The mechanism of the ATP-independent periplasmic chaperone SurA in outer membrane protein biogenesis

Julia Rose Humes

Submitted in accordance with the requirements for the degree of Doctor of Philosophy

The University of Leeds

Faculty of Biological Sciences

September 2018

Intellectual Property and Publication Statement

The candidate confirms that the work submitted is her own, except where work which has formed part of jointly-authored publications has been included. The contribution of the candidate and the other authors to this work has been explicitly indicated below. The candidate confirms that appropriate credit has been given within the thesis where reference has been made to the work of others.

Throughout this thesis the work directly attributable to the candidate is as follows:

(i) Literature research and compilation of the document.

(ii) The candidate performed all the experimental work and data analysis unless otherwise stated.

Chapters 3 contain work from the following publication:

Schiffrin, B. Calabrese A.N., Higgins A.J., Humes J.R., Ashcroft A.E., Kalli A.C., Brockwell D.J., Radford S.E.. Effects of Periplasmic Chaperones and Membrane Thickness on BamA-Catalyzed Outer-Membrane Protein Folding. J Mol Biol 429, 3776-3792 (2017).

In this publication B. Schiffrin designed and performed the kinetic experiments, computer modelling and molecular dynamics simulations. A. N. Calabrese designed and performed the mass-spectrometry experiments. A Higgins carried out crosslinking and kinetics. J Humes carried out the binding experiments. A Kalli, D Brockwell, A Ashcroft and S Radford provided experimental advice and helped with manuscript preparation.

Acknowledgments

Firstly, I would like to thank my supervisors Prof Sheena Radford and Dr David Brockwell who have been guided me through the last four years and pushed me to achieve things I didn't think I could. Thanks to the University of Leeds and the NIH for funding this project. I would also like to thank Dr Iain Manfeild, who trained me and allowed me to use the equipment in his lab to study the many molecular interactions in this thesis. Although my time in the NMR facility was brief, I learned so much and the help from Dr Arnout Kalverda has been invaluable.

The struggles I've have encountered during my research have been lessened by the wonderful people I've worked with in the Radford lab. There is always a friendly face to give advice on why an experiment hasn't worked and to go and have a drink with to help ease any science worries. In particular Nasir Khan our lab manager who always provides a smile and often delicious curries and really helped me settle into the lab all those years ago. Thanks to Jess Ebo and Matt Jackson who arranged so many social events to help turn work place proximity colleges into really good friends, as well as always having the kettle boiling when you needed a chat.

Within the Radford empire, the small group which took me in and who I worked with most were the OMPire headed up by Bob Schiffrin who trained my up in the lab when I didn't know which end of the pipette was which and has always come up with great suggestions and advice on my project. Anna Higgins, Jim Horne, Anton Calabrese, Paul White and Matt Iadanza who make up the OMPire are such a great group to work in and always willing to lend a hand as well as many terrible BAM jokes.

I need to give special thanks to Anna Higgins, Robb Hollis and Amy Swanston who have been there for me both in the lab and out to share triumphs and defeats with a large glass of wine.

My family have always been a constant support in everything I have achieved and they have always been there to cheer me on. My Mam and Dad have given me all the love I could ever need and many Sunday lunches to get me through. My big sister and my best friend Hannah, is always on the end of the phone through all my dramas she always knows what I need to hear.

Finally, a huge thank you to Dr Zak Mitchell who is the most supportive boyfriend I could ask for and has taken care of me through my turbulent Yorkshire Marathon training, the ups and downs of my research and the stress of thesis writing, I don't know what I would have done without him.

Abstract

Outer membrane proteins (OMPs) of Gram-negative bacteria travel from their site of synthesis in the cytoplasm, across the inner membrane and through the periplasm to the outer membrane (OM) prior to their folding to a functional form. To protect OMPs from misfolding or aggregation while traversing the periplasm a network of chaperones are employed. The OMPs must then reach the essential β-barrel assembly machinery (BAM) complex, which is involved in inserting OMPs into the OM. This process occurs in the absence of chemical energy as the periplasm is devoid of ATP and in a highly dynamic environment as the 'leaky' OM allows small molecules (<600 Da) to enter from the extracellular milieu.

The major periplasmic chaperone for OMPs, SurA, is known to interact with a number of substrates and has been crosslinked to the BAM complex *in vivo*. SurA is composed of four domains, an N-terminal domain, two peptidyl-prolyl isomerase (PPIase) domains and a short C-terminal helical domain. In this work wild-type *E. coli* SurA and SurA truncation variants lacking one (ΔP2) or both (N-Ct) of the PPIase domains have been studied. Using microscale thermophoresis, light scattering, native mass spectrometry and other biophysical techniques how each domain is involved in OMP binding, chaperoning and delivery to BAM is investigated.

The results demonstrate that SurA binds unfolded OMPs, tOmpA and OmpT with μM affinity, agreeing with previous findings. The core domain (SurA N-Ct) is sufficient for this interaction, but the addition of the PPIase domains leads to a tighter binding. Light scattering experiments shows that SurA WT can prevent aggregation of the two model OMPs, but the removal of the PPIase domains reduces the chaperoning ability for the larger, more aggregation-prone OMP, OmpT. These observations demonstrate that the acquisition of the PPIase domains is advantageous for both OMP binding and chaperoning. An interaction between SurA and the BAM complex is also observed for the first time *in vitro*. Overall, the results reveal new insights into

how SurA binds and chaperones OMPs before delivering them to the BAM complex for folding in the OM.

Table of Contents

List of Figures

List of Tables

List of Equations

Abbreviations

AF	Alexafluor
AFM	Atomic Force Microscopy
APS	Ammonium Phersulphate
ATP	Adenosine Triphosphate
AUC	Analytical Ultra-Centrifugation
Aβ	Amyloid β
BAM	β-barrel Assembly Machinery
BCA	Bicinchoninic Acid
BSA	Bovine Serum Albumin
CD	Circular Dichroism
CL	Cardiolipin
DDM	n-Dodecyl-β-D-Maltoside
DMSO	Dimethyl Sulfoxide
DNA	Deoxyribonucleic Acid
ΔP2	SurA with P2 domain deletion
DTT	Dithiothreitol
E. coli	*Escherichia coli*
EDC	(1-ethyl-3-(3-dimethylamino) propyl carbodiimide, hydrochloride
EDTA	Ethylenediaminetetraacetic Acid
ELISA	Enzyme-Linked Immunosorbent Assay
ER	Endoplasmic Reticulum
ESI	Electronspray Ionisation
FKPA	FK506-binding proteins
FRET	Flourescence resonance energy transfer
GAPDH	Glyceraldehyde-3-phosphate Dehydrogenase
Gdn-HCl	Guanidine Hydrochloride
HSQC	Heteronuclear Single Quantum Coherence
HT	Hexa-His tagged

IDP	Instrincally Disordered Protein
IM	Inner Membrane
Im7	Immunity Protein 7
IMS	Ion Mobility Spectrometry
IPTG	Isopropyl β-D-1-thiogalactopyranoside
ITC	Isothermal Titration Calorimetry
Koff	Off rate
Kon	On rate
LB	Lysogengy Broth
LPS	Lipopolysaccharide
M	Molar
MRE	Molar Residue Ellipticity
MS	Mass Spectrometry
MST	Microscale Thermophoresis
MWCO	Molecular Weight Cut Off
N-Ct	SurA containing on the N- and C-terminal domains
NHS	N-hydroxysuccinimide
NMR	Nuclear Magnetic Resonance
OM	Outer Membrane
OMP	Outer Membrane Protein
PCR	Polymerase Chain Reaction
PDB	Protein Data Bank
PDEA	(2-(2pyridinyldithio)ethaneamine
PE	Phosphatidylethanolamine
PG	Phosphatidylglycerol
PMSF	Phenylmethanesulfonyl Fluoride
POTRA	Polypeptide Transport Associated
PPIase	Peptide Prolyl Isomerase
RCMLA	Reduced Carboxymethylated Lactalbumin
SDS-PAGE	Sodium Dodecyl Sulfate-Polyacrylamide Gel Electrophoresis
SEC	Size Exclusion Chromatography

Skp	Seventeen kilodalton protein
SOC	Super Optimal Broth
SPR	Surface Plasmon Resonance
SurA	Survival Protein A
TBS	Tris Buffered Saline
TCEP	Tris(2-carboxyethyl)phosphine
TEM	Transmission Electron Microscopy
TEMED	Tetramethylethylenediamine
TF	Trigger Factor
TF RBD	Trigger Factor Ribosome Binding Domain
TF SBD	Trigger Factor Substrate Binding Domain
TROSY	Transverse Relaxation Optimized Spectroscopy
TY	Tryptone Yeast
UN	Unfolding
UV	Ultra Violet
VDAC	Voltage-Dependent Anion Channel
WHO	World Health Organisation
WT	Wild Type

Chapter 1 Introduction

1.1 Protein Folding and Proteostasis

In the 1950's Anfinsen discovered that small proteins can fold spontaneously upon dilution of denaturant, and that the only requirement to reach to correct folded state is the amino acid sequence [1]. Since that seminal work, the importance of molecular chaperones in aiding the folding of proteins in the crowded cellular environment has become apparent [2-6]. Chaperones are essential proteins found in all kingdoms of life which facilitate protein folding of nascent polypeptides, prevent self-association of aggregation-prone sequences and promote degradation of genetically mutated or irreversibly misfolded proteins [3,7,8].

Although some nascent polypeptides can fold spontaneously [9], the majority of proteins require the aid of chaperones however the chaperone network can become overloaded in the case of various cellular stresses and this problem is exacerbated by the crowded cellular environment [10]. Understanding the mechanisms of chaperones is critical to defining the proteostasis network and how this network can break down during cellular stress, genetic conditions and in ageing [7,11]. Protein misfolding diseases disrupt cellular proteostasis and evade chaperone control to form amorphous aggregates or amyloid fibrils [12-14]. Enhancing chaperone activity under these conditions may aid in slowing the progression of multiple human diseases such as Alzheimer's and Parkinson's [15,16] and targeting chaperones which are essential for oncoprotein activation is currently under investigation for new cancer therapeutics [17-19].

Controlling proteostasis of various cellular compartments is a challenge to both eukaryotic cells and Gram-negative bacteria [20-23]. The sorting of proteins into their native cellular compartments and the ability of the targeted polypeptides to reach their functional state in these different cellular environments requires specific

chaperone networks [24-26]. These networks often have homologous proteins between kingdoms, such as Hsp70 in the cytoplasm of eukaryotes and DnaK in cytoplasm of bacteria (Figure 1.1), and these pathways aid in the folding of most polypeptides which emerge from the ribosome. However, certain substrates or cellular compartments have evolved specialised chaperones such as those involved in disulphide bond formation [27].

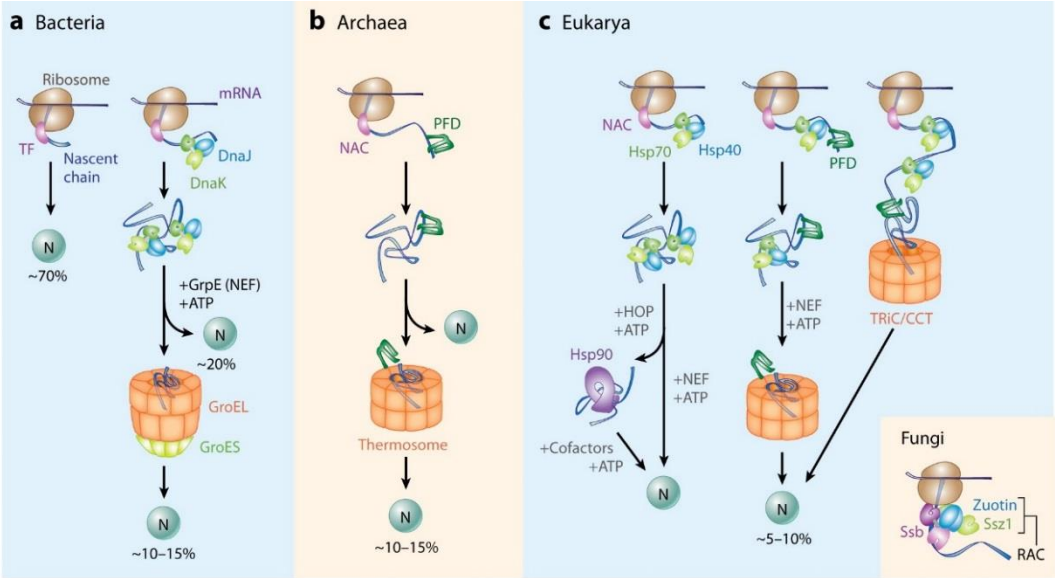

Figure 1.1 Cytoplasmic chaperone pathways in a) Bacteria b) Archaea c) Eukarya. Ribosome associated chaperones are found in all kingdoms of life Trigger factor (TF) in bacteria and nascent-chain-associated complex (NAC) in archaea and eukaryotes which bind to the nascent polypeptide and may lead to folding. For longer or more complex proteins, heat shock proteins (Hsp) Hsp70 in eukaryotes and DnaK in bacteria along with the Hsp40 family co-chaperones and nucleotide exchange factors aid in folding. Archaea which lack an Hsp system use prefoldin (PFD). Clients can then either be passed to Hsp90 in eukaryotes for proteins often found in signalling pathways or to a chaperonin system (TriC in eukaryotes, Thermosome in archaea and GroEL/ES in bacteria). Percentages represent average protein flux through each chaperone. Image reproduced from Kim *et al.* 2013 [28].

An example of specialised chaperones within cellular compartments is the periplasm of Gram-negative bacteria which is the space between the inner and the outer membranes of this class of bacteria. Proteins which require folding into the outer membrane for their function are synthesised in the cytoplasm then must be transferred across the inner membrane, across the periplasm and finally to the outer membrane all the while being protected from misfolding or aggregation by chaperones.

1.2 Gram-negative bacteria

The binding, chaperoning and delivery of β-barrel outer membrane proteins (OMPs) by chaperones in the periplasm of Gram-negative bacteria is investigated in this thesis. In 2017, the world health organisation published a list of twelve infectious bacteria for which new anti-biotic treatments are urgently needed (Table 1.1) [29]. Nine of these strains were Gram-negative including all infections in the critical category. Gram-negative infections often are harder to treat as these bacteria are surrounded by two membranes forming a barrier to most current antibiotics which act within the cytoplasm or periplasm to disrupt essential processes and can cause cell death.

Priority	Species	Gram positive of negative
Critical	*Acinetobacter baumannii*	Gram-negative
Critical	*Pseudomonas aeruginosa*	Gram-negative
Critical	*Enterobacteriaceae*	Gram-negative
High	*Enterococcus faecium*	Gram-positive
High	*Staphylococcus aureus*	Gram-positive
High	*Helicobacter pylori*	Gram-negative
High	*Campylobacter* spp.	Gram-negative
High	*Salmonellae*	Gram-negative
High	*Neisseria gonorrhoeae*	Gram-negative
Medium	*Streptococcus pneumoniae*	Gram-positive
Medium	*Haemophilus influenza*	Gram-negative
Medium	*Shigella* spp.	Gram-negative

Table 1.1 List of bacterial infections which require new antibiotic treatment published by the world health organisation (WHO) [29].

The inner most membrane, known as the inner membrane (IM) of Gram-negative surrounds the cytoplasm and is a symmetrical phospholipid bilayer in terms of the lipids it is comprised of, mainly comprised of phosphatidylethanolamine (PE) and phosphatidylglycerol (PG) lipids [30]. As bacteria lack intracellular organelles, all of the membrane-associated functions which are homologous to the eukaryotic organelles, are performed in the IM. The outer membrane (OM), by contrast, is asymmetric with the inner leaflet comprising of PE, PG and cardiolipin (CL), whereas the outer leaflet is comprised of glycolipids, principally lipopolysaccharide (LPS) [31] (Figure 1.2). The

outer membrane is densely packed with membrane proteins with mass ratios of 5:1:1 for protein: phospholipid: LPS.

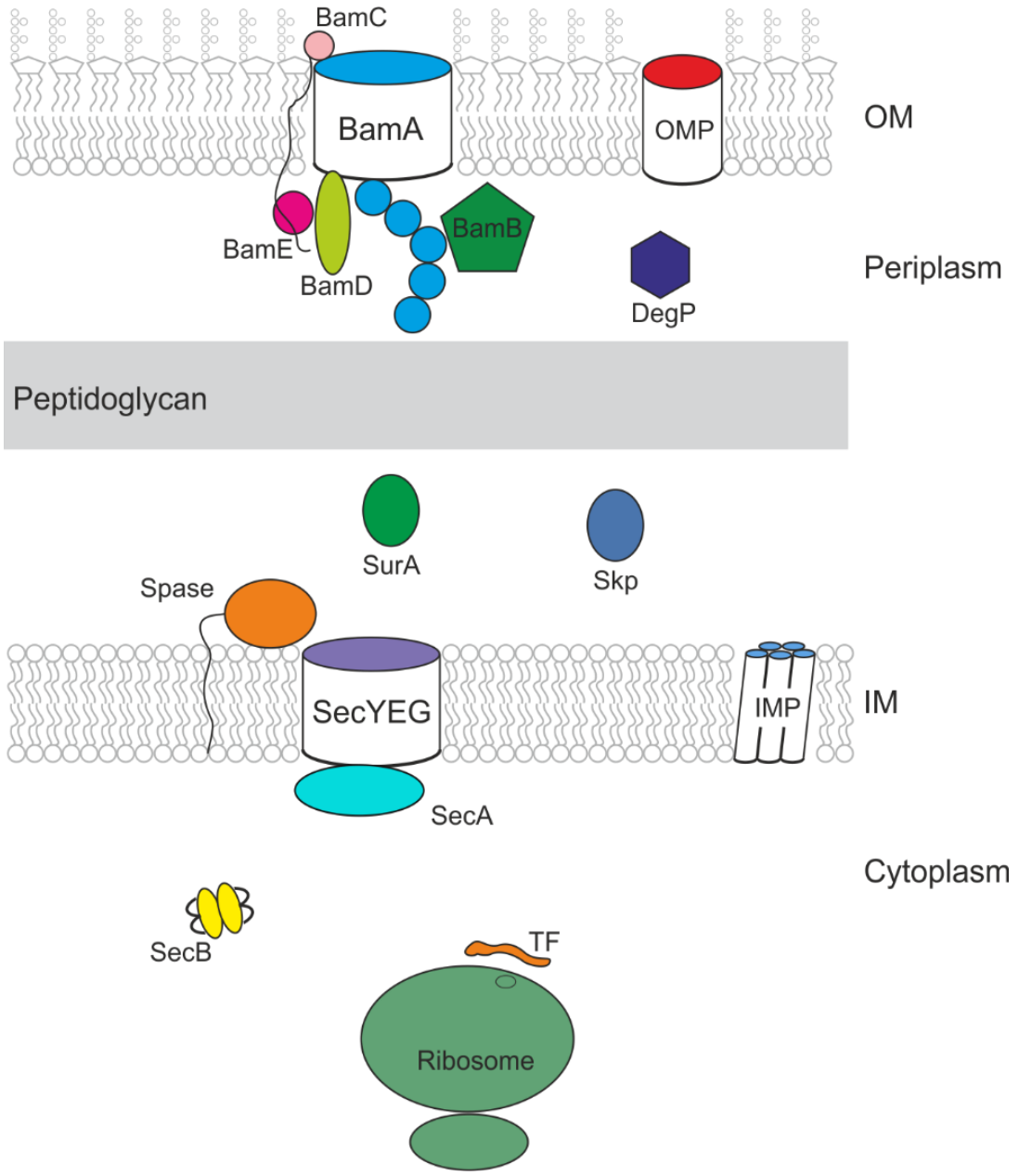

Figure 1.2 Schematic of the *E. coli* envelope. The main proteins involved in OMP biogenesis from the bacterial ribosome (dark green) via cytoplasmic chaperones Trigger Factor (TF) (orange) and the tetrameric SecB (yellow) OMPs are actively translocated through the Sec machinery (SecYEG) (purple) by the ATPase SecA (cyan). The signal sequence is cleaved by signal peptidase (SPase) (orange) and the nascent polypeptide bound by periplasmic chaperones Skp (blue), SurA (green) or DegP (purple) before being folded into the OM by the BAM complex (BamABCDE) as coloured in Figure 1.9. Schematic not to scale.

1.3 The Periplasm

The periplasm or periplasmic space separates the inner and outer membranes of Gram-negative bacteria (Figure 1.3). The periplasm was discovered after studies showing Gram-negative bacteria, which have no defined membrane bound organelles, contain ribonucleases and phosphatases without these enzymes causing toxicity in the cell [32]. Further extraction experiments led to the conclusion that these bacteria have a separate cellular compartment. This was then confirmed by electron microscopy imaging (Figure 1.3) [33,34]. Since this time, the periplasm has been shown to be important in many functions such as protein oxidation, disulphide bond formation, cell division, osmoregulation, as well as holding enzymes which would disrupt cytoplasmic processes [33,35-37].

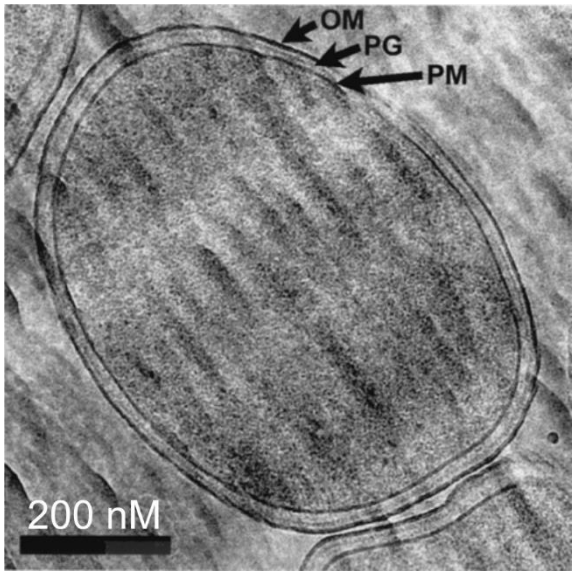

Figure 1.3 *E.coli* section electron microscopy image. Plasma membrane (PM), Peptidoglycan layer (PG) and Outer membrane (OM) labelled on the image. Adapted from Matias et al. [38].

The periplasm separates the inner and outer membranes and contains a layer of peptidoglycan necessary for cellular integrity, by maintaining cell shape and orchestrating division [36,39]. The presence of this peptioglycan layer in the periplasm has led to some debate in the field as to how outer membrane and secreted proteins traverse it. However, research demonstrating that outer membrane lipoproteins can coordinate peptidoglycan synthesis through direct contact with the peptidoglycan, indicates that at least some proteins may fit through pores in this layer [40]. The volume

of the periplasm was debated for many years but it has been shown to vary in size and can occupy up to 20% of the total cell volume under certain conditions [41]. Recent studies have shown that, Braun's lipoprotein which connects the OM to the peptidoglycan layer, is the 'molecular ruler' which determines periplasmic width [42] which has been estimated in the range of ~165 Å [43,44] to ~210 Å [45].

The OM allows free diffusion of molecules below 600 Da into the cell by transversing the lumen of non-specific porins [41,46]. This causes the periplasm to be highly dynamic as its composition depends on the environment the bacteria are in. For example, enterobacteria which cause human infections by ingestion must survive the passage through the highly acidic stomach (pH 1.5-3.5) to colonise the intestines. The periplasm is also devoid of ATP [47] and is more viscous than the cytoplasm [48]. These rapid changes and challenging environment within periplasm, may lead to unfolding or aggregation of soluble proteins or OMP during transport to the OM, and so periplasmic chaperones are essential to survival for Gram-negative bacteria [49,50].

1.4 Outer Membrane Proteins (OMPs)

Outer membrane proteins (OMPs) of Gram-negative bacteria are integral β-barrel membrane proteins that are involved in numerous functions such as the uptake of nutrients, release of waste materials, secretion of virulence factors, and resistance to host defence systems [30,31]. Membrane proteins in the outer membranes of mitochondria and chloroplasts are also mostly comprised of β-barrels [51]. Approximately 2-3% of genes in Gram-negative bacteria encode β-barrel OMPs [51] which are grouped into six families: porins, passive transporters, active transporters, enzymes, defensins and structural proteins [52]. Bacterial OMPs vary from 8-26 antiparallel β-strands and are always of an even number (Figure 1.4). An exception to this rule is the conserved eukaryotic protein voltage-dependent anion channel (VDAC), as the crystal structure of this barrel indicated 19 β-strands [53]. OMPs can also oligomerise, often into trimers, to form large functional structures in the membrane.

Although the distinguishing feature of these proteins is the β-barrel, they can also contain large domains either in the periplasm, on the outer surface of the cell or held within the barrel acting as a 'plug' which are often required for their function [51]. Although the importance of these OMPs is known, how they are translocated through the cell and inserted into the membrane remains to be fully elucidated.

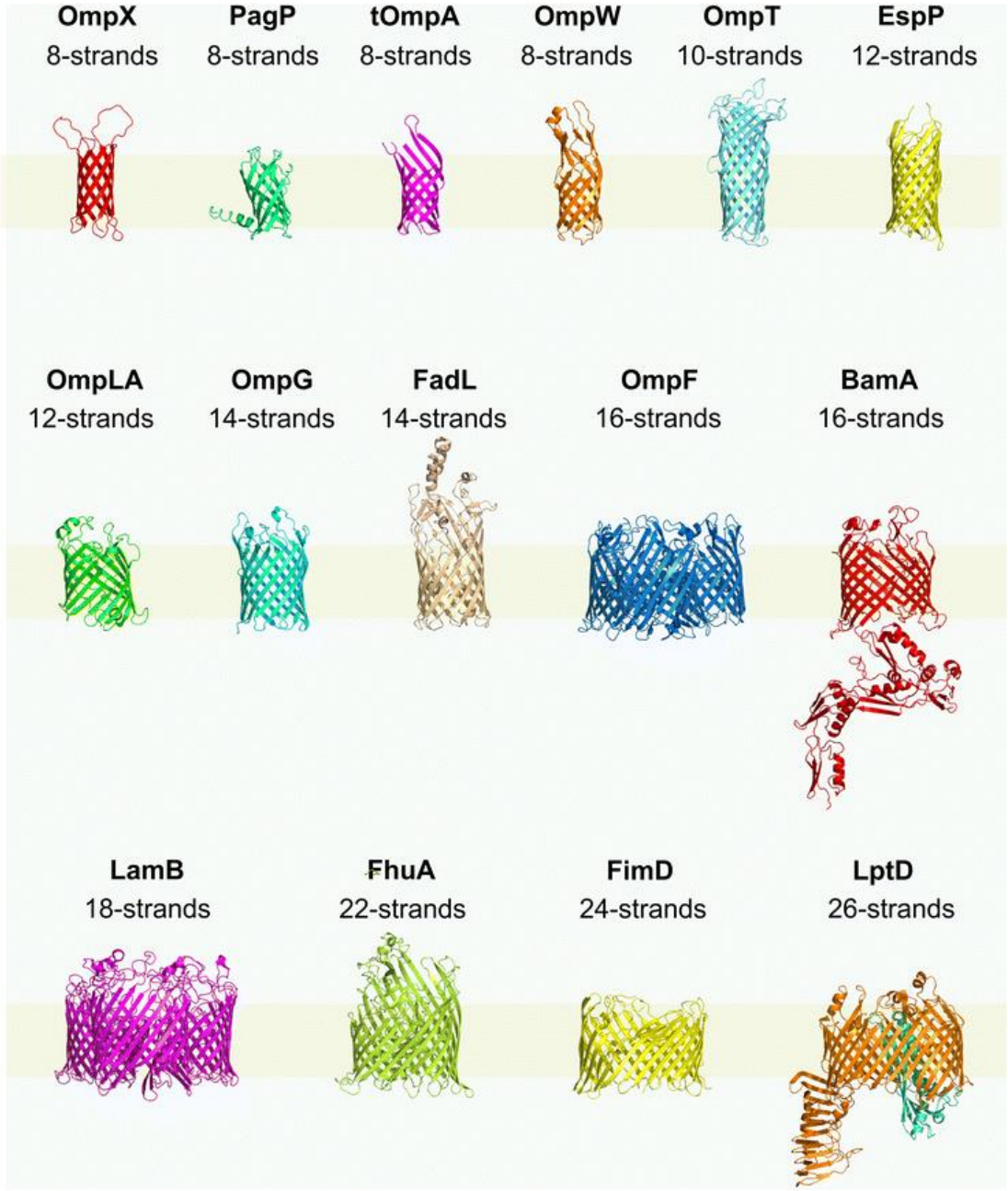

Figure 1.4 Crystal structures of Gram-Negative OMPs between 8 and 26 strands showing diverse architectures. OmpX (PDB: 2MO6)[54], PagP (PDB:3GP6)[55], tOmpA (PDB:1QJP)[56], OmpW (PDB:2F1V)[57], OmpT (PDB:1L78)[58], EspP (PDB: 2QOM)[59], OmpLA (PDB: 1QD5)[60], OmpG (PDB: 2IWV)[61], FadL (PDB:1T1L)[62], OmpF trimer (PDB:1OPF)[63], BamA (PDB:4K3B)[64], LamB trimer (PDB:1MAL)[65], FhuA (PDB:1BY3)[66], FimB (PDB: 3OHN)[67], (LptD PDB: 4Q35)[68]. Taken from Schiffrin et al. 2017[31].

1.5 Outer membrane protein translocation

Outer membrane proteins (OMPs) are translated by the bacterial ribosomes within the cytoplasm and so face a long journey from their site of synthesis to their native environment in the outer membrane (Figure 1.2). This journey requires a network of various chaperones, along with the SecYEG transporter, and although the main proteins in this network have been identified, and their crystal structures solved (Figure 1.5 and Section 1.8) [69-73] the exact interactions and mechanisms of these chaperones that aid OMP assembly remain to be discovered.

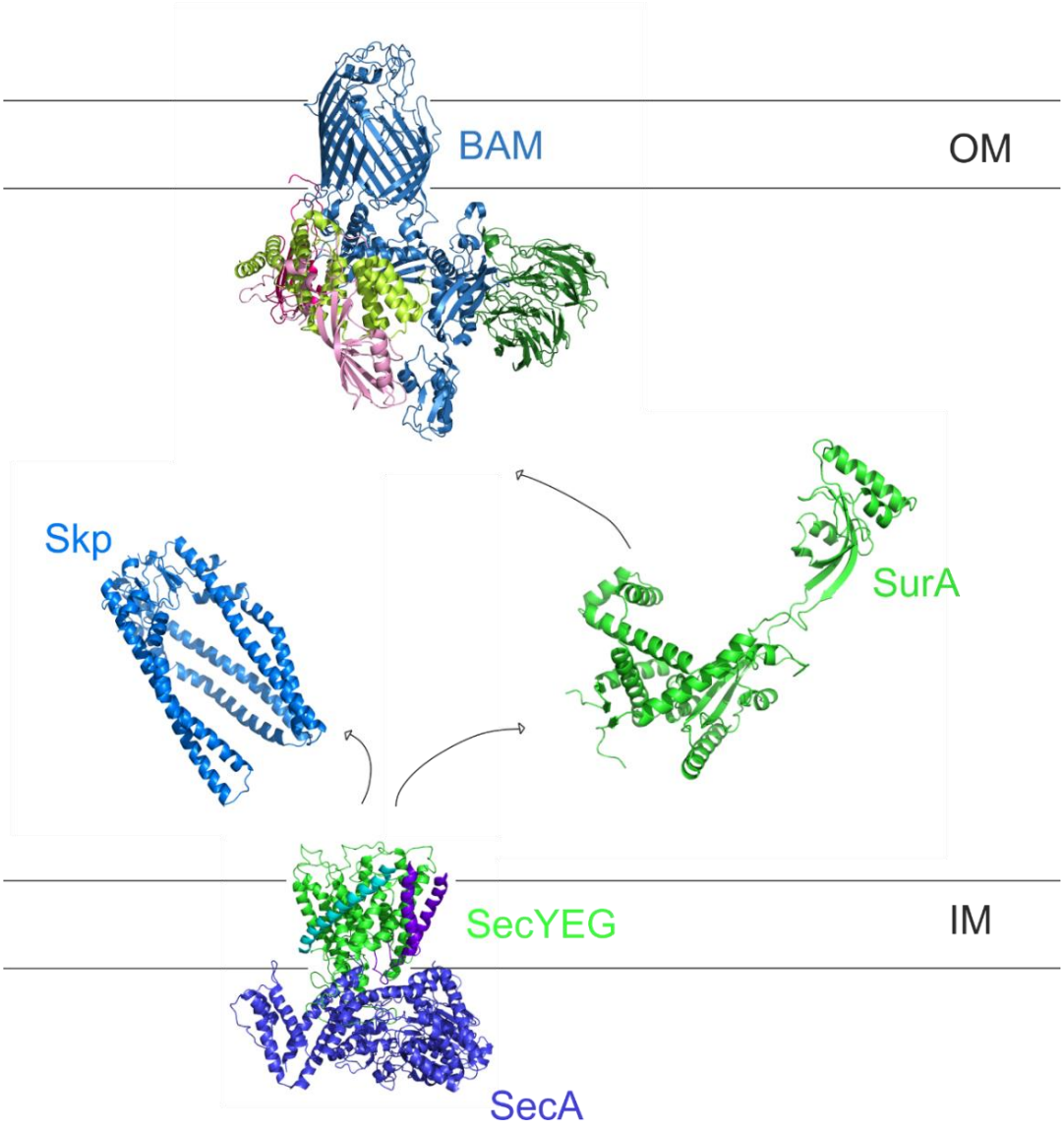

Figure 1.5 OMP transport across the pathway. OMPs are actively transported into the periplasm by the SecYEG complex utilising the ATP hydrolysis function of SecA (PDB: 3DL8)[74]. In the periplasm unfolded OMPs are bound by chaperones SurA (PDB: 1M5Y)[69] or Skp (PDB: 1U2M)[70] before interaction with the BAM complex (PDB : 5LJO)[71] for folding into the OM.

After the transcription and translation of OMP genes, the first contact with molecular chaperones occurs as the nascent protein emerges from the ribosome exit tunnel (Figure 1.2). Trigger factor (TF) has been shown to be an important OMP chaperone in the cytoplasm [24,75,76] and known to interact with the L23 subunit of the bacterial ribosome [77]. The crystal structure of trigger factor bound in a 1:1 stoichiometry to the 50S bacterial ribosome reveals its mode of action as it was described as a 'crouching dragon' (Figure 1.6) [78] which sits over the exit tunnel allowing its C-terminal domain, known to contain the chaperone activity [79], to interact with nascent substrates. Recent studies have shown that TF exists in the cell in a monomer-dimer equilibrium in the absence of substrates, with a K_d of dimerisation of 2.5 μM. The higher local affinity to substrates than to other TF monomers causes dimer dissociation [80,81]. TF has multiple hydrophobic binding sites across its surface that have been shown to keep alkaline phosphatase A (PhoA) in an unfolded and extended conformation [82]. This anti-aggregation mechanism is ubiquitous for the large range of substrates that TF is known to interact with, including OMPs which contain many hydrophobic residues and non-native interactions between these residues must be minimised to prevent protein misfolding.

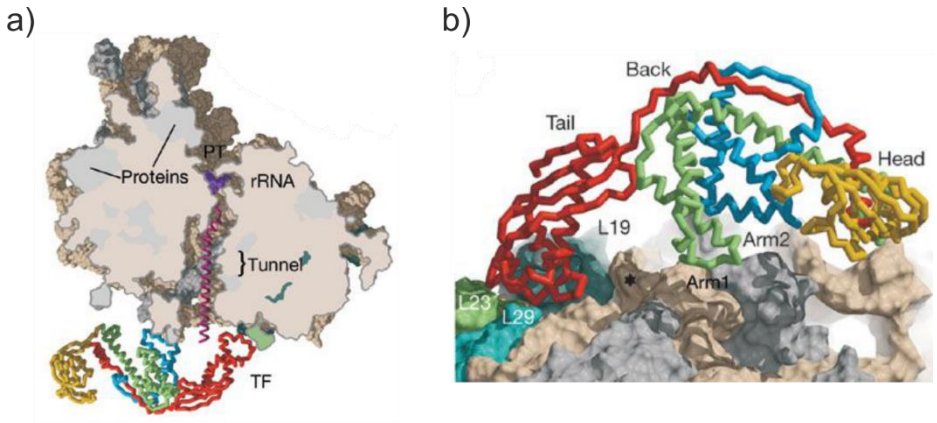

Figure 1.6 Structure of Trigger Factor guarding nascent polypeptides emerging from the Ribosome exit tunnel. a) 50S ribosome (beige) slice to observe the exit tunnel and the position of the Trigger Factor (TF) molecule in relation to the ribosome and modelled nascent chain in magenta. b) Zoom of a) with domains of TF labelled; tail or ribosome binding domain (RBD) in red, head or PPIase domain in yellow and arms 1 and 2 make up the substrate binding domain (SBD) in green and blue. Adapted from *Ferbitz et al.* 2004[78].

Although TF has been implicated in OMP biogenesis, it also aids in the folding of many cytoplasmic proteins. By contrast, a second cytoplasmic chaperone SecB works solely on proteins which require export from the cytoplasm [83]. SecB is a homo-tetrameric chaperone of 69 kDa which interacts with non-native precursor proteins (preproteins), which contain N-terminal signal peptides [83]. All bacterial secretory and outer membrane proteins contain a signal peptide which is 20-30 amino acids in length and contains a N-terminal domain of 1-8 positively charged amino acids, followed by a 4-16 amino acid helical hydrophobic segment and a C-terminal signal peptidase 1 (SPase 1) cleavage site [84,85]. SecB does not recognise the signal peptide [86], instead recognising basic and aromatic motifs [87], but still selectively interacts with pre-proteins, preventing their aggregation [88,89]. Like TF, SecB has also been shown to interact with substrates emerging from the ribosome but only to proteins of over 150 amino acids [87,90]. NMR studies showed that SecB binds substrates using hydrophobic grooves that run around the outer rim of the tetramer and can accommodate up to 250 interacting residues with Kd's of 0.05-0.5 μM (Figure 1.7) [89]. The SecB-substrate complex then interacts with SecA which is situated either in the cytoplasm or in association with the SecYEG complex. SecA is the ATPase motor which provides the energy for protein translocation through the inner membrane via the SecYEG translocon [74,84,91]. SecB is not essential for *E. coli* viability [92] and so there must be another pathway for OMPs to reach SecYEG, most likely using another chaperone such as TF, however this has not been well studied.

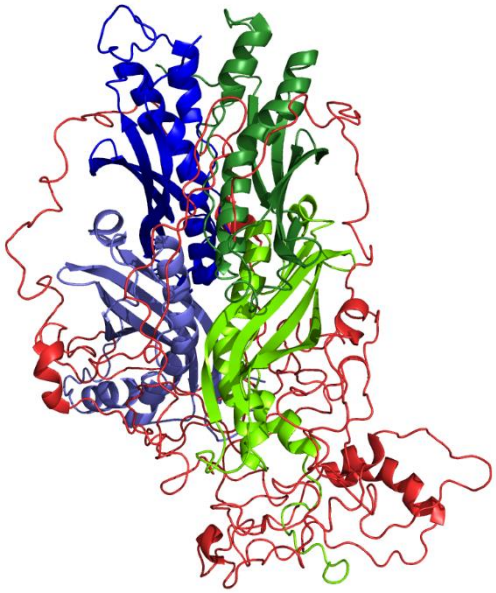

Figure 1.7 PhoA wraps around the SecB structure which prevents its aggregation. (PDB: 5JTL)[89] SecB in cartoon model, each monomer shown in light green, dark green, light blue and dark blue, PhoA in red.

The SecYEG complex is conserved across all domains of life and is essential for protein transport [84]. In Gram-negative bacteria the SecYEG complex is situated in the inner membrane and recognises the signal peptide of OMPs, periplasmic and secreted proteins [73,91]. SecY is a channel comprised of 10 transmembrane helices and is associated with SecE, that is responsible for stabilising SecY, and SecG which aids the interaction between SecA and SecY (Figure 1.8a) [73]. The current mechanism of translocation via SecYEG involves two-way communication between the two-helix finger of SecA that is held across the entrance of the SecY channel and the nucleotide binding region. As the unfolded protein is diffusing forward and backwards within the channel, bulky side chains cause structural perturbations of the two-helix finger which signals for nucleotide exchange and the binding of ATP. Binding of the ATP to SecA then causes conformational changes which are transduced through the structure causing an opening of the channel allowing the bulky side chain to pass. After ATP hydrolysis the channel constricts and the process is repeated (Figure 1.8b) [93,94]. This mechanism prevents the backsliding of proteins back into the cytoplasm while restricting the unwanted transport of water or ions across the inner membrane. Inner membrane proteins have an alternate signal sequence to that of OMPs which

directs SecY to laterally open to create an opening of its helical transmembrane domains and allow their folding into the membrane [95]. Once OMPs are in the periplasm the signal sequence is cleaved by SPase 1 which contains a serine-lysine catalytic pair within its hydrophobic cleft and the mature protein must then navigate the periplasm with the use of ATP-independent periplasmic chaperones to reach the BAM complex for folding and insertion into the OM (Figure 1.2) [96,97].

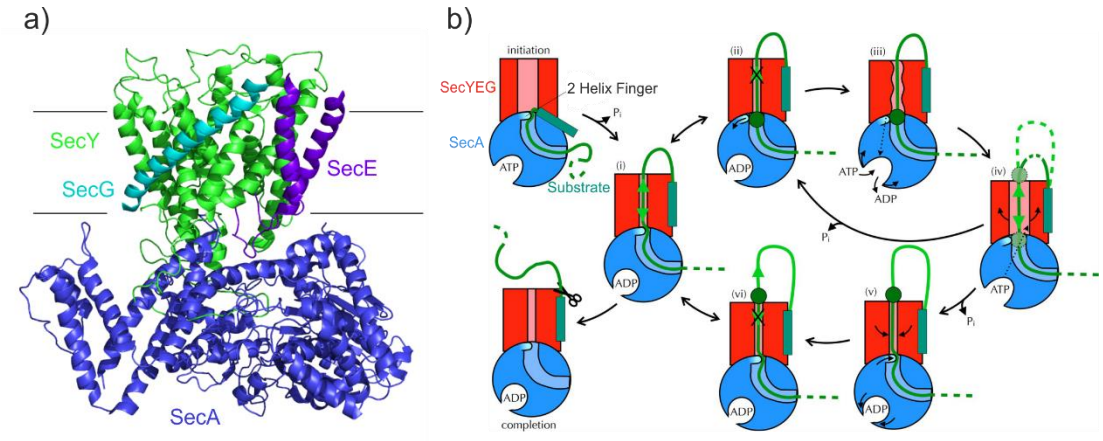

Figure 1.8 SecYEG structure and mechanism. a) Crystal structure of SecY (green) SecE (pruple) and SecG (blue) bound to SecA (purple) (PDB: 3DL8)[74] black lines indicate the position of the membrane. b) Mechanistic cycle of SecYEG (red), SecA (blue) with 2 helix finger labelled and substrate (green). After initiation the substrates can diffuse forward and backward in the SecYEG lumen (i) until it is blocked by a bulky side chain (ii), this induces nucleotide exchange in SecA (iii) which leads to opening of the lumen (iv). ATP hydrolysis causes closure of the lumen (v) trapping the bulky side chain on the periplasmic side (vi) this cycle continues until the full chain emerges through the channel and the signal sequence cleaved. Adapted from Allen *et al.* [93].

1.6 The BAM complex

The β-barrel assembly machinery (BAM) complex has been of much interest since BamA, the core component of the BAM complex, was shown to be involved in OMP biogenesis [96]. It has been shown that OMPs can fold spontaneously into detergent micelles or certain synthetic lipid bilayers when diluted out of denaturant *in vitro* [98-100], however in a complex cellular environment this process requires assistance by the BAM complex *in vivo*. The BAM complex is ubiquitous across all Gram-negative bacteria as well as having homologs in mitochondria and chloroplasts [51,101,102].

Bacterial strains lacking the BAM complex are non-viable, further demonstrating its importance [96].

The BAM complex from *E. coli* (Figure 1.9) comprises BamA which itself is a 16-stranded β-barrel within the OM that has five N-terminal polypeptide transport associated (POTRA) domains that protrude into the periplasm and are thought to interact with unfolded OMPs prior to their folding into the membrane [101,103]. BamA has four associated lipoproteins, BamB-E, which are arranged around the periplasmic portion of BamA [71,104]. Genetic knock-out studies have shown that BamA and BamD are the only essential components of the complex. Deletion of the other components however, display varying OMP assembly or growth defects [105].

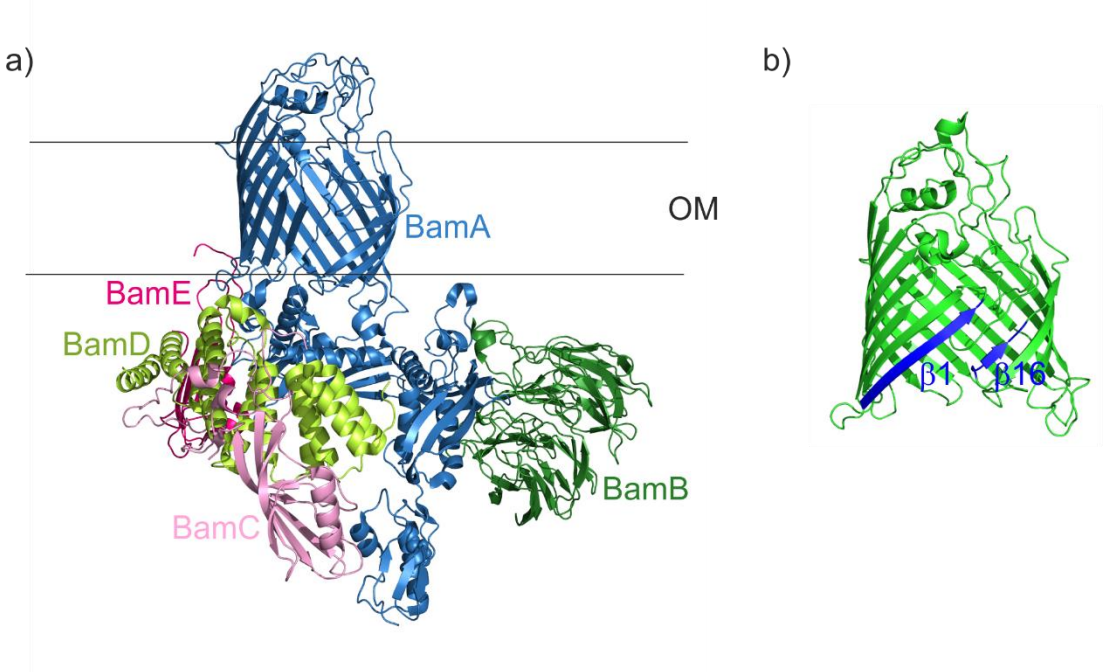

Figure 1.9 The BAM complex a) (PDB: 5LJO) [71] Cryo-EM structure of the full 5 domain BAM complex. BamA (β-barrel and POTRA domains) in blue, BamB in dark green, BamC in light pink, BamD in light green and BamE in dark pink b) BamA (PDB: 5D0O) [104] β1-β16 strands which form the lateral gate of the barrel in blue.

The mechanism of BAM complex associated OMP insertion is not fully understood, but through experimental evidence [64,97,105-107] multiple models have been proposed. Firstly, recent molecular dynamics simulations have shown a thinning of lipids on one side of the BamA barrel [64,97] and the rate enhancement of OMP folding by BamA was shown to be greater in thicker lipids of a carbon chain length of 14 compared to 12 [97]. Destabilisation of the lipids by the BAM complex may reduce the energy barrier for OMP folding in the membrane, passively creating a localised area for easier insertion of OMPs into the membrane (Figure 1.10a). Secondly, the incomplete hydrogen bonding network of the first and last β-strands of BamA (β1-β16) and the observation that cross-linking these strands is lethal *in vivo* [107], suggests a lateral opening of the BamA barrel and templating of the folding OMP onto the exposed β-strands of BamA before the OMP 'buds' of to complete its folding (Figure 1.10b). No direct evidence of either of these mechanisms has been found, however, further biochemical and structural evidence will be required to answer the questions that remain.

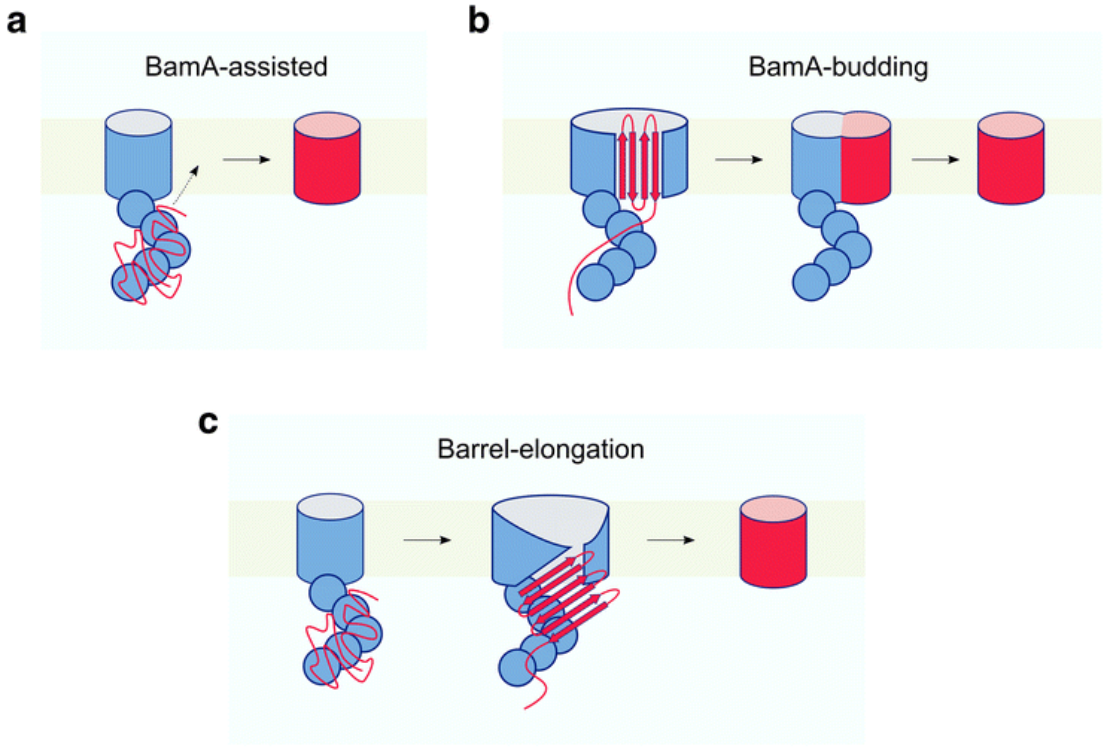

Figure 1.10 Proposed mechanisms of BAM mediated OMP folding and insertion into the OM. a) BAM assisted, OMPs interact with the POTRA domains and BAM disrupts the local lipids forming an area of easier insertion for OMPs. b) BamA-budding, OMPs template on the β-strands of the BamA lateral gate before the barrel closure buds the OMP from BAM. c) Barrel-elongation. OMPs interact with the POTRA domains and can template on the β1 strand of BamA forming β-strands in the periplasm and the OMP is then inserted into the membrane. Image adapted from Schiffrin et al. 2017[31].

1.7 Protein Folding of Bacterial Proteins

1.7.1 Cytoplasmic Protein Folding

Soluble proteins within the cytoplasm of prokaryotic and eukaryotic cells fold via a network of chaperones conserved from bacteria to man (Figure 1.1) [108,109] that assist in the folding and prevention of aggregation throughout their lifetime. I will briefly discuss the folding of soluble proteins in the context of cytoplasmic bacterial proteins. TF interacting with the ribosome protects nascent chains from degradation or aggregation and once the polypeptide is translated either it will fold with the aid of TF alone [110] or it will be passed to DnaK (the bacterial homologue of Hsp70). DnaK has been observed to have redundancy with TF as bacterial strains lacking either of the chaperones alone show no apparent folding defects when cultured at 37 °C [76], suggesting that DnaK can also bind to nascent chains in the absence of TF. DnaK

classically, however, acts by binding and releasing its substrate via cycles of ATP hydrolysis [111,112]. This is achieved by DnaK's co-factor DnaJ (or Hsp40 in eukaryotes) which accelerates ATP-hydrolysis, while the nucleotide exchange factor GrpE induces ADP release and ATP binding for the cycle to begin anew (Figure 1.11) [113]. DnaK binds sites on substrates that are approximately seven residues long and contain a hydrophobic central region with affinities of 5nM to 5µM [114]. The substrate forms hydrogen bonds and hydrophobic packing interactions with the chaperone [28] Once a protein has reached its native state, affinity for the chaperone decreases, as the hydrophobic amino acids required for chaperone binding are buried upon folding and the substrate is released.

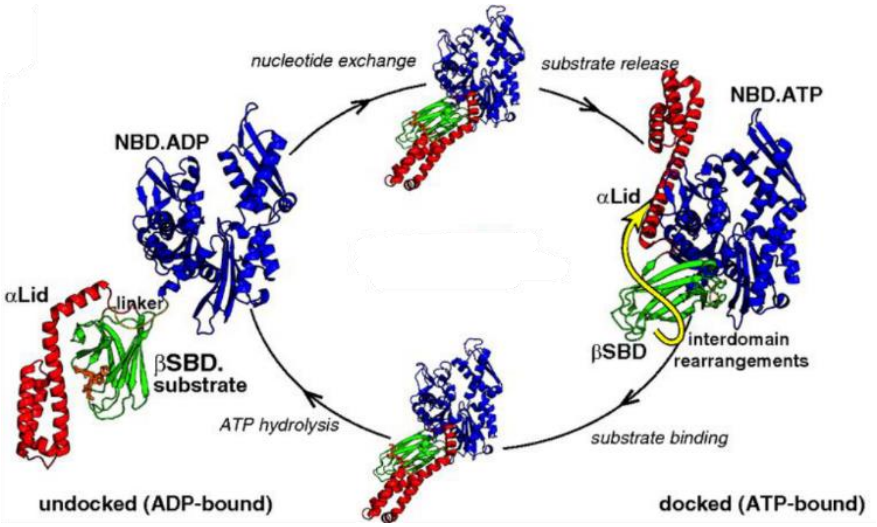

Figure 1.11 Structures and chaperone cycle of Hsp70 (DnaK). Nucleotide binding domain (NBD) in blue and Substrate binding domain (SDB) in green with the lid in red. The yellow arrow highlights ATP-induced Lid dissociation from the SBD. Conformational changes observed upon ATP binding and hydrolysis allow binding and release of substrates. Adapted from Zhuraleva *et al.* 2015[111]

If further assistance is needed for folding to the native state, proteins can be passed to chaperonins [12,115]. These cage-like structures comprise two rings and can be split into two groups [116]. In bacteria GroEL is a group 1 chaperonin which co-operates with GroES as its co-factor [117]. The second group, is found in archaea and eukaryotes and do not require co-chaperones, since the functionality of the co-chaperone function is included within the protein sequence. When unbound to a substrate GroEL has

exposed hydrophobic patches within the central cavity of the chaperone which bind hydrophobic amino acids on the surface of non-native proteins. The substrate is then sequestered into the centre of the cage by multiple contacts within the cylinder (Figure 1.12) [118]. Once the substrate is bound, ATP and the 'lid' co-chaperone, GroES, bind to form the cage structure which protects it from the crowded cellular environment [119]. Recent studies have shown that GroEL can interact directly with substrate folding intermediates and allow them to explore extended conformations not observed for the substrate in free solution [120]. With multiple rounds of ATP binding to the *cis* and *trans* rings and hydrolysis, GroEL/ES aids the folding and release of ~10% of all soluble bacterial protein in *E. coli* [12].

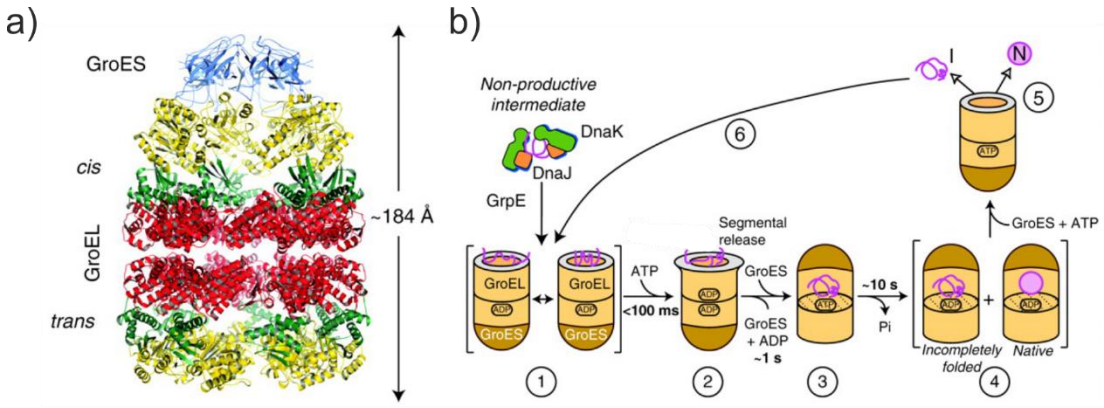

Figure 1.12 Structure and mechanism of GroEL. a) Crystal structure of GroEL-GroES complex (PDB: 1AON)[121], rings labelled *cis* and *trans*, GroES in blue. b) Mechanism of GroEL chaperonin, proteins are transferred from DnaK/J (1) ATP-dependent domain movement of the apical GroEL domains (2), GroES is recruited and encapsulates the substrate (3). Substrates are then either folded (4) and released (5), or go through the cycle again (6). Adapted from Hartl 2010[122].

1.7.2 Protein Folding in the Bacterial Periplasm

There are over 300 proteins present in the periplasm of Gram-negative bacteria [123]. Chaperones are required to assist folding of periplasm resident soluble proteins, along with prevention of aggregation of OMPs [122]. The chaperones which function in the periplasm must have distinct mechanisms of action from the cytoplasmic chaperones which cycle ATP for binding and release of substrates to aid folding, as there is no ATP present in the periplasm [47].

Soluble periplasmic proteins undergo the same translocation as OMPs via SecYEG [94]and they also undergo signal peptide cleavage via SPase 1 [85]. The subsequent folding of water soluble periplasmic proteins however, has not been well studied. The main chaperones for such proteins in the periplasm are Spy [124] and HdeA/HdeB [125] which are stress chaperones that are either at low concentrations under non-stressed conditions or are only activated under certain stresses. However, as the periplasm is so dynamic is it not known to what extent these chaperones are required.

1.7.2.1 Spy

Spy was first discovered as a molecular chaperone by an *in vivo* assay that linked protein stability to antibiotic resistance [124]. When *E .coli* was challenged to stabilise the bacteria test protein, Immunity protein 7 (Im7), the bacteria massively overproduces Spy, which increases the steady-state levels of the unstable protein mutants up to 700-fold [124]. Spy is a non-essential chaperone under both normal and stress conditions [126]. The Spy chaperone itself is a tightly bound dimer of kinked hairpin-like monomers, each with four α-helices (Figure 1.13) [127]. The dimer interface is of antiparallel orientation resulting in a novel cradle shape, not seen before in any class of chaperone [128]. Since its discovery, Spy has been found to be implicated in protecting *E .coli* when challenged with a wide range of stresses such as tannin, ethanol, butanol or excess metal ions [127,129]. Kwon *et al*. solved the crystal structure of Spy and subsequently proposed a model of its binding to an unfolded substrate [127]. On the concave surface of the cradle structure of Spy there are hydrophobic patches which could bind the exposed hydrophobic residues on the surface of unfolded proteins, thereby protecting it from irreversible misfolding or binding to other unfolded proteins which may lead to aggregation [129]. Further studies by Quan *et al.* support the hypothesis that the two hydrophobic patches in Spy are involved in client binding (Figure 1.13b) [127]. Mutants of Spy with increased chaperone activity were found to mainly increase the hydrophobic nature of the concave surface near the proposed binding regions. These mutants were also found to be less thermodynamically stable and have increased flexibility, suggesting that more flexible chaperones have increased activity as they are able carry out their

function by undergoing conformational changes upon substrate binding [129]. Structural analysis of the Spy-Im7 complex [130] demonstrated that Spy binds to locally frustrated regions of Im7. Frustration occurs when amino acids in a folded structure are in close proximity and are unable to minimise the free energy between them. Spy also destabilises partially folded states to aid in the search of the native client structure.

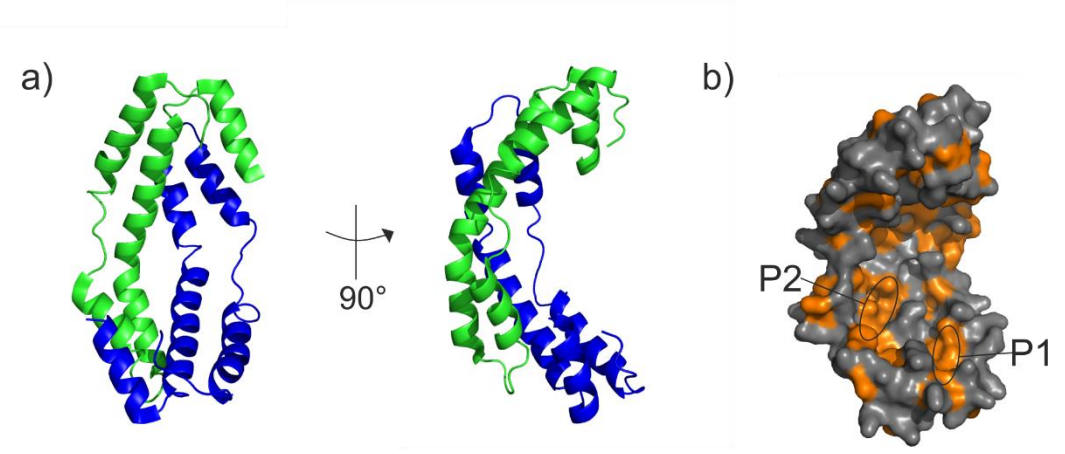

Figure 1.13 The homodimeric concave structure of Spy . (PDB: 3OEO) a) Monomers coloured in blue and green. b) Hydrophobic residues in orange on grey SurA surface structure proposed binding sites from Quan *et al.* **[129]** labelled as P1 and P2

Kinetic analysis of protein folding of Im7 in the presence of Spy demonstrated that Spy allows folding of the substrate while remaining bound to the chaperone [131] (See also Appendix where this publication is reproduced). These results propose a potentially widespread mechanism whereby ATP-independent chaperones can assist in protein refolding opposed to just buffering proteins against aggregation as has been shown previously for SecB and TF [82,89].

1.7.2.2 HdeA/HdeB

HdeA and HdeB are general chaperones in the periplasm of *E. coli* that protect a range of substrates as shown using the model proteins rhodanese, malate dehydrogenase and alcohol dehydrogenase [132]. However, these chaperones are only activated under acid-stress [133]. Under non-stress conditions HdeA/ HdeB dimerises and is inactive as

a chaperone (Figure 1.14) [134]. Once exposed to acid the complex dissociates into two active monomers that can bind to the exposed hydrophobic amino acids of unfolded periplasmic proteins [135,136]. Although HdeA and HdeB are structural homologues, they contain only 17% sequence identity, differences in their amino acid sequences leads to their differing functions [135,137]. HdeA monomerises and prevents aggregation of substrates between pH 1 and 3, whereas HdeB has only minimal activity at pH 3, with maximal acid-protective activity at pH 4 [137]. While both chaperones reversibly dissociate below pH 3, HdeB remains as a functional, flexible dimer that can bind a range of unfolded substrates at pH 4 [137]. HdeA and HdeB act synergistically in *E. coli* to protect the bacterium from a range of low pH's (including during transit through the acidic human stomach for example) that could unfold periplasmic proteins and lead to cell death.

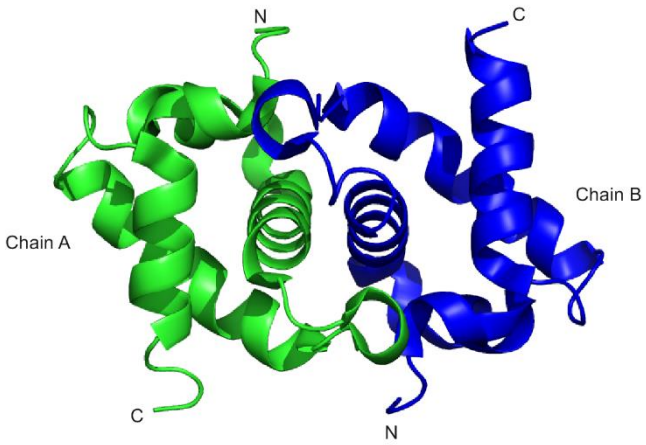

Figure 1.14 HdeA homodimer. (PDB: 1DJ8)[135] The dimer is present under neutral conditions and when exposed to acid-stress dissociates to bind its substrates.

Currently it is also not known whether the periplasmic water soluble proteins emerging from the Sec translocon need the assistance of chaperones to reach their native three-dimensional conformation and which chaperones, if any, are involved in folding specific clients.

1.8 Periplasmic Chaperones of Outer Membrane Proteins (OMPs)

1.8.1 Skp

Skp (Seventeen kilodalton protein) is a chaperone found within the periplasm of Gram-negative bacteria that has been shown to bind and prevent aggregation of OMPs [138,139]. In addition to acting on OMPs Skp has also been shown to improve the yield of recombinant soluble proteins [140] and to prevent the aggregation of lysozyme independently of ATP [70]. Genetic analysis has shown that in *E. coli,* Skp is non-essential for cell growth and survival and a proteomic approach discovered that deletion of Skp has no significant impact on the levels of OMPs within the cell [141]. This demonstrates the redundancy of the periplasmic chaperone network which has been suggested in multiple studies [142-144], as cellular conditions such as stress may determine which pathway is more prevalent.

The crystal structure of Skp, determined in 2004 [70], showed that the chaperone resembles a trimeric 'jellyfish', which is comprised of a core domain containing nine-stranded β-barrel which mediates trimerisation and helical tentacles which extend unidirectionally from the core, forming the walls of a cavity (Figure 1.15). This architecture is very similar to that of prefoldin, an ATP-independent cytoplasmic chaperone found in eukaryotes and archaea [145]. Although prefoldin is a hexamer containing 2 α and 4 β subunits, with the β-sheets forming the core, when compared to Skp it appears to be a dimer of trimers.

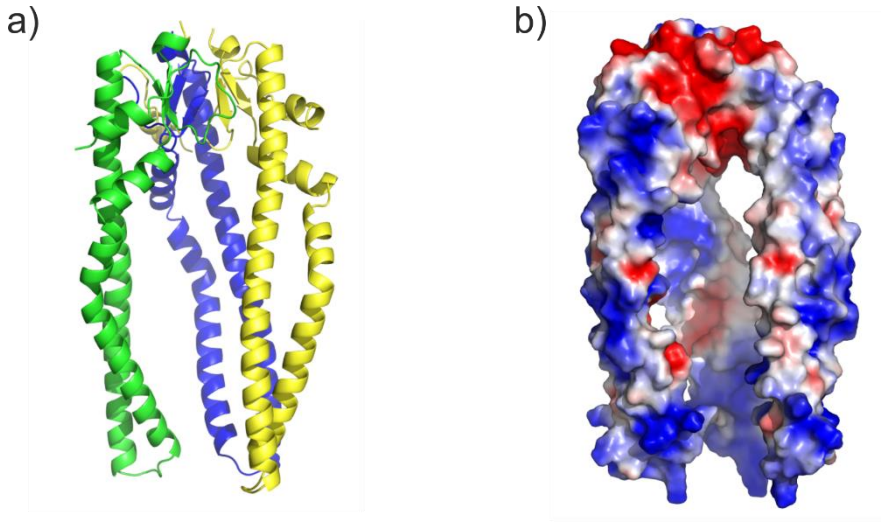

Figure 1.15 Crystal structure of Skp (PDB: 1U2M)[70]. a) Each monomer is individually coloured. b) Skp electropositive and electronegative surfaces are highlighted in blue and red, respectively. Electrostatic surface representations (-2 kT/e to +2 kT/e) were generated using the APBS plugin for PyMOL[146].

The tips of the Skp helices are enriched in conserved positive lysine and arginine residues, making the chaperone highly basic (pI 9.5) (Figure 1.15b). The tips are thought to interact with unfolded OMPs, which have pI values commonly around 6 and may also interact with BAM complex proteins or directly with the outer membrane (OM) which has an overall negative charge [44]. Within the cavity of Skp there is an even distribution of hydrophobic residues along the inner face of the tentacles (Figure 1.15b) [70] and this surface has been crosslinked to OmpA *in vitro* [147]. NMR studies have also suggested that unfolded OMP substrates are sequestered within the cavity [148,149] and that Skp holds the OMP in an unfolded 'dynamic globule' state to protect it from aggregation [149].

Skp binds a broad range of OMP substrates [138,150] ranging from 8 to 22 β-strands, yet despite the size difference, the stoichiometry of binding originally proposed to be 1:1 [151]. Schiffrin *et al.* observed using native mass spectrometry and fluorescence folding assays that for OMPs of ≥ 10 β-stands a 2:1 Skp:OMP complex can be formed [98]. As the extended OMPs cannot be contained within the cavity of a single Skp trimer, two

trimers were proposed to form a parallel side-by-side conformation to enlarge the cavity space in which to accommodate large unfolded OMPs (Figure 1.16). The affinity of Skp for OMPs has been measured in the nanomolar range [151] and equimolar Skp concentrations prevents OMP folding into liposomes in the absence of BAM [98]. However, it is not yet understood if or how Skp releases OMPs for folding into the membrane; and if Skp has any interaction with the BAM complex or delivers OMPs directly to the OM instead.

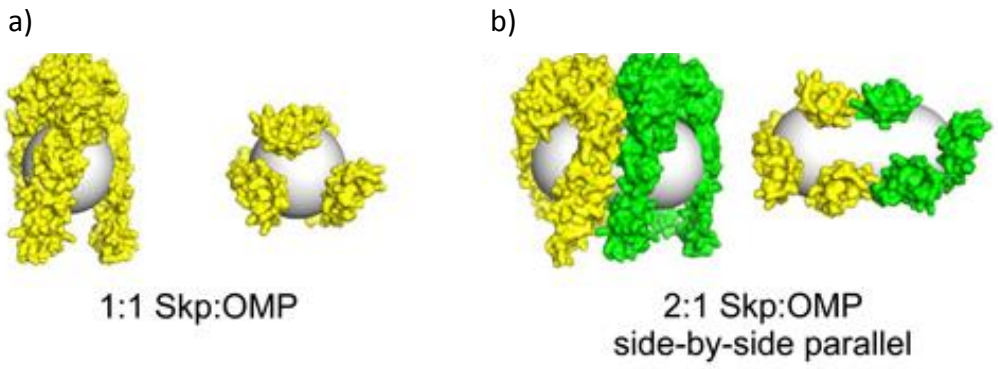

Figure 1.16 Proposed models of Skp-OMP interaction. a) Skp interaction of OMPs below 10 β-strands with a stoichiometry of 1:1. b) Skp binding larger OMPs with a 2:1 stoichiometry to encapsulate the larger substrate surface. Adapted from B. Schiffrin et al. 2016 [98].

1.8.2 FkpA

FkpA is a dual functional periplasmic chaperone as it also contains an active peptide prolyl isomerase (PPIase) domain [152]. FkpA was originally discovered as a periplasmic homologue of the macrophage infectivity potentiator (MIP) protein which is a FK506-binding protein [153]. FK506-binding proteins (FKBP) are a structural family of proteins which exhibit PPIase activity, FK506 binds these proteins and inhibits the catalytic activity by mimicking the transition state of proline *trans-cis* isomerisation [152].

FkpA is not essential and a deletion of the gene does not lead to an increase in σ^E stress response , which is caused by excess unfolded proteins in the periplasm (stress responses discussed in Section 1.9) [154]. However, overexpression of FkpA can reduce σ^E levels in strains of bacteria that have defects in LPS production or protein disulphide isomerases [154]. Although the chaperone activity of FkpA appears redundant to SurA at growth temperatures of 37 °C it appears to become more important during heat shock (44 °C) [142]. Under heat shock *ΔskpΔsurA* strains are lethal, but overexpression of FkpA can rescue growth and yield similar levels of folded OMP levels as wild-type strains [142]. FkpA is expressed at similar levels at 37 °C and 44 °C however at the higher temperature it binds to OmpC with higher affinity (23.2 ± 3.5 μM at 37 °C and 12.4 ± 3.7 μM at 44 °C) and also is more efficient at preventing

aggregation of OmpF [142]. These data suggest that FkpA is involved in OMP biogenesis and mainly acts upon heat shock when proteins are more likely to aggregate and other chaperones may be saturated by folding defects in the proteome as a whole. Further analysis found that FkpA can also prevent protein aggregation of MalE31, a folding deficient mutant of maltose binding protein, showing FkpA can also chaperone water soluble periplasmic proteins [152].

The crystal structure of FkpA (Figure 1.17) shows a symmetrical V-shaped homodimer with each 29 kDa monomer containing two domains. The N-terminal domain comprises of three α-helices which are involved in dimerisation and the C-terminal domain contains the FKBP activity. Analysis of the domains in isolation shows that the N-terminal domain is in a monomer-dimer equilibrium and retains chaperone activity, whereas the C-terminal domain remains monomeric, retaining PPIase activity [152]. This shows that the chaperone and catalytic activities reside in the N- and C- terminal domains, respectively. Multiple crystal structures show the C-terminus is different conformations [152] in accordance with NMR studies showing that the linker and C-terminal domain are highly dynamic [155]. These dynamics are reduced upon binding of a substrate (RNase A S-protein) to the hydrophobic residues lining the inside of the V structure. This is likely to position the PPIase domain in the correct orientation for catalysis [155].

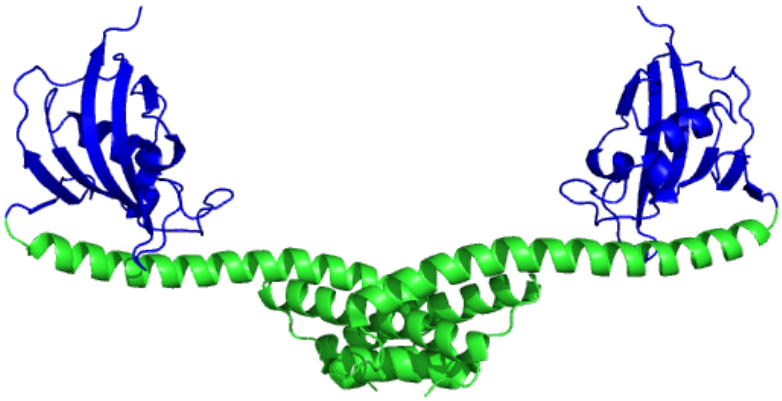

Figure 1.17 Crystal structure of the symmetrical FkpA dimer (PDB 1Q6U)[152] N-terminal chaperone domain in green and C-terminal FKBP PPIase domains in blue.

1.8.3 DegP

DegP is a periplasmic chaperone which also has serine protease function, that acts on unfolded proteins within the cellular envelope [156]. DegP is upregulated in the presence of excess unfolded proteins in the periplasm during heat shock [41] and temperature provides the switch which determines whether DegP acts as a chaperone or protease [157]. Above 37 °C DegP is required as a protease and is essential for bacterial survival at elevated temperatures [158,159]. Below 28 °C DegP is found to prevent protein aggregation and no degradation activity is observed [157,160].

Each monomer of DegP is 47 kDa and contains a protease domain and two PDZ domains which bind substrates (Figure 1.18a) [41]. The PDZ domains which gain their name from the protein in which they were originally discovered (post synaptic density protein) and are often found in signalling proteins to interact with downstream partners. The monomers pack together by interactions between protease domains into trimers, shielding the active site from binding and degrading native proteins under non-stress conditions [161]. The trimers can either remain in this state or go onto form hexamers by dimeristion of two trimeric units that involves a two-stranded β-sheet from each monomer protruding out to form a 'face-to-face' interaction (Figure 1.18b) [159]. These proteolytically-inactive stable hexamers and trimers have the ability to bind unfolded substrates which is thought to trigger the assembly of active polyhedral 12 or 24-mer cage structures [156]. It is thought that the disassembly of the stable hexamer occurs by a 'proteinquake' process, where a perturbation within one region causes the sequential unfolding of the β-sheets in the centre of the trimer-trimer interface [159]. The unfolded water soluble periplasmic protein or OMP can be degraded within the cage structures by the now inward facing protease domains, while restricting the access of native proteins, assisting cell survival. The formation of the polyhedral cage structures are seen at permissible temperatures as well as during heat shock [159], although they are most likely to remain inactive without a bound substrate to prevent wanton proteolysis [159].

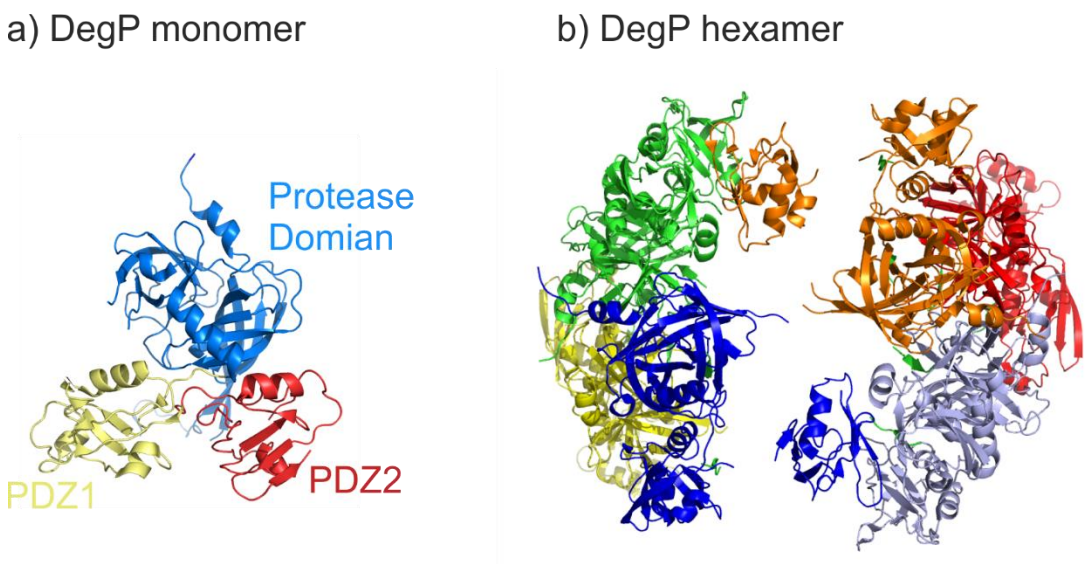

Figure 1.18 DegP Protease Structure a) DegP monomer (PDB: 1KY9)[72], protease domain in blue, PDZ1 in yellow and PDZ2 in red. b) DegP hexamer (PDB: 3OTP)[156] the hexamer structure (each monomer coloured individually) which binds to substrates before forming larger structures.

1.8.4 SurA

SurA was discovered due to its role in bacterial survival during stationary phase [162,163] which gave rise to the name survival protein A or SurA. Sequence analysis of SurA from *E. coli* identified two domains with homology to the peptide prolyl isomerase (PPIase) parvulin, flanked by a long N-terminal region and short C-terminal region [69]. Comparisons of the ability of SurA to aid in the folding of OMPs compared to soluble periplasmic proteins established SurA as specifically involved in OMP biogenesis [164] although it can prevent the aggregation of water soluble proteins [165].

In vivo, deletion of the SurA gene does not affect bacterial growth [166] but instead leads to: reduction of OM density [50], accumulation of unfolded proteins in the periplasm causing upregulation of the σ^E stress response [165], reduced antibiotic resistance [167] and increased sensitivity to hydrophobic agents (e.g. SDS/EDTA and rifampicin) [168]. Although SurA is not essential, deletion of both SurA and Skp or SurA and DegP as double deletions are lethal. By contrast, deletion of Skp and DegP is not

lethal [50,169]. This suggests the SurA is the major OMP chaperone within the periplasm and that Skp and DegP may function in an alternative redundant pathway. A recent single-molecule Förster resonance energy transfer (smFRET) study comparing the ability of SurA and Skp to disaggregate OmpC showed that Skp, but not SurA, could allow OmpC to reform monomeric species [144]. As SurA is at a higher concentration within the cell than Skp (7.2 μM and 0.73 μM respectively) [144] the authors propose that SurA deals with the OMP biogenesis under non-stressed conditions, while Skp is required under stress conditions when it is known to be over-expressed [50].

Although SurA is the major OMP chaperone in the periplasm, a proteomics study which examined the effect of SurA deletion, only eight proteins (out of 64 studied, 23 of which were β-barrel OMPs) were found to display reduced folded levels [170]. The proteins affected include porins OmpA, OmpF and LamB, as well as FadL, OmpX, FecA, FhuA and LptD. However, of these protein with reduced expression, only FhuA and LptD cannot be explained by decreased mRNA levels [170]. Depletion of SurA in a Skp null mutant strain diminished the levels of almost all OMPs measured [141], further implying that in the absence of a single periplasmic chaperone, redundant pathways can rescue any function required for OMP biogenesis.

The crystal structure of SurA, determined in 2002 [69], showed an asymmetrical dumbbell shape in which the N-terminal domain, the first PPIase domain (P1), and the C-terminal domain form the core of the molecule and the second PPIase domain (P2) is a satellite domain which is approximately 30 Å from the core (Figure 1.19). Although *E. coli* SurA contains two structural PPIase domains, only P2 displays PPIase activity [165] as P1 lacks the catalytic residues found in P2 and other pavulin homologues (Section 1.10). Mutations in these catalytic residues within the P2 domain prevent proline isomerisation but have no effect on SurA chaperone function [165]. Within the core of SurA an extended crevice was suggested to be a peptide binding channel and so an original hypothesis on the mechanism of SurA is that the

core domain is involved in binding OMPs and chaperone activity while the P2 domain is responsible for PPIase activity [165].

The 33 residue C terminal domain is mainly helical with a short β-strand (Figure 1.20) which forms an antiparallel β-sheet with a hairpin in the N-terminal domain thought to stabilise the core of SurA [171]. Deletion of between 2 and 20 residues from the C-terminal domain showed that removing only four amino acids increased susceptibly of bacterial strains to novobicin and that removal of 20 amino acids had the same effect as a deletion of full length SurA [171]. The sequence of the C-terminal domain however, appears to be less important as it can accommodate many varied mutations without compromising SurA function [172].

The surface features of SurA show that hydrophobic and electrostatics are at multiple locations across SurA (Figure 1.19). This suggests that SurA interacts with substrates using many small binding regions opposed to a singular binding site. This has been shown for both TF and SecB previously, as long unfolded substrates wrap around the chaperones in order to prevent the aggregation [82,89] (Figure 1.19).

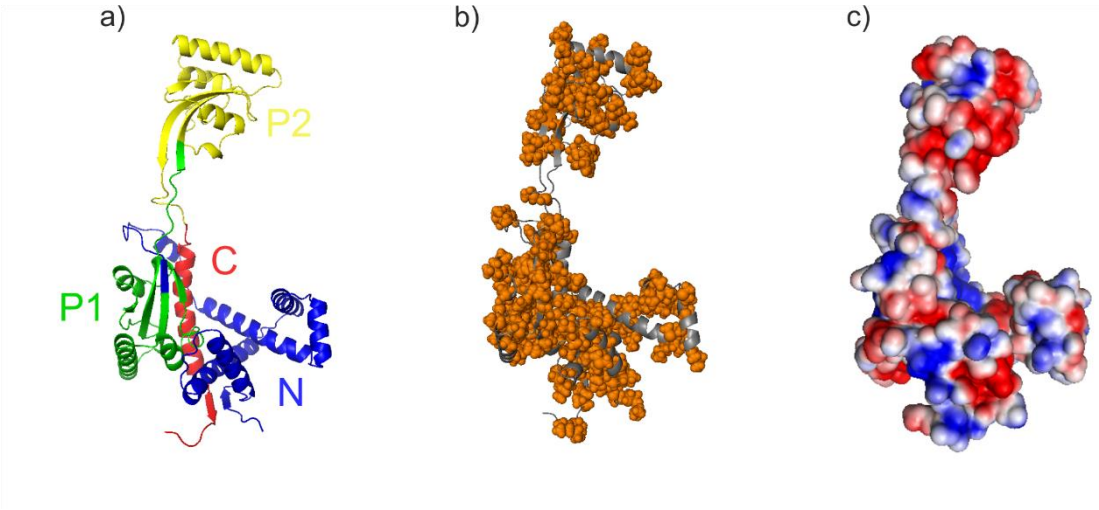

Figure 1.19 SurA physiological properties. a) Cartoon of SurA domains coloured as in Figure 1.20 (PDB: 1M5Y)[69] b) Hydrophobic residues in orange and as spheres on grey SurA structure c) SurA electropositive and electronegative surfaces are highlighted in blue and red, respectively. Electrostatic surface representations (-2 kT/e to +2 kT/e) were generated using the APBS plugin for PyMOL[146].

To examine the roles of the different domains within SurA domain deletions were created of all combinations such as the removal of P1 (SurA ΔP1), removal of P2 (SurA ΔP2), removal of both PPIase domains (SurA N-Ct) (Figure 1.20b). These experiments showed that in strains lacking SurA, σ^E activity is reduced almost to WT levels by plasmids containing SurA ΔP1, SurA ΔP2 and SurA N-Ct, but not by the PPIase domains alone [165]. *In vitro* assays have shown that SurA N-Ct is sufficient to prevent the aggregation of the thermally denatured water soluble protein citric synthase, and both SurA N-Ct and SurA ΔP2 were shown to have greater chaperone activity than SurA WT towards this protein [165]. It is interesting to note that SurA is highly conserved across protobacteria [173] and while the *E. coli* SurA contains two PPIase domains other homologues have been found with only one PPIase domain, often with higher sequence similarity to P2 than P1 (e.g. *Haemophilus influenzae*) or no PPIase domains (e.g. *Brucella ceti*) [174]. So understanding the functions of these domains will thus elucidate the requirement or lack of PPIase domains observed across bacterial species.

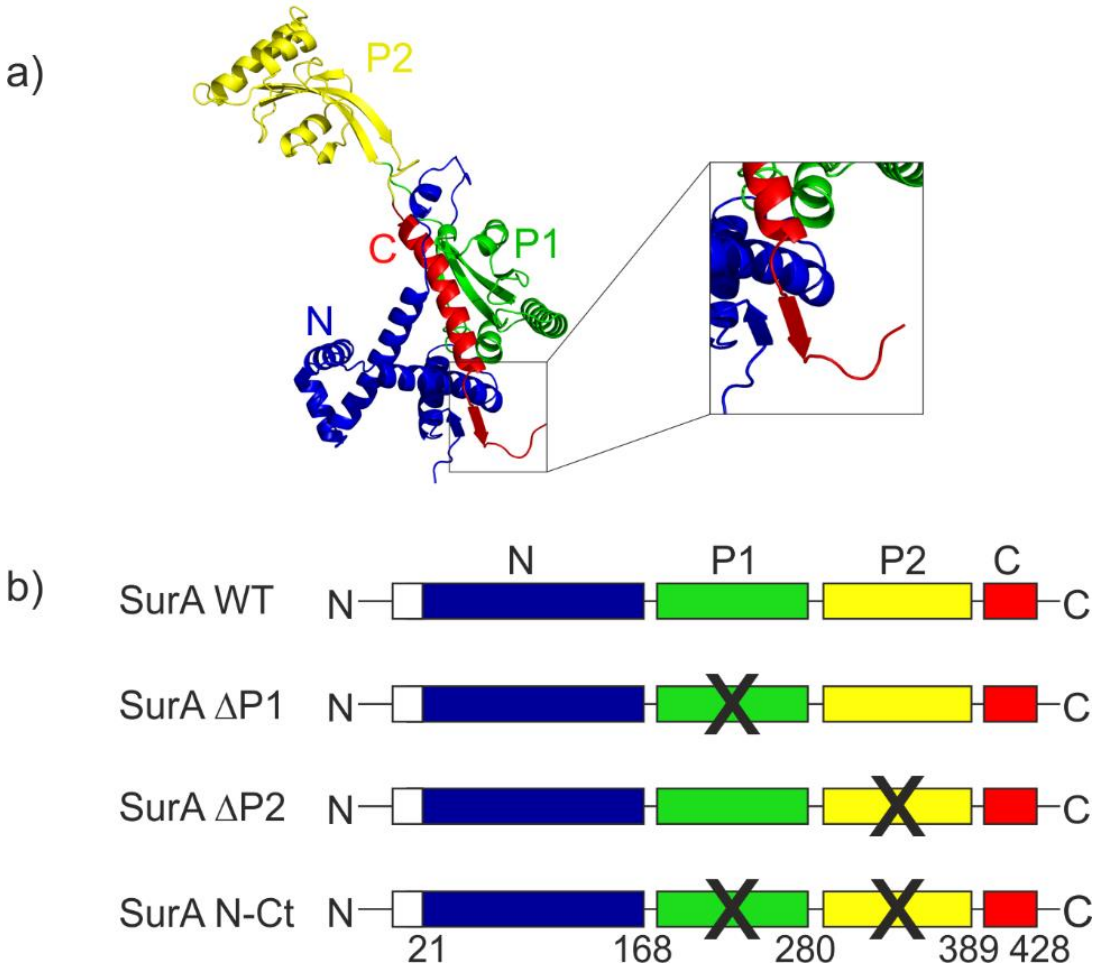

Figure 1.20 ATP-independent periplasmic chaperone SurA a) Crystal structure (PDB: 1M5Y)[69] domains coloured N terminal domain in blue, PPIase domain 1 (P1) in green, PPIase domain 2 (P2) in yellow and the C terminal domain in red. Boxed zoom of the C-terminus β-strand. b) The constructs of SurA used in this study, domains coloured as in a and black crosses indicate domain deletions.

SurA WT and SurA ΔP2 were found to interact preferentially with peptides which contain multiple aromatic (Ar) residues, in particular those which contain an Ar-X-Ar motif [175,176], which is common at the C-terminus of OMP sequences [175]. The affinities of SurA WT and SurA ΔP2 binding to peptides is between 1-14 μM and between 0.4-5.1 μM for full length OMPs (OmpF and OmpG) [177], whereas binding to reduced carboxymethylated lactalbumin (RCMLA), a representative water soluble unfolded protein, had reduced binding (33 ±11 μM and 38 ±11 μM for Sura WT and SurA ΔP2 respectively) [177]. Upon binding of SurA, OMPs are thought to be held in an extended and unfolded conformation as determined by FRET and NMR [144,149], which

presumably ensures that aggregation-prone regions of unfolded OMPs do not self-associate. Crystal structures of either the SurA ΔP2 variant, or of the P1 domain in complex with peptides, show binding to the P1 domain [178]. By contrast, crosslinking of peptides or full length OMPs in solution suggested that the N-terminal domain of SurA is the main site of OMP binding [179,180]. Similar crosslinking experiments suggested that mainly the N- and C-terminal residues of OMPs interact with SurA [180], consistent with the hypothesis that SurA recognises the Ar-X-Ar motif at the C-terminus of OMPs [175].

SurA's ability to aid in the folding of OMPs was measured by atomic force microscopy (AFM) studies. FhuA which were folded into proteoliposomes and the proteoliposomes absorbed to a mica surface. The folded FhuA was pulled via its plug domain out of the liposomes and the success of refolding was quantified under different conditions [181]. Without a chaperone present FhuA formed mainly non-native or misfolded structures. However, in the presence of SurA, 40% of refolding was successful compared to 7% without chaperone [181]. Skp was able to reduce the amount of misfolded species, but could not increase folding yield, further supporting the hypothesis that SurA is the main chaperone involved in OMP folding. SurA has also been shown to inhibit the aggregation of OmpF *in vitro* in a concentration-dependent manner at 37 °C, with a 20-fold excess of chaperone significantly reducing the amplitude of light scattering, however this inhibition is lost at 44 °C [142].

SurA is the only periplasmic chaperone which has been crosslinked to the BAM complex *in vivo* [50,180,182,183] and this interaction has been mapped to residue R64 of POTRA 1 [182] and between residues 311 and 316 in the P2 domain of SurA [180]. Disruption of this interaction by deletion of R64 causes an increase in antibiotic sensitivity, reduced OMP expression and is lethal in combination with the deletion of SurA [182]. There is a current focus to reveal the structure of SurA-OMP-BAM complex to identify if and how OMP substrates are handed over from SurA to BAM, and also the mechanism of BAM-mediated OMP folding and insertion into the membrane.

In uropathogenic *E. coli* strains (which cause infections within the unitary tract) the removal of SurA decreases binding and invasion of host cells and it has been shown that SurA N-Ct domain variant is sufficient to recover this function of SurA [184]. These results suggest the PPIase domains have no effect in bacterial virulence. SurA deletion strains have reduced pilus formation which is explained by the reduction in FimD pilus usher protein levels [166,184]. SurA has also been implicated for full virulence of salmonella and shigella [174] signifying that targeting SurA may be a promising route to developing novel antibiotics.

1.9 Periplasmic stress responses

Chaperones within the periplasm aid in the folding of water soluble, periplasmic proteins and OMPs proteins under non-stressed conditions within the cell. Under stress conditions Gram-negative bacteria have mechanisms to increase the concentrations of folding factors within the periplasm to prevent protein unfolding and misfolding which may lead to the cell death, reviewed in [21,41,185,186].

Three signal transduction pathways have been identified in *E. coli* which are activated in response to perturbations within the cellular envelope. Two of the responses are two-component systems (CpxAR and BeaSR) in which the first component (CpxA and BeaS) are membrane embedded histidine kinases which sense the stress through a cascade of phosphorylation events (Figure 1.21) the second component (which is a transcription factor) is activated to upregulate target genes [185]. Although these pathways function in the same way, they respond to different triggers and have different downstream effects [126,185,187]. The CpxAR system responds to a highly alkaline pH in the periplasm, overexpression of certain lipoproteins and misfolded pilus subunits and induces the expression of DegP, PpiA, PpiD and the disulphide bond catalyst DsbA to cope with these stresses. BeaAR senses environmental stresses such as presence of antibiotics, bile salts and ethanol, and responds by expression of a multi-drug efflux pump and stress response chaperone, Spy, to protect misfolding

of soluble periplasmic proteins [185]. These pathways are summarised schematically in Figure 1.21.

The third pathway which is induced by stress in the periplasm is the σ^E responses which is specifically activated when OMP biogenesis is disrupted. This pathway involves the RseA membrane protein which acts as an anti-σ^E factor by sequestering the transcription factor at the inner membrane. Upon the presence of excess unfolded OMPs in the periplasm [188] or incorrectly folded OMPs in the membrane RseA is cleaved allowing σ^E to translocate and interact with and upregulates its target genes such as DegP, FkpA, SurA and Skp [189]. These chaperones are known to prevent OMP aggregation, dissolve soluble OMP aggregates and degrade proteins in the periplasm which cannot fold correctly [72,142,165,181]. The σ^E response also reduces the translation of OMP genes via small RNAs [190] and also up-regulates BAM complex expression to reduces the pool of unfolded OMPs in the periplasm [189].

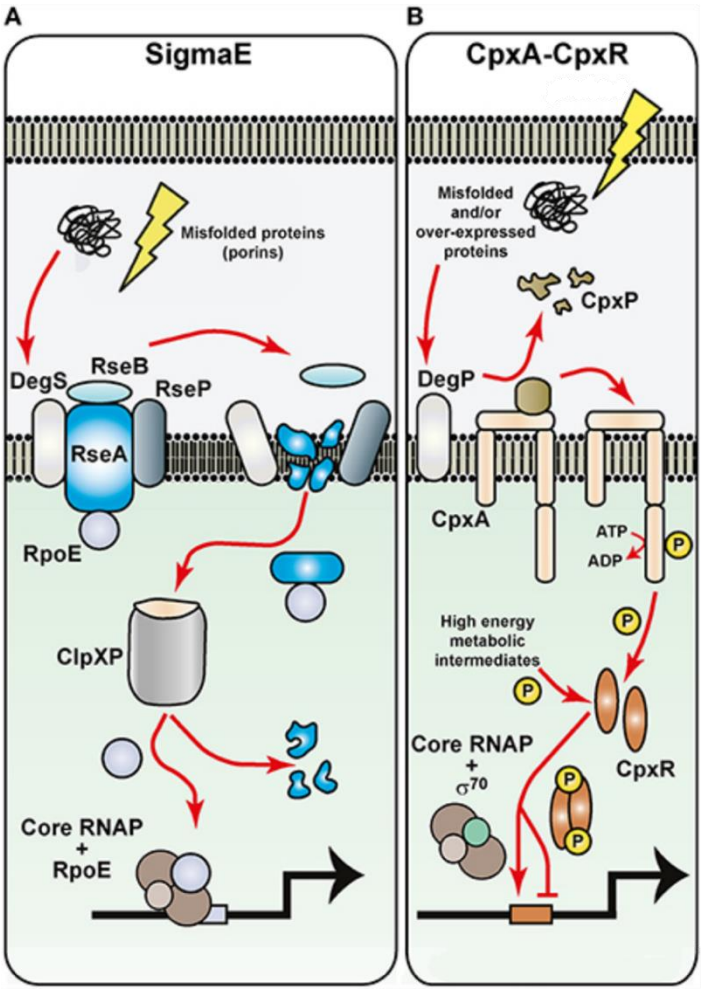

Figure 1.21 Stress response systems within the periplasm of Gram-negative bacteria. a) OMP misfolding in the periplasm initiates RseA digestion by proteases DegS, RseP and ClpXP which releases the sigma factor RpoE (σ^E) which upregulates required genes. b) CpxA-CpxR system initiated by unfolded proteins in the periplasm CpxP which inhibits CpxA is degraded by DegP, CpxA then initiates a phosphorylation cascade to the transcription factor, CpxR. Adapted from Chen *et al.*[188]

1.10 Peptiylprolyl Isomerases (PPIases) in protein folding

Peptidylprolyl isomerases (PPIases) are enzymes, found in prokaryotes and eukaryotes, that catalyse the conversion of *cis* to *trans* proline residues within protein sequences [191-193]. Under physiological conditions prolines within unfolded proteins are in an equilibrium between *cis* or *trans* conformations however, the trans form generally is found in natively folded proteins as the most stable isomer [194]. The interconversion of *cis* to *trans* isoforms as the rate-limiting step in protein folding has been observed to have a high energy barrier (84 kJ/mol) disfavouring spontaneous conversion [194]. PPIase's aid in *cis-trans* isomerisation by disruption of the partial double-bond character of the peptide bond [195].

There are three families of PPIase's: cyclophilins, FK506-binding proteins and parvulin-like domains [193], however there is currently no rationale for the structural diversity observed for this catalytic function. Parvulin is a 96 residue *E. coli* PPIase found in the cytoplasm and nucleus which has homologues in eukaryotes [196]. Larger proteins contain domains which are homologous to parvulin and also convey PPIase activity [196]. SurA for example, which in *E. coli* has two PPIase domains both with the $\beta\alpha_3\beta\alpha\beta_2$ parvulin fold, as found in all parvulin homologues [163]. Analysis of the PPIase domains of *E. coli* SurA in isolation showed that only the second PPIase domain had catalytic activity. Isolated P2, however has only approximately half the activity of the two PPIase domains together or the full length SurA [165]. The catalytic resides found in a eukaryotic homologue, Pin1, occurred in a hydrophobic pocket similar to that found in the second PPIase domain of SurA (His376 and Ile 378). Mutation of these residues in the context of the full length SurA led to little or no PPIase activity, demonstrating that these are the catalytic residues in SurA [165]. The first PPIase domain of *E. coli* SurA lacks the catalytic residue at the second position required for

activity showing although it is structurally a parvulin domain, it is not an active PPIase (Figure 1.22). The function of this domain remains unknown.

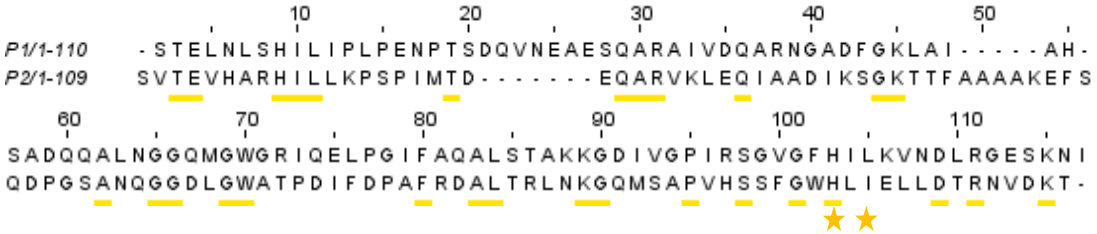

Figure 1.22 Alignment of PPIase domains P1 and P2 of SurA. Alignment done using the Clustal Omega software [197], conserved residues are underlined in yellow and catalytic residues in P2 (His376 and Ile 378) highlight with a yellow star.

The FK506-binding proteins (FKBP), such as FkpA, have no sequence or structural similarity to the other PPIase families (Figure 1.23) [198]. FKBP domains are 110 amino acids in length and have a conserved tertiary structure which contains five anti-parallel β-sheets. The loop between sheets 4 and 5 contain a short helix which caps the concave surface of the β-sheets allowing the hydrophobic residues to point into the centre of the protein forming the active site which binds polypeptides containing proline residues [192].

Alongside SurA and FkpA, other PPIase's found in the periplasm include PpiA and PpiD, which are members of the cyclophilin family of PPIases [199]. Cyclophilins have been found in mammals, plants, insects, fungi, and bacteria. The structure is conserved throughout evolution and all have PPIase activity [200]. The structure of proteins from this family have four β-strands with two α-helices on one side [201,202]. Cyclophilins have also been found in almost all cellular compartments such as mitochondria, the ER and the nucleus as well as the periplasm [200]. Many protein folding events depend on cylcophilins but they also have other functions such as a Cpy40 which form a complex with Hsp90, regulating its chaperone activity [19].

Analysis of the four known PPIases in the periplasm of *E. coli* (Figure 1.23) demonstrated that a quadruple deletion *ΔsurAΔfkpaΔppiaΔppid* strain had no more

phenotypic effects than *Δsura* single deletion, which is more sensitive to antibiotics and has reduced OmpA and LamB levels in the outer membrane [166]. It is unknown what the functions of the different PPIase proteins in the periplasm are, however *in vivo* PpiD has been shown to have partially overlapping substrate specificity with SurA [203] and also a similar structure (Figure 1.23). Furthermore, as the upregulation of PpiD and PpiA is caused by an alternative stress pathway to that of SurA and FkpA the enzymes may be more efficient under different conditions although this has not been tested.

Figure 1.23 Peptidyl prolyl isomerase (PPIase) domains of proteins present in the periplasm of *E.coli*. a) PpiA (PDB: 1W74) [202]. b) PpiD (PDB: 2KGJ) [201]. c) P1 domain of SurA (PDB: 2VP2) [178]. d) C-terminal domain of FkpA (PDB: 1Q6U) [152].

1.11 Current Questions in the Field and Aims of this Thesis

The role of periplasmic chaperones in OMP biogenesis has been studied over the past 30 years [46,162] however, many important questions in the field still remain:

1. How do ATP-independent periplasmic chaperones bind and transport OMPs?
2. What are the roles of SurA and Skp in OMP biogenesis? Do they have preference for certain substrates and are they required under different cellular conditions?
3. How does SurA interact with OMPs and the BAM complex and does it directly deliver OMPs to BAM for folding?

The main aim of this research is to study all aspects of the molecular mechanisms of SurA and shed light on these questions in the context of this chaperone. As SurA is the major chaperone involved in OMP biogenesis, studying the mechanism of this chaperone will aid in understanding the OMP biogenesis pathway as a whole. The initial binding of SurA to substrate, prevention of OMP aggregation and SurA's interaction with the BAM complex for OMP delivery is investigated here in order to better understand the journey of OMPs through the periplasm with the help of SurA.

Many biochemical and structural assays have been employed to examine the interaction between SurA and two model OMP substrates in the first results chapter. The ability of SurA to prevent the aggregation of these OMPs is then investigated and compared to other chaperones known to bind OMPs in *E. coli* in the second results chapter. Finally, in chapter 5, the interactions of SurA and Skp with the BAM complex are tested in order to understand the roles of these chaperones in OMP delivery for folding via the BAM complex. In this study PPIase domain deletion variants of SurA have been created and utilized to further elucidate the roles of the PPIase domains in binding, chaperoning, and delivering OMPs to the BAM complex. The results

presented have confirmed work within the literature, offered novel findings to the field and have also informed further study.

Chapter 2 Methods

2.1 Materials and Reagents

2.1.1 General Chemicals

Purite 18 MΩ water was used in all protocols. 30% (*w/v*) acrylamide and 10% (*w/v*) sodium dodecyl sulphate (SDS) was purchased from Severn Biotech Ltd., UK. Agar was purchased from Melford Laboratories, UK. Ready mixed LB-Broth (Miller) was purchased from Merck, Germany. Agarose, imidazole and ethylenediaminetetraacetic acid (EDTA) were purchased from Acros Organics, Belgium. Sodium chloride (NaCl), tris(hydroxymethyl)aminomethane (Tris), glycerol, glucose, sucrose, glacial acetic acid and hydrochloric acid (32% (*w/v*) HCl) were purchased from Fisher Scientific, UK. Carbenicillin, dithiothreitol (DTT) and isopropyl β-D-1-thiogalactopyranoside (IPTG) were purchased from Formedium, UK. Triton X-100 (protein grade) was purchased from Merck Millipore, USA. Urea *(>99% purity)* was purchased from MP Biomedicals, UK or Sigma-Aldrich, USA. Ethidium bromide, magnesium sulphate ($MgSO_4$), magnesium chloride ($MgCl_2$), chloramphenicol, bromophenol blue, guanidine hydrochloride (Gdn-HCl), ammonium persulphate (APS), ammonium acetate, ammonium hydroxide, tetramethylethylenediamine (TEMED), dimethyl sulfoxide (DMSO), tris (2-carboxyethyl)phosphine (TCEP), and ethanol were purchased from Sigma-Aldrich, USA. ^{15}N-labelled ammonium chloride and ^{13}C D-glucose were purchased from Cambridge Isotope laboratories, Inc

2.1.2 Molecular Biology Materials

E. coli strains BL21(DE3), BL21(DE3)pLysS and DH5α were purchased from Stratagene, UK. Site-directed mutagenesis was performed with the Q5 site-directed mutagenesis kit (NEB), using primers designed using NEBasechanger. Genes encoding tOmpA, PagP, OmpA and BamA (not including signal sequences) were initially provided by Prof Karen Fleming (John Hopkins University, USA) which previous members of the lab subsequently sub-cloned into pET11a plasmids. Prof Sebastian Hiller (University of Basel, Switzerland), Prof Daniel Kahne (Harvard University, USA), and Prof Harris

Bernstein (NIH, USA) kindly provided the HT-Skp-pET 28b, HT-SurA-pet 28b and HT-BamABCDE-pTrC 99a plasmids, respectively. OmpT was cloned by Lindsay M. McMorran (University of Leeds).

2.1.3 Protein Chemistry Materials

Analytical Superdex 75 10/300 GL, Sephacryl 200 10/300, HiLoad Superdex 75 prep grad and 5 ml HisTrap columns were purchased from GE Healthcare, UK. All buffers used during protein purification were filtered by vacuum filtration through 0.22 µM filters from Millipore, UK. Vivaspin 20 concentrators (MWCO 5 kDa or 10 kDa) were purchased from Sartorius, UK. SnakeSkin dialysis tubing (3.5 kDa MWCO), bicinchoninic acid (BCA) assay kits, and Alexa Fluor 488 C5 maleimide were purchased from Thermo Fisher Scientic, UK.

2.2 Molecular Biology

2.2.1 Bacterial strains

DH5α:

fhuA2 lac(del)U169 phoA glnV44 Φ80' lacZ(del)M15 gyrA96 recA1 relA1 endA1 thi-1 hsdR17

BL21(DE3) pLysS:

F– *ompT/tompA* hsdSB (rB–, mB–) *gal* [dcm] *[lon]* (DE3)

2.2.2 Growth Media

2.2.2.1 LB

E. coli cells were cultured in autoclaved lysogengy broth (LB) (Miller) medium (Merck, Germany) at 25 g/l and supplemented with carbenicillin (100 µg/ml) or kanamycin (50 µg/ml). For preparation of agar plates 25 g/l of LB and 15 g/l of agar were autoclaved for 20 minutes at 120 °C. On cooling to approximately 50 °C, antibiotic was added and 20-25 ml poured into sterile Petri dishes. For growth of BL21(DE3)pLysS cells, chloramphenicol (25 µg/ml) was added to the medium in addition to antibiotic.

2.2.2.2 HCDM1

To make ^{15}N or $^{15}N/ ^{13}C$ labelled proteins cells were grown in HCDM1 minimal medium:

- 10 g K_2HPO_4
- 10 g KH_2PO_4
- 7.5 g Na_2HPO_4
- 1 g NH_4Cl (^{15}N if using)
- 9 g K_2SO_4

These regents were made up to 1 litre with water and the following filter sterilised supplements were added after the media was autoclaved:

- 2 ml of 1 M $MgCl_2$
- 100 µl of 1 M $CaCl_2$
- 20 ml of 20 % (w/v) glucose (10 ml if ^{13}C labelling)

2.2.3 Preparation of competent cells

Cells of the commercial strain were plated out on LB/agar not containing antibiotics and grown overnight at 37 °C. A single colony was picked to inoculate 10 ml of LB and incubated overnight at 37 °C with 200 rpm shaking. The following morning the 10 ml was added to 100 ml of fresh LB and incubated to an OD_{600} of 0.4-0.45. The cells were harvested by centrifugation at 4000 rpm at 4 °C for 10 minutes. Pelleted cells were resuspended in 10 ml of sterile 100 mM $CaCl_2$ for 10 minutes and then centrifuged as before. The pellet was resuspended gently in 2 ml of pre-chilled 100 mM $CaCl_2$ 30% (v/v) glycerol. Cells were aliquoted (50 µl) into 1.5 ml Eppendorf tubes pre-cooled on dry ice and stored at -80 °C.

2.2.4 Transformation of *E. coli* strains

2µl of plasmid DNA containing the desired gene sequence was taken from a stock of approximately 100 ng/µl and added to 50 µl competent cells and incubated on ice for 30 minutes. The cells were then heat shocked at 42 °C for 45 seconds before being incubated on ice for 5 minutes. The 50 µl were then plated under sterile conditions

onto LB agar containing 100 µg/ml carbenicillin (or 50 µg/ml kanamycin for cells transformed with pET28b vectors), and incubated at 37 °C overnight.

2.2.5 Polymerase Chain Reaction (PCR) and mutagenesis

All PCR reactions for mutagenesis were carried out using the Q5 site-directed mutagenesis kit (NEB, E0554S). The following reagents were assembled in a thin wall PCR tube and place in the thermocycler:

- 12.5 µl Q5 Hit Start High-Fidelity Master Mix
- 1.25 µl forward primer (10 µM)
- 1.25 µl reverse primer (10 µM)
- 1 µl template DNA (1-25 ng/µl)
- 9 µl nuclease free water

Step	Temperature	Time
Initial Denaturation	98 °C	30 seconds
25 Cycles	98 °C	10 seconds
	50-72 °C*	10-30 seconds
	72 °C	20-30 seconds
Final Extension	72 °C	2 minutes
Hold	4 °C	

Table 2.1 PCR reaction for Q5 mutagenesis
*The temperature during the cycling reaction is optimised depending on the primers

After the PCR reaction the unmodified DNA was digested by KLD treatment using the Q5 kit reagents:

- 1 µl PCR product
- 5 µl KLD reaction buffer
- 1 µl KLD enzyme mix
- 3 µl nuclease-free water

The reagents were mixed then incubated at 25 °C for 5 minutes before 5 µl was added to 50 µl NEB 5-α cells. The DNA was incubated with the cells for 30 minutes on ice then heat shocked at 42 °C for 30 seconds. The cells were then added to 950 µl of

SOC medium and incubated at 37 °C with 200rpm shaking for 60 minutes. 50 µl was spread onto LB/agar plates containing carbenicillin or kanamycin and incubated overnight at 37 °C.

2.2.6 DNA Sequencing

All DNA sequencing was carried out by Genewiz. The T7 promoter forward primer (TAA-TAC-GAC-TCA-CTA-TAG-GG) and the T7 terminator reverse primer (CTA-GTT-ATT-GCT-CAG-CGG-TG) were used for sequencing of all pET vectors.

2.3 General Protein Methods

2.3.1 Sodium dodecyl sulphate polyacrylamide gel electrophoresis (SDS-PAGE)

Tris-Tricine buffered SDS-PAGE gels were used to monitor protein purification and tOmpA folding kinetics. The components in Table 2.2 were mixed, adding the TEMED and APS just prior to pouring into gel plates. The gels were made by adding resolving gel to ¾ full then adding the stacking gel on top, the comb was inserted and the gels left to set for at least 20 minutes.

	Resolving gel (mL)	Stacking gel (mL)
30% (w/v) acrylamide:0.8% (w/v) *bis*-acrylamide	7.5	0.83
3 M Tris, 0.3% (w/v) SDS (pH 8.45)	5.0	1.55
H_2O	0.44	3.72
glycerol	2.0	
10% (w/v) ammonium persulphate (APS)	0.1	0.2
N,N,N',N'-tetramethyl-ethylenediamine (TEMED)	0.01	0.01

Table 2.2 Tris-tricine buffered SDS-PAGE gel recipe

Sample solutions was added to an equal volume of 2x loading buffer (50 mM Tris-HCl pH 6.8, 100 mM DTT, 2 % (w/v) SDS, 0.1 % (w/v) bromophenol blue, 10 % (v/v) glycerol) and boiled for 5 minutes before loading approximately 15 µl of this solution to the gel. A protein molecular mass marker (Bio-Rad) was used to aid in identification. Anode (200 mM Tris-HCl, pH 8.9) and cathode buffers (100 mM Tris, 100 mM tricine, 0.1% (*w/v*) SDS, pH 8.25) were placed in the tank and a voltage of 30 mAmps for 30 minutes and 70 mAmps for a further hour was applied. The gels were stained with Instant blue stain (Expedeon, UK) for at least an hour then imaged with Syngene InGenius software. Densitometry quantification bands in kinetic assays or pelleting assays was performed using ImageJ.

2.3.2 Determination of protein concentration

The protein concentrations of all OMPs, BamA, SurA WT, SurA ΔP2 and SurA N-Ct were determined using their absorbance at 280 nm measured on a Nanodrop 2000 (Thermo Fisher). Theoretical molar extinction coefficients at 280 nm, calculated using the ExPASy protparam server were used to calculate the molar concentration of each protein. Skp and Spy have low molar extinction coefficients at 280 nm (1490 M^{-1} cm^{-1}) as their sequences contain no tryptophan residues, and only one tyrosine residue. For these proteins, concentrations were determined using a bicinchoninic acid (BCA) assay (Thermo Fisher Scientific, UK), according to the manufacturer's instructions.

2.4 Expression and purification of proteins in this study

2.4.1 SurA (WT/ ΔP2 /N-Ct) and Skp

The pET28b plasmid, containing the mature chaperone gene with an N-terminal hexa-histidine-tag and thrombin cleavage site, was transformed into *E. coli* BL21(DE3)pLysS cells (Stratagene). Cells were grown in LB medium containing 50 µg/ml kanamycin at 37 °C with shaking (200 r.p.m.) to an OD_{600} of ~0.6. The temperature was then lowered to 20 °C and expression induced by addition of IPTG to a final concentration of 0.4 mM. Following overnight expression at 20 °C (~18 h) cells were harvested by centrifugation (7000rpm, 4 °C, 30 minutes). The pelleted cells were resuspended in

25 mM Tris-HCl pH 7.2, 150 mM NaCl, 20 mM imidazole with EDTA-free protease inhibitor cocktail (Roche) for 1 hour then lysed using a cell disrupter (Constant Cell Disruption Systems, UK). Following centrifugation to remove cell debris (20 min, 4 °C, 25,000 g), the lysate was filtered then applied to a 5 ml HisTrap column (GE Healthcare), equilibrated with 25 mM Tris-HCl pH 7.2, 150 mM NaCl and 20 mM imidazole. His-tagged SurA/Skp was denatured on-column, to prevent any aggregation caused by the high protein concentration, with 25 mM Tris-HCl, 6 M Gdn-HCl, pH 7.2 and eluted with a gradient of 25 mM Tris-HCl, 6 M Gdn-HCl, pH 7.2 and 500 mM imidazole. Fractions containing pure protein (judged by SDS-PAGE) were pooled and refolded overnight by dialysis against 25 mM Tris-HCl pH 7.2, 150 mM NaCl with two changes and then into 50 mM glycine-NaOH pH 9.5, which is the buffer OMP binding assays are carried out to prevent OMP aggregation. The protein was concentrated to ~200 µM using Vivaspin 20 (5 kDa MWCO) concentrators (Sartorius, UK), aliquoted, snap-frozen in liquid nitrogen and stored at −80 °C.

2.4.2 SecB

E. coli BL21(DE3) cells (Stratagene, UK) were transformed with the plasmid containing the SecB gene. Cells were grown in TY (Tryptone Yeast) broth at 37 °C to an OD_{600} of 0.6, protein expression was then induced with 1 mM IPTG and grown for a further 3 hours before harvesting by centrifugation. The pellet was resuspended in 20 mM Tris-HCl, 50 mM KCl, pH 7.5 then lysed using a cell disrupter (Constant Cell Disruption Systems, UK), the debris was cleared by centrifugation (20 min, 4 °C, 39,000 g). The supernatant was filtered (0.2 micron polyvinylidene difluoride syringe filter, Sartorius, UK) then applied to a pre-equilibrated HisTrap 5ml column (GE Healthcare), washed with resuspension buffer then eluted with 330 mM imidazole. Fractions containing protein were pooled and dialysed against 20 mM Tris-HCl, 50 mM KCl, pH 7.5 overnight then bound to a 5ml HiTrap Q HP column (GE healthcare) pre-equilibrated with dialysis buffer. Protein was eluted with a gradient of 1 M KCl, then concentrated using Vivaspin 20 (5 kDa MWCO) concentrators (Sartorius, UK), snap-frozen in liquid nitrogen and stored at −80 °C.

2.4.3 Trigger Factor (TF)

The expression vector pCA528 was used to fuse *tig* (encoding TF) to the Ulp1-cleavable N-terminal $(His)_6$-SUMO tag [77,204]. BL21(DE3) cells were transformed and used for protein expression in LB supplemented with 40 µg/ml kanamycin at 30 °C. Gene expression was induced at an OD_{600} of 0.8 with 0.5 mM IPTG and cells were grown for 4 more hours. Harvested cell pellets were resuspended in lysis buffer (50 mM HEPES-KOH, pH 7.5, 150 mM KCl, 1 mM phenylmethanesulfonyl fluoride (PMSF), 5% v/v glycerol). Cell lysed by cell disruption and the lysate was cleared by centrifugation (30,000 g, 30 minutes, 4°C). Protein was purified using 5 ml HisTrap column (GE Healthcare) following standard procedures. The eluted material was supplemented with $(His)_6$-Ulp1 protease (Sigma Aldrich) and dialyzed overnight at 4 °C in storage buffer (25 mM HEPES-KOH, pH 7.5, 50 mM KCl, 5% glycerol). The next day, liberated $(His)_6$-Sumo and $(His)_6$-Ulp1 protease were removed by flowing over a HisTrap column. The flow through containing the desired protein was then bound to an anion-exchange column (5 ml ResourceQ, GE healthcare) and eluted with a linear gradient using storage buffer and high salt buffer (25 mM HEPES-KOH, pH 7.5, 500 mM KCl, 5% v/v glycerol). Finally, pooled peak fractions were dialyzed overnight at 4 °C in 50 mM HEPES-KOH, 150 mM KCl, pH 7.5 and snap frozen.

2.4.4 Expression and purification of outer membrane proteins (OMPs)

tOmpA and OmpT were purified using a method adapted from [143]. *E. coli* BL21(DE3) cells (Stratagene, UK) transformed with a pET11a plasmid containing the mature OMP gene were grown in 500 ml LB medium containing 100 µg/ml carbenicillin at 37 °C with shaking (200 r.p.m.). When the culture reached an OD_{600} of 0.6 protein expression was induced with 1 mM IPTG, cells were harvested by centrifugation (5,000 g, 15 min, 4 °C) after 4 hours of growth post induction. The pellet was resuspended in 50 mM Tris-HCl pH 8.0, 5 mM EDTA, 1 mM PMSF, 2 mM benzamidine for 1 hour then lysed by sonication (6 × 1 min bursts with 1 min cooling on ice between each sonication). The insoluble fraction was collected by centrifugation (25,000 g, 30 min, 4 °C), resuspended in 50 mM Tris-HCl pH 8.0, 2% (v/v) Triton X-100

and incubated for 1 hour at room temperature, with rocking. The insoluble fraction was again pelleted (25,000 g, 30 min, 4 °C) and the inclusion bodies washed twice by resuspension in 50 mM Tris-HCl pH 8.0, incubating for 1 hour at room temperature with rocking, followed by centrifugation (25,000 g, 30 min, 4 °C). The inclusion bodies were solubilized in 25 mM Tris-HCl, 6 M Gdn-HCl, pH 8.0 and centrifuged (20,000 g, 20 min, 4 °C). The supernatant was filtered (0.2 micron polyvinylidene difluoride syringe filter, Sartorius, UK) and protein purified further by gel filtration using a Superdex 75 HiLoad 26/60 column (GE Healthcare) equilibrated with 25 mM Tris-HCl, 6 M Gdn–HCl, pH 8.0. Peak fractions were concentrated to ~500 µM using Vivaspin 20 (5 kDa MWCO) concentrators (Sartorius, UK), and the protein solution then snap-frozen in liquid nitrogen and stored at −80 °C.

2.4.5 Expression and purification of the BAM complex in liposomes

The BAM complex used in this work, used to test binding to periplasmic chaperones was purified and prepared by A.Higgins. The BamABCDE complex was expressed and purified using a protocol adapted from [205]. Briefly, *E. coli* BL21(DE3) was transformed with plasmid pJH114 (provided by Harris Bernstein, NIH, USA) containing all five BAM genes (BamABCDE-$(His)_6$) and grown overnight (37 °C, 200 rpm) in LB containing 100 µg/ml carbenicillin. Cells were diluted 1:100 into 1 L TY broth and grown (37 °C, 200 r.p.m.) to an OD_{600} of 0.5–0.6 before addition of 0.4 mM IPTG to induce BAM expression. After 1.5 h, cells were harvested by centrifugation (4,000 r.p.m., 15 min, 4 °C) and the pellet resuspended and homogenized in 10 ml 20 mM Tris-HCl pH 8, lysed with a cell disruptor (Constant Cell Disruption Systems, UK), then centrifuged (6,000 g, 10 min, 4 °C). The membranes were pelleted by ultracentrifugation using a 50.2Ti rotor (45,000 rpm 30 min, 4 °C). Pelleted membranes were incubated with 10 ml cold 50 mM Tris-HCl pH 8, 150 mM NaCl, 1% (w/v) DDM at 4 °C for 2 h and the ultracentrifugation repeated to remove insoluble material. The BAM complex, which contains a $(His)_6$ tag on BamB, was then applied to Ni-NTA beads washed with 50 mM Tris-HCl pH 8, 150 mM NaCl, 1% (w/v) DDM and eluted. The protein was concentrated and gel filtered on a Superdex200, 10/300 GL column running in TBS with 0.05% (w/v)

DDM. Fractions were collected and those containing complete BamABCDE complexes were identified by SDS–PAGE, pooled, concentrated and flash frozen in liquid nitrogen. To create BAM containing proteoliposomes, DDM-solubilized BamABCDE was mixed with *E. coli* polar lipid films solubilized in 200 µl of TBS+0.05% (w/v) DDM using a 1:0.5 (w/w) ratio of lipid to protein. This was dialysed into detergent-free buffer (20 mM Tris-HCl pH 8, 150 mM KCl, 0.01% (w/v) sodium azide (dialysis buffer)) at 21 °C for 7 days. Reconstitution was tested by running boiled and unboiled samples on SDS-PAGE to check for BamA folding and presence of all BAM components.

2.4.6 Im7 purification

N-terminal cysteine variants of Im7 created by Q5 mutagenesis (New England Biolabs) and BL21(DE3) cells were transformed with chosen plasmid (containing Im7-WT, Im7-L53A I54A or Im7-L18A L19A L37A). Cells were cultured overnight in 150 ml LB 100 µg/ml carbenicillin at 37°C, 200 rpm. The overnight stocks were then used to inoculate 11 L of pre-warmed LB 100 µg/ml carbenicillin, 10 ml per litre. The cultures were grown to an OD_{600} of 0.6 and protein expression was induced by the addition of 1 mM IPTG. Bacteria were then grown for 5 hours at 37 °C before harvesting by centrifugation at 6000 rpm (Rotor JLA 8.1). The pellets were collected and stored at -20 °C. Lysis (50 mM Tris pH 8.0, 0.3 M NaCl, 10 mM imidazole) and elution (50 mM Tris pH 8.0, 0.3 M NaCl, 500 mM imidazole) buffers were prepared. Harvested cell pellets were thawed and re-suspended in 100 ml lysis buffer. PMSF and benzamidine proteinase inhibitors were then added to give a final concentration of 1 mM of each. The cells were then homogenised and lysed by cell disruption (Constant Cell Disruption Systems) and cell debris removed by centrifugation at 25000 rpm (JLA 25.50 Rotor) for 1 hour. The supernatant was syringe filtered (0.22 µm membrane filter) and bound to a Ni Sepharose column (5ml volume) (GE Healthcare) that was washed and pre-equilibrated with 25 ml lysis buffer. The protein was eluted using a gradient of 0-85% elution buffer and 3 ml fractions were collected. Fractions containing the desired protein were pooled and dialysed into 50 mM sodium phosphate buffer pH 6.0 overnight. The sample was then filtered and injected onto pre-equilibrated a Source 15Q resin 7 ml column (GE Healthcare). The protein was eluted with a gradient of 0-65% elution buffer (50 mM sodium phosphate buffer, pH

6.0, 1 M NaCl) and 3ml fractions were collected. The purity of the fractions was monitored by SDS-PAGE analysis. If the protein appeared pure a sample was analysed by the mass spectrometry facility (University of Leeds). Pure protein was dialysed into H_2O then freeze dried and stored at -20 °C.

2.5 CD spectra

Data were collected on a Chirascan spectropolarimeter (Applied Photophysics). Far-UV CD spectra were measured over a 190–260 nm range in 1 nm steps, in a 1 mm path-length cell and using a 2.5 nm bandwidth. At least two scans were measured and averaged. SurA variants were measured at a protein concentration of 5 µM in 50 mM glycine, pH 9.5 at 25 °C.

2.6 Urea Equilibration Denaturation

Equilibrium denaturation curves were measured using Photon Technology International (PTI) fluorimeter with a protein concentration of 0.2 mg/ml, in 50 mM glycine buffer pH 9.5 with 0-10 M urea in 0.2 M increments. Samples of SurA WT, SurA ΔP2 and SurA N-Ct at 5 µM were made up and incubated overnight at 25 °C to ensure the correct levels of denaturation for each urea concentration. Slit widths were set between 1-2 nm with a path length of 1 cm, excitation at 280 nm and emission at 350 nm was monitored and averaged over 1 minute at 25 °C. The average signal as a function of denaturant was fitted to a two state transition in Igor Pro 6.0 (Wavemetrics):

Equation 2.1 Two state fitting equation for equilibrium denaturation curves

$$\text{Obs Signal} = \frac{[(a[urea] + b)\exp\left(\Delta Gun - \frac{m[urea]}{RT}\right) + (c[urea] + d)]}{(1 + \exp(\Delta Gun - \frac{m[urea]}{RT})}$$

where ΔGun (kJmol^{-1}) is the equilibrium stability, and m is the equilibrium m-value, a and c represent the denaturant dependence of the folded and unfolded signal intensities respectively, and b and d are the signal intensities of the folded and

unfolded states, respectively, in the absence of denaturant. Data for the variants that could not be fitted to two-state equilibrium were fit to a three state equation.

Equation 2.2 Three state fitting equation for equilibrium denaturation curves

$$\text{Obs Signal} = \frac{[(a[urea]+b)\exp\left(\Delta G1un - \frac{m1[urea]}{RT}\right)+(c[urea]+d)]}{(1+\exp(\Delta G1un - \frac{m1[urea]}{RT})} + \frac{[(c[urea]+d)\exp\left(\Delta G2un - \frac{m2[urea]}{RT}\right)+(e[urea]+f)]}{(1+\exp(\Delta G2un - \frac{m2[urea]}{RT})}$$

2.7 Native Mass Spectroscopy

SurA–tOmpA complexes were prepared by rapid dilution of the denatured tOmpA (8 M urea and 50 mM glycine-NaOH, pH 9.5) to a final concentration of 1 µM into a solution of SurA (1 µM in 200 mM ammonium acetate, pH 9.5). Im7-SurA complexes were prepared 1:1 at 10 µM in 200 mM ammonium acetate buffer, pH 6.8. NanoESI–IMS–MS spectra were acquired with a Synapt HDMS mass spectrometer (Waters) with platinum/gold-plated borosilicate capillaries prepared in-house. Typical instrument parameters were: capillary voltage, 1.2–1.6 kV; cone voltage, 40 V; trap collision voltage, 6 V; transfer collision voltage, 10 V; trap DC bias, 20 V; backing pressure, 4.5 mbar; IMS gas pressure, 0.5 mbar; travelling wave height, 7 V; and travelling wave velocity, 250 ms^{-1}. Data were processed with MassLynx v4.1, Driftscope 2.5 (Waters) and Massign [206].

2.8 Analytical Size Exclusion Chromatography (SEC)

SurA WT/ ΔP2/ N-Ct with tOmpA complexes were formed at a 1:1 ratio both at a final concentration 10 µM in 50 mM glycine buffer, pH 9.5, 0.24 M urea. Size exclusion was performed using a Superdex 200 column on an ÄKTA pure system with a typical flow rate of 0.5 ml/min. The column was washed with 2 column volumes (CVs) of 2 M NaOH then 2 CVs of filtered H_2O to remove the 20 % ethanol in which it is stored and then equilibrated with 1.5 CVs of 50 mM glycine buffer, pH 9.5, 0.24 M urea. The

prepared sample is then loaded via injection. At the end of the analysis the column was washed with 2 CVs of water and 1.5 CVs of 20 % *(v/v)* ethanol and stored at 4 °C

2.9 Surface Plasmon Resonance (SPR)

SPR was used to monitor the kinetics of the association and dissociation of tOmpA with SurA variants. All proteins buffer exchanged into running buffer (50 mM glycine pH 9.5 0.24M urea) and the experiment was run at 5 µl/min. A CM5 chip (GE healthcare) which is a gold surface with covalently attached carboxymethylated dextran was loaded into a Biocore 3000 surface plasmon resonance system (GE healthcare). The chip was modified by 10 µl of a 1:1 EDC and NHS mixture both at 1 mg/ml and then 20 µl of 80 mM PDEA in 50 mM sodium borate buffer pH 8.5 leaving a reactive disulphide group. A N-terminal cysteine variant of tOmpA was then flowed over the surface at 20 µM for 7 minutes. Addition to the chip can be monitored by a change in the response units and should give a change of >1000 units. Any unreacted groups on the surface were then capped with L-cysteine at 9 mg/ml in 100 mM sodium acetate, 100 mM sodium chloride pH 4.0. Another cell was used as a blank and was treated with NHS/EDC, PDEA and L-cysteine in the absence of the immobilised substrate. Increasing concentrations of SurA WT (0.2, 1, 1.8, 5, 10 and 18 µM) was flowed over the chip, with a wash of 4 M urea between each concentration to denature the SurA, break the interaction and allow the SurA to be washed away. The titration was repeated at least twice for each concentration. The chip was then washed with urea and buffer before SurA ΔP2 / SurA N-Ct was applied at the same concentrations. The data was fit using the 1:1 Langmuir model (Equation 2.3) within the control software and the ka, kd and K_d were extracted from the fit.

$$Bound = \frac{C^A x\ Max}{C^A + Kd}$$

Equation 2.3 Langmuir Equation. Max is the maximum response (RUs). C^A is the concentration of injected analyte and K_d is in the same units as C^A (normally M)

2.10 Fluorescence Assay of OmpT folding

BAM complex purification and reconstitution into proteoliposomes was performed as described in Methods 2.4.5 [71]. BAM proteoliposomes were diluted to a concentration of 5 µM in 50 mM glycine-NaOH pH 9.5 containing 2 mM of the fluoropeptide Abz-Ala-Arg-Arg-Ala-Tyr(NO_2)-NH_2 (Peptide Synthetics). OmpT and chaperone (SurA WT, ΔP2, N-Ct, Skp, SecB) were then mixed to form a solution with final concentrations of 10 µM OmpT, 70 µM chaperone in 50 mM glycine-NaOH pH 9.5 and 0.8 M urea. This sample (chaperone-OmpT 'subreaction') was then immediately diluted 1:1 into the proteoliposome solutions to initiate the folding reaction. The final concentrations of the reaction components were 5 µM OmpT, 35 µM SurA, 0.25 µM BAM complex and 1 mM fluorogenic peptide. All OmpT folding reactions were carried out in 30 µl final reaction volume. Fluorescence emission following excitation at 325 nm was monitored at 430 nm with readings every 10 s for up to 5 h using a Clariostar plate reader (BMG Labtech GmbH). The signal was normalized following subtraction of the average background signal produced at the zero time point.

2.11 tOmpA folding kinetics gels

Outer membrane proteins migrate differently on SDS-PAGE gels depending if they are folded or unfolded. On Tris-tricine gels tOmpA in the folded state migrates faster than the unfolded state and the amount of folded vs unfolded can be monitored over time to measure the rate of folding. A sub-reaction of 20 µM SurA (or SurA variants) and 4 µM tOmpA is prepared in 20 mM Tris-HCl pH 8.0 150 mM NaCl 1.6 M urea. The sub-reaction is then mixed 1:1 to BAM complex in proteoliposomes (see 2.4.5). To give final concentrations of 1 µM BAM complex, 10 µM SurA and 2 µM tOmpA with a final urea concentration of 0.8 M. The reaction is measured at 25 °C and time-points are taken at defined intervals and mixed with 6x SDS-PAGE loading buffer then run un-boiled on tris-tricine gels (see 2.3.1) and the fraction folded over total protein is analysed by densitometry using ImageJ [207] and fit to a single exponential equation in Igor pro (Wavemetircs).

2.12 Isothermal Titration Calorimetry

Calorimetry measurements were performed with an ITC200 microcalorimeter (MicroCal Inc.). For each titration experiments, 350 µl WEYIPNV peptide solution at 20 µM in 20 mM sodium phosphate, pH 7.0 was added to the sample cell. SurA variants, dialysed into the same buffer as the peptide, was added to the injection syringe at a concentration 200 µM. An initial injection of 0.5 µl was made, followed by 19 injections of 2 µl every 4 seconds at 25 °C. The equilibration interval was 120 s between injections, and the stirring speed was 750 rpm. Binding isotherms were plotted and analysed using Origin Software (MicroCal Inc.).

2.13 Thioflavin T $A\beta_{40}$ aggregation assay

ThT plates were set up with 20 mM sodium phosphate, 0.2 mM EDTA, 10 µM ThT, 0.02% NaN_3, pH 7.4 either in the presence or absence of SurA WT, Skp or Spy at 10, 20 and 40 µM. $A\beta_{40}$ was dissolved from freeze dried stocks and added to the prepared wells at a final concentration of 20 µM. The assay was performed quiescently at 37 °C and the sample was excited at 450 nM wavelength and fluorescence at 482 nM [208] and measured over 4 days.

2.14 Microscale Thermophoresis

2.14.1 Labelling protein with Alexa fluor 488

Microscale thermophoresis is a technique based on the movement of molecules in a temperature gradient and the observation that this movement is altered by the interaction with a binding partner. The movement is monitored by fluorescently tagging one of the proteins which is then added to a titration of the unlabelled binding partner, the sample is heated to create the temperature gradient with an IR laser and the fluorescence excited with a LED, and the change in fluorescence in the heated area is measured. The change in fluorescence at each given binding partner

concentration can be plotted to give a binding curve in order to obtain the affinity of the interaction (Figure 3.11).

N-terminal cysteine mutants of tOmpA, OmpT, SurA WT, SurA ΔP2 and SurA N-Ct were created using Q5 mutagenesis (New England Biolabs) and purified as described for the wild-type proteins. Proteins were buffer exchanged into 6 M Gdn-HCl, 50 mM Tris pH 7.2 using 7 kDa MWCO Zeba spin desalting columns (Thermo Scientific) and diluted to a final protein concentration of 50 µM with a sample volume of 350 µl. A ten-fold molar excess of Alexa Fluor-488 C5 malemide (Thermo Scientific) dissolved in DMSO was added to the samples and incubated overnight at 4 °C. Following incubation, the reaction was quenched with excess β-mercaptoethanol. Then protein was separated from unbound dye using size exclusion chromatography on a Superdex 200 10/300 GL column (GE healthcare) and fractions containing labelled protein, determined by A_{280} and A_{488} on the AKTA prime (GE Healthcare) and Nanodrop 2000 (Thermo Fisher Scientific) were concentrated using Vivaspin 20 (5 kDa MWCO) concentrators (Sartorius, UK).

2.14.2 MST Protocol

From a 200 µM SurA stock solution in 50 mM glycine-NaOH, pH 9.5, a series of two-fold serial dilutions were performed to obtain sixteen 10 µl samples (100 µM- 3 nM). AlexaFlour 488 labelled tOmpA or OmpT buffer (buffer exchanged into 8 M urea 50 mM glycine pH 9.5 and then diluted to 200 nM in 0.48 M urea), was added 1:1 to give a final concentration of 100 nM OMP, 0.24 M urea in 50mM glycine pH 9.5 in all samples, 20 µl total volume.

In the case of SurA or Skp binding to the BAM complex, N-terminal cysteine mutants of the chaperone were labelled as in the same way as the OMPs. The BAM complex either in 50 mM TBS, 150 mM NaCl, pH 7, 0.05% DDM or within proteoliposomes (Methods 2.4.5). 50 mM TBS, 150 mM NaCl, pH 7 is used to create the dilution concentration series in 10 µl (1.2 nM-40 µM in DDM and 1.5 nM-50 µM in proteoliposomes). The labelled SurA or Skp is then added 1:1 to the dilution series to a final concentration of 100 nM in a volume of 20 µl.

The samples were loaded by capillary action into premium coated capillaries (NanoTemper Technologies GmbH) and measured using Monolith NT.115 (Nanotemper Tech.). Data were fitted to a Hill equation in Igor Pro (Wavemetircs).

$$S_{obs} = S_U + (S_B - S_U).\left(\frac{[L]^n}{K_D + [L]^n}\right)$$

Equation 2.4 Hill equation for MST fitting

Where S_{obs} is the observed signal, S_U and S_B are the signal of the unbound and bound state respectively, L is the ligand concentration which in these experiments is the OMP and n is the hill coefficient.

2.15 Nephelometry

2.15.1 Aggregation light scattering assay of OMPs

Nephelometry is a light scattering technique in which only light with is scattered up to 80 degrees is detected and light which passes directly through the sample is not measured. This leads to data which is less noisy than turbidity light scattering measurements which detects the amount of light scattered by detecting the loss of light passing directly through the sample. Nephelometry can detect particles of a certain size and number and so multiple small aggregates or larger aggregates can both be monitored (Figure 4.3).

Optimisation experiments were carried out in 25 mM Tris-HCl, pH 8.0. Stocks of tOmpA and OmpT were diluted to give the correct final concentration in 25 mM Tris-HCl, 0.24 M Gd-HCl, pH 8.0. 2 μM OMP concentration was chosen and under these conditions SurA WT, ΔP2 or N-Ct were added with 10-fold molar excess (20 μM) to tOmpA and 100-fold molar excess (200 μM) to OmpT.

Rapid dilution of unfolded OMPs from 8 M urea to 0.24 M urea containing 0.24 M NaCl causes aggregation monitored by an increase in light scattering. The OMP was buffer-exchanged into 8 M urea, 50 mM glycine buffer pH 9.5. A stock of 67 μM OMP in 8 M urea was diluted into 0 M urea buffer (50 mM glycine buffer pH 9.5) to give a final concentration of 2 μM protein in 0.24 M urea in 50 μl within the 96-well half area plate (Corning Product #3881). tOmpA and OmpT aggregation was monitored in buffer containing 0, 4, 10, 20, 40, 100 and 200 μM SurA WT, SurA ΔP2 or SurA N-Ct. The samples were read by a Nephelostar (BMG Labtech GmbH), at 635 ± 10 nm with a gain of 90, over 30 minutes at 25 °C. Values were processed by buffer blank subtraction and the minimum value in each data set was set as zero. Data were plotted in Origin Pro (OriginLab).

2.15.2 Aggregation assay of GAPDH

Freeze dried GAPDH (Sigma-Aldrich, USA) was solubilised to a stock of 250 μM in 20 mM potassium phosphate buffer pH 7.0, 100 mM KCl, 6 M Gdn-HCl. Rapid 100 fold dilution was carried out into 20 mM potassium phosphate buffer pH 7.0, 100 mM KCl in the presence or absence of 1.25 – 25 μM TF, SurA WT, SurA ΔP2 or SurA N-Ct with a final concentration of 0.06 M Gdn-HCl. Upon GAPDH addition, light scattering was measured at 635 ± 10 nm over 30 minutes at 25 °C. Values were processed by buffer blank subtraction and the minimum value in each data set was set as zero. Data were plotted in Origin Pro (OriginLab).

2.15.3 End point measurements of chaperone action on tOmpA/OmpT aggregation

End point analysis was also carried out to monitor the final light scattering values after the addition of 10- fold molar excess (20 μM) or 20-fold molar excess (40 μM) SurA WT, SurA ΔP2, SurA N-Ct, TF, SecB, Skp, Spy and BSA. These samples were incubated at 25 °C for 30 minutes and the light scattering was measured for 10 seconds and averaged. Data is presented from three replicates measured on the

same plate from the same protein stocks and standard deviation of the replicates is plotted as error.

2.15.4 Aggregation pelleting assay

After 30 minutes of kinetic aggregation analysis by nephelometry, the plate was removed and the samples containing tOmpA alone or tOmpA in the presence of SurA variants were transferred to an Eppendorph and centrifuged at 13,000 g on a benchtop centrifuge for 1 hour. 10 µl of the soluble fraction was taken and added to 2x SDS loading dye and the remaining 40 µl was discarded. 40 µl fresh buffer was used to resuspend to the pellet and 10 µl of this sample was added to 2x SDS loading dye. The samples were run on a Tris-glycine SDS-PAGE gel. The bands were then quantified by densitometry in image J (NIH) and normalised to soluble tOmpA alone.

2.15.5 Transmission electron microscopy of aggregate samples

tOmpA or OmpT samples, after 30 minutes of monitoring by nephelometry, were diluted to between 0.2 and 2 mg/mL then deposited onto carbon-coated EM grids for 45 seconds at room temperature. Excess sample was blotted onto filter paper and the grid washed three times with 20 µL H_2O, followed by staining in 10 µL of 2 % (w/v) uranyl acetate solution. Excess stain was removed by blotting and the grid allowed to air-dry. The grids were imaged using a JEOL JEM1400® transmission electron microscope at 120 kV. Images were recorded at 1000× and 10,000× magnification for each specimen using the AMT Image Capture Engine software Version 6.02 supplied with the instrument.

2.16 Nuclear Magnetic Resonance (NMR) experiments

2.16.1 Preparation of isotope-labelled SurA variants

For 2D NMR experiments, SurA variants were labelled with the heavy isotope of nitrogen (^{15}N) and, for 3D assignment experiments, both ^{15}N and carbon ^{13}C labelled protein. This was achieved by growing the bacteria in minimal HCDM1 medium (see

2.2.2.2) in the presence of the nitrogen and/or carbon isotope and in D_2O in the case of 3D experiments. Proteins were purified as detailed in section 2.4.1.

2.16.2 Acquiring ^{1}H-^{15}N spectra

2D NMR experiments were carried out at 25 °C on the 950 MHz Bruker Ascend Aeon™. SurA WT, SurA ΔP2 and SurA N-Ct were measured at 100 µM in 25 mM MES, 50 mM NaCl, pH 6.5 5% (*v/v*) D_2O. 300 µl was loaded into a Shigemi 3 mm symmetrical NMR microtube and placed in the spectrometer. BEST-TROSY 2D H^{1}- N^{15} HSQC spectra were generally acquired using 256 complex points in the indirect dimension, 1622 points in the direct dimension and 64 scans per increment with spectral widths of 11432 Hz and 3466 Hz in the ^{1}H and ^{15}N dimensions, respectively. For SurA ΔP2 in complex with tOmpA or OmpT, N^{15} SurA ΔP2 was diluted to 30 µM and tOmpA and OmpT were added at 5 or 2 µM respectively to achieve at least 5% binding, while avoiding aggregation, in order to observe any changes in chemical shift upon OMP binding. Watergate solvent suppression was used in all experiments and all NMR data were processed using NMRPipe and analysed in NMRview and CCPN analysis [209-211].

2.16.3 Assignment experiments

3D experiments are based on through-bond J-coupling effects and are designed to allow selective transfer of magnetisation between nuclei within the protein backbone. Measuring the resonances of different residues using a combination of the different experiments allows sequential residue assignment. Assignments are made by knowledge of distinct position for each residue in the CA, CB and CO dimensions and the connectivity of resonances in the protein sequence. Assignment of the backbone atoms of SurA ΔP2 were performed using uniformly labelled (N^{15} and ^{13}C) protein samples at 140 µM in 25 mM MES, 50 mM NaCl, pH 6.5 5% (*v/v*) D_2O. 3D experiments in the hydrogen, nitrogen and carbon dimensions were recorded at 35 °C on a 750 MHz Oxford NMR magnet equipped with TCI-cryoprobe. HNCO, HN(CA)CO, HNCA, HN(CO)CA, HN(COCA)CB and HN(CA)CB were measured to achieve good assignment for this large protein. The 3D NMR experiments preformed are

shown in Table 2.3. The data was processed in NMR pipe and then aligned and analysed in CCPN analysis [209,210].

Experiment	Correlations observed
HNCO	$^{1}HN_i$-$^{15}N_i$-$^{13}CO_{i-1}$
HN(CA)CO	$^{1}HN_i$-$^{15}N_i$-$^{13}C\alpha_i$-$^{13}CO_i$ $^{1}HN_i$-$^{15}N_i$-$^{13}C\alpha_{i-1}$-$^{13}CO_{i-1}$
HNCA	$^{1}HN_i$-$^{15}N_i$-$^{13}C\alpha_i$ $^{1}HN_i$-$^{15}N_i$-$^{13}C\alpha_{i-1}$
HN(CO)CA	$^{1}HN_i$-$^{15}N_i$-$^{13}C\alpha_{i-1}$
HN(COCA)CB	$^{1}HN_i$+1-$^{15}N_{i+1}$-($^{13}C\alpha_i$)-$^{13}C\beta_i$
HN(CA)CB	$^{1}HN_i$-$^{15}N_i$-($^{13}C\alpha_i$)/$^{13}C\beta_i$ $^{1}HN_i$-$^{15}N_i$-($^{13}C\alpha_{i-1}$)/$^{13}C\beta_{i-1}$

Table 2.3 Triple-resonance experiments used for sequential resonance assignments

Chapter 3 The role of the PPIase domains within SurA on outer membrane protein binding

3.1 Introduction

Outer membrane proteins (OMPs) are synthesised on the cytoplasmic ribosomes and must be transported from their site of synthesis to the OM via the periplasm in order to correctly fold and carry out their various functions. The periplasm is highly dynamic as it mirrors the extracellular conditions due to the 'leaky' OM, which can lead to an unstable environment for proteins. As OMPs are highly aggregation prone they require assistance to prevent them from inter- and intra- molecular interactions which can lead to aggregation, particularly in the unstable periplasmic compartment. The importance of chaperones within the periplasm is well known, as removal of SurA along with another chaperone (either Skp or DegP) is lethal to the cell [50] and a SurA deletion in a Skp depleted background leads to minimal levels of almost all OMPs folded into the OM [141]. Modelling of interactions of OMP chaperones with an unfolded substrate on route to the OM suggests that OMPs make hundreds of short lived interactions with various chaperones during their transport across the periplasm [212]. The kinetic control of chaperone interactions and the synthesis and degradation rates of these essential proteins must be tightly regulated to allow productive flux of OMP folding and OM homeostasis.

SurA, which is the major OMP chaperone, has been studied for a number of years leading to insights into how SurA binds OMPs in order to prevent their aggregation [178,180]. The crystal structure of SurA [69] which elucidated the positions of each domain in relation to each other, suggested a binding site for OMPs in the N-terminal domain, due to crystal packing of adjacent molecules, however it does not give many clues on SurA's mechanism. The 'asymmetrical dumbbell' structure of SurA appears to have a cavity within the concave surface between the core of SurA and the P2 domain (Figure 3.1). In addition, the crystal structure of the ΔP2 variant of SurA lacking the P2 domain in complex with a binding peptide obtained by scanning a peptide library

[178] showed the P1 domain dissociating from the N- and C- terminal domains that may be to compensate the loss the cavity upon the deletion of the P2 domain (Figure 3.1b). The concave surface of SurA may provide an extended binding region for OMP interactions, similar to the mechanism of the ATP-independent periplasmic chaperone, Spy, which is a homodimer that binds to substrates using a hydrophobic and charged surface [129-131]. Contradicting this hypothesis, crosslinking data has suggested that only the N-terminal domain of SurA is responsible for binding OMPs [179,180]. However, for unfolded OMP substrates the N-terminal domain of SurA alone may not provide a large enough binding surface to prevent OMP self-association. As the N-terminal domain within the crystal structure is in contact with the P1 domain and the C terminal domain it seems unlikely that only the N-terminal domain contacts the OMP, however there may be dynamics between the domains within the chaperone that cannot be observed in the crystal structure.

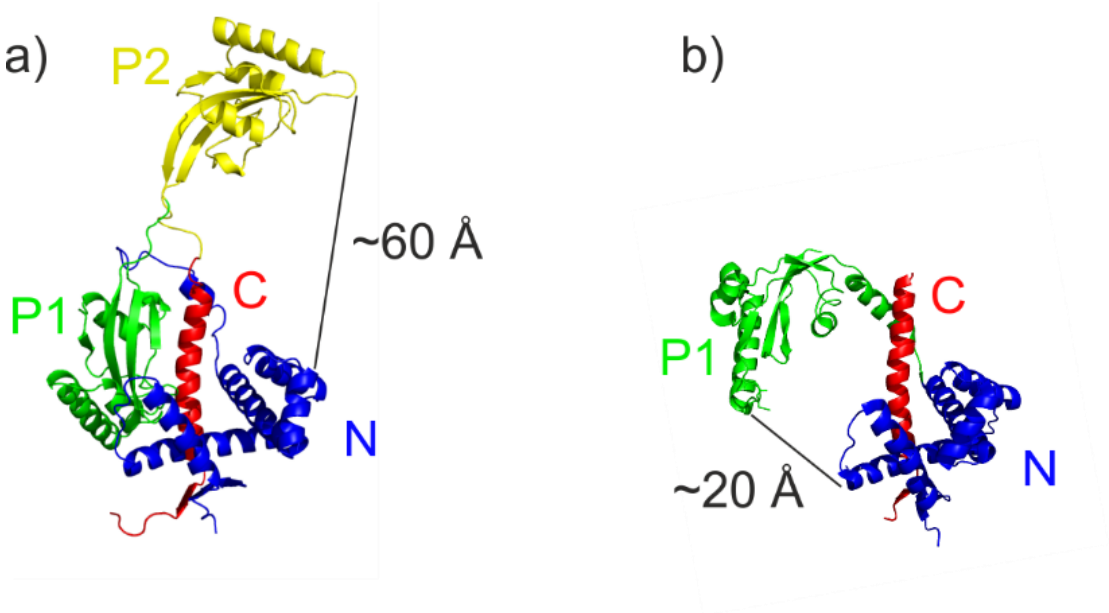

Figure 3.1 Crystal Structures of SurA WT and SurA ΔP2 a) SurA WT (PDB: 15MY) [69] N-terminal domain in blue, PPIase1 in green, PPIase2 in yellow and C-terminal domain in red b) SurA ΔP2 (PDB: 2PV3) [178]. Analysed in Pymol [213] to calculate the distances between atoms, colours as in a.

Although the regions of SurA that interact with OMPs are still to be discovered the affinities of SurA binding to peptides and a small number of OMPs have been documented (Table 3.1). The affinities of SurA WT and SurA ΔP2 binding OMPs are

not significantly different, suggesting that the P2 domain of SurA is not involved in binding OMPs or that the rearrangement of domains can compensate for the loss of P2 without a reduction in affinity. This poses several questions; if the P2 domain is not involved in binding of substrates and there are other PPIase's within the periplasm, does the P2 domain have any other role in chaperone activity? What are the roles of the P1 domain which does not have PPIase activity? In this chapter, experiments are described which address these questions using a range of techniques including MST, ITC, CD and SPR.

	K_d (μM)	
Substrate	SurA WT	SurA ΔP2
WEYIPNV	3.58 ±0.08	2.23 ±0.07
NFTLKFWDIFRK	6.62 ±1.03	5.57 ±0.64
OmpG	0.44 ±0.09	0.4 ±0.3
OmpF	5.2 ± 1.7	2.6 ±0.5
RCMLA	33 ± 11	38 ±11

Table 3.1 Table of known Kd's of SurA Interactions. SurA WT and SurA ΔP2 binding positive aromatic peptides, OMPs and a model soluble protein reduced carboxymethylated alpha-lactalbumin (RCMLA). Measured by competition ELISA assay in 20 mM phosphate buffer, pH 7.3 at 25 °C for WEYIPNV peptide, the OMPs and reduced carboxymethylated α-lactalbumin (RCMLA) [177] and in 50mM sodium acetate buffer, pH 5.0 at 25 °C for the NFTLKFWDIFRK [178].

The previously documented variants of SurA, ΔP2 and SurA N-Ct (Figure 1.20) [165] and SurA WT a used to compare their ability to bind two model unfolded OMPs. tOmpA is the 19 kDa 8-stranded transmembrane domain of the well-studied model OMP OmpA [56,97,214,215] and OmpT is a 33 kDa 10-stranded protease [58,216] (Figure 3.2). Comparing the binding ability of the SurA variants to these OMPs which are different sizes and have been shown to have different aggregation propensities [217] should help elucidate the roles of each of the domains within SurA. To this end, microscale thermophoresis (MST), was used to determine affinity. This technique has the advantage that it can be performed using low OMP concentrations (nM), and thus can be performed under conditions where OMPs remain in an unfolded, soluble form

in the absence of detergent or lipid and on time-scales in which OMP aggregation does not occur. The binding of SurA to OMPs was also tested by analytical size exclusion chromatography (SEC), native mass spectrometry (MS), circular dichroism (CD), surface plasma resonance (SPR) and NMR experiments, all of which were carried out under conditions which disfavoured OMP aggregation such as low protein concentration and the presence of denaturant.

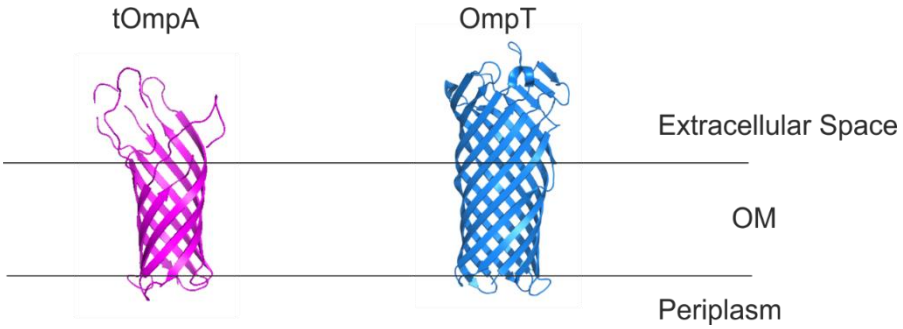

Figure 3.2 Crystal Structures of model OMPs. tOmpA (PDB: 1BXW)[218] and OmpT (PDB: 1I78)[58]

3.2 Expression and purification of SurA variants

All SurA variants used in this work (SurA WT, SurA ΔP2 and SurA N-Ct) (Figure 1.20) were created in Pet28b vectors containing a his tag and expressed and purified from the *E. coli* sequence lacking the N-terminal signal sequence. Proteins were expressed in the soluble fraction and purified by nickel affinity in its denatured state (6 M GdHCl, 25 mM Tris-HCl, pH 7.2) and refolded by dialysis (Methods 2.4.1). A typical A_{280} trace from SurA nickel affinity chromatography is shown in Figure 3.3a. The purity of each protein was determined by SDS-PAGE as shown in Figure 3.3b.

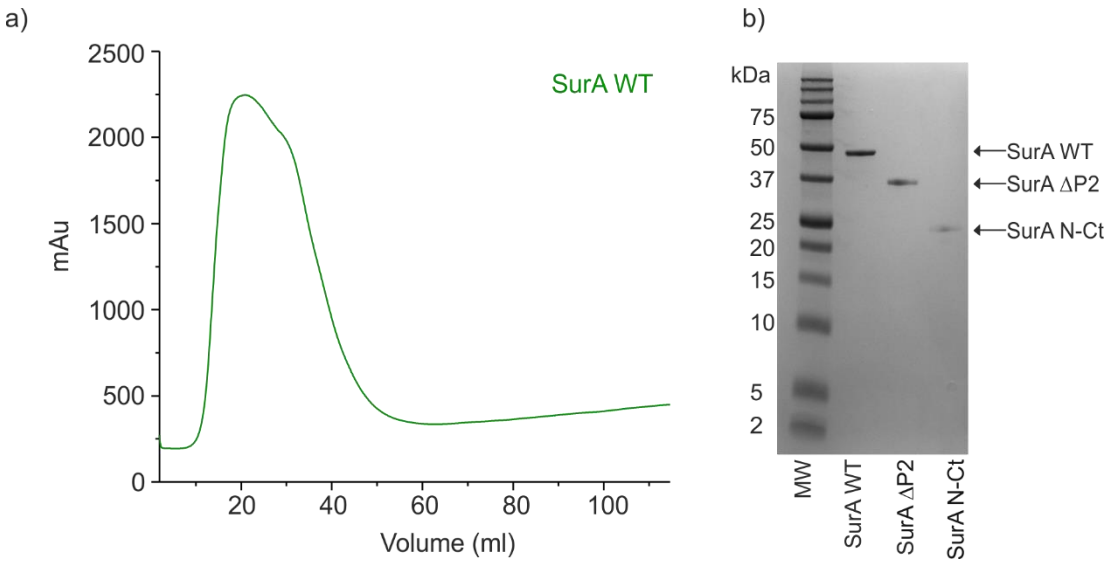

Figure 3.3 Purification of SurA variants a) Nickel affinity chromatography trace of the purification of SurA WT b) SDS-PAGE gel of pure SurA WT, SurA ΔP2 and SurA N-Ct.

3.3 Characterising SurA variants

3.3.1 Purified SurA variants are correctly folded and monomeric

To verify that the SurA variants, which were purified in a denatured state, were correctly folded and to investigate their structure, far UV-CD, native ESI-MS and analytical SEC were employed. All the experiments in this chapter are carried out in 50 mM glycine buffer pH 9.5. Unless stated otherwise, this buffer is used for many OMP experiments as the high pH aids in the retaining OMPs in a soluble conformation as their average pI is approximately 6 [219,220]. From the crystal structures of SurA the secondary structure was calculated to have 48% helical and 17% β-sheet content using standard methods [221]. The secondary structure of the purified SurA WT measured by CD and analysed by the CDSSTR algorithm using the Dichroweb software [222], suggests that the purified protein contains 46% helical and 19% beta sheet content (Figure 3.4a), showing the purified protein has the same secondary structure content as the crystal structure. The other purified SurA variants contained 50% and 46% helical content for SurA ΔP2 and SurA N-Ct, respectively, as determined by the same method as for SurA WT, suggesting there is no major conformational

rearrangements in the remaining domains when the PPIase domains are removed, consistent with the SurA ΔP2 crystal structure (Figure 3.1) [178].

Utilising native mass spectrometry (MS) at low protein concentration (1 µM) it was confirmed that these samples were folded, as they gave a characteristic distribution of charge state peaks at the correct mass to charge (m/z) ratio.

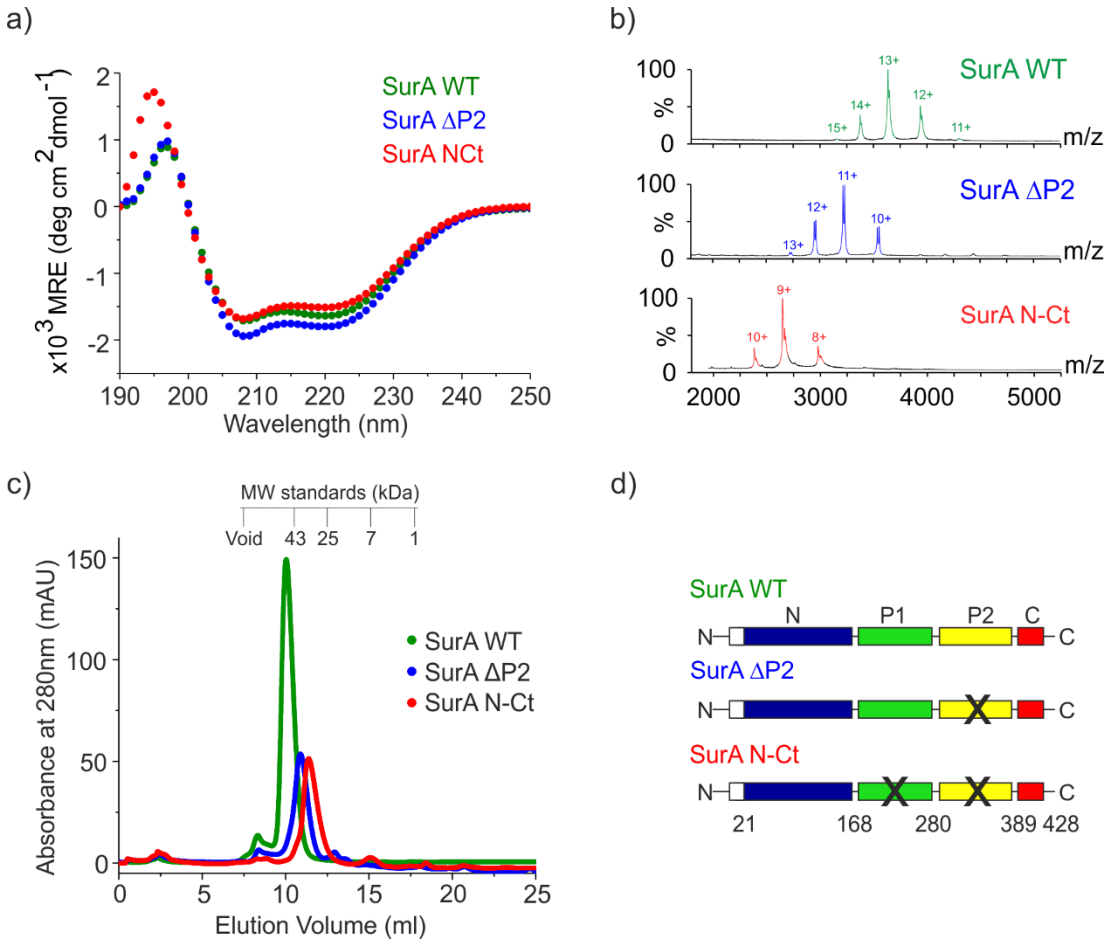

Figure 3.4 SurA variants are folded and monomeric a) Far UV Circular dichroism (CD) spectra of 5 µM SurA WT (green), SurA ΔP2 (blue), SurA N-Ct (red). b) Native ESI mass spectrometry (MS) of 1 µM SurA WT, ΔP2, N-Ct (colours as in a). c) Analytical SEC of 100 µM SurA WT, ΔP2 and N-Ct (colours as in a) d) SurA variants constructs.

Although the ESI-MS data show that, at low concentrations, the SurA variants are monomeric, binding assays for SurA interacting with OMPs require higher concentrations of chaperone, so analytical SEC of each variants was carried out at

100 μM, which is the highest concentration of SurA used in the MST experiments. The SEC traces show that SurA WT, SurA ΔP2 and SurA N-Ct elute as a mainly monomeric species at 47, 35 and 24 kDa respectively, with a small amount of a higher molecular weight species, presumably dimer (Figure 3.4c). The dimerisation affinity of SurA WT has been measured previously by AUC titration experiments which have Kd of 1160 ± 60 μM (1.1 mM) [223] which agrees that at the concentrations used in our experiments SurA should remain monomeric.

To confirm if the proteins were folded ^{1}H-^{15}N HSQC spectra is very powerful as it reports on the state of each residue, so the proteins were ^{15}N labelled (Methods 2.16.2) to obtain a spectrum. The ^{1}H-^{15}N HSQC spectra of each SurA variant showed they all have a well dispersed sets of peaks which again confirms that they are folded (Figure 3.5). There are a number of peaks for each protein which overlay with peaks in the spectra of another variant. However, as the spectra of these proteins have not been assigned further analysis is not possible here.

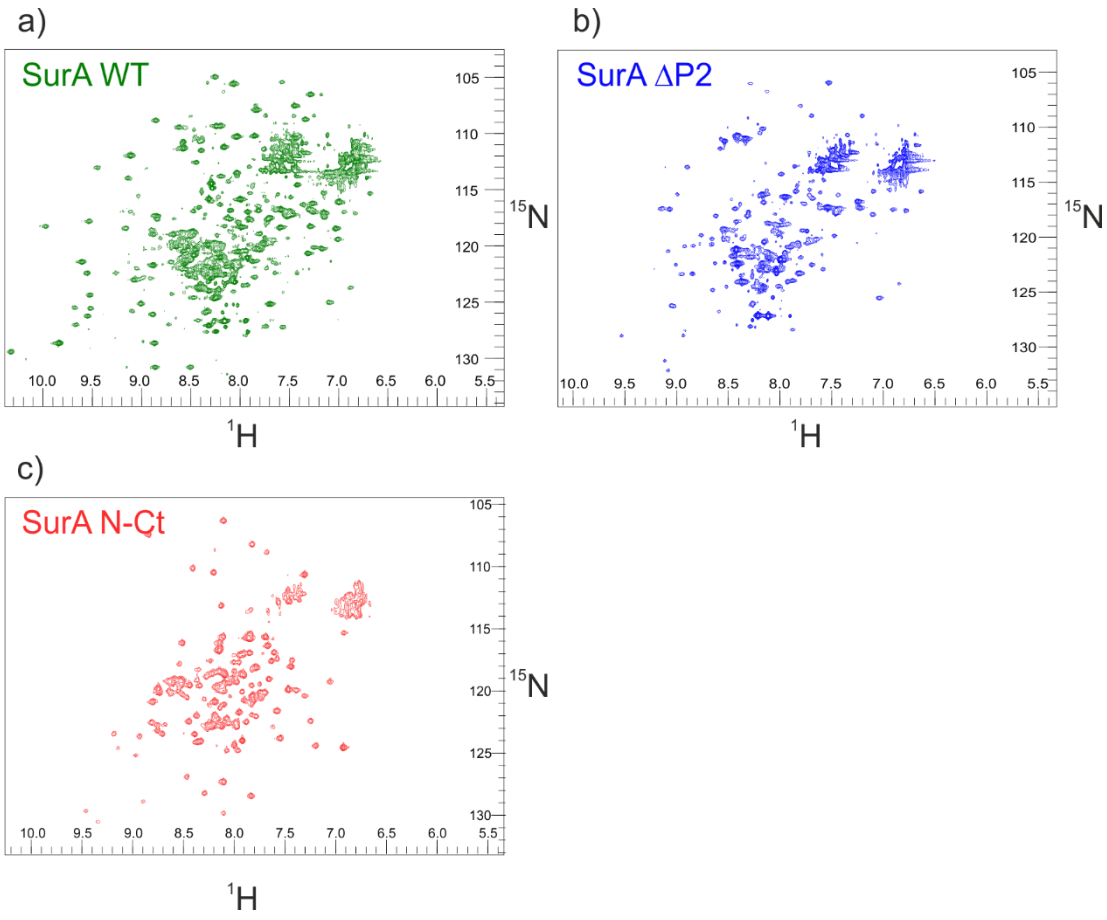

Figure 3.5 H^1-N^{15} TROSY NMR of SurA variants a) SurA WT (green) b) SurA ΔP2 (blue) c) SurA N-Ct (red) all variants were measured at 100 µM in 25 mM MES, 50 mM NaCl, pH 6.5 5% (v/v) D_2O

3.3.2 The PPIase variants of SurA fold and unfold uncooperatively

The structural information described above show that the SurA domain variants are all folded and monomeric under the conditions examined. The stability of the proteins was also analysed by urea denaturation equilibrium curves to investigate how the presence of absence of PPIase domains influence the folding and unfolding propensities of the different variants.

Fluorescence emission spectra were measured for each variant after equilibration in 0-10 M urea overnight to determine the % folded under these conditions, as the folded and unfolded species have distinct fluorescence emission spectra. Amino acids

with intrinsic fluorescence (Tryptophan and Tyrosine) in folded proteins are often in a hydrophobic environment (buried within the core of the protein) and in this environment they have a high quantum yield and therefore a high fluorescence intensity, compared to a low fluorescence when exposed to the solvent [224].

The results of the urea denaturation experiments show that each of the SurA variants are folded up to 3.4 M urea (Figure 3.6). However, the variants have distinct denaturation profiles. These complex profiles shows that SurA does not unfold cooperatively. SurA N-Ct, the variant lacking both PPIase domains, undergoes a single transition and it fully unfolded by approximately 6 M urea, suggesting is it unfolding as a single unit with a $\Delta G°_{UN}$ of 26.4 kJ.mol^{-1} and m-value of 6.1 kJ.mol^{-1}.M^{-1} (Figure 3.6c and Table 3.2). This supports the hypothesis that the C-terminal helix is involved in stabilising the larger N-terminal domain [171].

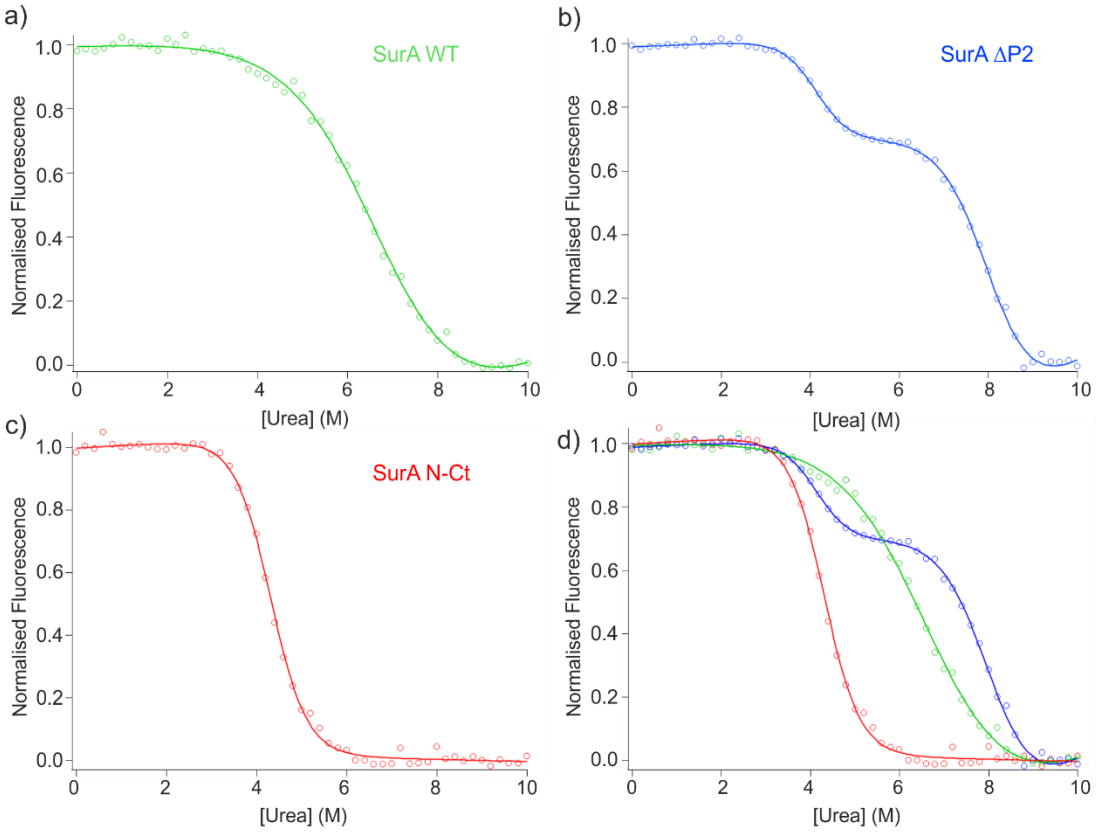

Figure 3.6 Equilibrium denaturation curves of SurA variants a) SurA WT (green) b) SurA ΔP2 (blue) c) SurA N-Ct (red) d) SurA WT, SurA ΔP2, and SurA N-Ct overlay. All proteins were measured at 5 µM at 25°C in 50 mM glycine, pH 9.5, 0-10 M urea and the data was fit to a two (SurA WT and SurA N-Ct) or three (SurA ΔP2) state transition in Igor Pro 6.0 .

SurA	$\Delta G°_{UN}1$ (kJ.mol^{-1})	m (kJ.mol^{-1})	$\Delta G°_{UN}2$ (kJ.mol^{-1})	m (kJ.mol^{-1})
WT	16.9 ± 0.9	2.5 ± 0.2		
ΔP2	24.3 ± 1.8	5.8 ± 0.5	37.9 ± 3.9	4.7 ± 0.5
N-Ct	26.5 ± 1.1	6.2 ± 0.2		

Table 3.2 ΔG° and m-values determined from the fits of each curve in Figure 3.6

The addition of a single PPIase domain (P1) in SurA ΔP2 alters the unfolding profile and shows two transitions that can be fit independently. These data have been modelled previously in a two domain protein [225] and shown that it is due to independent folding of the domains with a similar m-value and different $[D]_{50}$ values. $[D]_{50}$ is the urea value at which the protein is 50% unfolded. Fitting these data to a three state unfolding equation (Methods 2.6) gives two ΔG° values and m-values, the first of which ($\Delta G°_{UN}1$) is similar to that of SurA N-Ct unfolding alone, suggesting that this is reporting on the unfolding of the core domain in the SurA ΔP2 construct. These data suggest that the P1 domain unfolding is reported by the second transition ($\Delta G°_{UN}2$), and more stable than the N-Ct domain with a $\Delta G°_{UN}$ of 37.9 kJ.mol^{-1}.

The picture becomes more complicated for the full length SurA WT, as this protein has three domains with the potential to unfold independently. If there are three separate transitions for each domain, they are not resolved, but result instead as a single transition with a shallow slope, suggestive of uncooperative unfolding. The stability of the P2 domain in the context of the full protein cannot be identified by these data however, as the structure is the same as the P1 domain it is likely that it has a similar $\Delta G°_{UN}$. Fitting of the SurA WT data report a $\Delta G°_{UN}$ of 16.8 kJ.mol^{-1} and a m-value of 2.4 kJ/mol^{-1}. M^{-1}, which is much lower than expected. Published analysis of the two domain proteins (R1516 of spectrin) also has reported lower m-values than the individual domains and a single unfolding transition [226]. The independent folding and unfolding of the variants are in accord with the suggestion that the PPIase domains have been acquired during evolution of proteobacteria and they have been added to the ancestral core domain of SurA. The results show that the three

constructs all contain folded domains consistent with the CD and NMR analysis presented above.

3.4 Expression and Purification of tOmpA and OmpT

Unfolded tOmpA and OmpT are used in this study as model OMPs to examine the role of different domains of SurA in OMP binding as well as prevention of OMP aggregation and delivering OMPs to the BAM complex for folding. OMPs lacking their N-terminal signal sequence were expressed as insoluble inclusion bodies, which were isolated, solubilised in denaturant, then further purified by gel filtration in their denatured state (6 M GuHCl, 25 mM Tris-HCl, pH 8.0) (Methods 2.4.4) [143]. Typical A_{280} traces from tOmpA and OmpT gel filtration are shown in Figure 3.7a and b, with SDS-PAGE of peak fractions indicating pure protein Figure 3.7c.

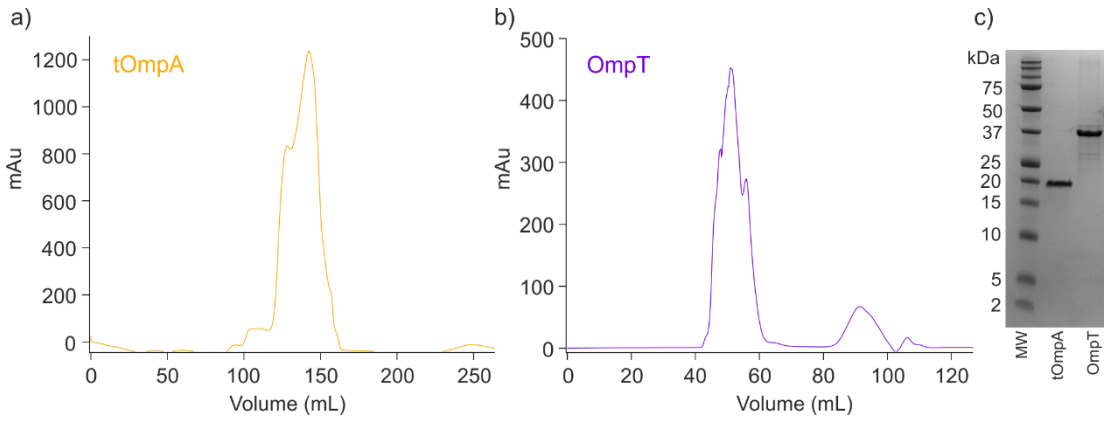

Figure 3.7 Purification of tOmpA and OmpT a) A_{280} elution of gel filtered tOmpA b) A_{280} elution of gel filtered OmpT 6 M Gdn-HCl, 25 mM Tris-HCl, pH 8.0. c) SDS-PAGE gel of pooled peak fractions from gel filtration of solubilised tOmpA and OmpT inclusion bodies. See Methods 2.4.4

3.5 Binding of SurA variants to tOmpA and OmpT

3.5.1 SurA variants interact with positive binding peptides

To verify that the SurA constructs are correctly folded and functional their ability to interact with peptides which were previously identified as positive binding peptides for SurA and SurA ΔP2, by an ELISA screening assay, was determined using ITC to reproduce the published data [178] (Methods 2.12). The experiments were carried out

with 20 µM peptide (WEYIPNV) and a titration of SurA variants upto 200 µM in 50 mM sodium phosphate buffer, pH 7.0, 25 °C.

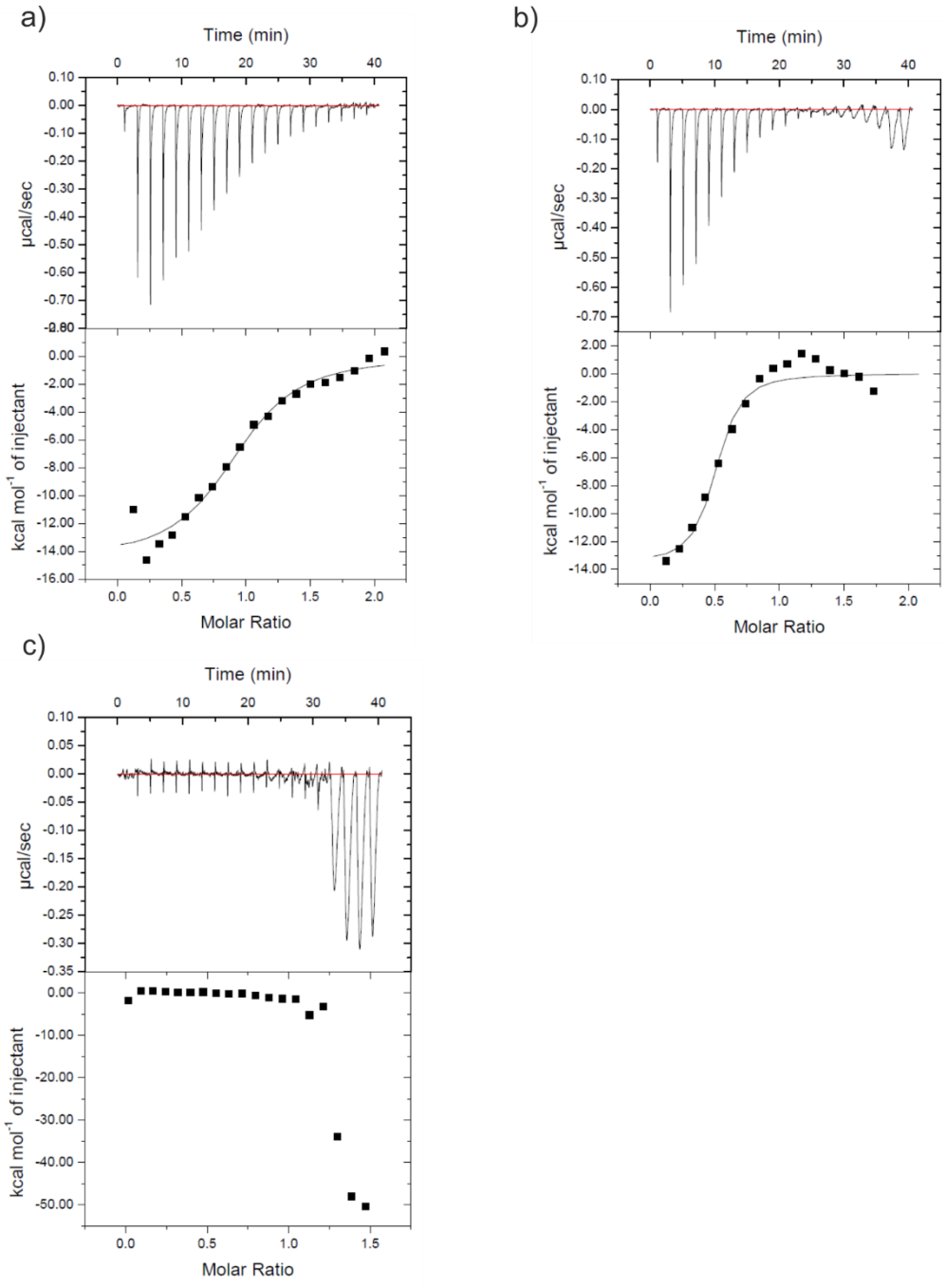

Figure 3.8 ITC of SurA WT, ΔP2 and N-Ct bind the WEYIPNV peptide. a) SurA WT, b) SurA ΔP2, c) SurA N-Ct. Raw ITC data (top) and binding isotherms created by plotting the integrated heat peaks against the molar ratio of the protein added (bottom).

SurA	K_d (μM)	N
WT	0.85 ± 0.3	1.02 ± 0.1
ΔP2	0.47 ± 0.3	0.77 ± 0.1
N-Ct	n/a	n/a

Table 3.3 ITC values of SurA binding to peptides. Kd and number of sites (N) from the fits of Figure 3.8

The ITC data (Figure 3.8 and Table 3.3) show that the peptide can bind to all three variants of SurA as revealed measured by a change in enthalpy over the concentration series, however the binding of SurA N-Ct to the peptide is reduced to the extent that a full binding curve could not be obtained (Figure 3.8c). The results show that SurA WT binds to the peptide with an affinity which is slightly tighter than the binding reported previously (0.85 ± 0.3 μM versus 3.58 ± 0.08 μM), however as the data sets were measured by a different method (competition ELISA) (Figure 3.8) and they are both low μM affinity binding the data are considered consistent. The same trend is seen for SurA ΔP2 as it is for SurA WT. The number of binding sites determined from the fit showed a binding stoichiometry of 1:1 which also agrees with the published data [177,178]. The binding of SurA N-Ct to peptides has not previously been measured and although there is a change in enthalpy at the high chaperone titration concentrations used, a full binding curve could not be fit to the data suggesting a reduced affinity compared to that of SurA WT or SurA ΔP2. This is consistent with the crystal structure of the NFTLKFWDIFRK peptide binding to SurA ΔP2 [178], as the interaction is observed to the P1 domain of the chaperone (Figure 3.9) and as the P1 is removed in the SurA N-Ct variant the higher affinity binding site is not available to interact with the peptide. These data suggest that when binding aromatic peptide sequences, the P1 domain is important for a high affinity interaction. However, removal of the P2 domain makes little difference to the interaction. Nevertheless, in the context of an unfolded OMP the binding surface of the P1 domain may not be sufficient and so model OMPs were next tested for binding to these SurA variants.

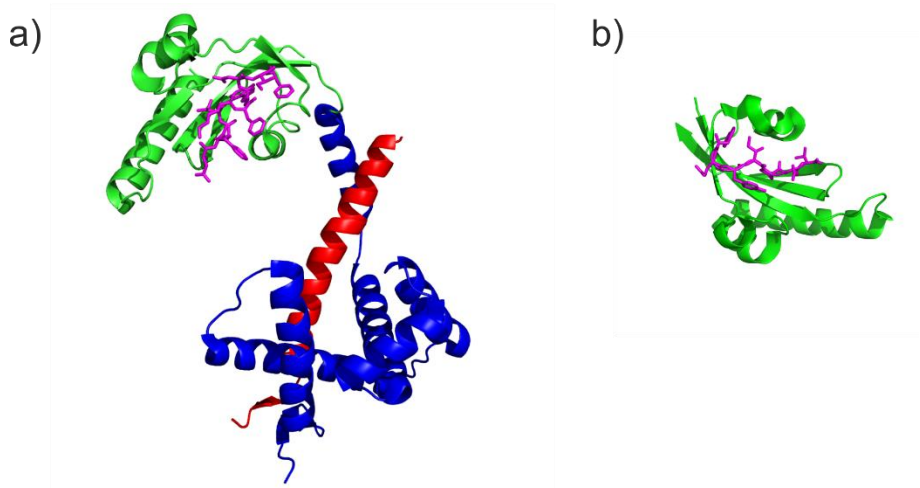

Figure 3.9 Positive binding peptides interact with the P1 domain of SurA. a) Crystal structure of SurA ΔP2 (N domain in blue, P1 in green and C in red) bound to the NFTLKFWDIFRK (magenta) (PDB: 2PV3) [178]. B) Crystal structure of the isolated P1 domain (green) in complex with WEYIPNV (magenta) (PDB: 2PV1) [178].

3.5.2 SurA PPIase domain variants interact differently with tOmpA and OmpT

Microscale thermophoresis (MST) was used to measure the affinity of each of the SurA variants for tOmpA and OmpT (Methods 2.14). In this technique one of the binding partners is fluorescently labelled and kept at a constant low (nM) concentration, and its movement in a temperature gradient is monitored in the presence of different concentrations of its potential binding partner [227]. N-terminal cysteine variants of tOmpA and OmpT were produced (Methods 2.4.4) and labelled via maleimide chemistry with AlexaFluor 488 dye (Methods 2.14.1) for use in the MST assay. Analytical size-exclusion chromatography indicated that all SurA variants were predominantly monomeric at the highest concentration used in the MST serial dilution (100 μM) (Figure 3.4). Aggregation assays were also carried out at 2 μM OMP under the same buffer conditions as MST, this concentration is higher than that in the MST assay (100 nM) but is required to test for aggregation. As no aggregation is visible at this higher concentration (Figure 3.10), it is implied there is none in the lower concentration.

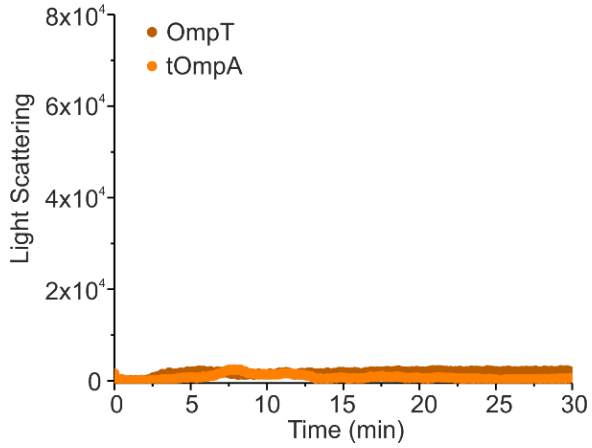

Figure 3.10 OMPs do not aggregate under MST conditions. Nephelometry light scattering assay of tOmpA and OmpT. OMPs were diluted to 2 µM in 50 mM glycine-NaOH, pH 9.5, 0.24 M urea (from 8 M urea) and light scattering measured immediately at 25 °C over 30 minutes.

In these experiments, all three SurA variants bind to tOmpA with similar low µM affinities (Figure 3.11, Table 3.4) in agreement with previous studies of binding of other OMPs (OmpG and OmpF) to SurA WT and SurA ΔP2 [97,177] (Table 3.1), although SurA N-Ct binding is slightly weaker. A different scenario is observed for binding of the SurA variants to OmpT. SurA WT binds to OmpT with low µM affinity, whereas SurA ΔP2 and SurA N-Ct, while still able to bind substrate OMP (shown by a change in the normalised fluorescence), have a weak affinity to OmpT, as a full binding transition could not be seen under these conditions (Figure 3.11). The data were fitted to a Hill coefficient and positive cooperativity [228] was observed for the interactions between all SurA variants and tOmpA, as well as SurA WT and OmpT. This suggests that multiple copies of SurA are interacting with a single unfolded OMP chain. These data demonstrate that the core region of SurA (SurA N-Ct) is sufficient for OMP binding, consistent with the observation that many SurA homologues in early proteobacteria lack PPIase domains [174,179]. However, SurA's affinity for the larger more aggregation-prone OMP substrate, OmpT, is dramatically increased by the presence of two PPIase domains, suggesting that the presence of the PPIase domains are involved in the interaction of some OMPs, perhaps especially OMP greater in size than the 8-stranded OmpA.

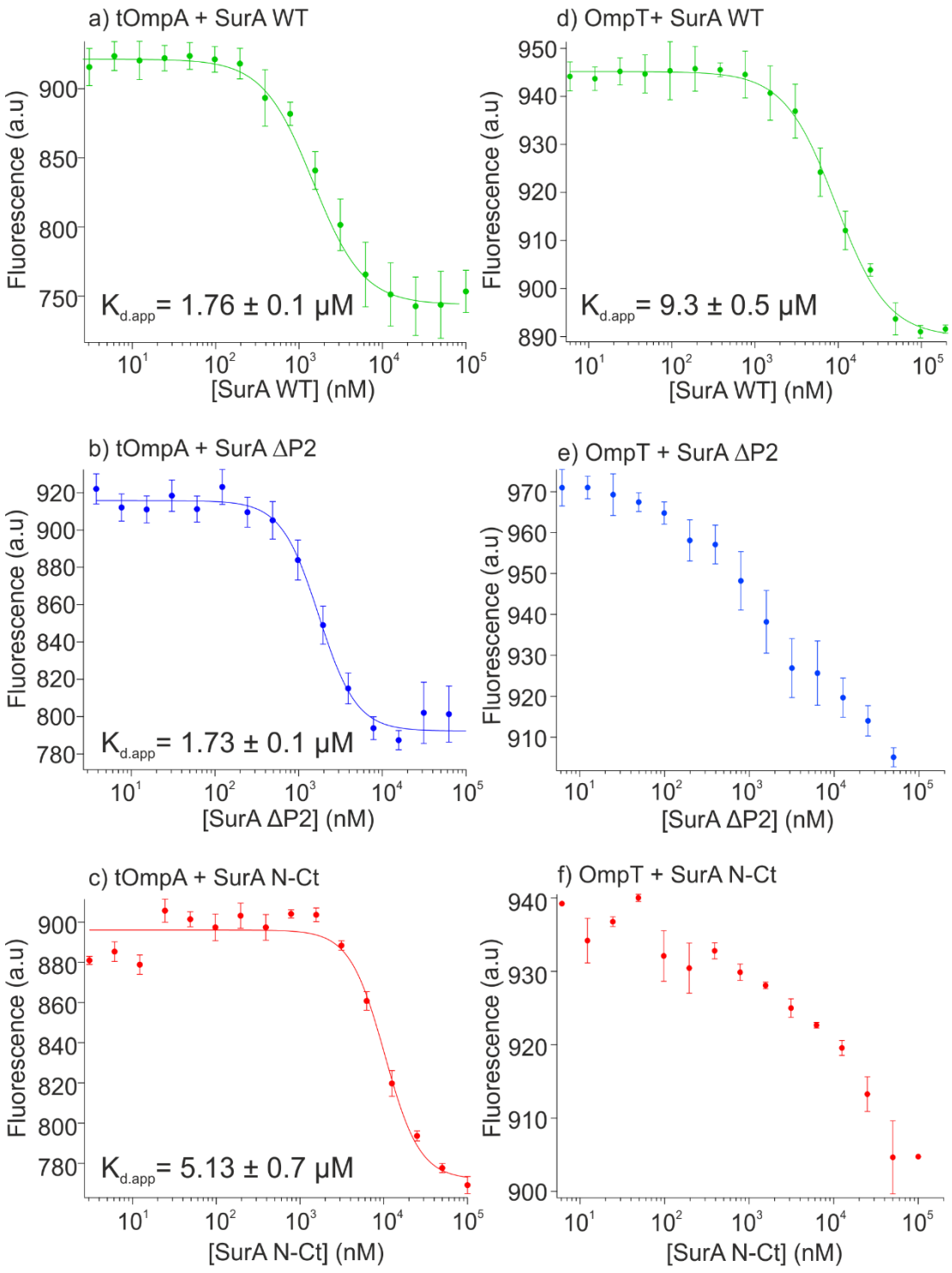

Figure 3.11 Binding curves of SurA variants for OMPs. Microscale thermophoresis binding curves of tOmpA binding to a) SurA WT (green), b) SurA ΔP2 (blue), and c) SurA N-Ct (red). d) OmpT binding to SurA WT (green), e) SurA ΔP2 (blue), f) SurA N-Ct (red). Data were fitted to a Hill equation (shown as a solid line) (Methods 2.14.2). Samples contained 100 nM Alexa Fluor 488-labelled OMP, 0.3 nm – 100 µM SurA variant, 0.24 M urea, 50 mM glycine-NaOH, pH 9.5, at 25 °C. Three replicates were recorded and averaged prior to fitting and the error of the fit plotted as error bars. Data in d-f were not able to be fitted (see main text).

	SurA WT		SurA ΔP2		SurA N-Ct	
	K_d (μM)	Hill coef.	K_d (μM)	Hill coef.	K_d (μM)	Hill coef.
tOmpA	1.76 ± 0.1	1.4 ± 0.1	1.73 ± 0.1	1.9 ± 0.2	5.13 ± 0.7	2.1 ±0.5
OmpT	9.30 ± 0.5	1.3 ± 0.1	N/A	N/A	N/A	N/A

Table 3.4 MST fitting data of SurA variants binding to tOmpA and OmpT. Each binding interaction was measured in triplicate and the data averaged prior to fitting. Data were fitted to the Hill equation (Methods 2.14.2) in Igor Pro. N/A: not applicable (data could not be fitted adequately)

3.5.3 The model bacterial protein Im7 does not bind SurA

As a test to investigate whether SurA can interact with water soluble proteins, Im7 was used to test its binding to SurA. Im7, or immunity protein 7, found in Gram-negative bacteria binds and inactivates the endonuclease domain of collicin toxin (ColE7) [229]. Im7 (an 87 amino acids, four α-helical protein) has been used for many years to investigate protein folding [230,231] and also to determine the effects of chaperones on protein folding [130,131]. Im7 folds via an intermediate state and mutations have been used to generate Im7 variants which are either fully unfolded (Im7 L18A L19A L37A) [232] or trapped in the intermediate structure (Im7 L53A I54A) [232,233].

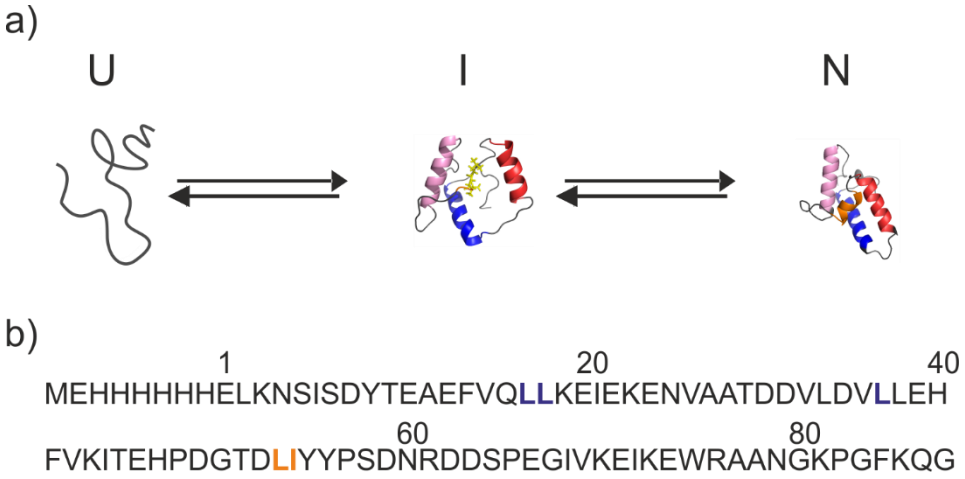

Figure 3.12 Im7 folding variants. a) Reversible folding pathway of Im7 from the unfolded chain via a partially folded intermediate (BMRD: 7316)[234] to the native folded protein (PDB: 1AYI) [235]. b) Sequence of wild type Im7, residues mutated to Ala in L18A L19A L37A (purple) and L53A I54A (orange).

The three N-terminally cysteine Im7 variants were purified (Methods 2.4.6) were labelled with with malemide AlexaFlour 488 (Methods 2.14.1) and used to investigate whether they bind to SurA WT or SurA ΔP2. The results (Figure 3.13) demonstrate that there is no detectable binding of any of the variants by MST with the concentrations of SurA used (3 nM – 100 µM). These mixtures of proteins were also analysed by native ESI-mass spectrometry (Methods 2.7) to determine whether complexes were observable by this method (Figure 3.14). SurA WT was tested with all the Im7 variants and only the unfolded variant (Im7 L18A L19S L37A) formed a complex with SurA WT, and ion from this complex were low intensity compared with the individual proteins in the mixture (Figure 3.14). These data suggest that SurA preferentially binds OMPs, with only a weak interaction with the water soluble protein (Im7), in an unfolded state, which agrees with previous data [177].

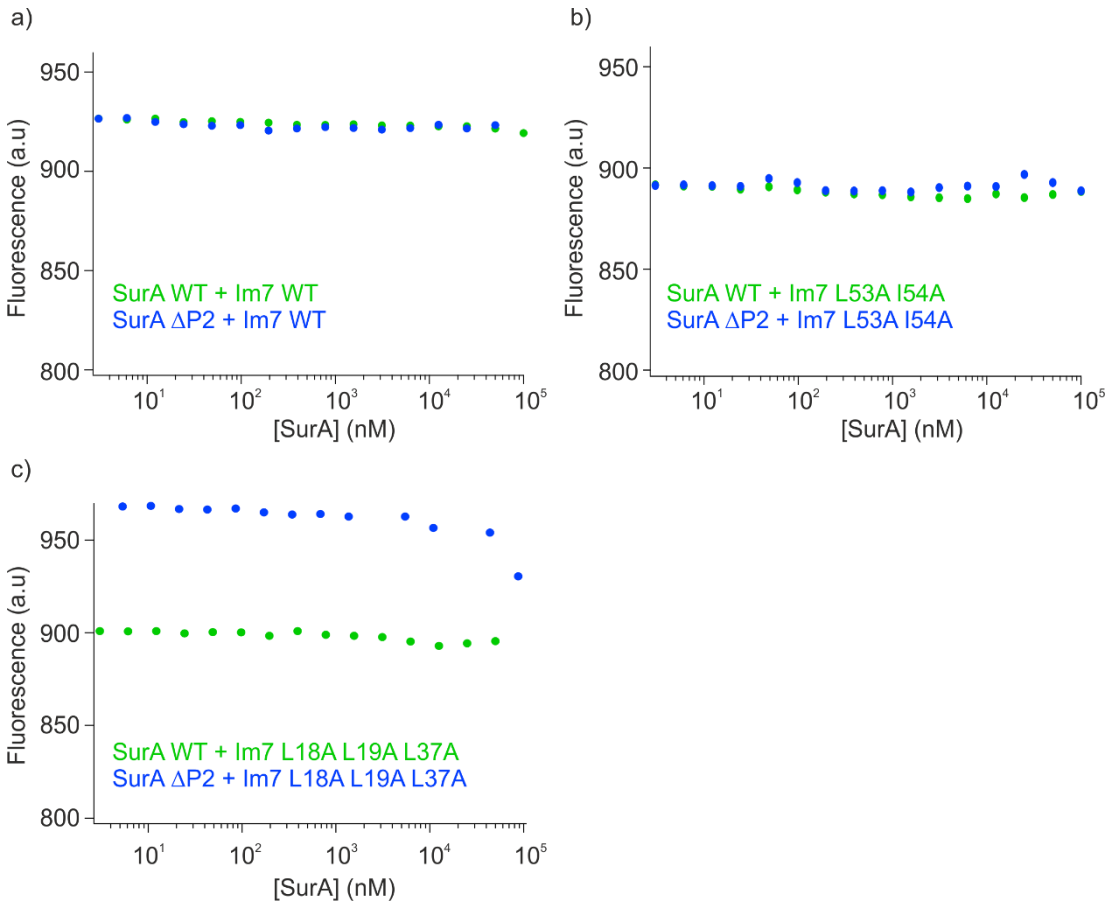

Figure 3.13 SurA does not bind Im7 in the unfolded, intermediate or native state. a) SurA WT (green) and SurA ΔP2 (blue) testing binding with native Im7 WT. b) SurA WT (green) and SurA ΔP2 (blue) testing binding with the variant Im7 L53A L54A. c) SurA WT (green) and SurA ΔP2 (blue) testing binding with variant Im7 L18A L19A L37A. All MST experiments were carried out in 50 mM sodium phosphate buffer pH 7.0 with 100 nM Im7-AF488 and 3 nM – 100 µM SurA variant (WT or ΔP2), any changes in fluorescence intensity is due to the % labelling of the Im7 variant. (AF488: Alexafluor 488 labelled).

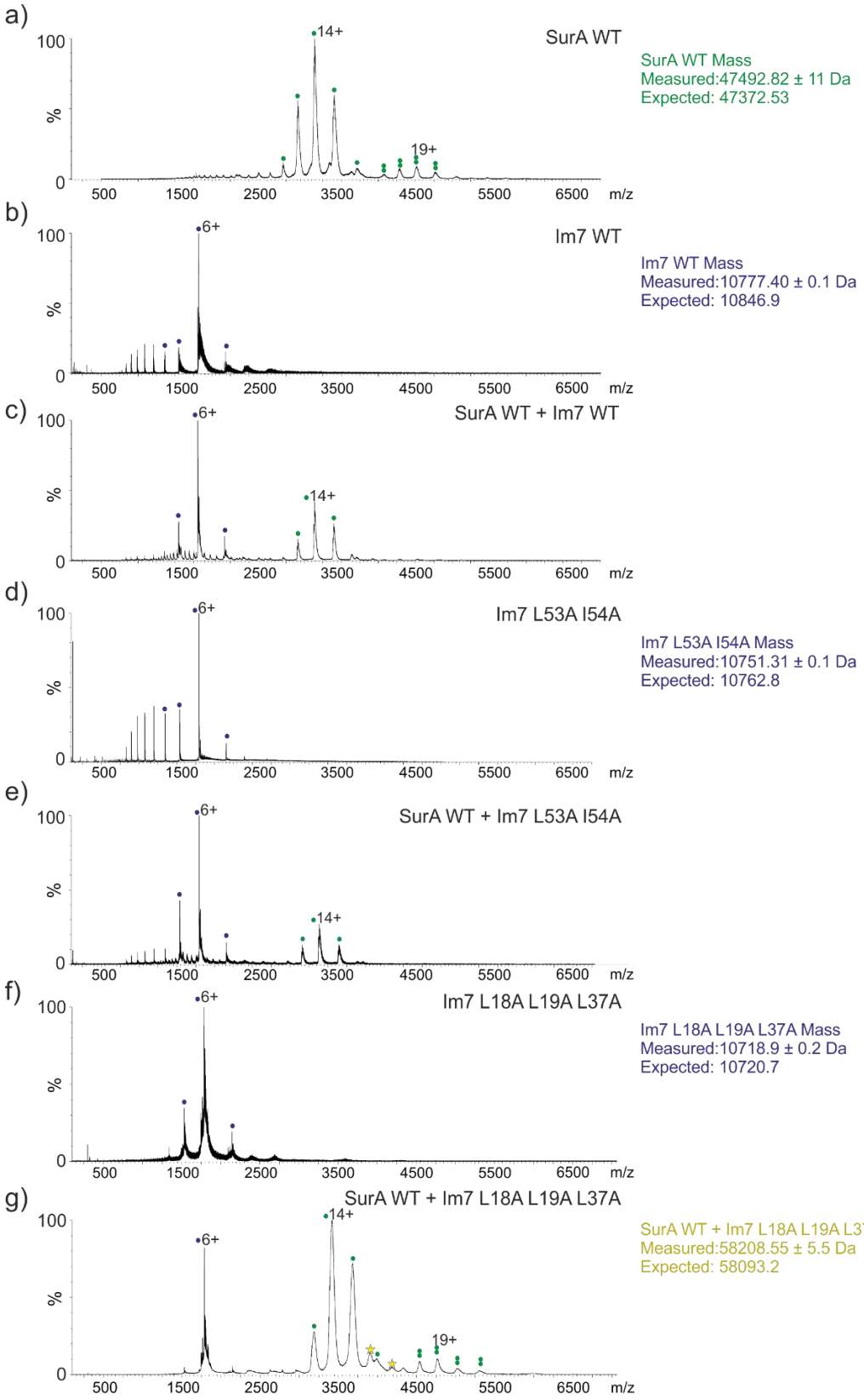

Figure 3.14 Native ESI-MS of SurA WT and Im7 variants. a) SurA WT alone (10 µM), single green dots indicate monomer and double green dots indicate dimer. b) Im7 WT (10 µM) c) SurA WT 1:1 Im7 WT (10 µM) d) Im7 L53A I54A 10 µM e) SurA WT 1:1 Im7 DM f) Im7 L18A L19A L37A 10 µM g) SurA WT 1:1 Im7 TM. All Im7 monomers represented by blue dots and SurA-Im7 complex peaks are denoted with a yellow star. The complexes were formed by 1:1

mixture of the proteins to a final concentration of 10 μM in 200 mM ammonium acceate 6.8 (Methods 2.7).

3.5.4 SPR of SurA binding to tOmpA

Surface plasmon resonance (SPR) is another technique that can determine affinity but it also can measure the kinetics of the binding interaction [236]. The N-terminal cysteine variant of tOmpA was immobilised on the SPR chip as described in Methods 2.9. SurA variants were titrated and flowed over the surface and the change in reflectance on the chip surface was monitored by response units (Figure 3.15).

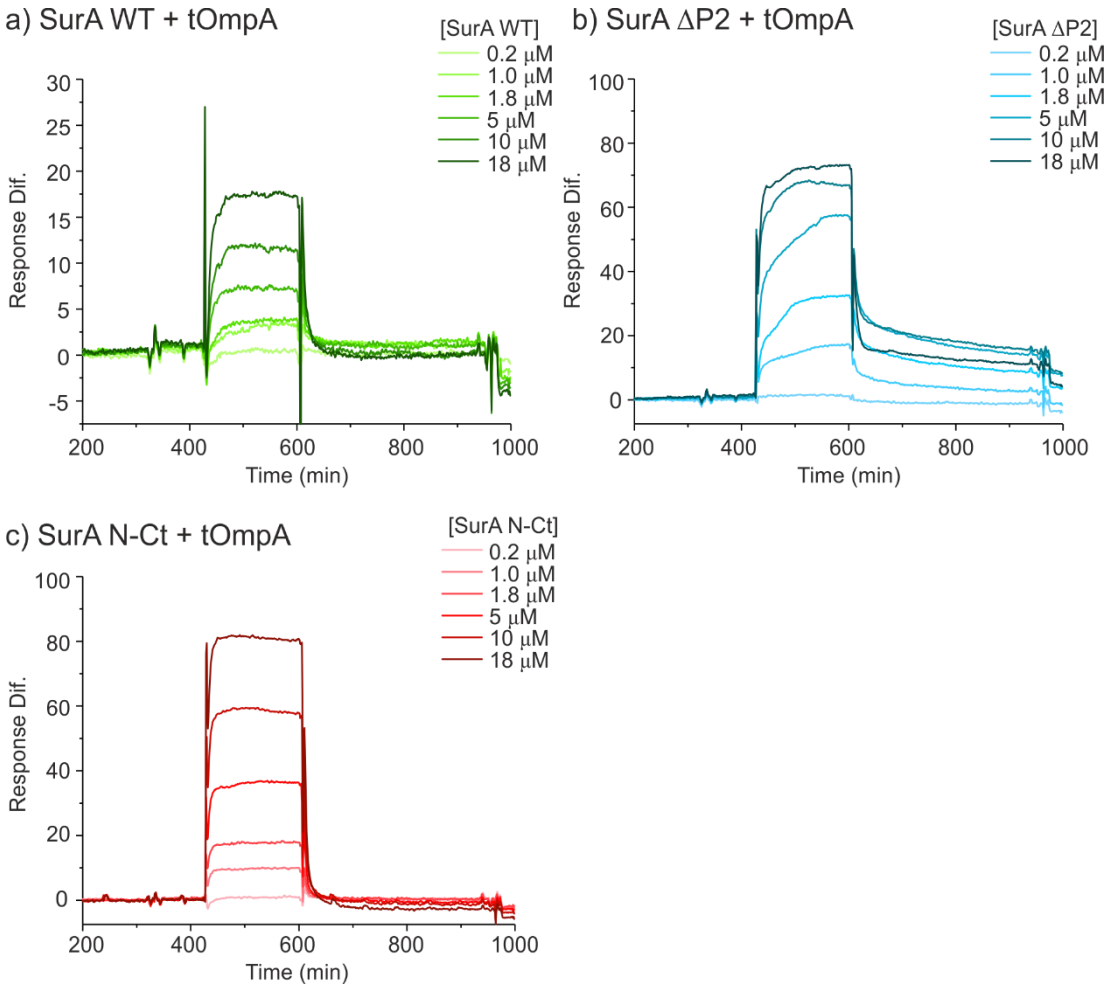

Figure 3.15 SPR response curves of tOmpA binding SurA WT/ ΔP2/ N-Ct. a) SurA WT analyte interacting with tOmpA on the surface at 0.2, 1.0, 1.8, 5, 10 and 18 μM. b) SurA ΔP2 interacting with tOmpA at the same concentrations c) SurA N-Ct interacting with tOmpA at the same concentrations. All experiments carried out in 50 mM glycine buffer, 0.24 M urea pH 9.5.

	k_{on} (M^{-1} s^{-1})	k_{off} (s^{-1})	K_d (µM)
SurA WT + tOmpA	6.17×10^3	0.0231	3.74
SurA ΔP2 + tOmpA	4.6×10^3	0.004	0.87
SurA N-Ct + tOmpA	1.34×10^3	0.117	8.81

Table 3.5 Fitting data from SPR curves. The titration data were fitted to a 1:1 Langmuir model using BIAevaluation software to extract the k_{on}, k_{off} and Kd (Equation shown in 2.9).

Together the results presented above show that the Kds of SurA WT/ ΔP2/ N-Ct for tOmpA can be measured by SPR and MST and all are low µM and show the same trend that SurA N-Ct has slightly weaker binding than SurA WT and SurA ΔP2 to tOmpA. The kinetics of these interactions suggest a slow on rate and a slow off rate which may suggests conformational changes occur upon binding and release (given typical diffusion limited values of k_{on} are 10^6 -10^8 M^{-1} s^{-1}) [237]. These data contrast with the findings of Costello et al. [212] who reported rapid association and dissociation of chaperones to OMPs traversing the periplasm by simulation, with calculated on and off rates from FRET experiments. However, the results presented here are the first direct measurement of association and dissociation rates of SurA with an OMP. Further investigation into the conformational changes occurring on OMP binding and how this changes for different OMPs is now required.

3.5.5 Analytical SEC of SurA WT/ ΔP2/ N-Ct tOmpA complexes

After the binding affinities of SurA WT/ ΔP2/ N-Ct for tOmpA were determined, analytical SEC was used next to analyse complexes formed. SurA-tOmpA complexes were formed at a 1:1 molar ratio (10 µM) and the samples analysed on an analytical Superdex 200 column (Methods 2.8).

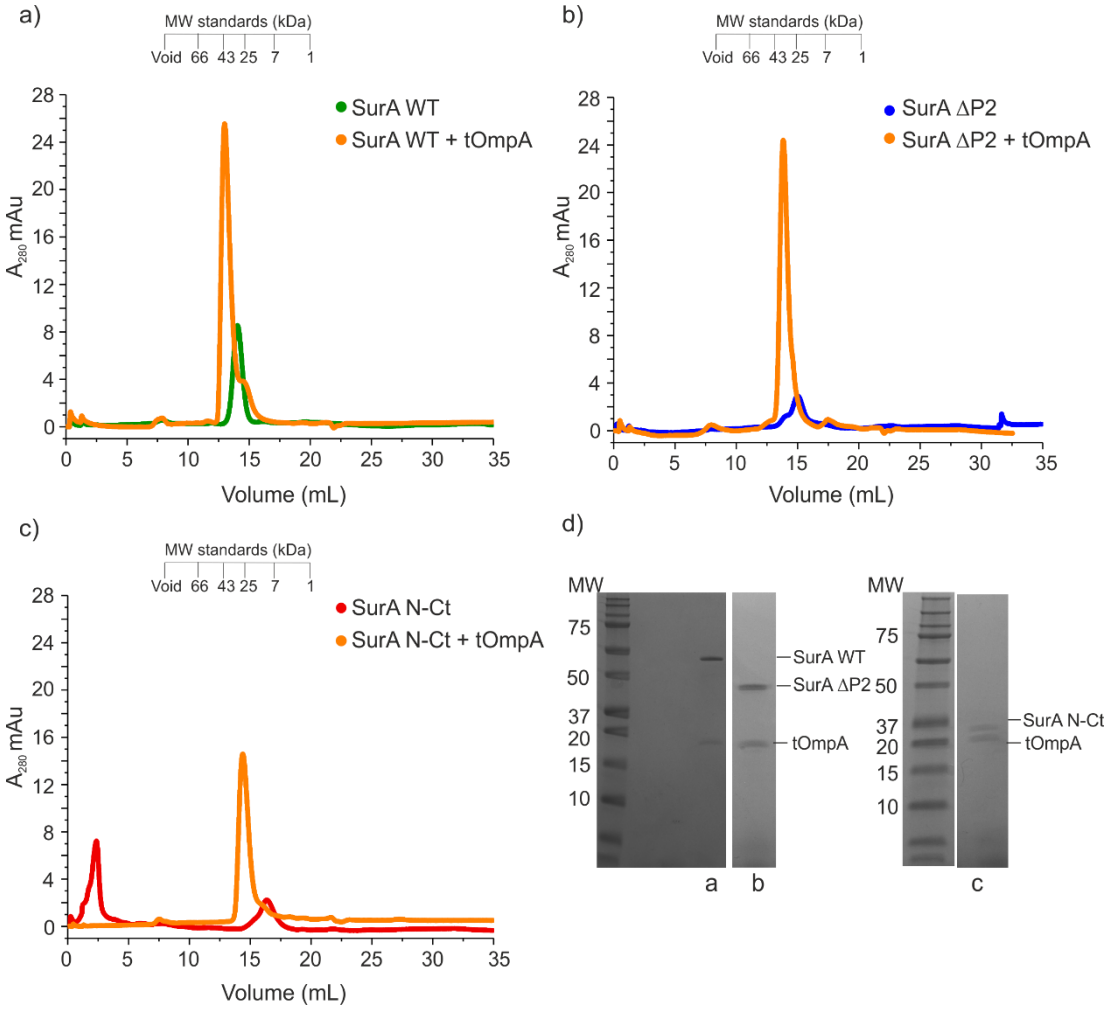

Figure 3.16 Analytical SEC of SurA WT/ ΔP2/ N-Ct bound to tOmpA. a) SurA WT 5 µM (green) and in 1:1 complex with tOmpA (10 µM) (orange). b) SurA ΔP2 5 µM (blue) and in 1:1 complex with tOmpA (10 µM). c) SurA N-Ct 5 µM (red) and in 1:1 complex with tOmpA (10 µM) (orange). d) SDS-PAGE of SurA-tOmpA complex peaks from a, d and c

The addition of tOmpA shows a clear peak shift in all SurA variants, which is expected as, at these concentrations, SurA and tOmpA should be approximately 50-60% bound for all variants (Figure 3.16). The peaks from the SurA-tOmpA samples were analysed by SDS-PAGE to confirm the presence of both proteins in the complex peaks (Figure 3.16d). The small amount of dimeric population seen in Figure 3.4 at 100 µM is not observed under these conditions, so only the monomeric interactions with tOmpA are observed.

3.5.6 SurA can form 1:1 and 2:1 complexes with tOmpA

The experiments above show that SurA binds to OMPs with low μM affinity and that this affinity is reduced for certain OMPs by the removal of the PPIase domains. To better understand the stoichiometries of these complexes, native ESI-MS was employed as it gives a more detailed picture of the masses of the complexes (Methods 2.7). SurA WT/ ΔP2/ N-Ct complexes with tOmpA were prepared by diluting tOmpA from 8 M urea to 1 μM tOmpA in 200 mM ammonium acetate pH 9.5 containing SurA at 1 μM at a final urea concentration of 0.24 M urea (Figure 3.17).

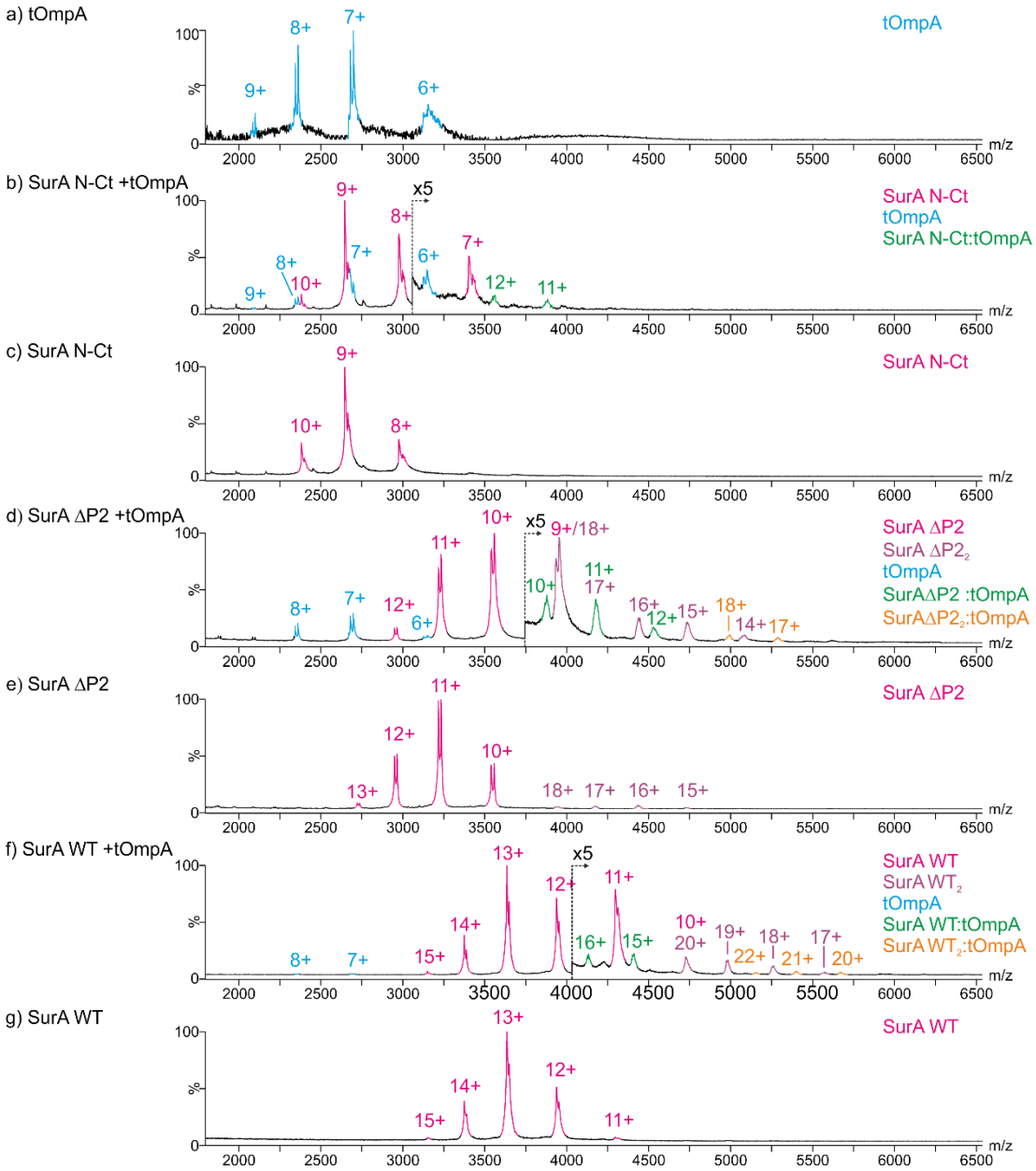

Figure 3.17 ESI mass spectra of tOmpA (1 µM) in the presence of 1 µM SurA WT a) tOmpA alone and in complex with b) SurA N-Ct d) SurA ΔP2 f) SurA WT. The spectra of SurA variants alone at 1 µM alone are shown c) SurA N-Ct e) SurA ΔP2, and g) SurA WT. For ease all SurA species including variants are shown in magenta, any dimeric SurA species (e.g. SurA WT_2) are shown in light pink and tOmpA alone is in blue. SurA 1:1 tOmpA complexes are in green and SurA 2:1 tOmpA complexes in orange. Experiments were performed in 200 mM ammonium acetate, pH 9.5. Expected and observed masses are shown in Table 3.6.

Native MS of SurA WT was measured as an observed mass of 47255.3 ± 1.0 (Da) compared to the expected mass of 47372.53 Da from the protein sequence there is a loss of 117 Da that can be accounted for by the loss of the N-terminal methionine and glycine located prior to the hexa-histidine tag on the SurA constructs. The SurA ΔP2 and SurA N-Ct variants also showed the loss of the N-terminal methionine. The reported, observed and expected masses are reported in Table 3.6 and all the measured masses are consistent with expected given the proteins are measured under native conditions.

The results revealed that a 1:1 complex was observed as the predominant complex species for all variants binding to tOmpA, Aggregation of OmpT unfortunately precluded analysis by ESI-MS. Interestingly, the charge state distribution for the SurA N-Ct:tOmpA complex has a lower intensity than the 1:1 complexes of SurA WT and ΔP2 (Figure 3.14), which is consistent with SurA N-Ct having a lower affinity for tOmpA, as shown by MST (Table 3.4). SurA WT and SurA ΔP2 both show 1:1 and 2:1 SurA to tOmpA complexes (Figure 3.17) suggesting that more than one SurA molecule is able to interact with a single non-native OMP. This is consistent with the Hill coefficients of >1 measured by MST (Figure 3.11). Mass spectrometry however does have the limitation that in the gas phase certain conformations are favoured and complexes with a higher stoichiometry and weak binding that may exist in solution may not be detected by mass spectrometry. It may be the case that 2:1 SurA to OMP complexes can be formed for each of the SurA variants however under these conditions using this technique that are not observed.

Protein or complex	Expected mass (Da)	Observed mass (Da)
SurA	47241.3	47255.3 ± 1.0
$SurA_2$	94745.0	94951.6 ± 6.4
tOmpA	18743.7	18746.5 ± 1.0
1:1 SurA-tOmpA	65985.0	66146 ± 2.0
2:1 SurA-tOmpA	113226.3	113397.0 ± 6.5
SurA ΔP2	35317.9	35394.5 ± 1.0
SurA $\Delta P2_2$	70635.8	70794.3 ± 1.2
1:1 SurA ΔP2 - tOmpA	54061.6	54088.5 ± 3.0
1:1 SurA ΔP2 - tOmpA	89379.5	89526.1 ± 6.9
SurA N-CT	23741.9	23804.2 ± 0.8
1:1 SurA N-CT-tOmpA	42485.6	42567.0 ± 3.3

Table 3.6 Observed and expected masses of SurA-tOmpA complexes. The masses shown are for the proteins without the initiator methionine (and for SurA WT, the subsequent Gly as this was removed proteotypically during the preparation).

3.5.7 SurA does not induce secondary structure of OMPs upon binding

To investigate whether SurA alters the conformation of OMPs in the chaperone-substrate complex, far-UV circular dichroism (CD) was used to analyse the secondary structure of the proteins within the complex (Methods 2.5). As seen in Figure 3.4, SurA alone is approximately 50% helical as is observed in Figure 3.18. The spectra of the OMPs alone were also measured in 8 M urea, showing that, as expected these proteins are fully unfolded with no secondary structure persisting. Spectra of tOmpA and OmpT were also measured in 0.24 M urea in 50 mM glycine pH 9.5. As previously

measured (Figure 3.10) under these conditions the OMPs do not aggregate over 30 minutes. The far-UV CD spectra were recorded within 5 minutes of the dilution of OMPs out of 8 M urea to avoid any possibility of aggregation in the samples. tOmpA in 0.24 M urea remains as a random coil, however OmpT under these conditions contains some secondary structure. This agrees with previously published data which observed a change in tryptophan fluorescence when OmpT is diluted from 8 M to 0.24 M urea in the absence of lipids or detergent [98]. Together these data suggest that OmpT in low concentrations of urea has some structure, which is likely formed by the portion of the protein which is not contained in the membrane in the final folded structure (Figure 3.18).

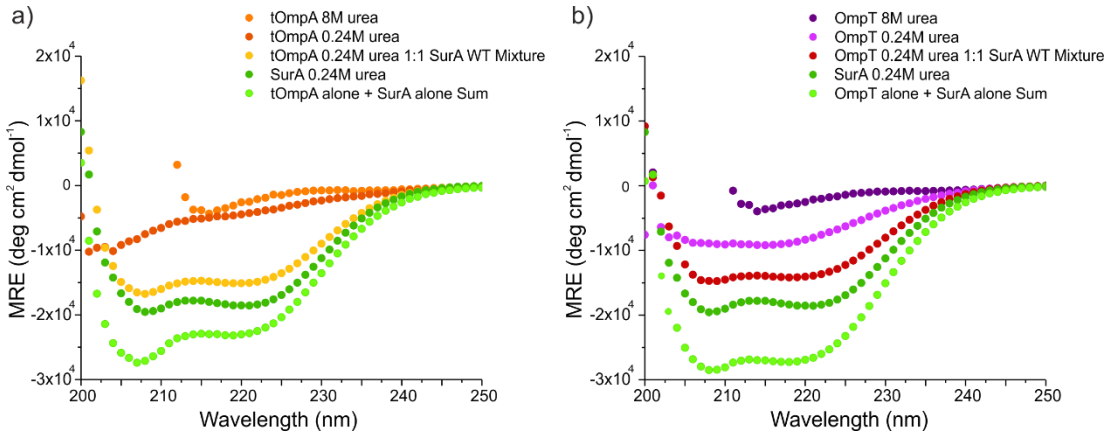

Figure 3.18 Differential CD of SurA tOmpA/OmpT complexes. a) tOmpA alone in 8 M and 0.24 M urea (light and dark orange), tOmpA 1:1 SurA (yellow), SurA alone (dark green), the addition of tOmpA and SurA individual spectra (light green) and the spectra of SurA alone from the tOmpA 1:1 SurA complex spectra (grey). b) OmpT alone in 8 M (purple) and 0.24 M urea (pink), OmpT 1:1 SurA (red), SurA alone (dark green), the addition of tOmpA and SurA individual spectra (light green) All experiments were done at 5 µM protein in 50 mM glycine pH 9.5 on a Chirascan circular dichroism spectrometer (Methods 2.5)

Upon 1:1 addition of SurA WT to tOmpA or OmpT, the spectra remain helical which is to be expected as the helical contribution of SurA will outweigh the random coil of the OMP (Figure 3.18). However, this complex has less helical content than SurA alone suggesting that SurA must undergo a change in secondary structure upon substrate binding. Addition of the individual spectra of tOmpA or OmpT with SurA alone, compared with the spectra of the SurA-OMP complex spectra, show that the summed spectra contains more secondary structure (as seen by a more negative MRE value). This suggests that there are conformational changes in one or both of the

proteins that are not observed in the proteins in solution on their own. As previous reports have documented, OMPs bind to SurA in an extended conformation. The data suggest that in complex with SurA the OMPs remain unfolded but there may be conformational changes in the SurA chaperone upon substrate binding.

3.5.8 2D NMR spectra of SurA ΔP2 interaction with tOmpA and OmpT

Binding of SurA to OMPs has been observed by a plethora of methods discussed in this chapter, however these techniques could not determine the regions on SurA involved in the interaction. NMR is a powerful tool, which can be used to monitor binding at a residue-specific level and to observe conformational changes, as well as many other features of proteins [211,238]. In this study we aimed to monitor the binding of SurA ΔP2 to tOmpA and OmpT. SurA ΔP2 is more amenable to NMR studies as it is smaller than SurA WT but can still interact with OMPs as determined by MST and MS. As the crystal structure of SurA ΔP2 shows that the remaining domains are similarly structured to SurA WT, assignments for these residues could be transferred from SurA ΔP2 to the spectrum of SurA WT. TROSY-NMR was used as it allows the study of larger proteins (above 25 kDa), as larger proteins have broad line widths in typical HSQC spectra, whereas TROSY-HSQC selectively detects only the narrowest component [238].

30 μM SurA was ^{15}N labelled, purified and then buffer exchanged into 50 mM glycine, pH 7.5 5% (v/v) D_2O which contained 5 μM tOmpA. Glycine buffer was used to keep the conditions consistent with previous binding experiments (Figure 3.11, Figure 3.15) however the pH was lowered to 7.5 as high pH leads to difficulty in observing exchangeable amide protons using ^{1}H-detected NMR methods. Under these conditions, SurA is 16% bound to tOmpA (assuming a Kd of 1.7 μM, Figure 3.11, Table 3.4) which should be sufficient to see if there are chemical shifts in the presence of OMP, a higher concentration of OMP lead to precipitation. Once the tOmpA was added, the spectra was acquired as soon as possible to prevent aggregation, with a

dead time of approximately 5 minutes, then a TROSY-HSQC acquired for 1 hour. Figure 3.19 shows that although many of the peaks of SurA ΔP2 are not observed in this experiment of the residues which are observed many undergo chemical shifts. However, some are not altered in the presence of tOmpA.

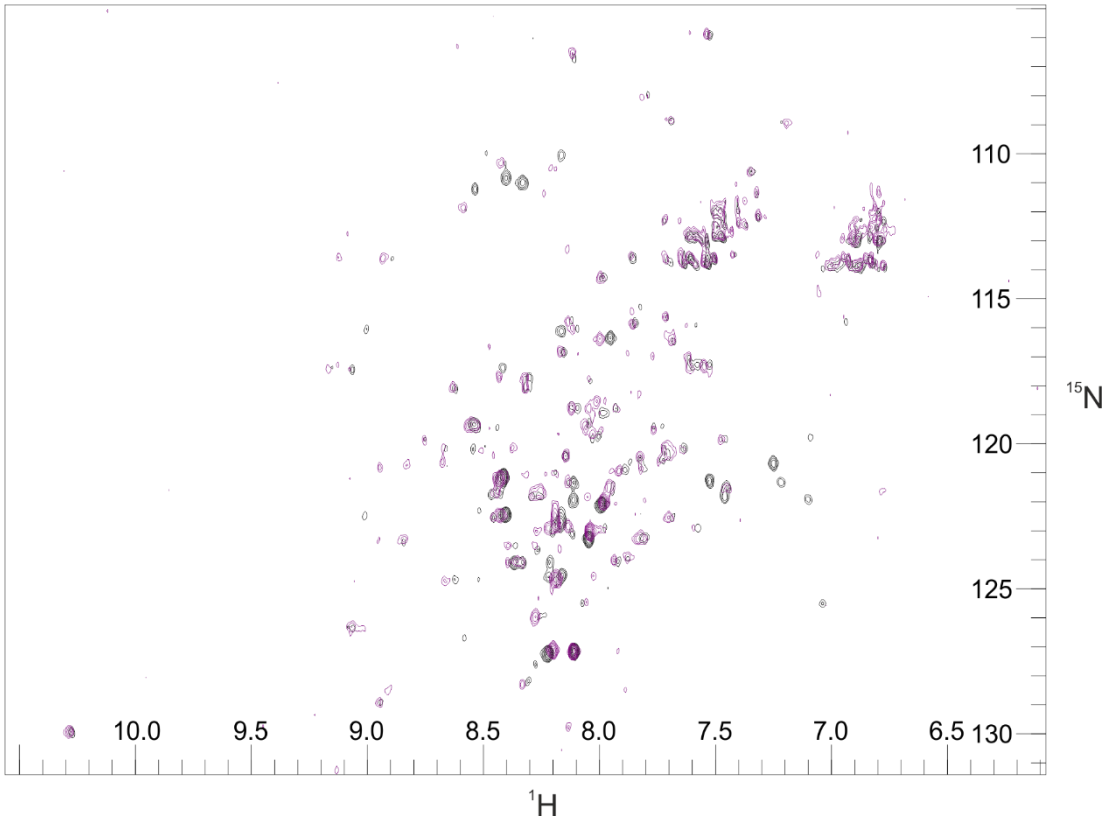

Figure 3.19 TROSY-^{1}H-^{15}N HSQC spectra of SurA ΔP2 in the presence and absence of tOmpA. Overlay of 30 µM ^{15}N SurA ΔP2 alone (black) and 30 µM ^{15}N SurA ΔP2 + 5 µM tOmpA (pink) both measured in 50 mM glycine pH 7.5 5% (v/v) D_2O, 950 MHz (Methods 2.16.2).

^{1}H- ^{15}N TROSY-HSQC spectra of SurA ΔP2 was also monitored in the presence of OmpT (Figure 3.20). However, as this OMP has been shown to be more aggregation-prone than tOmpA [217], it is more liable to precipitate during the experiment. A lower concentration of OmpT (2 µM) was added than was present in the tOmpA experiment. As the Kd of SurA ΔP2 and OmpT could not be determined (Figure 3.11), the % of SurA bound under these conditions cannot be calculated. Chemical shifts are observed in the complex spectra compared to the apo protein in spite of a low % bound and again some peaks move while others are not affected. These data show

that multiple residues of SurA ΔP2 are involved in binding tOmpA and OmpT opposed to a small binding motif and that these residues are likely spread throughout the protein.

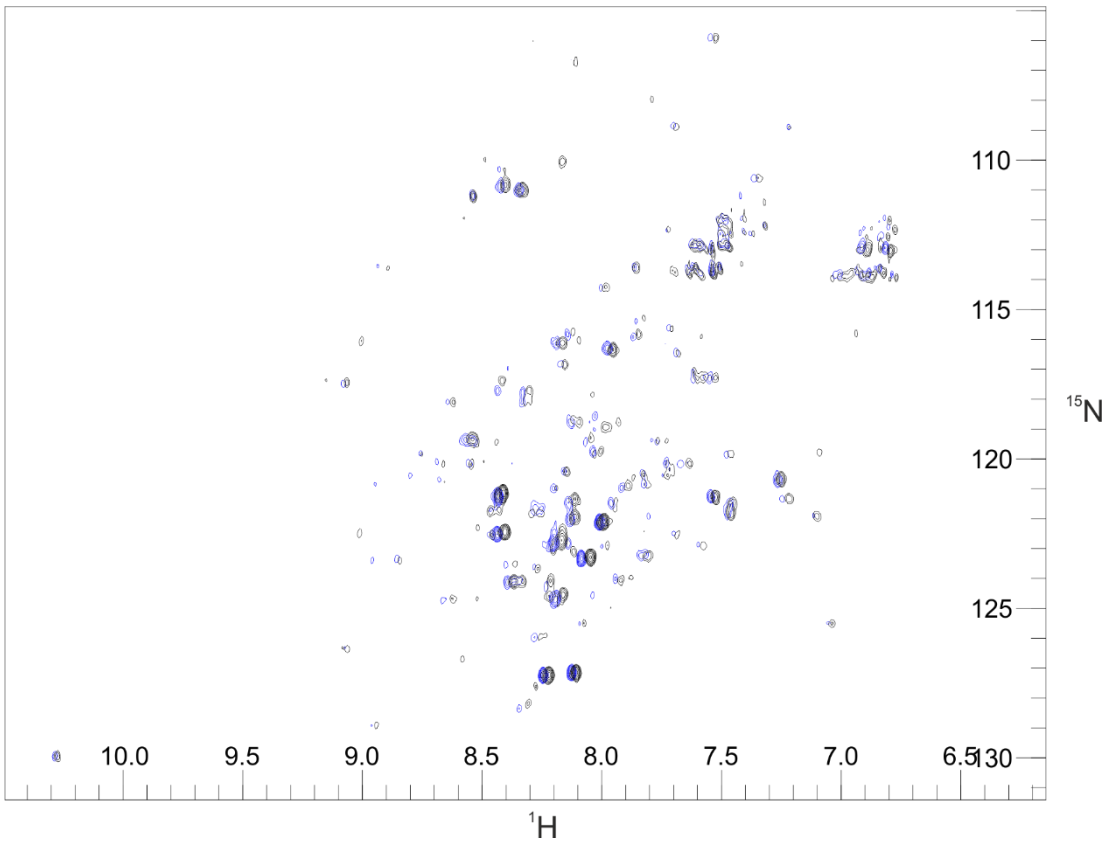

Figure 3.20 TROSY-^{1}H-^{15}N HSQC spectra of SurA ΔP2 in the presence and absence of OmpT. Overlay of 30 µM ^{15}N SurA ΔP2 alone (black) and 30 µM ^{15}N SurA ΔP2 + 2 µM OmpT (blue) both measured in 50 mM glycine pH 7.5 5% (v/v) D_2O, 950 MHz (Methods 2.16.2).

A comparison of the spectra of SurA ΔP2 alone and in complex with either tOmpA (pink) or OmpT (blue) (Figure 3.21) shows that although some peaks remain the same in all three conditions, peaks which do move do not do so uniformly in the presence of OMPs. This suggests that different OMPs cause different environments for the residues in SurA involved in binding. Assignment of these spectra would allow determination of which regions of SurA are involved in binding to OMPs. As many of the peaks appear to move, it also suggests there may be global conformational changes in the chaperone upon substrate binding.

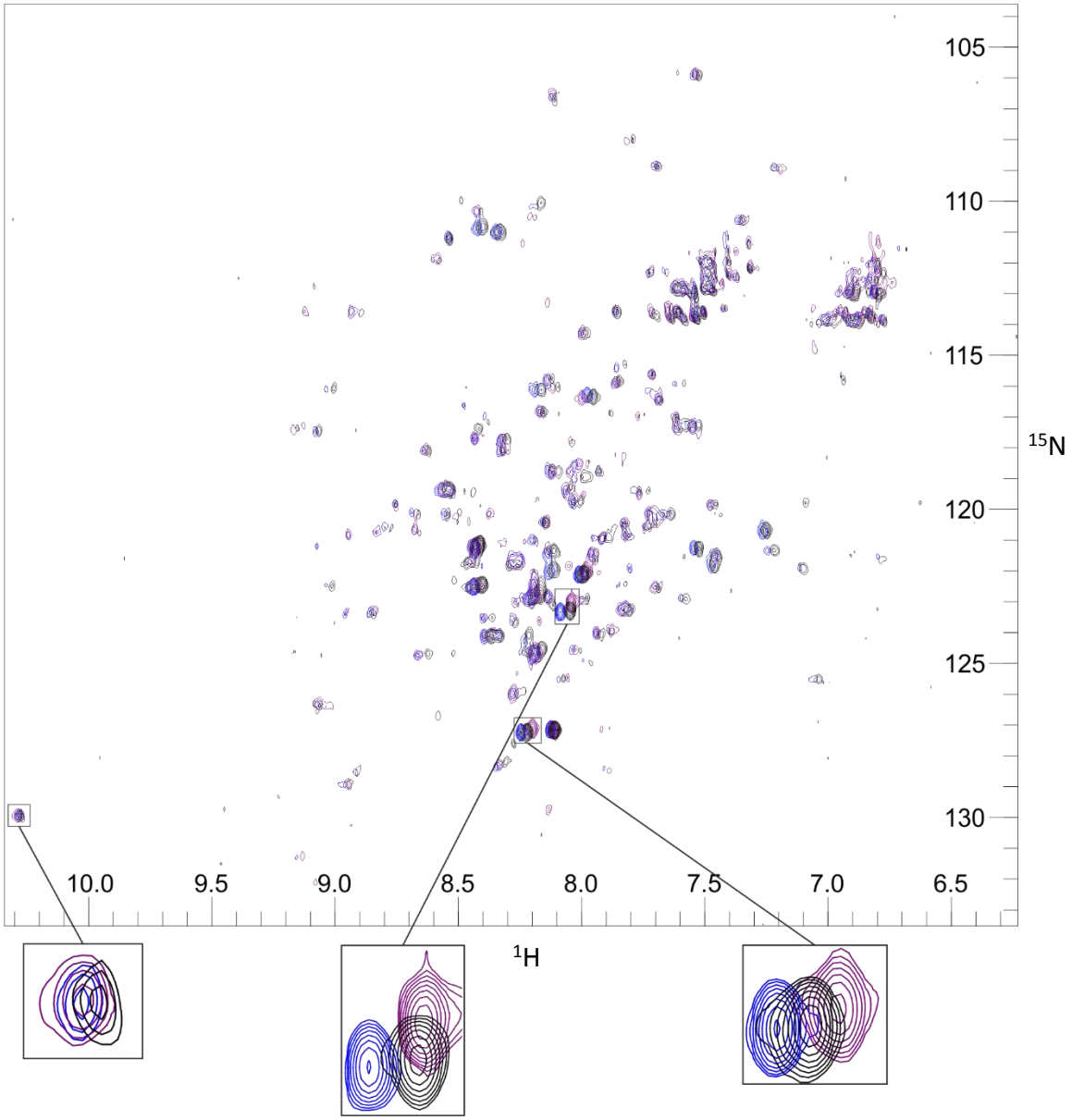

Figure 3.21 tOmpA and OmpT cause different effects upon binding to SurA ΔP2. Overlay of the ^{1}H-^{15}N TROSY-HSQC spectra of 30 µM ^{15}N SurA ΔP2 alone (black) and ^{15}N SurA ΔP2 + OmpT (blue) and ^{15}N SurA ΔP2 + tOmpA (pink). All measured in 50 mM glycine pH 7.5 5% (v/v) D_2O, 950 MHz.

3.5.9 Preliminary Assignment of N^{15} C^{13} SurA ΔP2

After preliminary data showing that the addition of OMPs cause chemical shifts in SurA ΔP2, this spectrum was optimised in order to give clean enough spectra for good assignments. The TROSY-HSQC spectra of the 35 kDa SurA ΔP2 at 100 µM (Figure 3.5)

was well dispersed indicative of folded protein and did not have many overlapping peaks however some of peaks were quite broad and some peaks were not observed. From the initial test the protein concentration was reduced to 70 µM to prevent any dimer interaction which could occur at high concentrations and the temperature was increased from 25°C to 35°C which does alter the peaks chemical shift but also increases the resolution (Figure 3.22).

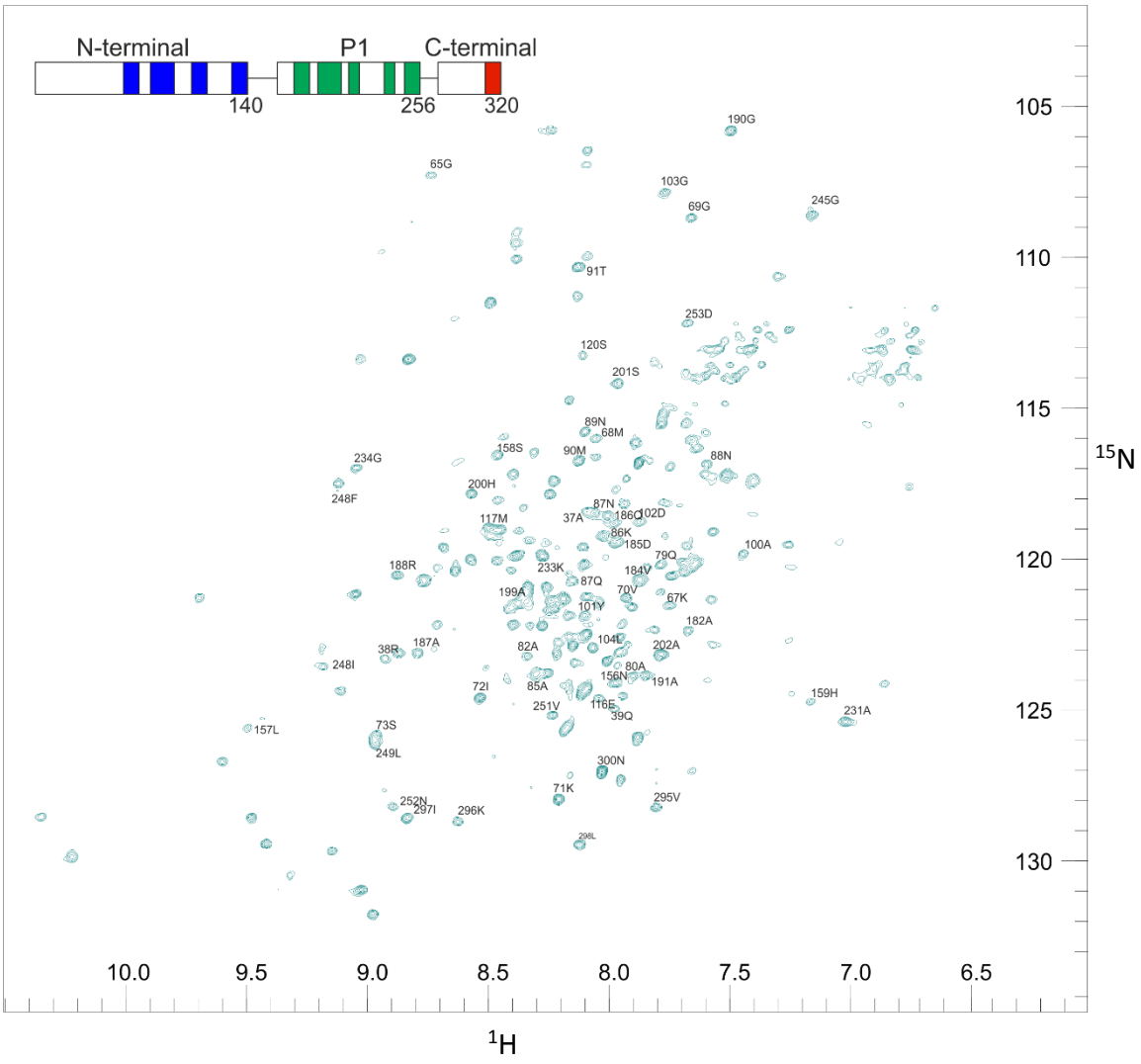

Figure 3.22 Partial assignment of SurA ΔP2. TROSY-HSQC spectra of N^{15} and C^{13} SurA ΔP2 in 25 mM MES, 50 mM NaCl, pH 6.5 5% (v/v) D_2O at 35°C, 750 mHz bruker NMR spectrometer and analysed using CCPN analysis. Inset is a schematic of regions in which the residues have been assigned, coloured as in Figure 3.4d.

After optimisation of the NMR conditions 238 peaks were observed of the 320 residues expected for the SurA ΔP2 construct, so there are still 82 peaks which cannot be observed. These peaks may be in highly dynamic unstructured regions within the protein which have linewidths too broad to detect. Triple resonance spectra (HNCO, HN(CA)CO, HNCA, HN(CO)CA, HN(COCA)CB and HN(CA)CB) of N^{15} and C^{13} labelled SurA ΔP2 as described in Methods 2.16.3 were measured to give i and i-1 peaks for the Cα, Cβ and Co of each residue allowing backbone chemical shift assignment. Due to the size of the protein leading to many peaks in the triple resonance spectra

overlapping and limited time, 73 of the peaks in the TROSY were assigned, however these residues are well distributed throughout the protein with assigned regions in all domains of SurA ΔP2 as shown by the inset of Figure 3.22.

As the tests of SurA ΔP2 interacting with OMPs were carried out in a different buffer and at a different temperature, unfortunately the assignments cannot be used to determine which peaks shift upon the addition of OMPs. However, residue specific information on SurA's binding regions is possible to obtain by 2D-NMR and further study will soon elucidate the regions of SurA that interact with OMPs.

3.6 Discussion

Previous studies have determined the importance of SurA in OMP biogenesis [164,170], demonstrating its preference to interact with aromatic sequences [175] and its higher affinity for OMPs than unfolded model proteins [177]. In this chapter, multiple biochemical assays were employed to analyse SurA binding to OMPs in their unfolded state as they would be in the periplasm. This was achieved by tailoring the experimental conditions such as OMP concentration and urea concentration to ensure that aggregation was prevented. Light scattering was used to investigate aggregation of tOmpA and OmpT alone and no siginificant increase in light scatering was observed sugesting that the OMPs remain soluble and do not form large aggregates under these binding conditions.

Native ESI-MS, analytical SEC, SPR and MST revealed that the core of SurA (the N and C terminal domains lacking the PPIase domains) is sufficient for interacting with OMPs. Interestingly, studies of SurA homologues in different Gram-negative bacteria have determined that some bacterial species only contain a single PPIase domain (often with higher sequence similarity to the P2 domain of the *E. coli* SurA) or no PPIase domains [174]. These data suggest that in cases of SurA homologues which do not contain PPIase domains, the chaperone retains the ability to interact with OMPs.

Further bioinformatics analysis (B.Schiffrin unpublished) of the domains within SurA homologues across different proteobacteria has been carried out from a dataset of 1176 genes from 1160 unique species. Results suggest that the core domain of SurA (N-Ct) is the ancestoral protein as it is more common to find a single or no PPIase domains in the older bacterial classes. It also suggests that the PPIase domains have been aquired and retained over the evolution of proteobacteria as the later bacterial classes mostly contain two PPIase domains (Figure 3.23). Overall it appears that there is an adventageous role for the PPIase domains which has been selected for, however this role is not yet fully understood. The binding data from the SurA domain variants presented here gives insights into the functions of the PPIase domains and suggestions as to their importance.

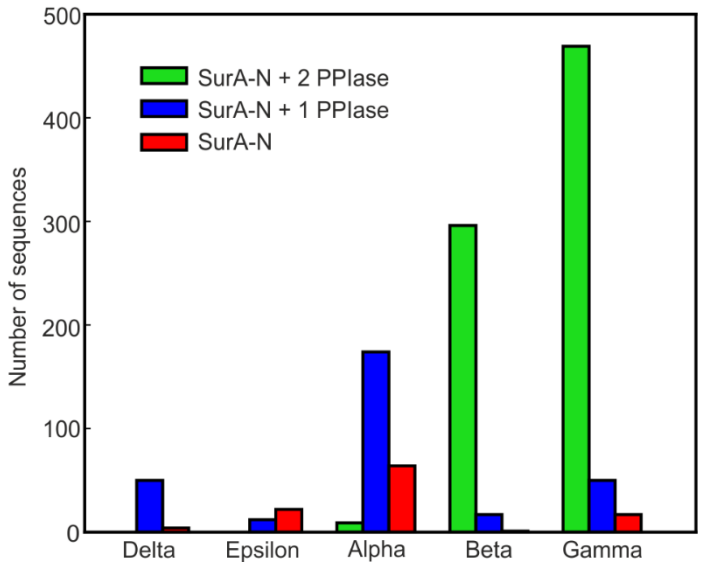

Figure 3.23 Bioinformatics analysis of presence of PPIase domains in SurA homologues. Proteins homologous to *E. coli* SurA in δ-, ε-, α-, β- and γ-proteobacteria were analysed for the presence or absence, of PPIase domains. Sequences were obtained from the PFAM database and belong to the SurA_N PFAM family (PF09312).

As an initial test of binding, a small aromatic peptide which has previously been shown to interact with SurA by an ELISA assay was analysed by ITC for binding to the SurA variants to observe any change caused by the presence of absence of the PPIase domains. The crystal structure of SurA domains in contact with aromatic peptides show they interact with the P1 domain. In agreement with this, the ITC shows that

removing the P1 domain significantly reduces SurA affinity for the peptide (Figure 3.8). The role of the P1 domain in binding OMPs is less dramatic. For tOmpA, removal of P2 or both PPIase domains does not prevent SurA's interaction with this OMP. However, in the absence of P1, the SurA N-Ct variant shows a reduction in affinity (Figure 3.11, Table 3.4), suggesting that a region of SurA involved in the interaction has been lost. Taken together these data suggest that the P1 domain of SurA may be an important point of contact for substrates. It also appears that the P1 domain can recognise aromatic residues which are common in OMP sequences [175] and hence conveys specificity for OMPs over other unfolded proteins.

The role of the PPIase domains was also analysed in the interaction of SurA with OmpT. For this OMP, the PPIase domains are required for an efficient interaction. SurA ΔP2 and SurA N-Ct has a change in fluorescence with OmpT over the titration showing that there is binding occuring. However, as a full binding curve cannot be measured these interactions appear to have very low affinity (Figure 3.11, Table 3.4). Another explanation for the change in fluorescence could be aggregation of OmpT which is changing the thermophesis properties, however this is unlikely as the final conentration of OmpT in this assay in 100 nM. OmpT has been shown to contain some amount of secondary structure under these conditions demonstrated by CD (Figure 3.18) and so the binding of this substrate may not be as simple as that of the unfolded chain of tOmpA. However, OmpT and SurA WT do interact with low μM afffinity suggesting that SurA has the ability to chaperone this more complex substrate.

The MST of tOmpA and OmpT binding the SurA variants showed that, for interactions where a full binding curve could be obtained, using a hill equation rather than a quadratic equation allowed a better fit to the data (Figure 3.24). Fitting the data by the two different methods gave a very similar kD, however using the hill equation showed that all the interactions that could be fitted have a hill coefficient of >1 (Table 3.4) indicative of positive cooperativity. It appears that there is a complex binding mechanism of SurA to OMPs and the MST suggests that this is substrate dependent.

From this data, two hypotheses may be formed, either the binding of a single SurA molecule to a unfolded OMP polypeptide chain causes an increase in the affinity for a second SurA molecule to bind elsewhere, in a 'beads on a sting' mechanism. The other posibility is that an initial contact of a small region of SurA with the OMP increases the affinity for further binding regions on the same SurA molecule, causing the OMP to wrap around the chaperone and interact with multiple sites on the chaperone surface, as has been previously shown for PhoA interacting with trigger factor [82]. This second mechanism is mostly supported by the mass spectrometry data suggesting mostly a 1:1 interaction, however the limitaions of this technique in monitoring large complexes is discussed in section 3.5.6. Either of these mechanisms would be able to prevent aggregation prone regions of the OMP chain self-associating and therefor prevent aggregation and it may be the case that this chaperone can interact using both mechanisms depending on the conditions within the cell however more detailed structural analysis of this complex would be required to determine if this is the case.

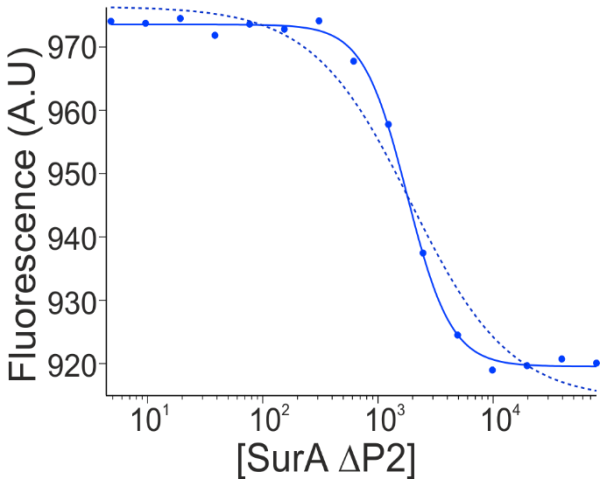

Figure 3.24 Comparison of quadratic and Hill equation fitting. SurA ΔP2 binding tOmpA (50 mM glycine pH 9.5 0.24M urea) fit to a Hill (solid line) or quadratic (dotted line) equation.

Analysis of the secondary structure of SurA WT on the binding of tOmpA or OmpT shows that SurA appears to have altered secondary structure when in complex with a substrate, as determined by CD (Figure 3.18). The NMR analysis of the complex shows that in the presence of OMPs many residues in SurA have an altered chemical

environment (Figure 3.21), which suggests that multiple regions of SurA are interacting with the OMP, or that the chaperone is undergoing conformational chages or a combination of the two effects. These data together suggest that there are extensive conformational changes occuring in SurA upon substrate binding which may be required for the chaperones mechanism of action. Structural determination of this complex by NMR will determine the extent of this change and help elucidate the role of structural movements in the mechanism of SurA.

In summary the data presented here show that the the core domain of SurA is sufficient for OMP interaction, however the PPIase domains play a role in the interation with more complex substrates such as OmpT. SurA preferentially binds OMPs over water soluble proteins. SurA is able to bind OMPs of different sizes and aggregation propensities and how it then prevents the self-association or aberrant interactions during the transport of these OMPs through the periplasm is a critical factor in OMP biogenesis and is the focus of the next chapter.

Chapter 4 SurA PPIase domain variants and other OMP chaperones have varying abilities to prevent OMP aggregation

4.1 Introduction

The periplasm is highly dynamic with rapidly changing conditions such as pH and viscosity. The presence of these stresses can lead to protein unfolding and aggregation [33]. In addition to this challenging environment, OMPs traversing the periplasm are in an unfolded or partially folded state and, as they are amphipathic molecules with stretches of hydrophobic residues, this makes them prone to self-association and aggregation [239]. Chaperones interact with OMPs and have been shown to hold them in an unfolded and extended conformation [149] which prevents intramolecular interactions of the OMP chain. It has also been observed that these chaperones have a very diverse range of substrates as SurA has been shown to interact with OMPs of between 8 and 26 strands [170]. The mechanism by which SurA and other periplasmic chaperones can prevent the aggregation of OMPs of different sizes, sequences and aggregation propensities remains to be understood.

The aggregation propensity of eight OMPs has been studied using sedimentation velocity analytical ultra-centrifugation (AUC) and demonstrated that unfolded OMPs have differing propensities to self-associate and form higher order oligomers [217]. A pH titration showed that an increase in pH led to the OMPs forming lower weight oligomers and at pH 9, all OMPs except OmpT have average weights of less than tetrameric species. The addition of KCl induced OMP aggregation, however OmpA and OmpX (the 8-stranded OMPs tested) remained monomeric to a higher salt concentration (200 mM) in comparison to the other OMPs. Urea was also monitored, which showed that, at 4 M urea, all OMPs were monomeric, with the exception of PagP. Below 4 M urea however, the OMPs had varying amounts of self-association. Armed with this knowledge, during the development of the aggregation assay in this

chapter, pH, urea and salt concentration were carefully monitored to find conditions in which reproducible aggregation kinetics could be monitored.

Monitoring the inhibition of protein aggregation by chaperones *in vitro* is common in the study of ATP-dependent chaperones that interact with soluble proteins to test chaperone activity [15,82,118,240]. Thermal denaturation or rapid dilution from high denaturant conditions can induce aggregation of test proteins, a titration of chaperone is then used to observe the concentration of chaperone required to prevent aggregation. In the case of GroEL, a 1:1 ratio of chaperone to rhodanese is sufficient to prevent aggregation [117] while trigger factor (TF) can prevent Glyceraldehyde 3-phosphate dehydrogenase (GAPDH) aggregation with a 0.5:1 chaperone to substrate ratio [82]. Only a limited number or studies have monitored OMP aggregation.

A study which investigated the ability of FkpA to chaperone OMPs at high temperature showed that FkpA can reduce the aggregation of OmpF in a concentration dependent manner and that this chaperone is more active at 44 °C than 37 °C [142]. The titration of FkpA to 20-fold excess over the substrate could not inhibit aggregation but showed a significant decrease in light scattering amplitude [142]. In comparison, a 20-fold molar excess of SurA WT could reduce but not eliminate aggregation at 37 ° C and had little effect at 44 °C. Skp showed a only a slight reduction in OmpF aggregation at both temperatures [142]. A separate study which monitored unfolded OmpC aggregation in the presence of periplasmic chaperones showed that 2x, 5x and 20x molar excess of DegP, Skp and SurA, respectively, caused inhibition of OmpC aggregation as monitored by light scattering [241]. SurA has also been tested for chaperone activity against a 49 kDa water soluble protein, citrate synthase [165]. Although a 1:1 mixture had some effect on the aggregation, a 64x excess of SurA was required to fully inhibit the aggregation of this non-native substrate [165]. These data suggest that periplasmic chaperones are required in a higher excess to prevent the aggregation of their substrates than cytoplasmic chaperones. This could be due to

their substrates having a higher aggregation propensity or simply for the reason that periplasmic chaperones have a distinct mechanism of action to cytoplasmic chaperones.

Light scattering is often used to monitor protein aggregation as it is sensitive to an increase in particle size and number in solution and so self-association and precipitation of large OMP aggregates causes an increase in light scattering [242]. This increase in light scattering by aggregation can be prevented by the formation of a soluble complex between the molecular chaperones and the substrates. Typically, light scattering is monitored by turbidity, which monitors the loss of transferred light in a straight path caused by particles in the solution deflecting the light. Another technique to monitor aggregation is nephelometry which measures only the light that is scattered within the sample up to 80° and traps light that passes directly through the sample [243]. Nephelometry is more sensitive than turbidity and also often leads to data with a better signal to noise [244]. To this end a nephelometry assay was developed to monitor aggregation of OMPs and to determine the roles of the PPIase domains of SurA in chaperoning OMPs. In this chapter the domain variants of SurA (SurA ΔP2 and SurA N-Ct) (Figure 1.20) along with SurA WT were tested to determine their effects on tOmpA and OmpT aggregation. To complement this detailed analysis, a comparison of multiple *E. coli* chaperones which have been shown to interact with OMPs during their biogenesis was also carried out by an end point analysis. The end point analysis allows direct comparison of different chaperones to determine their ability to prevent OMP aggregation and to identify whether the chaperones have specificities for certain substrates.

4.2 OMP aggregation assay development using Nephelometry

A small number of previous studies have monitored OMP aggregation by light scattering [142,241], however this was performed either as a control to determine if aggregates will be formed in other experiments or under only limited conditions. Here, I have determined conditions under which tOmpA and OmpT reproducibly

aggregate and carried out chaperone titrations to pick apart the effects that different chaperones have on OMP self-association.

4.2.1 tOmpA and OmpT aggregate upon dilution from 6 M Gdn-HCl

tOmpA and OmpT were expressed, purified and snap frozen in 6 M Gdn-HCl, 25 mM Tris-HCl, pH 7.2 as detailed in Methods 2.4.4. As an initial test to monitor whether the aggregation of the OMPs can be monitored by nephelometry, a concentration series of 2-8 µM OMP was tested by dilution from 6M Gdn-HCl at different stock concentrations so the final concentration of Gdn-HCl was held at 0.24 M.

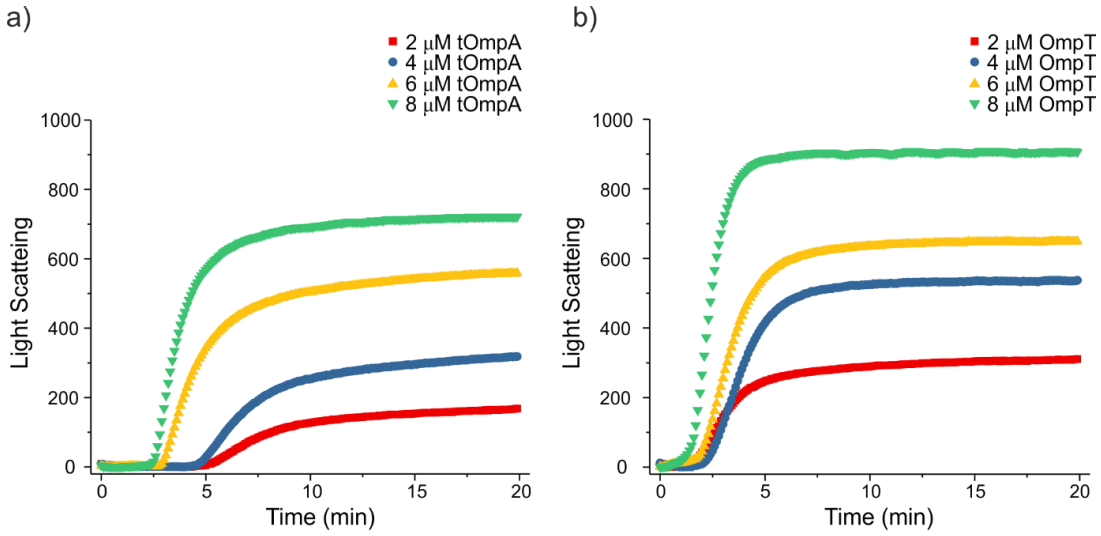

Figure 4.1 Concentration dependence of tOmpA and OmpT aggregation measured by nephelometry. a) tOmpA and b) OmpT at 2 µM (red), 4 µM (blue), 6 µM (yellow) and 8 µM (green). Both proteins were diluted from 6 M Gdn-HCl to a final concentration of 0.24 M Gdn-HCl in 50 mM glycine buffer pH 9.5. Nephelometry was measured at 635 ± 10 nm with a gain set to 50.

When measured under the same conditions (50 mM glycine buffer pH 9.5, 0.24 M Gdn-HCl) tOmpA and OmpT both aggregate at 2 µM, however tOmpA has a longer lag time before sufficient and large enough species are formed that scatter light and a lower final amplitude than OmpT (Figure 4.1). This suggests that tOmpA aggregates to a lesser extent than OmpT under these conditions, which is in agreement with previous reports that OmpT is more aggregation prone as measured by AUC [217]. An

increase in OMP concentration causes a decrease in lag time and an increase in amplitude for both tOmpA and OmpT, as expected for a multi-molecular reaction. As aggregation can be monitored at 2 μM OMP and a lower concentration of OMP allows a higher relative molar excess of chaperone to be added, 2 μM OMP was chosen to carry out all nephelometry experiments.

4.2.2 SurA WT can inhibit the aggregation of tOmpA and OmpT however removal of the PPIase domains reduces chaperone activity

SurA WT, ΔP2 or N-Ct were then added to the buffer prior to the dilution of the OMP to initiate aggregation. If the chaperone can bind to the OMP and prevent self-association, it should reduce the light scattering output. SurA WT was titrated into each OMP to determine the concentration which was able to prevent aggregation. For tOmpA this requires a 10x molar excess of SurA WT, however for OmpT complete inhibition over a 25 minute time-scale requires 100x excess of chaperone (Figure 4.2). The difference in SurA excess required to prevent the two OMP substrates suggests that the chaperone mechanism is not simply monomer sequestration, where a single SurA interacts with an unfolded OMP to prevent it for self-association, but there is a more complex mechanism of chaperoning these aggregation prone substrates. This agrees with the binding data that SurA may interact by different mechanisms to different substrates which may affect the substrates aggregation. The PPIase domain variants, SurA ΔP2 and SurA N-Ct, were then tested at the same concentration of SurA WT that could prevent aggregation to determine whether the removal of the PPIase domains affected SurA's ability to chaperone OMPs. Under these conditions SurA ΔP2 is slightly less effective than SurA WT in preventing the aggregation of tOmpA and SurA N-Ct is worse again although N-Ct still reduces aggregation slightly (Figure 4.2). The results suggest that sequential removal of the PPIase domains leads to constructs that are progressively less effective at preventing aggregation, although they have similar Kds at least for binding tOmpA (Figure 3.11). Removal of the PPIase domains has a dramatic effect on the aggregation of OmpT as SurA ΔP2 and SurA N-Ct slow the aggregation of OmpT, but result in a higher final light scattering

amplitude, suggesting that the chaperones may be pulled into the aggregates. These data show that the PPIase domains play an important role in preventing self-association of OMPs, in particular the larger more aggregation prone OMPs, such as OmpT.

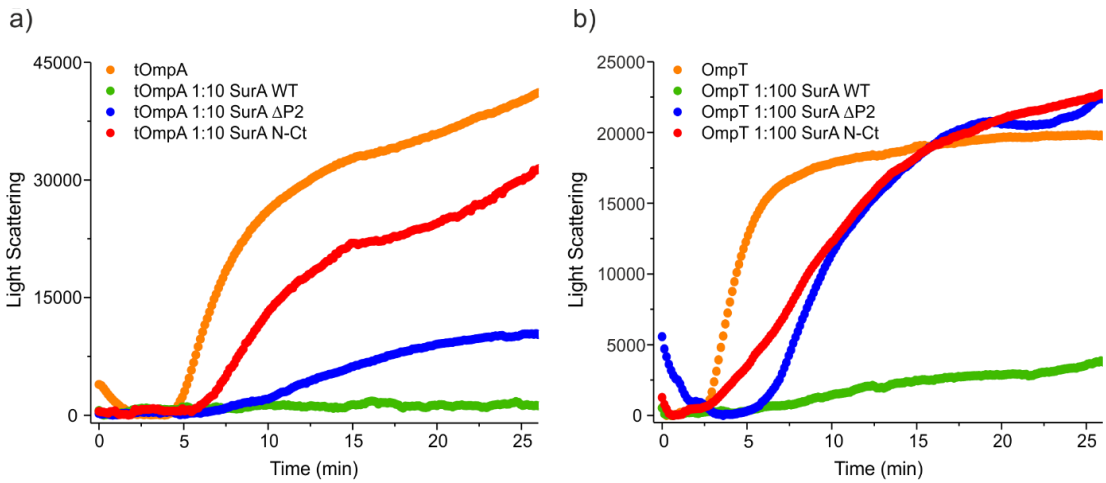

Figure 4.2 SurA variants have differing effects on OMP aggregation. Aggregation of a) tOmpA (orange) and b) OmpT (orange) alone and in the presence of SurA WT (green), SurA ΔP2 (blue) and SurA N-Ct (red). a) 10x excess of chaperone is added to tOmpA and b) a 100x of SurA variants excess added to OmpT to inhibit. All samples contained 50 mM glycine buffer pH 9.5, 0.24 M, Gdn-HCl at 25 °C.

4.2.3 Aggregation of OMPs in urea requires NaCl

After the preliminary experiments carried out in a final concentration of 0.24 M Gdn-HCl, the conditions were next altered to determine whether aggregation could be carried out to monitor OMP aggregation from denaturation in urea to remain consistent with the binding data that were carried out in 50 mM glycine buffer, pH 9.5, 0.24 M urea (Methods 2.15.1). The OMPs were buffer exchanged into 8 M urea from 6 M Gdn-HCl to keep them in an unfolded state, they were then diluted to a stock concentration of 66.7 μM OMP in 8 M urea before rapid 33x dilution to give a final concentration of 2 μM protein in 50 μl final volume.

Interestingly, little or no aggregation was observed upon dilution of the OMPs from urea, as was seen under conditions used for MST experiments, 50 mM glycine buffer pH 9.5, 0.24 M urea (Figure 3.9). However the addition of 0.24 M NaCl to the buffer to create an ionic strength identical to that measured above (0.24 Gdn-HCl) (Figure 4.2) can induce aggregation of tOmpA and OmpT, by pelleting assay, it was also observed that there was no soluble tOmpA or OmpT in solution after 30 minutes of aggregation (Figure 4.3b). It is interesting to note that under these conditions, OmpT has a longer lag time and a lower final amplitude than tOmpA, which is the opposite of the previous observation following dilution from Gdn-HCl (Figure 4.2). This may be due the denaturants having different effects on the conformation of the OMP or if OmpT is significantly more aggregation prone it may have formed insoluble aggregates which have fallen out of solution to the bottom of the well and so are not observed in the kinetics analysis. Despite the differences dependent on the denaturant used, the change in the light scattering for both OMPs alone is reproducible and allows further analysis to test the effects of the presence of chaperone.

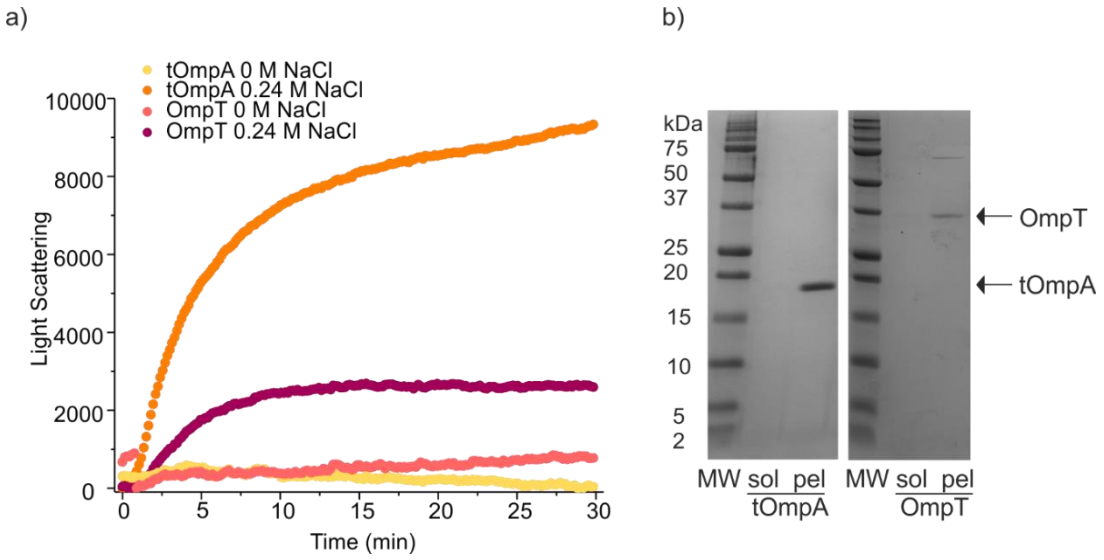

Figure 4.3 tOmpA and OmpT require NaCl to induce aggregation in urea. a) tOmpA and OmpT at 2 μM (final urea concentration 0.24 M) in the presence or absence of 0.24 M NaCl in 50 mM glycine buffer pH 9.5. tOmpA without NaCl (yellow) and with NaCl (orange) and OmpT without NaCl (pink) and with (purple). b) Pelleting assay of tOmpA and OmpT (50 mM glycine buffer pH 9.5, 0.24 M urea, 0.24 M NaCl) after 30 minutes, soluble (sol) and pelleted (pel) material separated by centrifugation and run on SDS-PAGE gel.

4.3 PPIase domains of SurA increase the ability to prevent aggregation

Once conditions were optimised to reproducibly analyse OMP aggregation following dilution from 8 M urea the ability of the chaperones to inhibit tOmpA or OmpT aggregation was tested again. The buffer (50 mM glycine buffer pH 9.5, 0.24 M NaCl) was prepared in the presence or absence of a SurA variant (SurA WT, SurA ΔP2, SurA N-Ct) at concentrations in excess of the substrate OMP (2x-100x) with a final volume of 50 μl (Methods 2.15.1). Rapid dilution of tOmpA or OmpT to a final concentration of 2 μM in 0.24 M urea was carried out and the measurements which monitor the increase in light scattering associated with aggregation using nephelometry were started immediately. The experiment was allowed to proceed for 30 minutes, at which time aggregation was complete as judged by the plateau in light scattering signal and the fact that the OMPs are fully insoluble in the pelleting assay (Figure 4.3). The data were analysed using both the light scattering kinetics which shows changes in lag time and apparent rate of aggregation and also were presented as end-point analysis where the final amplitude over three replicates are to allow easy comparison between conditions (Figure 4.4).

The results show that the presence of SurA WT inhibits both tOmpA and OmpT aggregation in a dose-dependent manner (Figure 4.4, Figure 4.5). A 50-fold molar excess of SurA WT prevents aggregation of tOmpA, demonstrated by no significant increase in light scattering over 30 min. By contrast, a 50-fold molar excess of SurA WT is insufficient to fully prevent OmpT aggregation, which requires a 100-fold chaperone excess as was seen upon dilution from Gdn-HCl (Figure 4.2). The requirement for higher SurA WT concentrations to prevent the aggregation of OmpT compared with tOmpA may be due to the larger size of OmpT, its higher aggregation propensity [217], a lower affinity of SurA WT for OmpT compared to tOmpA (Figure 3.11), the kinetics of the binding reaction, or a combination of these effects.

tOmpA aggregation was also inhibited by a 50 fold molar excess of SurA ΔP2 and SurA N-Ct (Figure 4.4) suggesting that removal of the PPIase domains has no effect on SurA's ability to chaperone this OMP and that again the N-Ct, the core module of SurA is a functional chaperone. The end point analysis of the effect of the SurA variants on tOmpA aggregation allows subtle differences to be detected, and reveals that at a 10-fold excess SurA WT and SurA ΔP2 both reduce the end point amplitude by approximately 50%, whereas SurA N-Ct has only a small effect at this concentration. This improvement of aggregation inhibition with the addition of the PPIase domain also correlates with the slight reduction in affinity for SurA N-Ct for tOmpA compared to the other PPIase variants (Figure 3.11).

Removal of the P2 domain alone, or both PPIase domains from SurA has a dramatic effect on the ability of SurA to prevent OmpT aggregation. Not only is aggregation of OmpT not prevented by addition of SurA ΔP2 or SurA N-Ct, but the addition of either variant increased both the rate and final amplitude of the OmpT aggregation reaction in a dose-dependent manner, reflecting an increase in the number and/or size of the aggregates formed. This also correlates with the binding data for these variants for OmpT, as the affinity is significantly reduced compared with SurA WT (Figure 3.10).

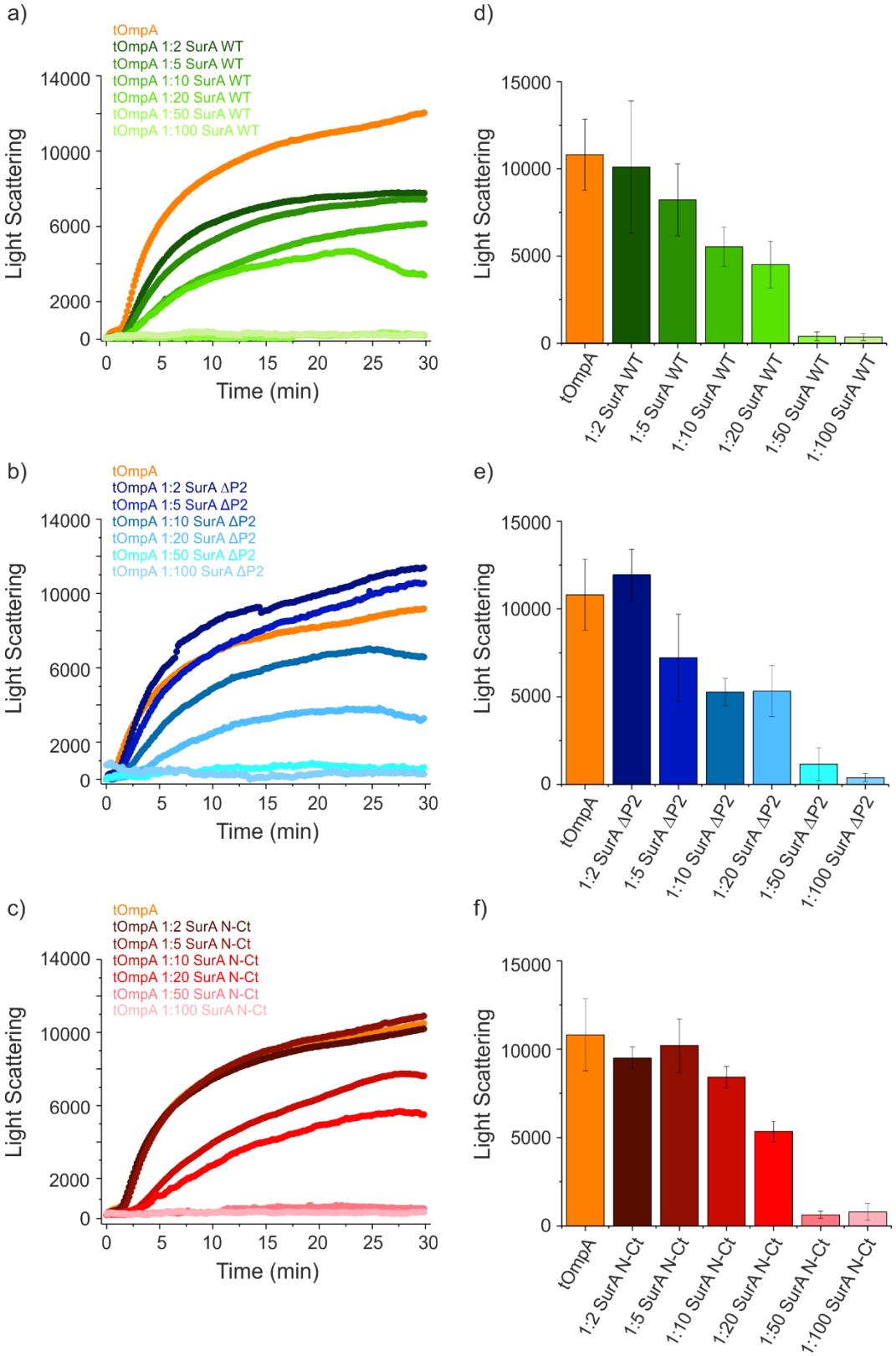

Figure 4.4 SurA variants inhibit tOmpA aggregation. (a,b,c) Aggregation of tOmpA alone (orange), and in the presence of (a) 2-100x molar excess of SurA WT (dark to light green), (b) SurA ΔP2 2-100x (dark to light blue) and (c) SurA N-Ct 2-100x (dark to light red). (d,e,f) Bar charts showing light scattering value after 30 minutes of at least three replicates of the conditions monitored in a,b and c respectively, errors are standard deviation of the replicates. Samples contained 2 μM tOmpA, 0-200 μM SurA variant, 0.24 M urea, 0.24 M NaCl, 50 mM glycine-NaOH, pH 9.5, at 25 °C.

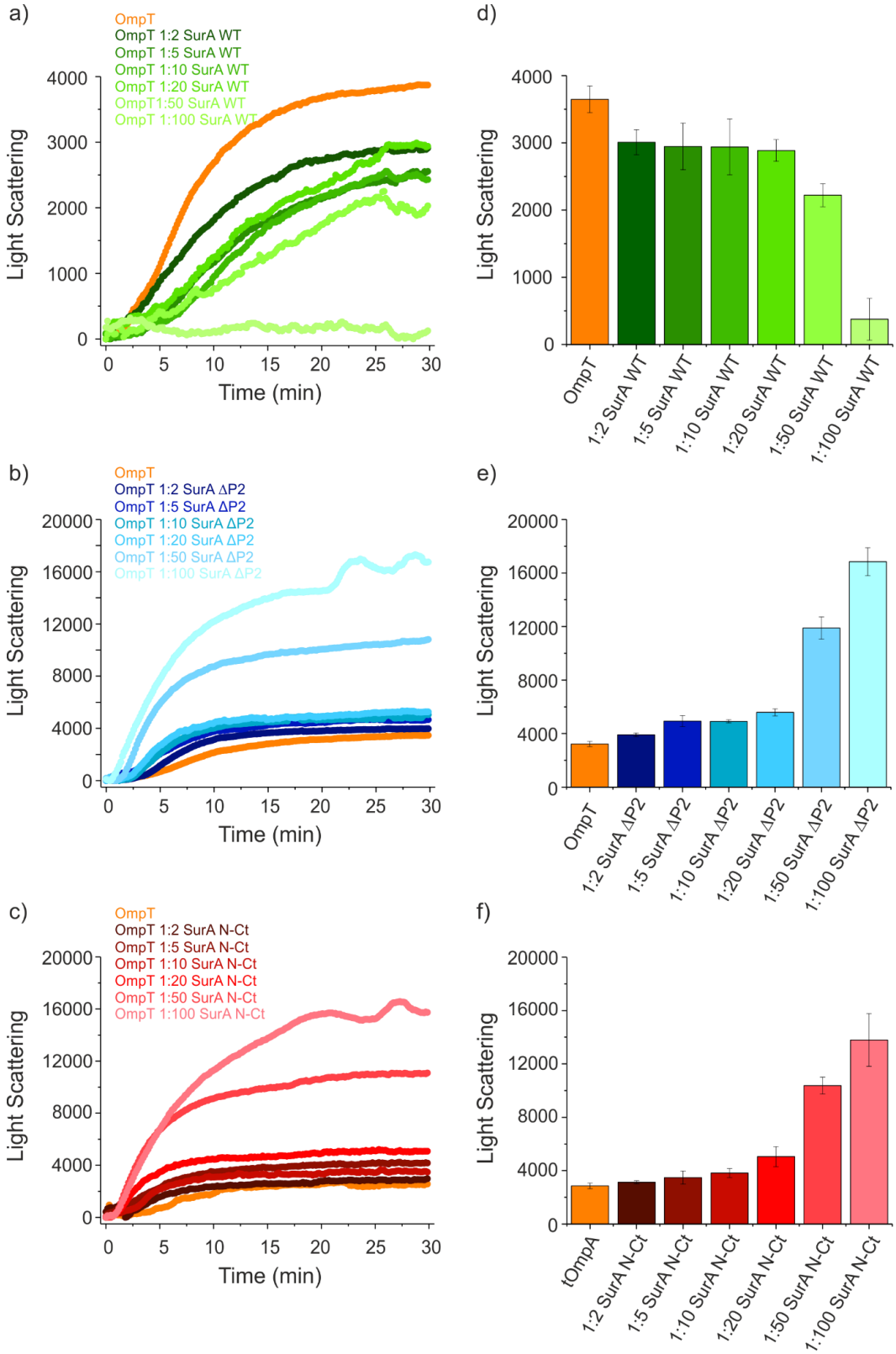

Figure 4.5 SurA WT inhibits OmpT aggregation but SurA ΔP2 and N-Ct do not. (a,b,c) Aggregation of OmpT alone (orange), and in the presence of (a) 2-100x molar excess of SurA WT (dark to light green), (b) SurA ΔP2 2-100x (dark to light blue) and (c) SurA N-Ct 2-100x (dark to light red). (d,e,f) Bar charts showing the light scattering value after 30 minutes of at least three replicates of the conditions monitored in a, b and c respectively. Errors are standard deviation of the replicates. Samples contained 2 µM OmpT/0-200 µM SurA variant, 0.24 M urea, 0.24 M NaCl, 50 mM glycine-NaOH, pH 9.5, at 25 °C.

Lag time analysis of the aggregation data sets in Figure 4.4 and Figure 4.5 was also carried out to better understand the effect of the SurA variants on OMP aggregation. A threshold of 300 light scattering units was chosen, above which the aggregation was determined to be in the exponential phase. The lag times demonstrate that the time taken to reach exponential phase is related to the concentration of chaperone added and therefor shows the same trend as the endpoint analysis.

For tOmpA the lag times increase with the a larger excess of SurA (Figure 4.6 a-c) which suggests that the SurA variants can bind to monomeric OMPs or small oligomers which are not observed in the Nephelometry assay and can slow the progression of larger or more numerous OMP aggregates forming, as well as reducing the final amplitude. OmpT with the addition of SurA WT also has a general trend of increasing lag time with increasing excess of chaperone agreeing with the final amplitude analysis. SurA ΔP2 and SurA N-Ct which were observed to increase the final amplitudes (Figure 4.5) also increased the rate of large enough aggregates to be observed in the assay. This suggests that the SurA variants which increase the rate of aggregation do so by interacting with small oligomers or monomeric OMPs to promote aggregation perhaps by being incorporated into the aggregates to drive the aggregate size. The lag time analysis has demonstrated that the SurA variants which interact with OMPs to either prevent or promote aggregation do so by altering the rate at which the enter the exponential phase, suggesting that SurA is not interacting with multimeric OMPs to disassemble aggregates but instead with monomeric or small aggregates at early time points in the reaction.

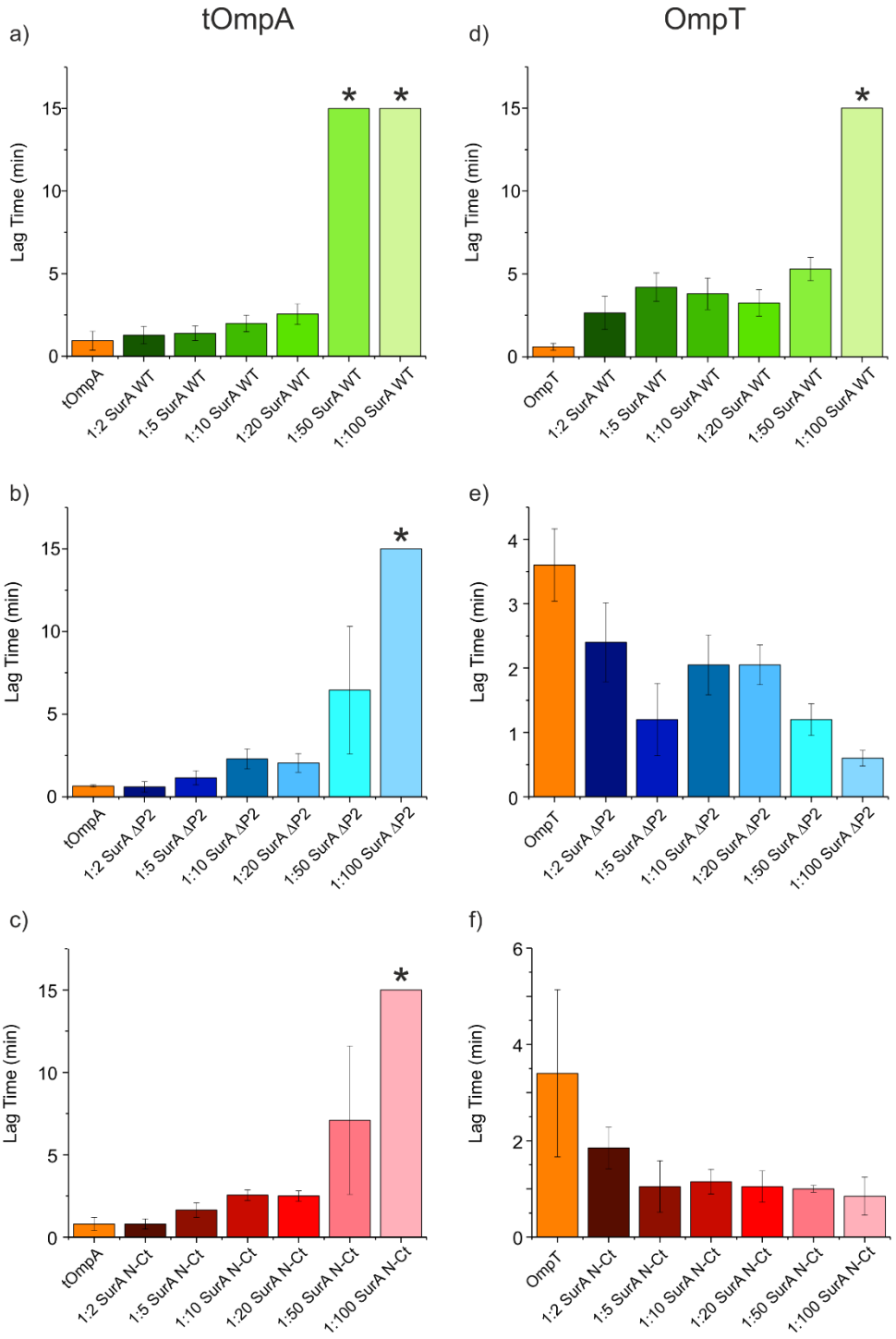

Figure 4.6 Effect of SurA variants on the lag times of tOmpA and OmpT aggregation. (a-c) Lag time values for aggregation assays in Figure 4.4 of tOmpA alone (orange) or in the presence of 2-100 molar excess of (a) SurA WT (dark to light green), (b) SurA ΔP2 (dark to light blue), or (c) SurA N-Ct (dark to light red). (d-f) Lag time values for aggregation assays in Figure 4.5 of OmpT alone (orange) or in the presence of 2-100 molar excess of (a) SurA WT (dark to light green), (b) SurA ΔP2 (dark to light blue), or (c) SurA N-Ct (dark to light red). Conditions highlighted by a star symbol indicate those in which no aggregation was detected over the experimental timescale (30 min). Lag time was measured where a light scattering value >300 was measured. Samples contained 2 µM tOmpA/OmpT, 4-200 µM SurA variant, 0.24 M urea, 0.24 M NaCl, 50 mM glycine-NaOH, pH 9.5, at 25 °C, quiescent.

4.3.1 Light scattering is caused by aggregation and the addition of SurA variants to tOmpA can prevent insoluble OMP aggregate formation

In order to determine whether the aggregation of OMPs is complete after 30 minutes and to test the extent to which the addition of chaperone prevents the formation of insoluble material, pelleting assays were carried out on tOmpA alone and in the presence of SurA WT, ΔP2 or N-Ct. The samples were prepared in the same way as is described for the nephelometry assay (Methods 2.15.1) and incubated at 25 °C for 30 minutes before centrifugation at 13,000 *g* for 1 hour to separate soluble protein from protein which has formed insoluble aggregates. The soluble and pelleted material was then run on a SDS-PAGE gel and quantified by densitometry to identify the percentage of protein in each fraction. OmpT was unfortunately not able to be monitored by this technique as it has the same molecular weight as SurA ΔP2 and the higher excess of SurA required to have an effect on OmpT aggregation causes the gel to be overloaded with SurA which prevented accurate densitometry analysis.

The results of these experiments showed that tOmpA alone after 30 minutes is mostly in the pellet as was observed in (Figure 4.3). However densitometry reveals that a small amount of soluble tOmpA is detected which cannot be observed without computational analysis (Figure 4.7 a,b). The addition of SurA at 10-fold molar excess of chaperone to tOmpA reduces the amplitude of aggregation for SurA WT and ΔP2 but N-Ct has little effect (Figure 4.4) so this concentration was used to monitor the aggregation with a pelleting assay. The amount of tOmpA in the pelleted fraction in the presence of a 10-fold molar excess of SurA WT reduced compared to pelleted tOmpA alone and the majority of tOmpA remains soluble (Figure 4.7 a,b). SurA ΔP2 appears slightly less effective than SurA WT at reducing the amount of pelleted tOmpA. However, this may be due to variability in the experiment and repeating the experiment may show that these data are actually more similar. SurA N-Ct can retain tOmpA mostly in the soluble fraction but is not as good at preventing tOmpA aggregation as SurA WT or ΔP2, consistent with the nephelometry assay (Figure 4.4).

To monitor the morphology of the aggregates formed at the end of a nephelomerty assay negative-stain transmission electron microscopy (TEM) was used as it was previously observed that thioflavin T (Tht) interacted with OmpA aggregates [215], suggesting that the aggregates formed are fibrillar in structure. tOmpA and OmpT were sampled after 30 minutes' incubation at 25 °C, deposited on a carbon-coated EM grids and stained with uranyl acetate (Methods 2.15.3). Both tOmpA and OmpT form amorphous aggregates under these conditions (Figure 4.7 c,d) which is inconsistent with the previous reports [215]. It may be the case however that there is β-structure within the amorphous aggregates, which may lead to ThT fluorescence. The pelleting assay and EM data taken together show that the light scattering output observed in the nephelometry assay is caused by OMP aggregation and that SurA can inhibit aggregation by maintaining OMP solubility.

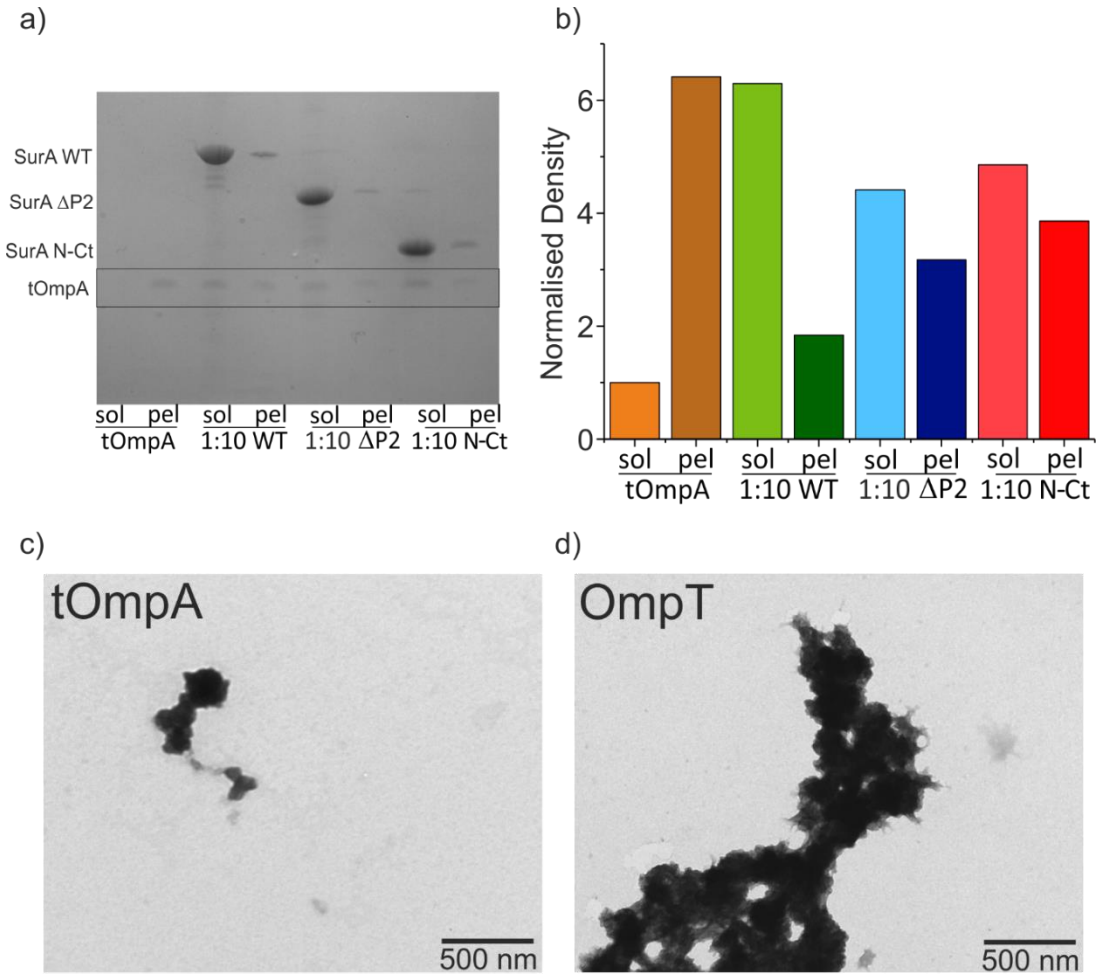

Figure 4.7 tOmpA and OmpT form amorphous aggregates a) At 30 minutes of aggregation the samples were pelleted and soluble and pelleted fractions run on an SDS PAGE gel, tOmpA band indicated by the asterisk. b) The bands were quantified by densitometry and normalised to soluble tOmpA alone (orange) to monitor the effect of 10x SurA WT (green), SurA ΔP2 (blue) and SurA N-Ct (red). b) Transmission electron microscopy (TEM) images of 2 μM tOmpA and OmpT after 30 minutes aggregation at 25 °C 50 mM glycine buffer pH 9.5, 0.24 M urea, 0.24 M NaCl.

4.4 Comparison of SurA variants with E. coli ATP-independent chaperones in preventing OMP aggregation

The finding that the PPIase domain variants have differing effects in preventing the aggregation on the two OMP substrates monitored here suggested that SurA may have specificity for certain OMPs. In order to test whether other chaperones that interact with OMPs can prevent tOmpA and OmpT aggregation, a panel of chaperones were investigated using aggregation of these two OMPs as measured by nephelometry. Here, Skp, Trigger Factor (TF), SecB, Spy and BSA as a non-chaperone control were compared to SurA WT for chaperone ability. As above, aggregation assays were performed by rapid dilution of tOmpA or OmpT stock solutions, into buffer alone or containing a 10-fold molar excess of each chaperone for tOmpA or a 20-fold molar excess of chaperone for OmpT. The solutions were incubated at 25 °C for 30 minutes and then an end-point light scattering value was measured. Importantly the chaperones do not aggregate alone under these conditions (Figure 4.8) and so any effects caused are due to the interaction of the OMP with the chaperone.

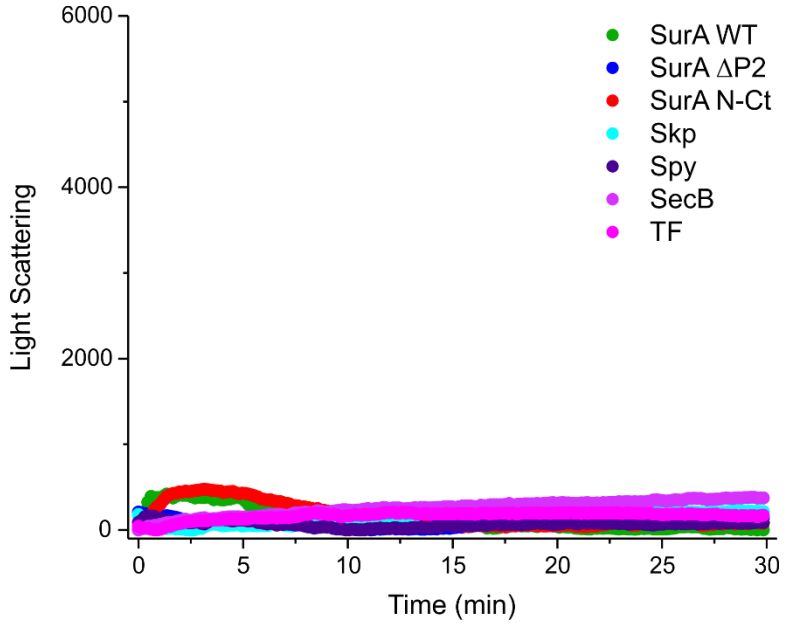

Figure 4.8 Chaperones alone do not aggregate. SurA WT (green), SurA ΔP2 (blue), SurA N-Ct (red), Skp (cyan), Spy (dark purple), SecB (light purple) and TF (pink) all at 200 μM in 50 mM glycine buffer pH 9.5, 0.24 M urea, 0.24 M NaCl.

The results for tOmpA aggregation show that a 10-fold molar excess of SurA WT considerably reduces the aggregation of tOmpA, as shown in Figure 4.4. Skp also significantly reduces tOmpA aggregation to a similar extent to SurA WT , as expected given its well-established role as an OMP chaperone [98] and nM affinity for OMP substrates [151]. SecB and TF, both of which interact with OMPs in the cytoplasm [75,245], can also significantly inhibit tOmpA aggregation, though to a lesser extent than SurA WT or Skp (Figure 4.9). Interestingly, the periplasmic chaperone Spy, which is known to be important under stress conditions [131] but had not been reported to interact with OMPs, has no significant effect on tOmpA aggregation. No reduction in scattering is seen by the addition of BSA for either tOmpA or OmpT showing that the effects caused by the chaperones are not due to the presence of any protein in solution (Figure 4.9).

OmpT was also tested with the chaperones at a 1:20 molar ratio of OMP to chaperone and the end-point analysis shows that SurA WT at this concentration does not significantly inhibit OmpT aggregation, agreeing with the kinetic analysis (Figure 4.5). Skp also cannot inhibit aggregation of OmpT under these conditions which may be due to the pH of this experiment as it is close to that of Skp (pI 9.7), which may prevent Skp's interaction with certain substrates. The cytoplasmic chaperones TF and SecB can significantly prevent OmpT aggregation than SurA WT. Interestingly, although they are carried out at different molecular excess of chaperone, TF and SecB can prevent both tOmpA and OmpT aggregation by approximately 50 % (Figure 4.9). This may be due to the cytoplasmic chaperones having a wide specificity that includes both water soluble and membrane proteins. Spy again reduced OmpT aggregation, but less well than SecB and TF, as it did for tOmpA. These data suggest that as well as chaperoning soluble proteins the excess of Spy which is observed under stress conditions [124], can also aid in the inhibition of OMP self-association, likely by interaction with hydrophobic stretches on the unfolded OMP [129-131]. Taken together these data highlight that *E. coli* chaperones have differential effects on OMP

substrates and that specificity in periplasmic chaperones plays a role in preventing the aggregation of OMPs in this dynamic environment.

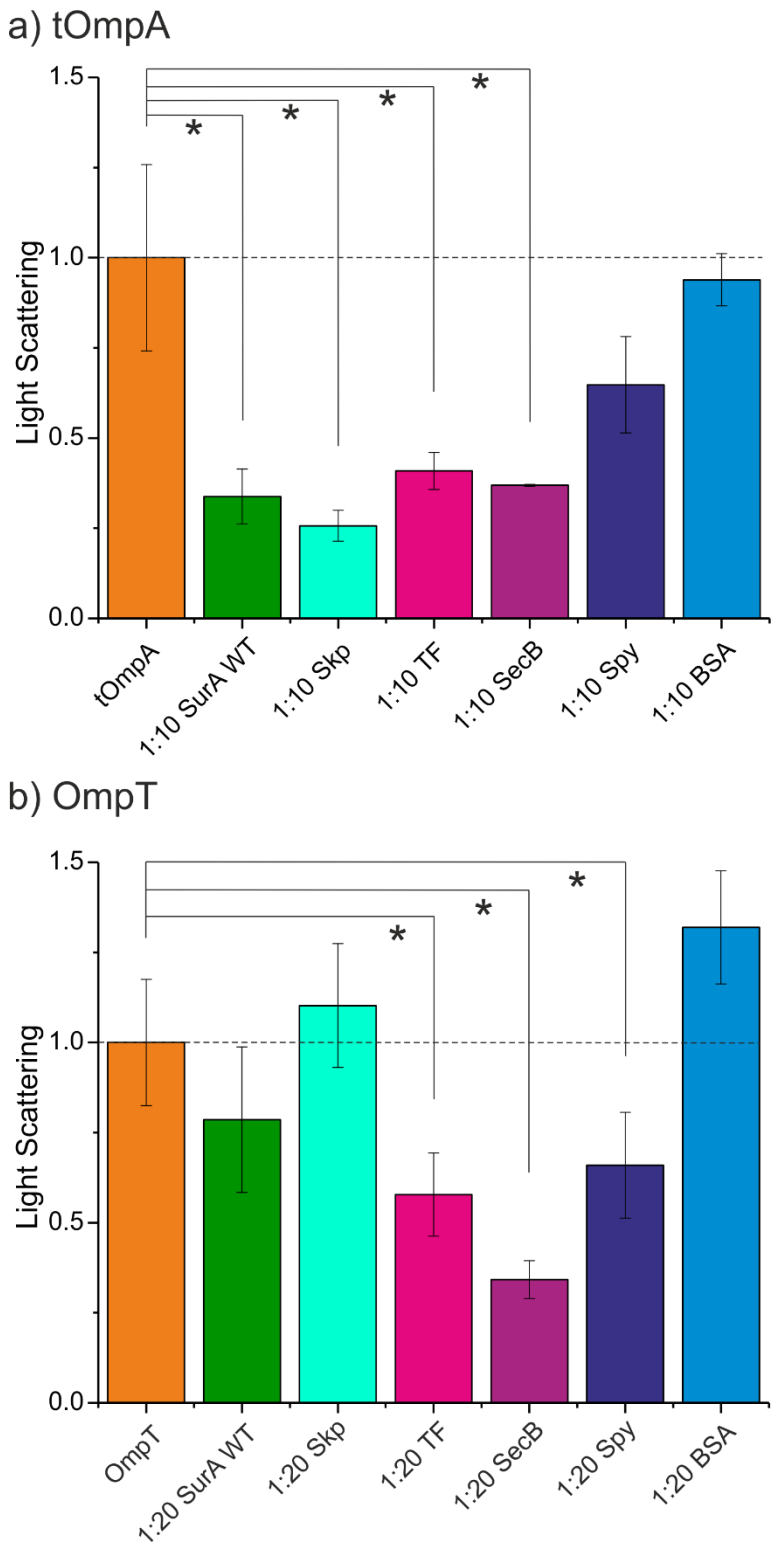

Figure 4.9 *E. coli* ATP-independent chaperones have varied effects on tOmpA and OmpT aggregation. Samples contained 2 µM tOmpA/OmpT (orange), 20 µM chaperone/BSA for tOmpA and 40 µM chaperone/BSA for OmpT 50 mM glycine buffer pH 9.5, 0.24 M urea, 0.24

M NaCl. Concentrations of Spy, Skp and SecB, are of the dimeric, trimeric and tetrameric species, respectively. Light scattering was monitored by nephelometry at 635 nm, and values were taken following 30 minutes' incubation at 25° C. Light scattering values are normalised to OMP alone normalised to 1 and horizontal dotted line to compare. * Indicate statistical difference (P-value <0.05) as tested by two sample unequal variance T-test. TF: Trigger Factor.

4.4.1 SecB can bind and prevent the aggregation of tOmpA and OmpT

The data presented above demonstrated that the cytoplasmic chaperones SecB and TF can inhibit the aggregation of both tOmpA and OmpT which has not been previously demonstrated. The binding affinities are already determined for SurA and the PPIase variants (Figure 3.11), Skp's interaction with OMPs has been documented in the nM range [151,246] and Spy has been shown to bind unfolded soluble substrates (Im7 L18A L19A L37A) with a K_d of 10.4 ± 0.1 μM [131]. However, how SecB and TF binds a range of unfolded OMPs has not been studied. Through their mechanism of binding water soluble proteins, it would appear that substrates wrap around the chaperone and bind to hydrophobic patches on the chaperone surface [82,89]. MST was used along with kinetic nephelometry assays to observe the binding and chaperoning of these chaperones for tOmpA and OmpT.

The results obtained using MST show that SecB binds to tOmpA with a Kd similar to that of SurA WT (K_d = 2.05 ±0.08 μM compared to 1.76 ±0.1 μM for SecB and SurA WT, respectively) (Figure 4.10) and these chaperones can both significantly reduce the aggregation of this OMP (Figure 4.9). SecB binds to OmpT, however, with a K_d of 0.6 ± 0.04 μM which is a significantly higher affinity than SurA WT binding OmpT (9.30 ± 0.5 μM) showing that SecB can tightly interact with this larger more aggregation-prone OMP. Interestingly when fitting uaing a Hill equation, both interactions have a Hill coefficient of >1, suggesting it may bind in a mechanism similar to that of SurA to interact with unfolded OMPs.

The inhibition of OmpT aggregation by SecB demonstrated that a 12.5- fold molar excess of tetrameric SecB could almost fully inhibit OmpT aggregation (Figure 4.10)

however a 100x excess of SurA WT is required to reduce the light scattering output to a similar level (Figure 4.5). The addition of a higher excess of SecB (25-fold molar excess) did not the increase the inhibition. This may be due to SecB having a rapid off rate for OMPs allowing a period of time in which the OMPs can aggregate before being rebound to the chaperone. This is the first evidence that SecB can interact with OMPs which have a range of sizes and that this chaperone can efficiently inhibit the aggregation of OmpT.

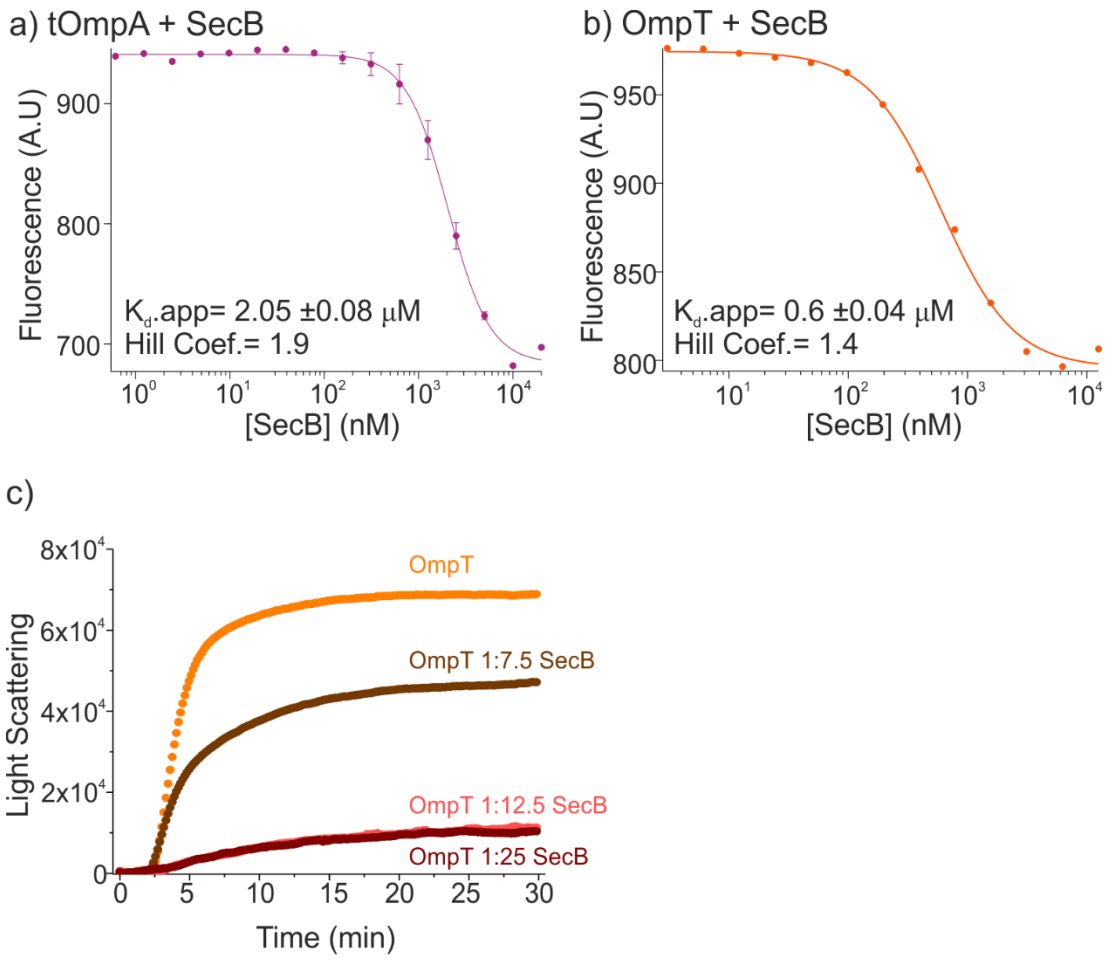

Figure 4.10 SecB can bind tOmpA and OmpT and inhibits OmpT aggregation. a) MST of tOmpA-488 with a concentration series of SecB. b) MST of OmpT-488 with a concentration series of SecB both in 50 mM glycine buffer pH 9.5, 0.24 M urea. c) Nephelometry of OmpT alone (orange) and in the presence of 7.5x (brown), 12.5x (pink) and 25x molar excess (red) SecB 50 mM glycine buffer, pH 9.5, 0.24 M urea, 0.24 M NaCl, 25 °C. All SecB concentrations are of the tetrameric species.

4.4.2 Trigger Factor can bind and prevent the aggregation of tOmpA and OmpT

SecB is thought to act specifically on proteins which are exported through the IM via the SecYEG complex [245,247]. However, TF can also interact with the ribosome and bind substrates during translation [78,82] so is likely to have a broader set of clients than SecB. Trigger factor binds both tOmpA and OmpT (Figure 4.11a,b) with a similar affinity (K_d = 4.8 ±0.2 μM and 4.2 ±0.4 μM respectively). The affinities measured for TF binding OMPs are similar to those of SurA WT, suggesting that TF may be a general chaperone in the cytoplasm which can interact with water soluble and membrane proteins. As seen for SecB, the binding of TF to tOmpA and OmpT also has positive cooperativity observed by a Hill coefficient of >1. The addition of TF to tOmpA inhibits aggregation in a concentration-dependent manner (Figure 4.11c) and at 10-fold molar excess can significantly reduce aggregation as seen in Figure 4.9. Trigger factor can bind both OMPs tested here despite them having different properties, suggesting that TF does not distinguish between OMPs.

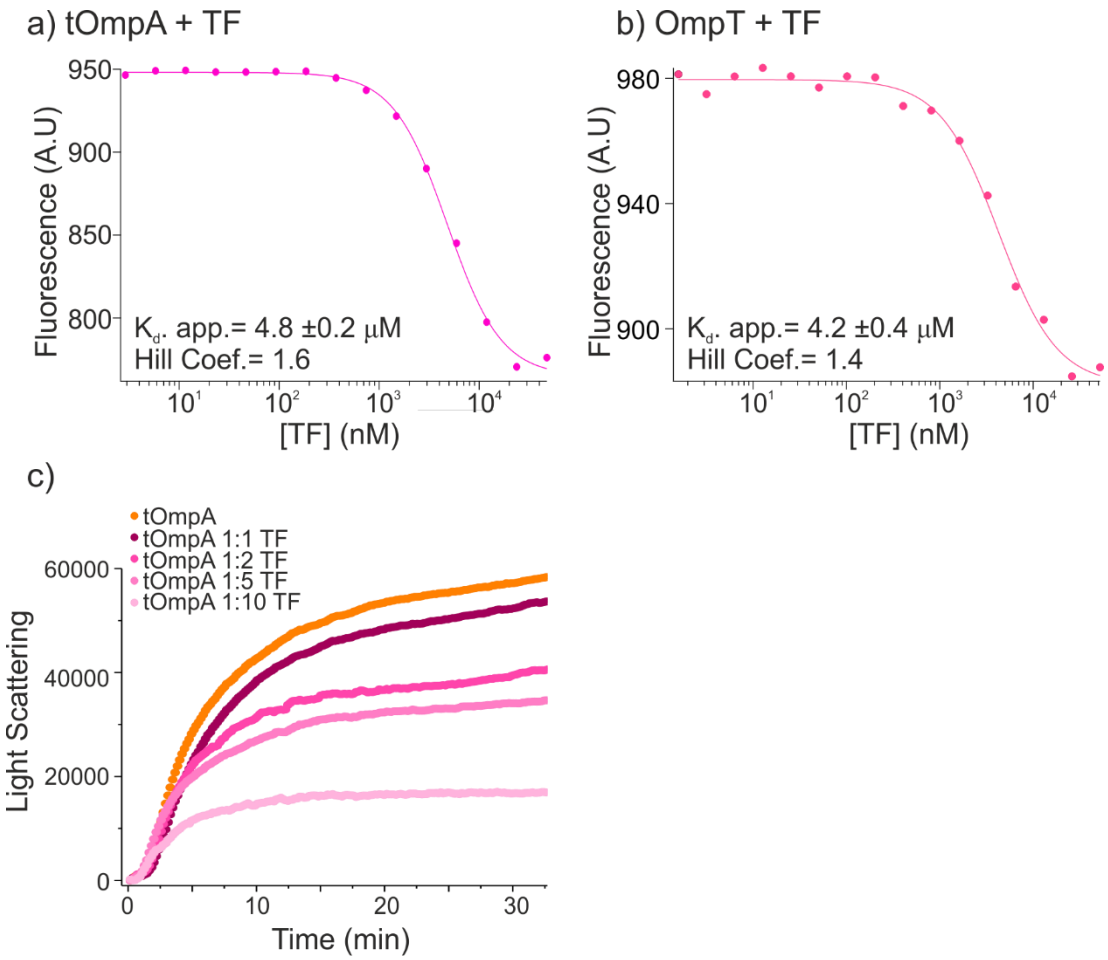

Figure 4.11 TF can bind tOmpA and OmpT. a) MST of tOmpA-488 with a concentration series of TF. b) MST of OmpT-488 with a concentration series of TF both in 50 mM glycine buffer pH 9.5, 0.24 M urea. c) Nephelometry of tOmpA alone (orange) and in the presence of 1x ,2x, 5x, 10x molar excess (dark to light pink) TF 50 mM glycine buffer pH 9.5, 0.24 M urea, 0.24 M NaCl, 25 °C.

To compare directly the effect of TF on OMPs and soluble proteins, its ability to inhibit the aggregation of tOmpA was compared to inhibition of glyceraldehyde-3-phosphate dehydrogenase (GAPDH) aggregation. GAPDH is a soluble 36 kDa protein which has previously been shown to aggregate upon dilution from 3 M Gdn-HCl into 20 mM Potassium phosphate (KPi), 100 mM KCl, 0.06 M Gdn-HCl, pH 7.0 , where a 0.5-fold TF can inhibit this aggregation [82]. A titration of 0.5-10-fold molar excess of TF over GAPDH was carried out and the concentration of chaperone required to prevent aggregation measured. The results (Figure 4.12) showed that a 5-fold molar excess prevented any significant increase in light scattering. As TF at 10x excess cannot fully inhibit the aggregation of tOmpA but can fully prevent aggregation of this soluble

substrate, it does appear that TF is more efficient at preventing soluble protein aggregation.

The SurA PPIase domain variants were also tested on GAPDH aggregation to observe if these chaperones are specialised for OMP substrates or can act as general chaperones to prevent water soluble protein aggregation. SurA variants were added to the buffer in which GAPDH was then diluted to observe any changes in light scattering. SurA WT increased the rate and final amplitude of GAPDH aggregation in a dose-dependent manner (Figure 4.12) showing that it does not prevent the aggregation of this soluble protein and even exaggerates aggregation, as was observed for SurA ΔP2 and N-Ct for OmpT (Figure 4.5). The addition of SurA ΔP2 and N-Ct also cannot prevent the aggregation of GAPDH although at certain concentrations (0.5-fold molar excess), can slightly lower the final amplitude of aggregation although it does not appear to be a significant change.

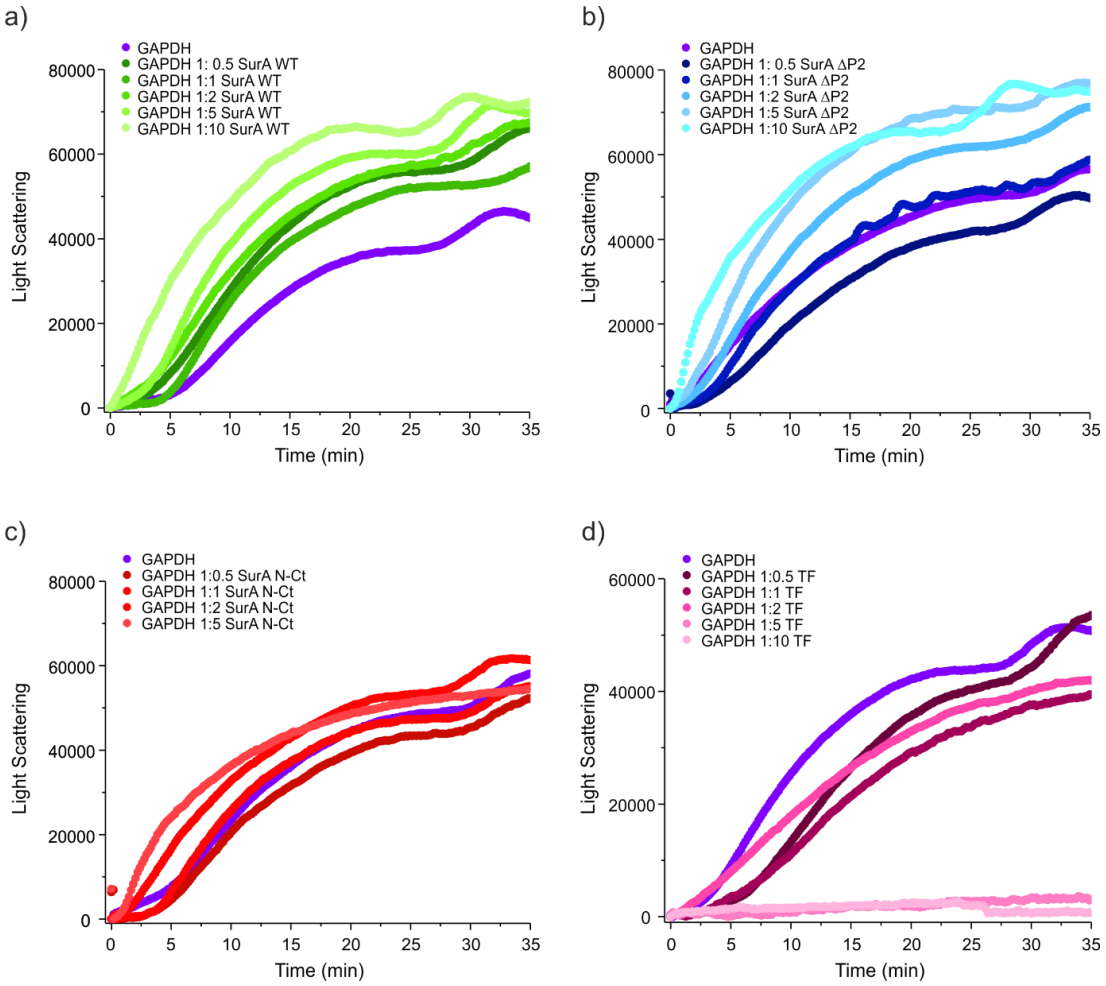

Figure 4.12 The effect of SurA WT, SurA ΔP2, SurA N-Ct and TF on GAPDH aggregation. GAPDH aggregation alone at 2 μM (purple) with the addition of 0.5 to 10-fold molar excess a) SurA WT (dark to light green), b) SurA ΔP2 (dark to light blue), c) SurA N-Ct (dark to light red) and d) TF (dark to light pink). All experiments carried out in 20mM potassium phosphate buffer pH 7.0, 100mM KCl 0.06M Gdn-HCl and light scattering measured by nephelometry at 365 nm.

4.4.3 SurA can prevent the fibril formation of Aβ40 but Skp and Spy cannot

Multiple chaperones have been observed to prevent the aggregation of disease-related amyloid-forming proteins such as Hsp40 family proteins [248], Hsp70, Hsp90 [15,249] BRICHOS domains [250] and others. Here we use Amyloid-β 40 (Aβ40) as a test protein as it is intrinsically disordered and is highly aggregation prone and so may mimic the collapsed state of an OMP in the periplasm, which is the state that these chaperone will encounter and must prevent from self-association. Amyloid formation

and the inhibition thereof is often monitored by ThT fluorescence assays [208]. ThT is a small molecule that gives a strong fluorescence signal upon binding to beta-sheet amyloid fibrils [208] and so a change in lag time or a reduction in final amplitude of fluorescence can indicate that the chaperones are having an effect on amyloid formation [251,252]. $A\beta_{40}$ has been well studied [251,253] and it gives reproducible aggregation kinetics [254]. SurA WT, Skp and Spy were added to $A\beta_{40}$ at a 2:1, 1:1 and 1:2 chaperone to substrate molar ratio to observe any changes in aggregation. The results show that SurA can prevent $A\beta_{40}$ aggregation even at sub-stoichiometric concentrations over 60 hours whereas, at a 2-fold molar excess, Spy and Skp increase the aggregation lag time, but do not inhibit the aggregation (Figure 4.13). This demonstrates that these ATP-independent periplasmic chaperones have differing effects on amyloid forming non-native substrates and may suggest that they equally do not have the same mechanism on unfolded OMP substrates.

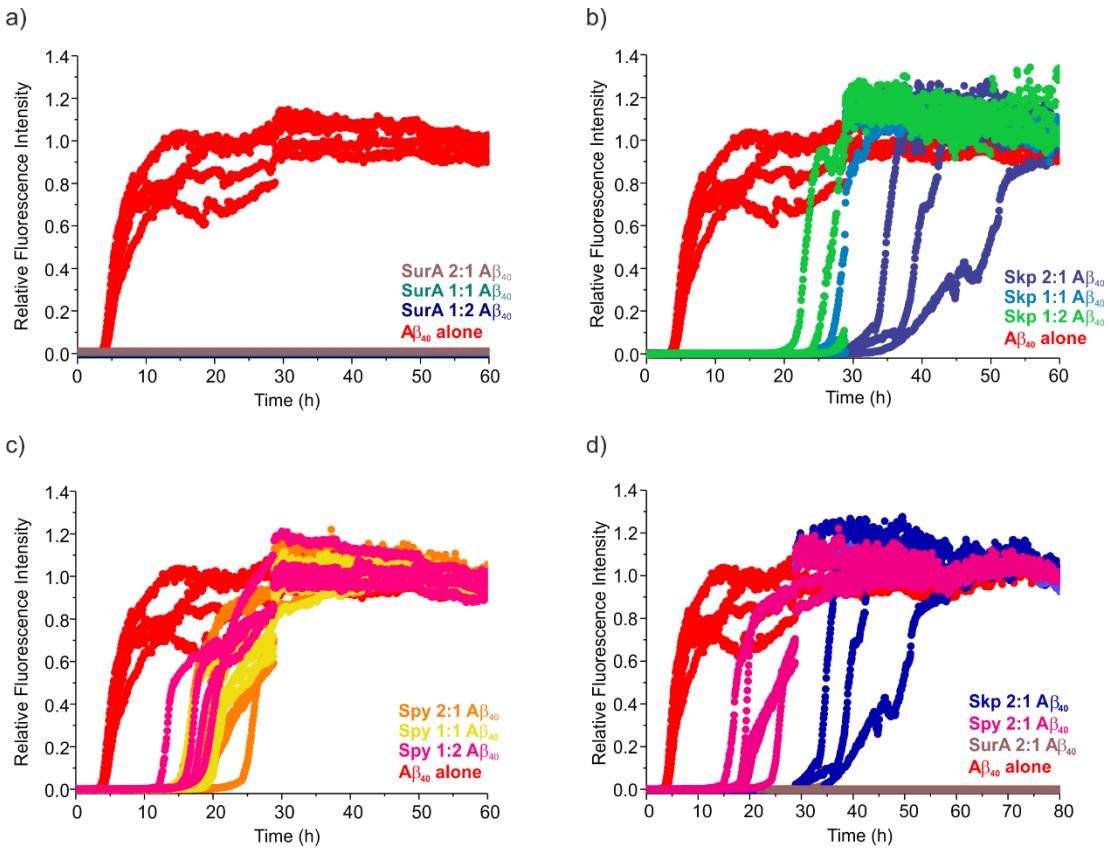

Figure 4.13 ATP-independent periplasmic chaperones SurA WT, Skp and Spy have differing effects on $A\beta_{40}$ amyloid formation. $A\beta_{40}$ alone in red and the addition of a) SurA WT, b) Skp

and c) Spy at 2:1, 1:1 and 1:2 chaperone: substrate molar ratios. Final concentration of $A\beta_{40}$ is 20 µM in 20 mM monobasic sodium phosphate, 0.2 mM EDTA, 0.02% NaN_3, pH 7.4.

4.5 Discussion

The role of SurA in OMP biogenesis is well documented through *in vivo* studies as the removal of SurA causes membrane defects and reduced levels of OMPs folded into the OM [50,167,168]. However, how SurA can hold its substrates in an extended conformation and prevent aberrant inter- and intra-molecular interaction has not been well studied. This is the first detailed analysis of SurA's function in preventing the aggregation of native OMP substrates, looking at the role of the PPIase domains and comparing SurA to other ATP-independent *E. coli* chaperones.

An interesting finding from the development of the nephelometry assay is that the OMPs (tOmpA and OmpT) have different aggregation propensities when diluted from high concentrations of Gdn-HCl or urea. OmpT alone, in particular, aggregates rapidly with a lag time of 2.5 minutes and has plateaued after 10 minutes suggesting that all the OmpT is insoluble by this time in Gdn-HCl (Figure 4.2). OmpT has a higher final light scattering signal than tOmpA suggesting that it forms larger or more numerous aggregates than tOmpA which agrees with previous studies [217]. Dilution of OmpT from 8 M urea, however, results in a lower final signal than tOmpA (Figure 4.3) suggesting that the denaturant and salt concentration plays a role in the ability of certain OMPs to form aggregates.

The titration of SurA domain variants allows detailed analysis of the role of PPIase domains in chaperoning. Removal of one or both PPIase domains slightly reduced SurA's ability to prevent the aggregation of tOmpA however all three variants have some effect (Figure 4.4), consistent with *in vivo* findings that bacterial strains lacking SurA WT and containing SurA homologues lacking PPIase domains are viable [165]. Along with the binding data which showed that SurA N-Ct binds tOmpA with a similar affinity to SurA WT (Figure 3.11), these data show that SurA N-Ct is a functional chaperone however appears to work best on smaller OMPs such as tOmpA.

SurA WT can reduce the light scattering amplitude of tOmpA by approximately 50% with a 10-fold molar excess and 50-fold molar excess fully preventing aggregation (Figure 4.4), however even at a 50-fold molar excess of SurA WT the aggregation of OmpT is only reduced by around 30%, with 100-fold molar excess being required to inhibit OmpT aggregation (Figure 4.5). The difference in the excess of SurA WT required to retain different OMPs in a soluble form may be linked to the OMP molecular weight as OmpT is almost twice the size of tOmpA (37 kDa compared to 19 kDa). However, a larger sample size will be needed to reveal other features that may also play a role, such as the presence of soluble domains, the binding affinity of chaperone to OMP and the aggregation propensity of the OMP sequence. The large excess of chaperone required may also be due to a small amount of the chaperone getting incorporated into the aggregates as observed in (Figure 4.7) for SurA WT, ΔP2 and N-Ct during tOmpA aggregation. The finding that the excess of chaperone required to prevent OMP aggregation is much larger than the Kd measured for these interactions which suggests that the interaction is more complex than a 1:1 sequestration in order to prevent self-association and there is a more complex mechanism of the chaperone. These findings alongside the demonstration that this interaction is positively cooperative, as suggested by the hill coefficient, suggest that multiple chaperone molecules are binding along an unfolded OMP chain, akin to the 'beads on a sting' model which has proposed for other chaperones. Many chaperone molecules binding likely to the exposed hydrophobic patches along the OMP could efficiently prevent self-association and aggregation, and further structural analysis, such as cryo-EM, would be needed to test this hypothesis.

The removal of one or both PPIase domains has a strikingly different effect on OmpT aggregation compared with its effect on tOmpA. Addition of either SurA ΔP2 or SurA N-Ct to the OmpT aggregation mixture increases the rate and final amplitude of aggregation (Figure 4.5). The increase in final amplitude suggests that larger aggregates are formed and it may be that these chaperone variants are incorporated into the OmpT aggregates. The ability of SurA WT to inhibit OmpT aggregation while

SurA ΔP2 and N-Ct cannot suggests one explanation for the acquisition and retention of the PPIase domains through the evolution of bacterial classes (Figure 3.23). SurA homologues with two PPIase domains may be able to chaperone a more diverse range of substrates which may also be larger in size and also more aggregation-prone in sequence. As it has previously been shown that SurA N-Ct is more effective than SurA WT at preventing the aggregation of citrate synthase [165] it may be that the addition of the PPIase domains have increased the range of OMPs that SurA can bind at the expense of chaperoning soluble proteins. However, the findings presented here suggest that SurA N-Ct is not effective at preventing the aggregation of GAPDH. Bacterial strains with SurA homologues that lack these domains may have a smaller set of substrates which they can chaperone or larger OMPs such as OmpT may not interact with SurA but instead rely on different periplasmic chaperones. Further studies will be needed *in vivo* to test this hypothesis.

Previous studies have suggested that the periplasmic chaperones SurA, Skp and DegP act in a redundant pathway [143,169]. Although SurA has been identified as the major OMP chaperone, it is not known if all OMPs are chaperoned by SurA under normal conditions and other chaperones are employed under stress conditions, or whether certain OMPs have specificity for certain chaperones. To test this, the nephelometry assay was used to compare *E. coli* chaperones from the periplasm (SurA, Skp and Spy) with cytoplasmic OMP chaperones (TF and SecB) and BSA as a non-chaperone control. A 10-fold molar excess of all chaperones was used to monitor changes in tOmpA aggregation and a 20-fold molar excess was used for OmpT as differences can be identified between the SurA domain variants at these concentrations. Under these conditions, Skp was shown to be as effective as SurA WT at preventing tOmpA aggregation, however Skp has no effect on OmpT (Figure 4.9). Skp is also not as effective as SurA WT at preventing the fibrillation of $A\beta_{40}$ (Figure 4.13). Taken together, these data suggest that Skp specifically can prevent the aggregation of certain substrates. SurA WT, however, is effective at preventing the aggregation of a range of OMPs and also the amyloid forming $A\beta_{40}$ suggesting that it has evolved to

chaperone many substrates and is not as specialised as Skp, at least for the range of outer membrane protein substrates studied here.

TF and SecB, the cytoplasmic chaperones tested, are effective at preventing the aggregation of both tOmpA and OmpT, demonstrating that they may be better general chaperones of aggregation-prone clients. SecB binds to the larger OMP, OmpT with higher affinity than for tOmpA and also is very effective at preventing OmpT aggregation (Figure 4.10) providing evidence that SecB may have evolved to interact with larger or more aggregation-prone substrates. A lower excess of TF is required to prevent aggregation of the soluble protein, GAPDH, (Figure 4.12) than is needed to prevent aggregation of tOmpA (Figure 4.11), suggesting that for this chaperone is better at chaperoning soluble substrates than OMPs while maintaining its ability to prevent aggregation of very different substrates. It has been noted that structurally similar elements are observed in the core domain of SurA and the substrate binding domain of TF (Figure 4.14) [255]. As this work has shown that the N- and C-terminal domains of SurA can bind and chaperone substrates, it is likely that TF and SurA may interact with clients in a similar manner and may have evolved from a common ancestral chaperone. However, they now reside in different cellular compartments. If this is the case the *E. coli* TF and SurA will have evolved specialised functions as TF interacts with the ribosome [78,81] and SurA interacts with the BAM complex [180,182].

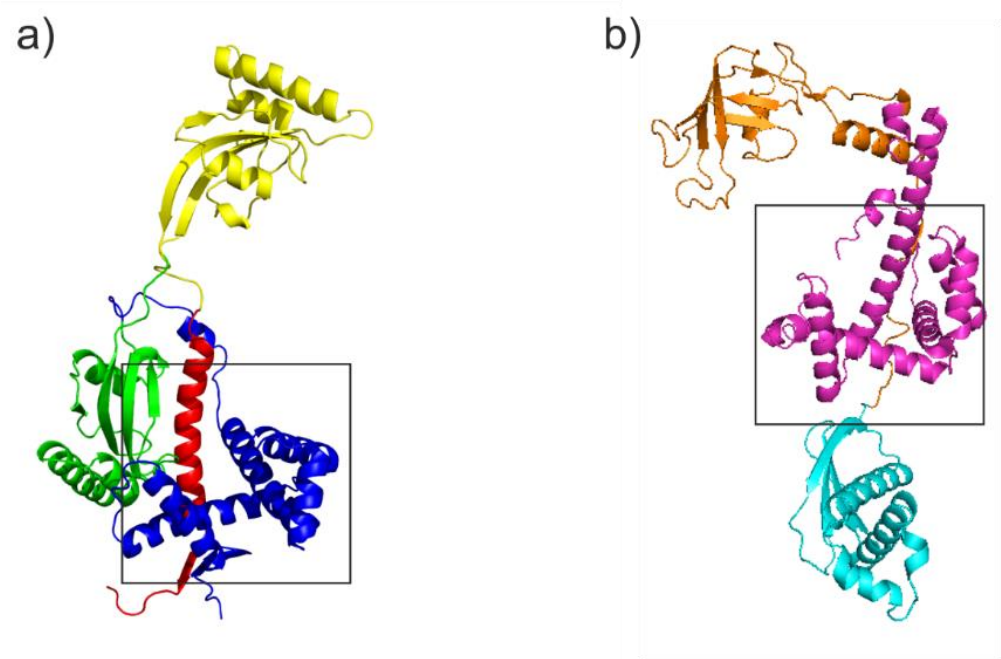

Figure 4.14 Comparison of 'clamp domains' of SurA and trigger factor. a) Crystal structure of SurA (PDB: 1M5Y) [69]. N-terminal domain in blue, P1 in green, P2 in yellow and the C-terminal domain in red. b) Crystal structure of trigger factor (TF) (PDB: 1W26) [33,78]. N-terminal ribosome binding domain (RBD) in blue, PPIase domain in orange and C-terminal substrate binding domain (SBD) in magenta. Boxes indicate the region of structural similarity between the core domain of SurA and the substrate binding domain of TF

Overall, the comparison between the *E. coli* chaperones show that their interactions with OMPs all show positive cooperativity and that if they do have the ability to inhibit OMP aggregation this requires a molar excess of chaperone, of at least 10-fold excess. The results thus suggest a new model for a general mechanism of ATP-independent chaperones, in which multiple chaperones interact with an unfolded OMP chain in order to prevent aggregation by multiple rounds of substrate binding and release.

Chapter 5 Investigating the mechanism by which SurA interacts with and delivers OMPs to the BAM complex

5.1 Introduction

The previous chapters have investigated how SurA interacts with OMPs and prevent their aggregation. Here, the interaction of SurA with the BAM complex is tested. OMPs require chaperones for their transport to the inner membrane [92,256] and then across the periplasm [6,212], however how they are the delivered to the BAM complex and inserted into the membrane is currently not known. The hypothesis that periplasmic OMP chaperones directly interact with the BAM complex, delivering OMPs for folding has been proposed as SurA has been crosslinked to BAM *in vivo* [50,180,182,183] and mutations within SurA alter the levels of OMPs folded into the membrane [257]. However, whether this is solely due to proximity of the chaperone to the OM remains unsolved. In this chapter, MST is used to detect whether there is an interaction of SurA or Skp with the BAM complex folded into detergent micelles and to determine the role of the SurA PPIase domain variants in delivering tOmpA and OmpT to BAM for folding.

Many studies have reported the spontaneous folding of OMPs into lipid bilayers [99,220,258] however the kinetics is too slow to be biologically relevant [97]. As removal of the BAM complex is lethal *in vivo* [96] and *in vitro* assays have demonstrated that this complex increases the rate of folding of OMPs into membranes [97], it is thought that the BAM complex must catalyse folding of OMPs. The mechanism by which BAM aids in the folding and insertion of OMPs into the outer membrane is currently unknown, however multiple methods have been proposed based on several studies [64,259,260]. Destabilising of the lipids in close proximity to BAM may reduce the energy barrier for folding in the membrane, passively creating a localised area for easier insertion of OMPs [64,97]. Alternatively, the incomplete hydrogen bonding network between β1 and β16 strands of the BamA barrel may present a surface on which new β-strands may template [71]. Otherwise, BAM may function by a combination of these along with

other features to catalyse OMP insertion (Figure 1.9). Further structural analysis of BAM in contact with a folding substrate will elucidate which of these hypothesis are correct.

The method by which OMPs reach the BAM complex also remains enigmatic. SurA has been crosslinked to the BamA subunit POTRA domain 1 as determined by SDS-PAGE pull down analysis [50,183] however a complex of SurA and BamA could not be co-purified suggesting that this interaction is weak or transient [50]. Deletion of the N-terminal POTRA 1 domain from BamA , showed OMP folding defects [182] and it was thought to be caused by an interruption of SurA binding BamA. Single site mutations of POTRA 1 suggested that SurA not only interacts with the POTRA 1 domain of BamA, but it interacts in close vicinity to the R64 residue of the α2 helix [182] (Figure 5.1a). An independent study then observed that the residues between 311 and 316 of the P2 domain of SurA could be crosslinked to the BAM complex [180] (Figure 5.1b). Sucrose density gradient analysis of cells showed that under non-stressed conditions SurA is found in both the inner and outer membrane fractions however in BamA-depleted cells, SurA is no longer found at the outer membrane [180]. Taken together, it appears that SurA interacts with the BAM complex *in vivo.* Whether this interaction is on the OMP folding pathway and if this interaction can occur in the presence of an unfolded OMP substrate is not known.

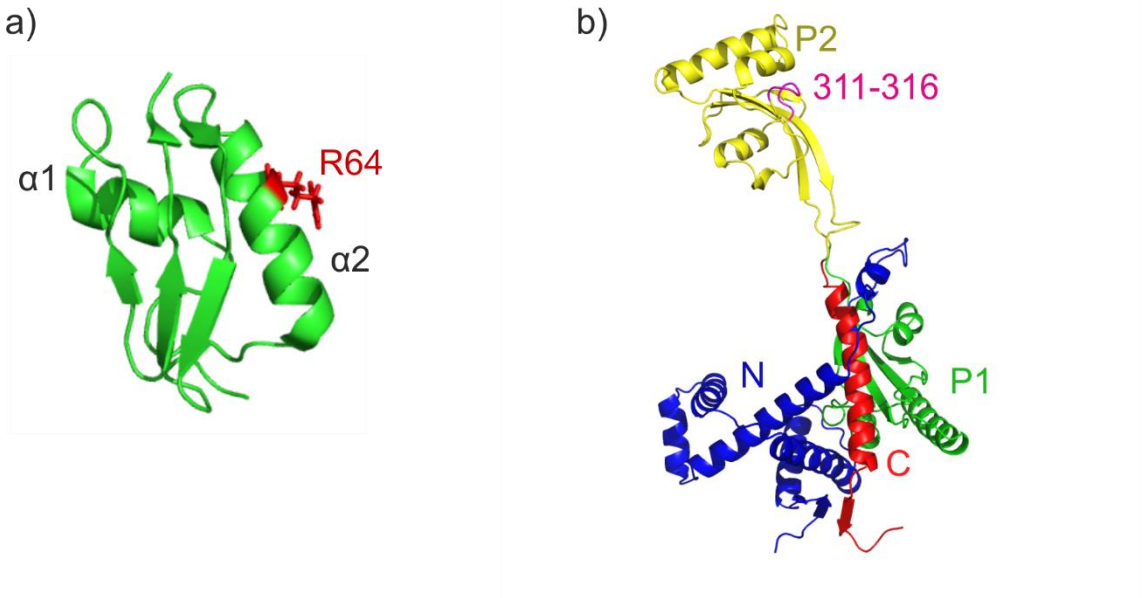

Figure 5.1 Regions of POTRA 1 and SurA found to interact by crosslinking. a) POTRA 1 (PDB: 5LJO)[71] and R64 in the α2 helix highlighted in red b) SurA (PDB: 1M5Y)[69] residues 311-316 in the P2 domain (yellow) highlighted in pink.

The presence of parallel redundant pathways that utilise different periplasmic chaperones have been proposed by genetic studies [50,169]. As SurA was observed to crosslink to BAM yet under the same conditions no interaction between Skp or DegP and BAM could be observed, it was suggested that the chaperones may have some substrate specificity with a handover to SurA which can then interact with BAM [52] for OMPs folding This was tested by mass spectrometry analysis of these complexes *in vitro* [98] however, no handover events were observed when tOmpA-loaded Skp was added to SurA [97]. The tight binding of Skp to OMPs in the nM range [151,241,246] and the encapsulation of OMPs in the cavity of Skp [98,149] make it unlikely that Skp can spontaneously release OMPs to another chaperone or into solution for folding. However, other mechanisms by which Skp substrates interact with the BAM complex have not been proposed. An alternative pathway in which Skp delivers substrates directly to the OM and bypasses BAM, is supported by *in vitro* data which have shown that the highly positively charged 'tentacle' tips of Skp can deliver OMPs directly to negatively charged bilayers [143]. Indeed, recent data which suggest that Skp can deliver substrates into membranes *in vivo* [261].

The choreogrpahy of OMP release from chaperones and subsequent interaction with the BAM complex is an important step for OMP folding. Depending on the mechanism by which OMPs are incorporated into the membrane via BAM, large portions of the unfolded OMP chain may remain in the periplasm which must be protected from aggregation or degredation. The role of chaperones in the delivery of OMPs to BAM is studied in this chapter.

In the work presented in this chapter, Anna Higgins (University of Leeds) prepared the BAM complex in DDM and proteoliposomes as described in [71] and carried out the OmpT folding assay. The tOmpA folding assay was carried out with Dr Bob Schiffrin (University of Leeds).

5.2 SurA directly interacts with the BAM complex and the interaction is mediated by the P2 domain of SurA

The interaction of SurA with the BAM complex has been detected using an *in vivo* crosslinking approach [180,182]. This result could however be down to a non-specific interaction due to proximity of the proteins within the crowded periplasm. To determine whether there is a direct binding event between SurA and the BAM complex, MST was employed. The BAM complex was purified in DDM detergent (Methods 2.4.5) and confirmed to be folded. N-terminal cysteine variants were created in SurA WT, SurA ΔP2 and SurA N-Ct and were labelled with Alexafluor 488 dye (Methods 2.14.1). Labelled SurA was then mixed with a titration of BAM complex folded in DDM.

The results of these experiments showed that, SurA WT binds to the BAM complex folded into DDM with a K_d of 0.09 ± 0.01 μM (90 nM) (Figure 5.2). This is the first direct evidence of SurA's interaction with the BAM complex *in vitro*. The binding curve was fitted to a 1:1 binding model as this fit the data well, suggesting that multiple SurA molecules do not bind to BAM. Replacing SurA WT with either of the

domain variants (SurA ΔP2 or SurA N-Ct) in this assay showed that although there is some binding shown by a change in fluorescence intensity, the affinity of SurA lacking a single or both PPIase domains for BAM is significantly reduced. Neither of the binding curves of SurA ΔP2 or SurA N-Ct binding to BAM can be fitted as there is no post transition baseline making it difficult to estimate a K_d. However, a change in fluorescence is only observed above 1000 nM (1 μM) concentration of BAM where a significantly lower concentration of BAM (~20 nM) is required to initiate a transition upon binding to SurA WT.

As an interaction is still observed for SurA N-Ct binding to the BAM complex (Figure 5.2 c) this suggests that multiple regions of SurA are involved in the interaction and that these regions are spread across the whole of the SurA molecule, including the core domain. The main region of interaction of SurA appears to be in the P2 PPIase domain as removal of this domain alters the affinity dramatically, in accord with *in vivo* binding studies (Figure 5.1b) [180].

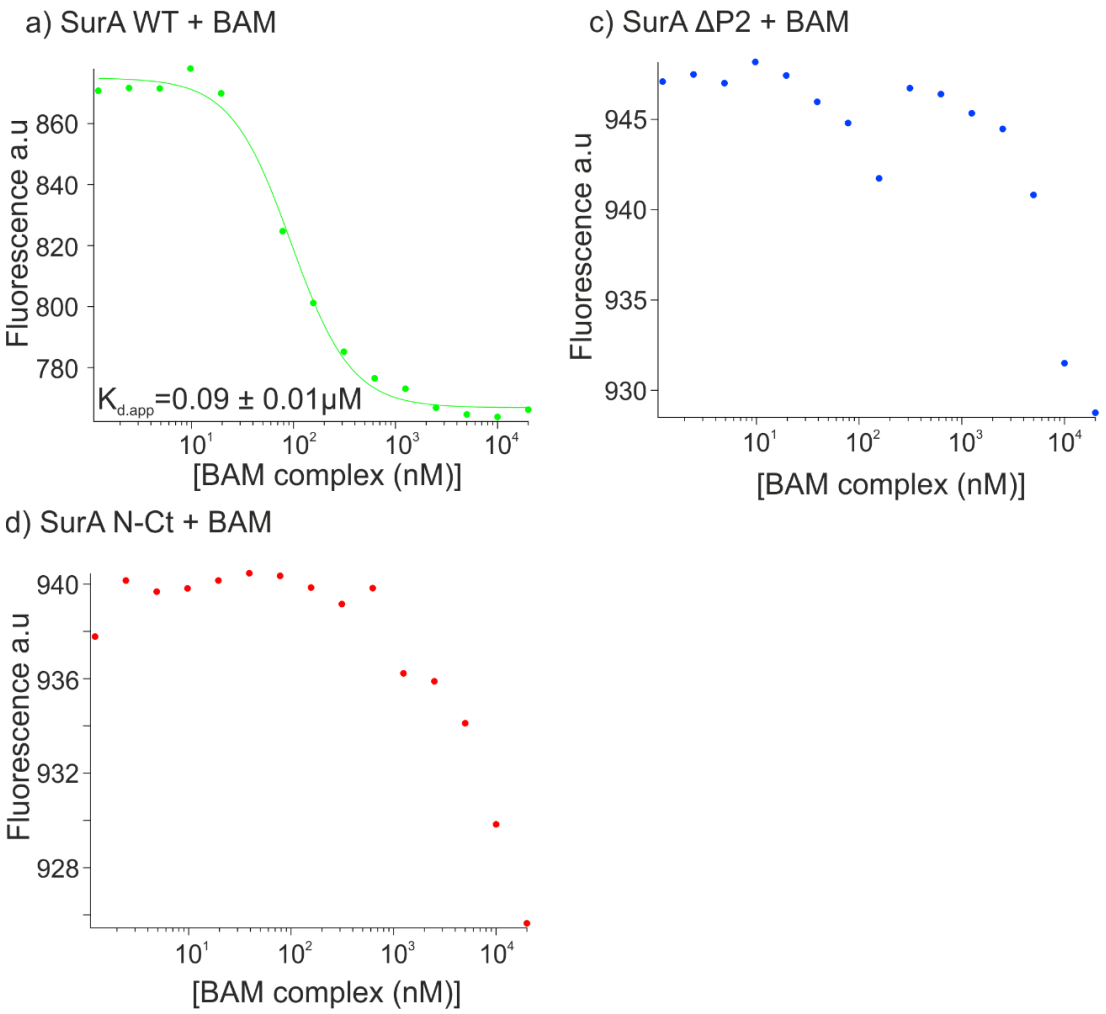

Figure 5.2 Removal of the P2 domain reduces SurA's ability to bind the BAM complex. Microscale thermophoresis binding curves of a) SurA WT-AF_{488}, b) SurA ΔP2-AF_{488}, c) SurA N-Ct-AF_{488}, binding to BAM folded in DDM. Samples contained 100 nM SurA-AF_{488}, 1.2 nM -40 µM BAM complex, 50 mM TBS, 150 mM NaCl, pH 7 at 25 °C. Three replicates were recorded and averaged prior to fitting and the error of the fit plotted as error bars. AF_{488} : AlexaFluor 488 dye

The binding of SurA WT to BAM was then quantified in liposomes. The BAM complex was reconstituted into *E. coli* polar lipid extract using dialysis (Methods 2.4.5) and concentrated to a stock of 100 µM allowing a titration of 50 µM- 1.5 nM of BAM against labelled SurA WT (100 nM).

Interestingly, the tight interaction observed between SurA WT and BAM in DDM is not replicated in proteoliposomes formed from *E.coli* polar lipids. Again a change in fluorescence is observed indicating that there is an interaction, but under these

conditions the binding has a weak affinity. Labelled SurA WT was also tested against a titration of empty liposomes to observe if this change in fluorescence is due to the chaperone interacting with the increasing concentration of lipids and not directly with BAM. When empty liposomes are added no change in fluorescence is observed over these concentrations (Figure 5.3b), suggesting that the interaction seen in Figure 5.3a is reporting on a direct interaction between SurA and BAM and that SurA does not simply interact with lipids.

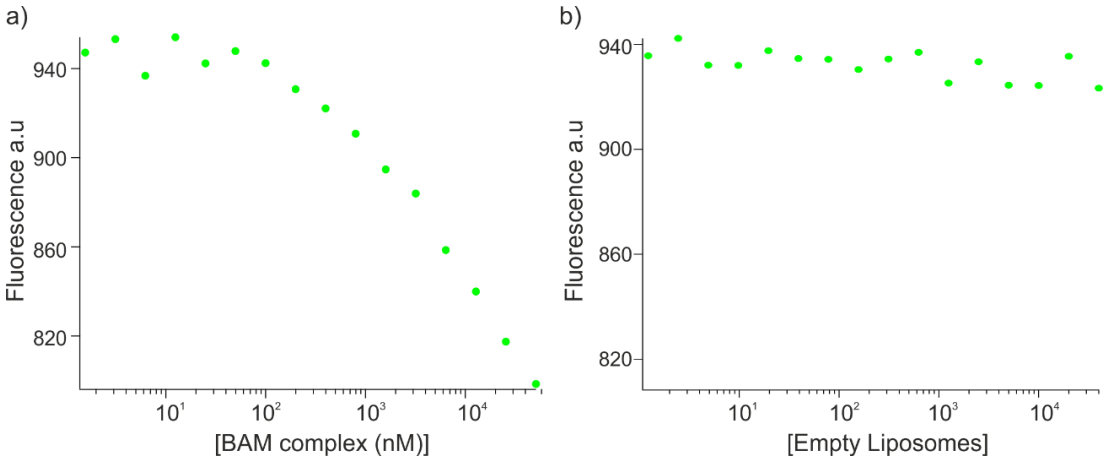

Figure 5.3 SurA WT has reduced binding of BAM in proteoliposomes compared to detergent. Microscale thermophoresis binding curves of SurA-AF_{488} binding to a) BAM folded in proteoliposomes, b) empty liposomes. Samples contained 100 nM SurA-AF_{488}, 1.5 nM -50 μM BAM complex, 50 mM TBS, 150 mM NaCl, pH 7 at 25 °C. Three replicates were recorded and averaged. AF_{488} : AlexaFluor 488 dye

The binding of SurA with BAM was also tested by 2D-TROSY NMR as described in Methods 2.16.2. ^{15}N labelled SurA was buffer exchanged into 25 mM MES, 150 mM NaCl, 0.05% (w/v) DDM, pH 6.5 at 70 μM and measured alone to observe the apo state of the chaperone in detergent (Figure 5.4a). Although only a few residues are observed, any major changes induced by the addition of BAM should still be detected. The low abundance of peaks is likely caused by the size of SurA WT, production and purification of the sample in deuterium would result in a better spectrum [262]. The BAM complex in the same buffer was added to a final concentration of 35 μM, so the SurA is 50% bound under these conditions, given the K_d.

The spectrum of ^{15}N SurA in the presence of BAM has fewer peaks than SurA alone and the peaks which remain are less intense (Figure 5.4). The loss of peaks occurs as a result of line broadening, and suggests that the residues that give rise to them are involved in the interaction with BAM. Another explanation could be that there is a conformation change upon binding which alters the environment of these residues. As the peaks which do remain do not undergo a significant change in chemical shift, a major shift in the structure of SurA upon binding to the BAM complex is unlikely. As many of the peaks are lost, it suggests that multiple regions of SurA are involved in the interaction with BAM which agrees with the binding data (Figure 5.2).

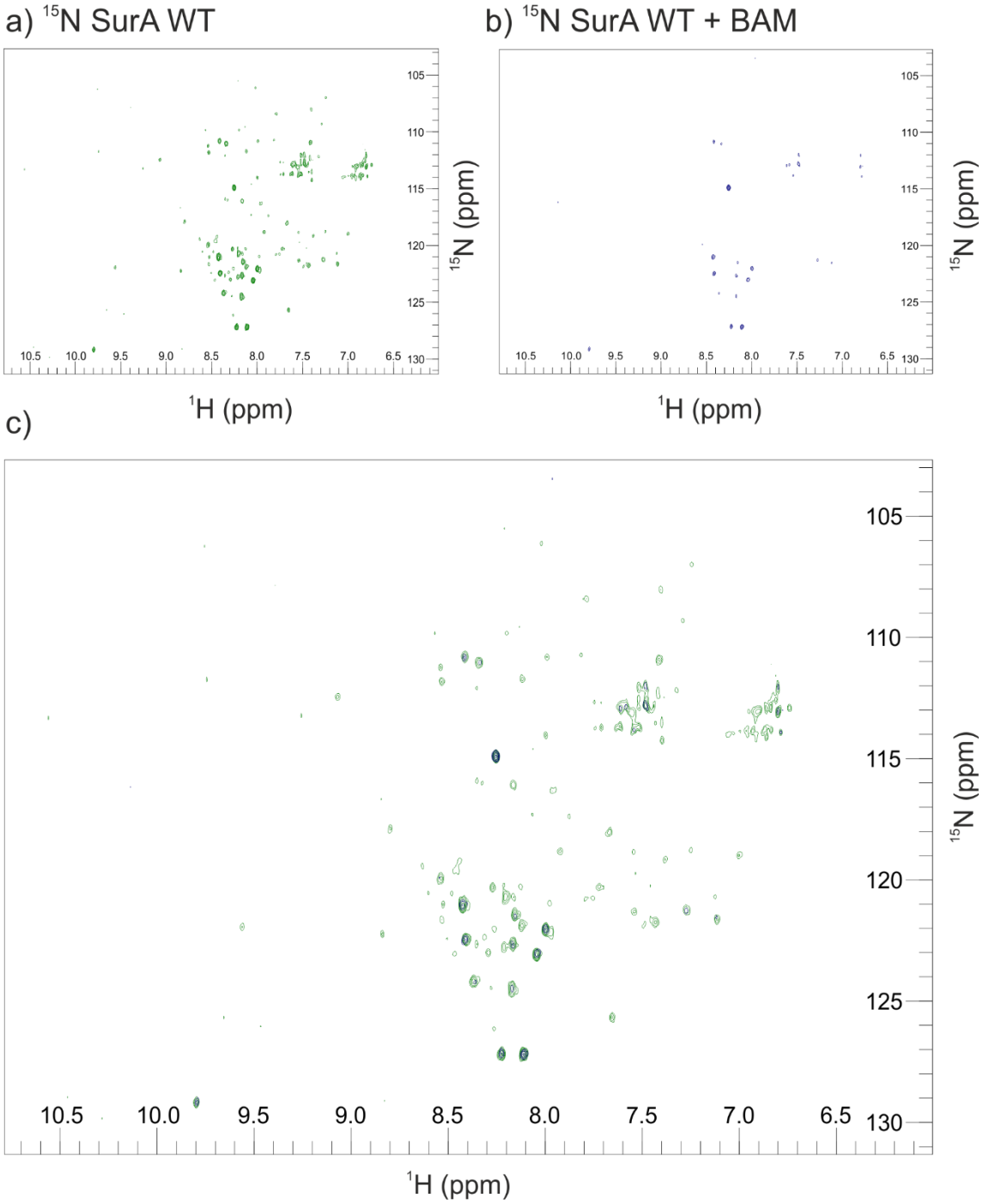

Figure 5.4 Multiple regions of SurA are involved in the interaction with the BAM complex. 2D-TROSY ^{15}N-^{1}H NMR spectrum of a) ^{15}N SurA WT (70 µM), b) ^{15}N SurA WT + BAM complex (35 µM), c) overlay of a and b. All spectra measured in 25 mM MES, 150 mM NaCl, 0.05% (w/v) DDM, pH 6.5 at 950 mHz.

5.3 Removal of the P1 domain slows the delivery of OmpT to BAM

A previously established fluorescence assay that monitors OmpT folding into liposomes via the BAM complex requires SurA to observe efficient folding of OmpT

[71,216,263]. This assay has been used to observe changes in the efficiency of BAM assisted OMP folding [71] and is adapted here to monitor the effects of SurA domain variants on this process. In the assay, a sub-mixture of unfolded OmpT and SurA is added to BAM-containing liposomes at concentrations of 0.25 µM BAM proteoliposomes, 5 µM OmpT, 1 mM fluorogenic peptide and 35 µM SurA. OmpT folding is then monitored by fluorescence, as upon correct folding, the enzymatic site of OmpT is formed and can cleave a fluorescently quenched peptide (Abz-Ala-Arg-Arg-Ala-Tyr(NO_2)-NH_2) which becomes fluorescent. The fluorescence output is used as an indirect measure of OmpT folding via BAM. No fluorescence output is observed in the absence of any single component including SurA (Figure 5.5) which suggests SurA is required to maintain OmpT in a soluble state and delivers OMPs to the BAM complex for insertion into the liposomes [71].

The results of these experiments showed that SurA WT can efficiently deliver OmpT to BAM (Figure 5.5), consistent with previous findings [71,263]. Replacing SurA WT with SurA ΔP2 does not greatly affect OmpT delivery. This result was unexpected as SurA ΔP2 has a significantly reduced binding affinity to OmpT compared to SurA WT (Figure 3.11) and also the P2 domain of SurA is required to maintain high affinity interaction of SurA to BAM at least in DDM. To ensure that OmpT was not aggregating in the presence of SurA PPIase domain variants a nephelometry assay was carried out under the same conditions as the OmpT folding assay. No significant increase in light scattering was observed for OmpT alone or in the presence of SurA variants (Figure 5.5b), these data are consistent with other aggregation assays carried out in the absence of NaCl (Figure 4.3). As there is no aggregation of the OMP, it appears that SurA ΔP2 can compensate for the reduced affinity of OMP and of BAM and retain the ability to efficiently deliver OmpT to BAM for folding. The SurA N-Ct variant however, is substantially slower than SurA WT at aiding OmpT insertion (Figure 5.5). As aggregation cannot account for a reduced folding rate this suggests that the P1 domain of SurA is not essential, but is involved, in delivery of OmpT to BAM.

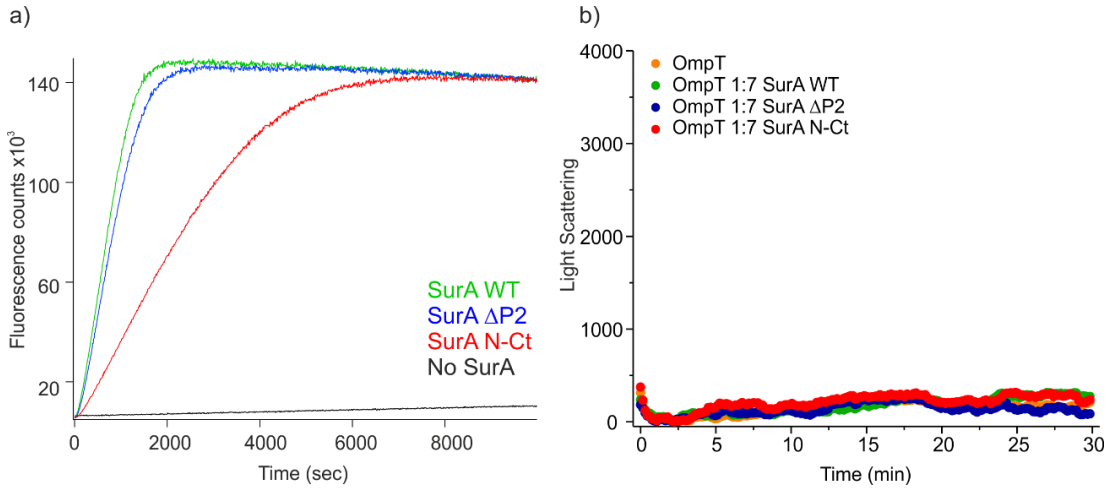

Figure 5.5 SurA N-Ct is less efficient at delivering OmpT to BAM than SurA WT or SurA ΔP2. a) Kinetic traces of OmpT folding measured by fluorescence quantification following proteolytic cleavage of the peptide (Abz-Ala-Arg-Arg-Ala-Tyr(NO_2)-NH_2) in the presence of SurA WT (green), SurA ΔP2 (blue), SurA N-Ct (red) or no SurA (black). All experiments were performed with final concentrations of 0.25 µM BAM proteoliposomes, 5 µM OmpT, 1 mM fluorogenic peptide, 35 µM SurA and performed in 50 mM glycine-NaOH pH 9.5, 25 °C. b) Nephelometry light scattering assay to test for OmpT aggregation under the conditions of the OmpT folding assay in (a) (5 µM OmpT, 35 µM SurA in 50 mM glycine-NaOH pH 9.5, 25 °C).

5.4 Removal of P2 domain slows the delivery of tOmpA to BAM

As the OmpT folding assay can only monitor the effects of BAM and SurA on one substrate, a second method to monitor OMP folding was developed. OMPs are highly stable and are SDS resistant upon folding [97,264]. This feature causes the unfolded and folded species of OMPs to run at different apparent molecular weights on a SDS-PAGE gel. A folding assay was developed in which aliquots of the reaction (unfolded tOmpA into liposomes via the BAM complex) are taken at given time points and the folding quenched by the addition of 6x SDS loading buffer to disrupt the liposomes and prevent further folding (Methods 2.11, Figure 5.6a). After optimisation by Dr B. Schiffrin, reproducible tOmpA folding kinetics were obtained which showed a decrease in the unfolded band and an increase in the folded band over time (Figure 5.6a). The fraction folded is then calculated by the density of the folded band compared to the sum of the folded and unfolded bands.

This band shift assay was next used to determine the effect of SurA domain variants on BAM-dependent folding of tOmpA. The results showed that if no SurA is added to the folding mixture, the folding of tOmpA is very slow (Figure 5.6b). However, the addition of SurA WT increases the delivery of tOmpA to BAM for folding, such that tOmpA is fully folded after 1 hour (3600 seconds). This agrees with the OmpT folding data which showed no folding in the absence of SurA (Figure 5.5) and confirms that SurA is required in these assays to deliver OMPs to the BAM complex for folding.

Replacing SurA WT in this assay with SurA ΔP2 or SurA N-Ct reduces the rate of tOmpA folding (Figure 5.6). This suggests that for the substrate tOmpA at least, the P2 domain is important for delivery to BAM and that further removal of P1 has no effect. Again an aggregation assay confirmed that, under these conditions, there is a small amount of tOmpA aggregation alone but the addition of SurA WT, SurA ΔP2, SurA N-Ct prevents any detectable aggregation (Figure 5.6c). Thus, the differences observed between SurA variants is not caused by the depletion of soluble tOmpA. The effect of removal of the P2 domain on tOmpA folding is not consistent with the results seen for OmpT which showed that removal of the P2 domain had no effect on the apparent rate of folding. Here removal of the P2 or both P1 and P2 have the same effect of a reduced rate of folding.

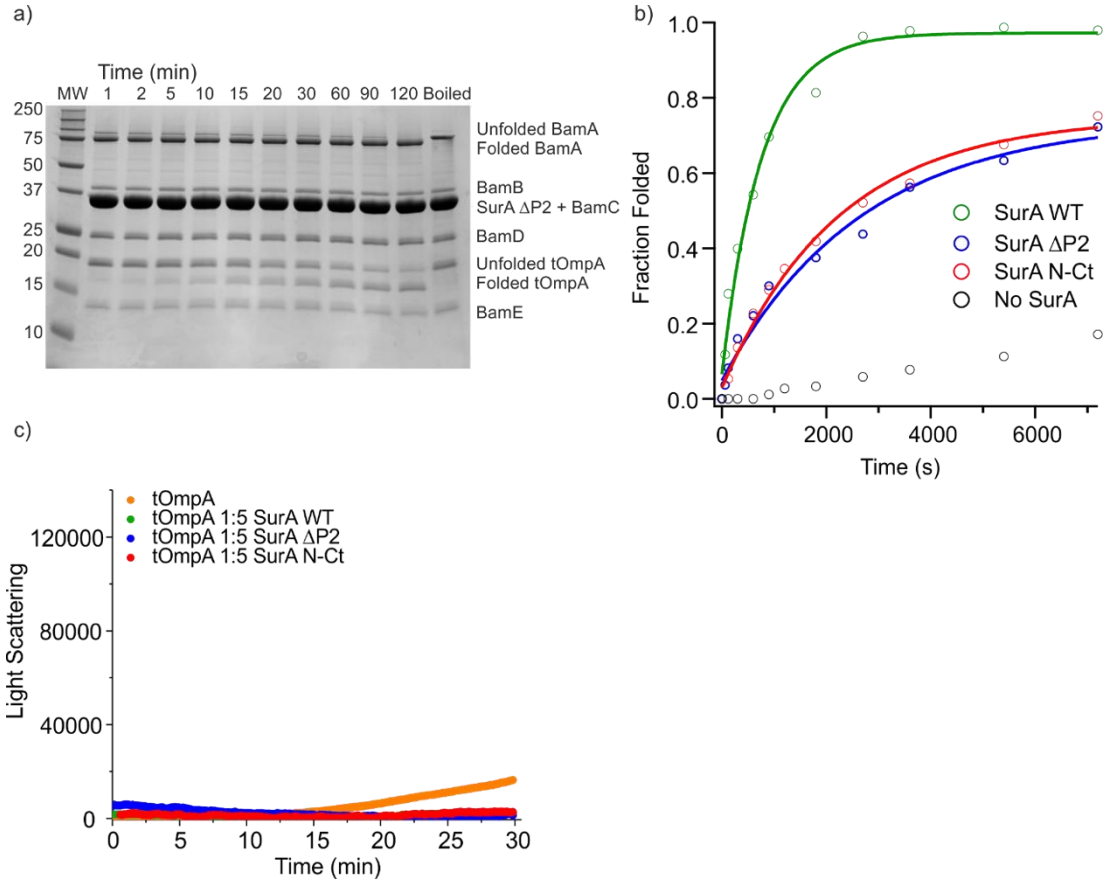

Figure 5.6 Delivery of tOmpA by SurA PPIase domain variants to the BAM complex. a) tOmpA folding assay, tOmpA is added to a SurA variant which is then added to the BAM complex in liposomes and the extent of folding is measured over time. (Final concentrations 1 μM BAM complex, 10 μM SurA and 2 μM tOmpA, 0.8 M urea, in 20 mM Tris-HCl, pH 8.0, 150 mM NaCl 25 °C.) b) Comparison of tOmpA folding assays for SurA WT (green). SurA ΔP2, SurA N-Ct (red) and no SurA (black) over 8000 seconds (2.2 hours). c) Nephelometry light scattering assay to test for aggregation under conditions of tOmpA folding assay (2 μM tOmpA, 10 μM SurA in in 20 mM Tris-HCl, pH 8.0, 150 mM NaCl, 25 °C)

5.5 Skp can interact with BAM but with a lower affinity than SurA WT

SurA is the only chaperone within the periplasm to have been observed to bind the BAM complex [50,182,183]. Furthermore, no crosslinks of Skp or DegP has been detected [50]. However, deletion of SurA in bacterial strains is non-lethal [170]. This suggests that there may be another chaperone which is able to interact with BAM in the absence of SurA to deliver OMPs which rely on the BAM complex for folding. Consequently, Skp was used therefore in the MST assay to determine whether this chaperone which is known to bind OMPs can interact with BAM *in vitro*.

The same experimental setup was used as described for SurA binding to BAM in DDM (Methods 2.14.2). The results of these experiments (Figure 5.7) showed that under these conditions Skp binds to BAM with a K_d of 0.49 ±0.04 μM (500 ±40 nM) (Figure 5.7a), and this is the first evidence that Skp can bind BAM *in vitro*, and hence may do so *in vivo*. It is also interesting that this binding has a Hill coefficient of 2.4 which suggests positive cooperativity and that multiple Skp trimer molecules can interact with the BAM complex at once.

As the binding of Skp to OMPs is higher affinity (in the nM range) [151] than the interaction between Skp and BAM measured here it is unclear if Skp can deliver OMPs to BAM. The OmpT folding assay was used to determine whether Skp can release OmpT for folding via BAM to test this. The results show that Skp can deliver OmpT to BAM which agrees with previous findings that demonstrate that prefolded BamA can release tOmpA from Skp and allow tOmpA folding which is not observed in the absence of BamA [97]. Compared to SurA WT, Skp is slower at delivery of OmpT to BAM (Figure 5.7b) which may be due to the difference in the binding affinities as SurA binds tighter than Skp to the BAM complex 0.09 ±0.01 μM and 0.49 ±0.04μM respectively, or could be due to the mechanism by which the chaperones deliver OMPs to BAM.

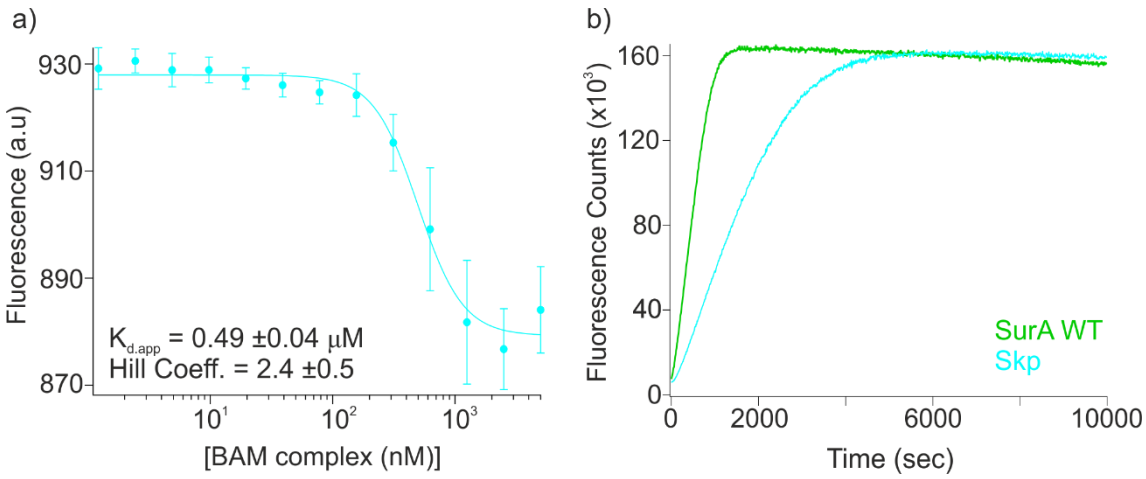

Figure 5.7 Skp can bind the BAM complex. Microscale thermophoresis binding curves of Skp-AF_{488} binding to BAM folded in DDM. Data were fitted to a Hill equation (shown as solid line). Samples contained 100 nM Skp-AF_{488}, 1.2 nM -40 µM BAM complex, 50 mM TBS, 150 mM NaCl, pH 7 at 25 °C. Three replicates were recorded and averaged prior to fitting and the error of the fit plotted as error bars. b) Kinetic traces of OmpT folding measured by fluorescence quantification following its proteolytic cleavage of the peptide (Abz-Ala-Arg-Arg-Ala-Tyr(NO2)-NH2) in the presence of SurA WT (green), Skp (cyan). All experiments were performed with final concentrations of 0.25 µM BAM proteoliposomes, 5 µM OmpT, 1 mM fluorogenic peptide, 35 µM SurA/Skp and performed in 50 mM glycine-NaOH pH 9.5, 25 °C.

5.6 Discussion

This study shows the first direct evidence that SurA interacts with the BAM complex and this binding is altered depending on the membrane environment surrounding the complex. Published structures of the BAM complex as determined by cryo-EM and X-ray crystallography show two conformations of the barrel of BamA. In the 'lateral open' conformation [71] the BamA β-barrel is distorted leading to the separation of the β1 and β16 strands and an opening of the barrel to the lipids (Figure 1.9). Conversely, the 'lateral closed' conformation [104] has the β-strands 1-16 hydrogen bonded. This observation suggests that the barrel domain of BamA may undergo conformational changes between an open and closed state as part of its function. The POTRA domains also undergo a conformational shift and when the BamA barrel is in the open conformation, the POTRAS are extended ~20Å away from the membrane compared to the lateral closed structure [104,106]. These changes in conformation of the β1-β16 strands appear to depend on the membrane mimic that the structure is solved in. In accord with this notion, the structure of the BAM complex in nanodiscs containing the same *E.coli* polar lipid extract used in this study

for the MST experiment of SurA biding to BAM appears to be highly dynamic and can convert between multiple different conformations (unpublished Dr M. Iadanza). A recent study by Hartmann *et al.* demonstrated that in both detergent micelles and in nanodiscs, the BamA barrel populates multiple conformational states which are modulated by changes in the gate region [265].

From the cryo-EM structure it appears that BAM in DDM is held in a single conformation which has allowed structural characterisation. This structure reveals that the BamA barrel is laterally open with extended POTRA domains [71]. Previous findings have shown that SurA binds to POTRA 1 of BamA [182] (Figure 5.1). This conformation of the BamA barrel may place in a POTRA 1 conformation preferential for binding. Taken together the MST alongside the structural data it suggests that SurA WT binds to the BAM complex in a laterally open conformation with high affinity (Figure 5.2).

The difference in binding of SurA WT, SurA ΔP2 and SurA N-Ct to BAM suggests that that binding occurs primarily via the P2 domain of SurA. It could also be interesting to investigate the binding of SurA PPIase domain variants to the BAM complex of different bacterial species as SurA homologues which lack PPIase domains may have an altered mode of binding or differences in the BAM complex to allow binding. The unpublished nanodisc data and recent NMR data [265] suggests that in proteoliposomes the BAM complex is more dynamic and the binding of SurA under these conditions is reduced compared to that in detergent micelles (Figure 5.3) this suggests that there is a preferred conformation of BAM which SurA can bind and a highly dynamic BAM complex causes a reduction in the ability of SurA to bind.

The results described(Figure 3.11 and Figure 5.2) demonstrate that SurA binds to BAM in DDM more tightly than it does to OMP substrates, in agreement with other studies [97,177]. This may allow efficient handover of substrates from SurA to the BAM

complex for folding. The observation that SurA preferentially binds to BAM in the open conformation presents a hypothesis that SurA delivers OMPs to BAM and the OMPs can template onto the unbound β-strands of the BAM complex to initiate OMP folding.

Chaperone	K_d binding to BAM	Hill coefficient
SurA WT	0.09 ± 0.01 μM	1
Skp	0.49 ± 0.04 μM	2.4 ± 0.5

Table 5.1 Affinities of SurA WT and Skp binding the BAM complex in DDM. 100 nM Skp/SurA-AF_{488}, 1.2 nM -40 μM BAM complex, 50 mM TBS, 150 mM NaCl, pH 7 at 25 °C.

Comparing the folding of tOmpA and OmpT via the BAM complex showed that the PPIase domains appear to play different roles in the delivery of different substrates. OmpT was efficiently delivered by both SurA WT and SurA ΔP2 whereas SurA ΔP2 has reduced ability to deliver tOmpA to BAM and SurA N-Ct could deliver both OMPs but had reduced ability compared to SurA WT (Figure 5.5, Figure 5.6). The chaperoning data suggests that the P2 domain of SurA is required to prevent aggregation of OmpT (Figure 4.5). The P2 region of SurA is also shown here to be primarily used for BAM complex interaction, suggesting a duel role of the P2 domain. Firstly, P2 is needed to chaperone certain substrates and secondly, it is involved in the interaction with the BAM complex for delivery of OMPs for folding.

Using MST, Skp has been shown here to interact with the BAM complex in DDM detergent (Figure 5.7, Table 5.1), which has not previously been reported. This finding suggests that OMPs can be chaperoned and delivered to BAM via Skp which provides an explanation as to why deletion of SurA is not lethal to cells [50,169,170]. Studies found that deletion of SurA only caused a reduction in a small number of OMPs [170] and it may be that Skp and SurA have overlapping substrates and Skp can largely compensate for the absence of SurA. SurA, however, still binds to the BAM complex

with a 5x higher affinity than Skp (0.09 ±0.01μM and 0.49 ±0.04μM) (Table 5.1) under the same conditions, supporting findings that SurA is the major chaperone that interacts with the BAM complex and may explain why crosslinks have not been observed between Skp and BAM *in vivo*.

In summary, the data presented here show for the first time *in vitro* that SurA directly binds to the BAM complex and suggest that this interaction is preferable when the BamA barrel is in the open confirmation and the POTRA domains are extended. It appears that the P2 domain is not essential but highly important in the binding of SurA to BAM. However, the P2 domain appears less significant for delivery when SurA is bound to OmpT, which required P2 to prevent its aggregation. In this case, the P2 domain may not be free to bind BAM. Skp has also been observed to bind to BAM for the first time, however with a lower affinity than SurA WT. Together, these data have revealed some new aspects of the roles of SurA, the SurA PPIase domain variants and Skp and their contact with the BAM complex.

Chapter 6 Conclusions and Discussion

OMPs require chaperones to prevent their self-association and aggregation [41,174,212] and for efficient folding into the OM [50,170]. After translation on cytoplasmic ribosomes, OMPs are bound by chaperones such as TF and SecB [75,92]. They are then trafficked to the SecYEG complex in the IM [94] for active translocation into the periplasm, facilitated by ATP-hydrolysis by SecA [91]. As the environment within the periplasm is highly variable [33], chaperones such as SurA, Skp and DegP bind OMPs to prevent their aggregation in this cellular compartment [21]. The OMPs then must reach the BAM complex which aids their folding and insertion to the OM [96] allowing them to carry out their various functions.

SurA has been shown to be the major OMP chaperone within the periplasm of *E. coli* through genetic analysis *in vivo* [141,169,170]. Previous studies have shown that SurA interacts with OMPs with K_d's in the μM range [177,178] and that SurA can halt the aggregation of the water soluble protein citrate synthase [165]. SurA is also the only periplasmic chaperone for which crosslinks to the BAM complex have been detected [50,180,182,183]. Bioinformatic analysis of SurA homologues in various classes of proteobacteria (Figure 3.23) showed that the PPIase domains have been acquired and conserved through evolution, suggesting that these domains convey some advantage to the function of SurA.

The aims of this project were to analyse the binding of SurA to OMPs, determine the mechanism by which SurA prevents aggregation of substrates and investigate whether SurA directly binds the BAM complex for delivery of OMPs. In addition, the roles of the PPIase domains in these functions was also adressed. To achieve these aims, variants of SurA from *E. coli* lacking either the P2 domain (SurA ΔP2) or both PPIase domains (SurA N-Ct) (Figure 1.20) were designed, based on previous publications [165,178] to observe the function of these domains in the context of the full length chaperone.

The binding of SurA to two model OMPs (tOmpA and OmpT) was measured using multiple different biochemical assays. Native ESI-MS, analytical SEC, SPR and MST demonstrated that the core domain of SurA, the N- and C-terminal domains lacking both PPIase domains, retains the ability to bind the OMPs tested. Demonstrating that SurA homologues which do not contain PPIase domains can interact with OMP substrates. The addition of the PPIase domains increased the affinity of binding to both OMPs. However, as SurA N-Ct retained a low μM K_d for binding to tOmpA, the enhancement in affinity is minimal for the binding to this 8-stranded OMP substrate (Figure 3.11). On the other hand, the presence of the PPIase domains are required for SurA to bind OmpT with low μM affinity (Figure 3.10). These data suggest that the acquisition of the PPIase domains has increased the ability of SurA to bind large, aggregation-prone OMPs such as OmpT.

Measurement of the binding affinity between SurA and OMPs using MST showed that the K_d's obtained agreed with previous findings [178], and also showed that the interaction has positive co-operativity (Figure 3.11, Table 3.4). Native ESI-MS also demonstrated that SurA WT and SurA ΔP2 form both 1:1 and 2:1 chaperone to tOmpA complexes, which has not been observed previously. This proposes a new model of SurA binding in which multiple SurA molecules bind to several sites along the unfolded OMP chain. This 'beads on a string model' has been proposed previously for Trigger Factor [82] and SecB [266], in which the substrates interact with hydrophobic patches on the surface of the chaperone and for long chains multiple chaperones are required to interact with various hydrophobic regions along the length of the substrate. Another hypothesis is that two SurA molecules can come together to form a cage like structure around a collapsed OMP chain such as been observed for Skp [98,149].

Evidence of which of these models of the mechanism of SurA is correct was tested further by studying the interaction between SurA and water soluble proteins. Im7 wild-type and Im7 folding variants which are either fully unfolded or trapped in an

intermediate state, were tested for binding to SurA. Although, no interaction could be observed using MST (Figure 3.13), a small population of 1:1 complex of SurA WT and Im7 L18A L19A L37A was detected by native MS (Figure 3.14). Aggregation data of the water-soluble GAPDH shows that addition of any of the SurA variants has no effect on the aggregation of this 37 kDa protein which has a complex final fold (Figure 4.12). However, SurA WT could prevent amyloid formation of the intrinsically disordered $A\beta_{40}$ with sub-stoichiometric concentrations of chaperone to monomer (Figure 4.13). Taken together these data suggest that SurA is also able to interact with water soluble proteins which do not contain any secondary structural elements such as the unfolded Im7 L18A L19A L37A [232] and the intrinsically disordered $A\beta_{40}$ [267], while retaining a preference for binding OMP substrates. This provides evidence that SurA binds its substrates in an extended conformation opposed to in a collapsed state and that the interaction is likely to occur via the 'beads on a string' model.

Investigating the ability of SurA and the PPIase domain variants to prevent the aggregation of tOmpA and OmpT revealed that a higher excess of SurA WT is required for OmpT (100-fold excess) than for tOmpA (50-fold excess) (Figure 4.4,Figure 4.5). OmpT is both more aggregation prone [217] and is larger in size than tOmpA, the results suggest that properties of the OMP dictate the excess of chaperone required to keep the substrate soluble. If the concentration of SurA required is related to the chain length of the OMP which this observation supports the 'beads on a string model' of SurA interaction. This model would allow efficient chaperoning as it prevents aberrant interactions but would require high concentrations of chaperone *in vivo*. In accord with this hypothesis, recent studies, documented that the cellular concentration of SurA is between 2.07-7.2 μM [144,268] in *E. coli* and unfolded OMP concentrations are approximately 94.7 nM [212] under non stressed conditions suggesting that there is an excess of SurA over unfolded OMP substrates in the periplasm in order to prevent OMP aggregation.

The difference in ability of the SurA PPIase variants to chaperone the model OMPs was striking, SurA ΔP2 and SurA N-Ct, as well as SurA WT could prevent the aggregation of tOmpA with 50-fold molar excess (Figure 4.4). By contrast, only SurA WT could prevent the aggregation of OmpT, with the SurA variants increasing both the rate and final amplitude of aggregation (Figure 4.5). This reflects the binding data which showed that all SurA variants could bind tOmpA with low μM affinity, but had significantly reduced binding affinity for OmpT compared to SurA WT (Figure 3.11). Together, these data support the hypothesis that the PPIase domains of SurA have been acquired and conserved to aid in both binding and chaperoning of larger, more aggregation-prone substrates. Genetic studies analysing the change in OMP levels *in vivo* showed that the concentration of OmpA (the full length form of tOmpA including the periplasmic domain) and OmpT were reduced upon SurA depletion in a *Δskp* strain lacking SurA [141]. By contrast, removal of SurA with normal levels of Skp showed that OmpA levels were reduced, but those of OmpT were not [170]. This suggests that OmpT may not rely on SurA but instead is bound by Skp, or another chaperone, in the periplasm, indicating OMP specificity of chaperones which has not been proposed previously. These findings also provide a rationale as to why the domain variants of SurA have no effect on preventing the aggregation of OmpT, whereas other chaperones may be more effective in preventing OmpT aggregation.

In this study the first observation that Skp interacts with the BAM complex is measured by MST (Figure 5.7). As shown in Figure 5.7b, Skp allows OmpT folding via BAM and no folding is observed in the absence of a chaperone. Together with previous studies which showed that there is no hand-over events between Skp and SurA [98]. The results suggest that Skp can bind substrates in the periplasm and directly deliver them to BAM. Although the removal of Skp from bacterial strains shows no change in the levels of OMP monitored in the OM [141], these data demonstrate that in the absence of SurA, Skp is an effective chaperone which can carry out the same functions in a redundant pathway. On the other hand, there may be substrates which are preferentially chaperoned by Skp under non-stress conditions, but can also be bound by SurA and *vice versa*.

Comparison of the ability of *E.coli* OMP chaperones to prevent substrate aggregation revealed that TF and SecB appear to be general chaperones for both water soluble and OMP substrates (Figure 4.9). A closer look at TF showed that a lower concentration of TF was required to prevent the aggregation of GAPDH than is required to prevent the aggregation of tOmpA (Figure 4.11). The opposite is seen for SurA, as it has no effect on GAPDH but can chaperone OMPs (Figure 4.12). SurA and TF have similar structures in the domains which are responsible for binding substrates, the N- and C-terminal core domain or SurA and the substrate binding domain (SBD) in the centre of the TF structure (Figure 4.14). These findings suggest that TF and SurA may have evolved from a common ancestor however now reside in different cellular compartments and so have acquired different abilities such ribosome binding for TF and the ability of SurA to interact with the BAM complex. Both of these chaperones contain at least a single PPIase domain which are dispensable to the chaperone activity [165,269]. As the domains are from different PPIase families (SurA contains parvulin domains and TF has a FK506-binding protein homology) (Section 1.10), it is likely that they have also been acquired independently.

SecB binds to nascent polypeptide chains in the cytoplasm which are targeted to the periplasm, OM, or for secretion out of the bacterium [266]. SecB then interacts with SecA with high affinity (0.6 nM) [270] before SecA interacts with the SecYEG complex in the inner membrane [93]. From this study it appears that SecB preferentially binds OmpT over tOmpA, given the K_d's of 0.6 ± 0.04 μM and 2.05 ± 0.08 μM, respectively (Figure 4.10) but it can inhibit the aggregation of both substrates (Figure 4.9). Genetic analysis of SecB null strains of *E. coli* showed 12 substrates which are reduced and therefore appear to be dependent on SecB [92], one of which was OmpT. This suggests that the reason that SecB binds with such high affinity to OmpT (Figure 4.10) is that OmpT requires SecB *in vivo* in order to reach the SecYEG complex, and their interaction may be driven by specialised recognition regions.

SurA is the only periplasmic chaperone that has been crosslinked with the BAM complex *in vivo* [50,180,182,183], however this observation may have been due to the high concentration of SurA in the periplasm [144,212]. In this thesis, SurA WT is observed to bind the BAM complex *in vitro* with a K_d of 0.09 ± 0.01 μM (Figure 5.2). The affinity of this interaction is dependent on the membrane environment in which the BAM complex is folded. From structural analysis it appears that the membrane environment alters the conformation of the BamA barrel and POTRA domains [71,104]. Together with the data collected here, the results suggests that SurA preferentially interacts with certain conformations of the BAM complex. This mechanism may prevent chaperone binding while BAM is in the process of inserting a substrate as binding may inhibit necessary conformational changes. Biochemical assays have aided in forming this hypothesis and further structural analysis of the SurA-OMP-BAM complex at different time points of OMP folding determined by cryo-EM or X-ray crystallography will help to answer the questions regarding precisely how SurA interacts with the BAM complex.

A comparison of the ability of different of SurA PPIase domain variants to bind the BAM complex shows that, while the P2 domain is not essential, it plays an important role in the interaction, as removal of this domain reduces the affinity (Figure 5.2). Further deletion of the P1 domain appears to have no additional effect on the affinity suggesting that the P1 domain may not be involved in BAM binding. The PPIase domains also play a role in the delivery of OMPs to BAM, although this appears to be OMP dependent. For OmpT, removal of the P2 domain does not alter the delivery to BAM but the additional deletion of P1 slows delivery rate, compared to SurA WT (Figure 5.5), suggesting that the P1 domain is involved in OmpT delivery. Conversely, for tOmpA removal of the P2 domain reduces folding via BAM, compared to SurA WT (Figure 5.6), and removal of P1 has no further effect. This provides a rationale for the acquisition of two PPIase domains in SurA as it appears that these domains may aid in the delivery of certain substrates to the BAM complex depending on the properties of the substrate.

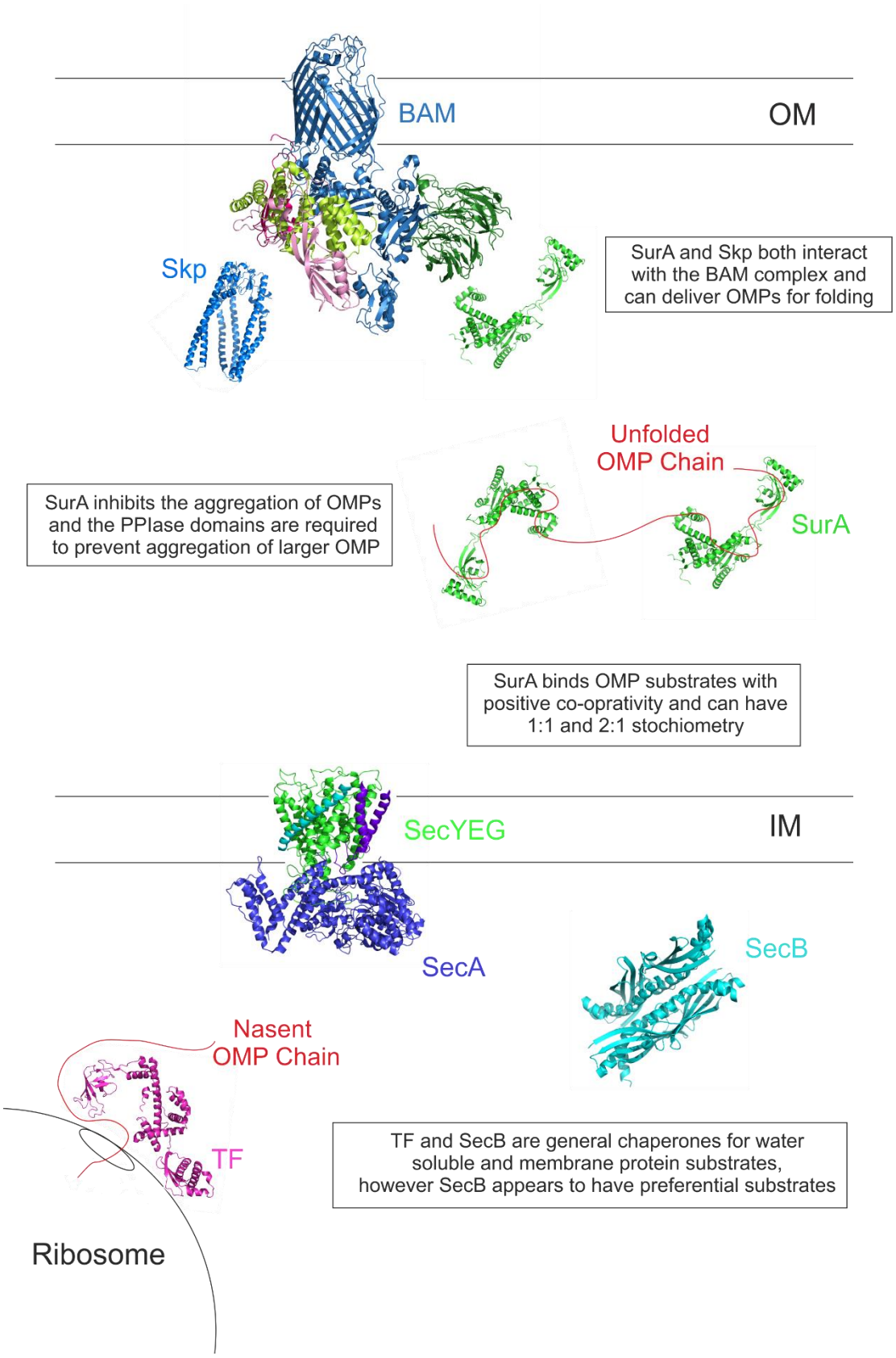

Figure 6.1 Main findings of this study. PDB ID of structures TF (1W26)[78], SecB (1OZB)[271], SecYEG-SecA (3DL8)[74], Skp (12UM)[70], SurA (1M5Y)[69], BAM complex (5LJO)[71].

In addition to understanding OMP biogenesis, this work may also aid in the development of new therapeutics. The outer membrane of gram-negative bacteria is a major defence as it is a potent permeability barrier against toxic molecules such as antibiotics. As the majority of antibiotics exert their effect in the cytoplasm, these drugs must first permeate the cell. As well as chaperoning OMPs, SurA has been implicated in pathogenicity, with roles in the correct assembly of virulence factors such as pili and adhesins [166,272]. The essential and conserved BAM complex within the OM may also be a promising target for therapeutics and a recent study developed a monoclonal antibody which antagonises BamA function and is therefore bactericidal [273]. In the urgent search for novel antibiotics to treat Gram-negative bacterial infections, disruption of the OMP biogenesis pathway may provide targets both on the surface of and within the cell.

This work has provided valuable insights into the mechanism of SurA and its roles in OMP binding, OMP chaperoning and delivery of OMPs to BAM, with the major findings summarised in Figure 6.1. The results have elucidated that the core domain of SurA is sufficient for binding however, new functions of the PPIase domains of SurA in binding and chaperoning have rationalised the acquisition and conservation of these domains during proteobacterial evolution. Investigating the interaction between periplasmic chaperones and the BAM complex has demonstrated that SurA binds BAM with nM affinity, however the affinity is dependent on the membrane environment. It has also shown that Skp is able to interact with BAM, which has not been previously shown. Comparison of cytoplasmic OMP chaperones showed that TF and SecB appear to be good general chaperones for OMPs, but SecB has preferential substrates with which to interact. Together the data both answers questions in the field of OMP biogenesis and provides new hypotheses which can be tested and should go on to inform further discoveries.

References

1. Anfinsen, C.B. Principles that govern the folding of protein chains. *Science* **181**, 223-30 (1973).
2. Balchin, D., Hayer-Hartl, M. & Hartl, F.U. In vivo aspects of protein folding and quality control. *Science* **353**, aac4354 (2016).
3. Saibil, H. Chaperone machines for protein folding, unfolding and disaggregation. *Nat Rev Mol Cell Biol* **14**, 630 (2013).
4. Bardwell, J.C. & Jakob, U. Conditional disorder in chaperone action. *Trends Biochem Sci* **37**, 517-25 (2012).
5. Horwich, A.L. Molecular chaperones in cellular protein folding: the birth of a field. *Cell* **157**, 285-288 (2014).
6. Mas, G. & Hiller, S. Conformational plasticity of molecular chaperones involved in periplasmic and outer membrane protein folding. *FEMS Microbiol Lett* **365**, 121 (2018).
7. Hartl, F.U., Bracher, A. & Hayer-Hartl, M. Molecular chaperones in protein folding and proteostasis. *Nature* **475**, 324-32 (2011).
8. Kettern, N., Dreiseidler, M., Tawo, R. & Hohfeld, J. Chaperone-assisted degradation: multiple paths to destruction. *Biol Chem* **391**, 481-9 (2010).
9. Finkelstein, A.V., Bogatyreva, N.S. & Garbuzynskiy, S.O. Restrictions to protein folding determined by the protein size. *FEBS Lett* **587**, 1884-90 (2013).
10. Ellis, R.J. Macromolecular crowding: obvious but underappreciated. *Trends Biochem Sci* **26**, 597-604 (2001).
11. Morimoto, R.I. & Cuervo, A.M. Proteostasis and the Aging Proteome in Health and Disease. *J Gerontol* **69**, S33-S38 (2014).
12. Hartl, F.U. & Hayer-Hartl, M. Molecular chaperones in the cytosol: from nascent chain to folded protein. *Science* **295**, 1852-8 (2002).
13. Valastyan, J.S. & Lindquist, S. Mechanisms of protein-folding diseases at a glance. *Dis Model Mech* **7**, 9-14 (2014).
14. De Strooper, B. Loss-of-function presenilin mutations in Alzheimer disease. Talking Point on the role of presenilin mutations in Alzheimer disease. *EMBO Rep* **8**, 141-146 (2007).
15. Evans, C.G., Wisen, S. & Gestwicki, J.E. Heat shock proteins 70 and 90 inhibit early stages of amyloid beta-(1-42) aggregation in vitro. *J Biol Chem* **281**, 33182-91 (2006).
16. Rekas, A. et al. Interaction of the molecular chaperone alphaB-crystallin with alpha-synuclein: effects on amyloid fibril formation and chaperone activity. *J Mol Biol* **340**, 1167-83 (2004).
17. Wang, X. et al. A study on the biological function of heat shock factor 1 proteins in breast cancer. *Oncol Lett* **16**, 3821-3825 (2018).
18. Mahalingam, D. et al. Targeting HSP90 for cancer therapy. *Br J Cancer* **100**, 1523-1529 (2009).
19. Whitesell, L. & Lindquist, S.L. HSP90 and the chaperoning of cancer. *Nat Rev Cancer* **5**, 761 (2005).
20. Mogk, A., Huber, D. & Bukau, B. Integrating Protein Homeostasis Strategies in Prokaryotes. *Cold Spring Harb Perspect Biol* **3**, a004366 (2011).

21. Merdanovic, M., Clausen, T., Kaiser, M., Huber, R. & Ehrmann, M. Protein quality control in the bacterial periplasm. *Annu Rev Microbiol* **65**, 149-68 (2011).
22. Hipp, M.S., Park, S.H. & Hartl, F.U. Proteostasis impairment in protein-misfolding and -aggregation diseases. *Trends Cell Biol* **24**, 506-14 (2014).
23. Radwan, M., Wood, R.J., Sui, X. & Hatters, D.M. When proteostasis goes bad: Protein aggregation in the cell. *IUBMB Life* **69**, 49-54 (2017).
24. Bhandari, V. & Houry, W.A. Substrate Interaction Networks of the Escherichia coli Chaperones: Trigger Factor, DnaK and GroEL. *Adv Exp Med Biol* **883**, 271-94 (2015).
25. Petrakis, N., Alcock, F. & Tokatlidis, K. Mitochondrial ATP-independent chaperones. *IUBMB Life* **61**, 909-914 (2009).
26. Voos, W. Chaperone-protease networks in mitochondrial protein homeostasis. *Biochim Biophys Acta* **1833**, 388-99 (2013).
27. Shouldice, S.R. et al. Structure and function of DsbA, a key bacterial oxidative folding catalyst. *Antioxid Redox Signal* **14**, 1729-60 (2011).
28. Kim, Y.E., Hipp, M.S., Bracher, A., Hayer-Hartl, M. & Hartl, F.U. Molecular chaperone functions in protein folding and proteostasis. *Annu Rev Biochem* **82**, 323-55 (2013).
29. Tacconelli, E. & Magrini, N. Global priority list of antibiotic-resistant bacteria to guide research, discovery and delvelopment of new antibiotics. (World Health Organisation (WHO), 2017).
30. Malinverni, J.C. & Silhavy, T.J. Assembly of Outer Membrane beta-Barrel Proteins: the Bam Complex. *EcoSal Plus* **4**(2011).
31. Schiffrin, B., Brockwell, D.J. & Radford, S.E. Outer membrane protein folding from an energy landscape perspective. *BMC Biol* **15**, 123 (2017).
32. Neu, H.C. & Heppel, L.A. Some obervations on the "latent" ribonuclease of Escherichia coli. *Proc Natl Acad Sci USA* **51**, 1267-74 (1964).
33. Miller, S.I. & Salama, N.R. The gram-negative bacterial periplasm: Size matters. *PLoS Biol* **16**, e2004935 (2018).
34. Bladen, H.A. & Mergenhagen, S.E. Ultrastruture of veillonella and morphological correlation of an outer membrane with particles associated with endotoxic activity. *J Bacteriol* **88**, 1482-92 (1964).
35. Denoncin, K. & Collet, J.F. Disulfide bond formation in the bacterial periplasm: major achievements and challenges ahead. *Antioxid Redox Signal* **19**, 63-71 (2013).
36. Nanninga, N. Cell division and peptidoglycan assembly in Escherichia coli. *Mol Microbiol* **5**, 791-5 (1991).
37. Schlapschy, M. & Skerra, A. Periplasmic chaperones used to enhance functional secretion of proteins in E. coli. *Methods Mol Biol* **705**, 211-24 (2011).
38. Matias, V.R.F., Al-Amoudi, A., Dubochet, J. & Beveridge, T.J. Cryo-Transmission Electron Microscopy of Frozen-Hydrated Sections of Escherichia coli and Pseudomonas aeruginosa. *J Bacteriol* **185**, 6112-6118 (2003).
39. Gan, L., Chen, S. & Jensen, G.J. Molecular organization of Gram-negative peptidoglycan. *Proc Natl Acad Sci USA* **105**, 18953-7 (2008).

40. Typas, A. et al. Regulation of peptidoglycan synthesis by outer-membrane proteins. *Cell* **143**, 1097-109 (2010).
41. Goemans, C., Denoncin, K. & Collet, J.F. Folding mechanisms of periplasmic proteins. *Biochim Biophys Acta* **1843**, 1517-28 (2014).
42. Cohen, E.J., Ferreira, J.L., Ladinsky, M.S., Beeby, M. & Hughes, K.T. Nanoscale-length control of the flagellar driveshaft requires hitting the tethered outer membrane. *Science* **356**, 197-200 (2017).
43. Plummer, A.M. & Fleming, K.G. From Chaperones to the Membrane with a BAM! *Trends Biochem Sci* **41**, 872-882 (2016).
44. Silhavy, T.J., Kahne, D. & Walker, S. The Bacterial Cell Envelope. *Cold Spring Harb Perspect Biol* **2**, a000414 (2010).
45. Du, D. et al. Structure of the AcrAB-TolC multidrug efflux pump. *Nature* **509**, 512-515 (2014).
46. Decad, G.M. & Nikaido, H. Outer membrane of gram-negative bacteria. XII. Molecular-sieving function of cell wall. *J Bacteriol* **128**, 325-36 (1976).
47. Wülfing, C. & Plückthun, A. Protein folding in the periplasm of Escherichia coli. *Mol Microbiol* **12**, 685-692 (1994).
48. Mullineaux, C.W., Nenninger, A., Ray, N. & Robinson, C. Diffusion of green fluorescent protein in three cell environments in Escherichia coli. *J Bacteriol* **188**, 3442-8 (2006).
49. Konovalova, A. et al. Inhibitor of intramembrane protease RseP blocks the σE response causing lethal accumulation of unfolded outer membrane proteins. *Proc Natl Acad Sci USA* **115**, 6614-662 (2018).
50. Sklar, J.G., Wu, T., Kahne, D. & Silhavy, T.J. Defining the roles of the periplasmic chaperones SurA, Skp, and DegP in Escherichia coli. *Genes Dev* **21**, 2473-84 (2007).
51. Wimley, W.C. The versatile beta-barrel membrane protein. *Curr Opin Struct Biol* **13**, 404-11 (2003).
52. Bos, M.P., Robert, V. & Tommassen, J. Biogenesis of the gram-negative bacterial outer membrane. *Annu Rev Microbiol* **61**, 191-214 (2007).
53. Hiller, S. et al. Solution Structure of the Integral Human Membrane Protein VDAC-1 in Detergent Micelles. *Science* **321**, 1206-1210 (2008).
54. Hagn, F., Etzkorn, M., Raschle, T. & Wagner, G. Optimized phospholipid bilayer nanodiscs facilitate high-resolution structure determination of membrane proteins. *J Am Chem Soc* **135**, 1919-25 (2013).
55. Cuesta-Seijo, J.A. et al. PagP Crystallized from SDS/Cosolvent Reveals the Route for Phospholipid Access to the Hydrocarbon Ruler. *Structure* **18**, 1210-1219 (2010).
56. Pautsch, A. & Schulz, G.E. High-resolution structure of the OmpA membrane domain. *J Mol Biol* **298**, 273-82 (2000).
57. Hong, H., Patel, D.R., Tamm, L.K. & van den Berg, B. The outer membrane protein OmpW forms an eight-stranded beta-barrel with a hydrophobic channel. *J Biol Chem* **281**, 7568-77 (2006).
58. Vandeputte-Rutten, L. et al. Crystal structure of the outer membrane protease OmpT from Escherichia coli suggests a novel catalytic site. *EMBO J* **20**, 5033-9 (2001).

59. Barnard, T.J., Dautin, N., Lukacik, P., Bernstein, H.D. & Buchanan, S.K. Autotransporter structure reveals intra-barrel cleavage followed by conformational changes. *Nat Struct Mol Biol* **14**, 1214-20 (2007).
60. Snijder, H.J. et al. Structural evidence for dimerization-regulated activation of an integral membrane phospholipase. *Nature* **401**, 717-21 (1999).
61. Yildiz, O., Vinothkumar, K.R., Goswami, P. & Kuhlbrandt, W. Structure of the monomeric outer-membrane porin OmpG in the open and closed conformation. *EMBO J* **25**, 3702-13 (2006).
62. van den Berg, B., Black, P.N., Clemons, W.M., Jr. & Rapoport, T.A. Crystal structure of the long-chain fatty acid transporter FadL. *Science* **304**, 1506-9 (2004).
63. Cowan, S.W. et al. The structure of OmpF porin in a tetragonal crystal form. *Structure* **3**, 1041-50 (1995).
64. Noinaj, N. et al. Structural insight into the biogenesis of β-barrel membrane proteins. *Nature* **501**, 385-390 (2013).
65. Schirmer, T., Keller, T.A., Wang, Y.F. & Rosenbusch, J.P. Structural basis for sugar translocation through maltoporin channels at 3.1 A resolution. *Science* **267**, 512-4 (1995).
66. Locher, K.P. et al. Transmembrane signaling across the ligand-gated FhuA receptor: crystal structures of free and ferrichrome-bound states reveal allosteric changes. *Cell* **95**, 771-8 (1998).
67. Phan, G. et al. Crystal structure of the FimD usher bound to its cognate FimC-FimH substrate. *Nature* **474**, 49-53 (2011).
68. Qiao, S., Luo, Q., Zhao, Y., Zhang, X.C. & Huang, Y. Structural basis for lipopolysaccharide insertion in the bacterial outer membrane. *Nature* **511**, 108-11 (2014).
69. Bitto, E. & McKay, D.B. Crystallographic structure of SurA, a molecular chaperone that facilitates folding of outer membrane porins. *Structure* **10**, 1489-98 (2002).
70. Walton, T.A. & Sousa, M.C. Crystal structure of Skp, a prefoldin-like chaperone that protects soluble and membrane proteins from aggregation. *Mol Cell* **15**, 367-74 (2004).
71. Iadanza, M.G. et al. Lateral opening in the intact beta-barrel assembly machinery captured by cryo-EM. *Nat Commun* **7**, 12865 (2016).
72. Krojer, T., Garrido-Franco, M., Huber, R., Ehrmann, M. & Clausen, T. Crystal structure of DegP (HtrA) reveals a new protease-chaperone machine. *Nature* **416**, 455-9 (2002).
73. Collinson, I. The structure of the bacterial protein translocation complex SecYEG. *Biochem Soc Trans* **33**, 1225-30 (2005).
74. Zimmer, J., Nam, Y. & Rapoport, T.A. Structure of a complex of the ATPase SecA and the protein-translocation channel. *Nature* **455**, 936 (2008).
75. Oh, E. et al. Selective ribosome profiling reveals the co-translational chaperone action of trigger factor in vivo. *Cell* **147**, 1295-1308 (2011).
76. Deuerling, E., Schulze-Specking, A., Tomoyasu, T., Mogk, A. & Bukau, B. Trigger factor and DnaK cooperate in folding of newly synthesized proteins. *Nature* **400**, 693-6 (1999).
77. Kramer, G. et al. L23 protein functions as a chaperone docking site on the ribosome. *Nature* **419**, 171-4 (2002).

78. Ferbitz, L. et al. Trigger factor in complex with the ribosome forms a molecular cradle for nascent proteins. *Nature* **431**, 590-6 (2004).
79. Kramer, G. et al. Functional Dissection of Escherichia coli Trigger Factor: Unraveling the Function of Individual Domains. *J Bacteriol* **186**, 3777-3784 (2004).
80. Morgado, L., Burmann, B.M., Sharpe, T., Mazur, A. & Hiller, S. The dynamic dimer structure of the chaperone Trigger Factor. *Nat Commun* **8**, 1992 (2017).
81. Kaiser, C.M. et al. Real-time observation of trigger factor function on translating ribosomes. *Nature* **444**, 455 (2006).
82. Saio, T., Guan, X., Rossi, P., Economou, A. & Kalodimos, C.G. Structural basis for protein antiaggregation activity of the trigger factor chaperone. *Science* **344**, 1250494 (2014).
83. Sala, A., Bordes, P. & Genevaux, P. Multitasking SecB chaperones in bacteria. *Front Microbiol* **5**, 666 (2014).
84. Chatzi, K.E., Sardis, M.F., Karamanou, S. & Economou, A. Breaking on through to the other side: protein export through the bacterial Sec system. *Biochem J* **449**, 25-37 (2013).
85. Auclair, S.M., Bhanu, M.K. & Kendall, D.A. Signal peptidase I: Cleaving the way to mature proteins. *Pro Sci* **21**, 13-25 (2012).
86. Gannon, P.M., Li, P. & Kumamoto, C.A. The mature portion of Escherichia coli maltose-binding protein (MBP) determines the dependence of MBP on SecB for export. *J Bacteriol* **171**, 813-8 (1989).
87. Knoblauch, N.T. et al. Substrate specificity of the SecB chaperone. *J Biol Chem* **274**, 34219-25 (1999).
88. Ullers, R.S. et al. SecB is a bona fide generalized chaperone in Escherichia coli. *Proc Natl Acad Sci USA* **101**, 7583-7588 (2004).
89. Huang, C., Rossi, P., Saio, T. & Kalodimos, C.G. Structural basis for the antifolding activity of a molecular chaperone. *Nature* **537**, 202-206 (2016).
90. Randall, L.L. et al. Binding of SecB to ribosome-bound polypeptides has the same characteristics as binding to full-length, denatured proteins. *Proc Natl Acad Sci USA* **94**, 802-807 (1997).
91. Denks, K., Vogt, A.S., I, Petriman, N.A., Kudva, R. & Koch, H.G. The Sec translocon mediated protein transport in prokaryotes and eukaryotes. *Mol Membr Biol* **31**, 58-84 (2014).
92. Baars, L. et al. Defining the role of the Escherichia coli chaperone SecB using comparative proteomics. *J Biol Chem* **281**, 10024-34 (2006).
93. Allen, W.J. et al. Two-way communication between SecY and SecA suggests a Brownian ratchet mechanism for protein translocation. *Elife* **5**, e15598 (2016).
94. Fessl, T. et al. Dynamic action of the Sec machinery during initiation, protein translocation and termination. *ELife* **7**, e35112 (2018).
95. Ge, Y., Draycheva, A., Bornemann, T., Rodnina, M.V. & Wintermeyer, W. Lateral opening of the bacterial translocon on ribosome binding and signal peptide insertion. *Nature Commun* **5**, 5263 (2014).
96. Voulhoux, R., Bos, M.P., Geurtsen, J., Mols, M. & Tommassen, J. Role of a highly conserved bacterial protein in outer membrane protein assembly. *Science* **299**, 262-5 (2003).

97. Schiffrin, B. et al. Effects of Periplasmic Chaperones and Membrane Thickness on BamA-Catalyzed Outer-Membrane Protein Folding. *J Mol Biol* **429**, 3776-3792 (2017).
98. Schiffrin, B. et al. Skp is a multivalent chaperone of outer-membrane proteins. *Nat Struct Mol Biol* **23**, 786-793 (2016).
99. Stanley, A.M. & Fleming, K.G. The process of folding proteins into membranes: challenges and progress. *Arch Biochem Biophys* **469**, 46-66 (2008).
100. Surrey, T. & Jahnig, F. Refolding and oriented insertion of a membrane protein into a lipid bilayer. *Proc Natl Acad Sci USA* **89**, 7457-61 (1992).
101. Pfitzner, A.K. et al. Mitochondrial-bacterial hybrids of BamA/Tob55 suggest variable requirements for the membrane integration of beta-barrel proteins. *Sci Rep* **6**, 39053 (2016).
102. Ulrich, T., Gross, L.E., Sommer, M.S., Schleiff, E. & Rapaport, D. Chloroplast beta-barrel proteins are assembled into the mitochondrial outer membrane in a process that depends on the TOM and TOB complexes. *J Biol Chem* **287**, 27467-79 (2012).
103. Warner, L.R., Gatzeva-Topalova, P.Z., Doerner, P.A., Pardi, A. & Sousa, M.C. Flexibility in the Periplasmic Domain of BamA Is Important for Function. *Structure* **25**, 94-106 (2017).
104. Gu, Y. et al. Structural basis of outer membrane protein insertion by the BAM complex. *Nature* **531**, 64 (2016).
105. Kim, K.H., Aulakh, S. & Paetzel, M. The bacterial outer membrane beta-barrel assembly machinery. *Protein Sci* **21**, 751-68 (2012).
106. Bakelar, J., Buchanan, S.K. & Noinaj, N. The structure of the β-barrel assembly machinery complex. *Science* **351**, 180-186 (2016).
107. Noinaj, N., Kuszak, A.J., Balusek, C., Gumbart, J.C. & Buchanan, S.K. Lateral opening and exit pore formation are required for BamA function. *Structure* **22**, 1055-1062 (2014).
108. Nakamoto, H. et al. Physical interaction between bacterial heat shock protein (Hsp) 90 and Hsp70 chaperones mediates their cooperative action to refold denatured proteins. *J Biol Chem* **289**, 6110-9 (2014).
109. Bishop, O.T., Edkins, A.L. & Blatch, G.L. Sequence and domain conservation of the coelacanth Hsp40 and Hsp90 chaperones suggests conservation of function. *J Exp Zool B Mol Dev Evol* **322**, 359-78 (2014).
110. Haldar, S., Tapia-Rojo, R., Eckels, E.C., Valle-Orero, J. & Fernandez, J.M. Trigger factor chaperone acts as a mechanical foldase. *Nature Commun* **8**, 668 (2017).
111. Zhuravleva, A. & Gierasch, L.M. Substrate-binding domain conformational dynamics mediate Hsp70 allostery. *Proc Natl Acad Sci USA* **112**, E2865-73 (2015).
112. Kityk, R., Kopp, J., Sinning, I. & Mayer, M.P. Structure and dynamics of the ATP-bound open conformation of Hsp70 chaperones. *Mol Cell* **48**, 863-74 (2012).
113. Melero, R. et al. Modulation of the chaperone DnaK allosterism by the nucleotide exchange factor GrpE. *J Biol Chem* **290**, 10083-92 (2015).
114. Bukau, B. & Horwich, A.L. The Hsp70 and Hsp60 Chaperone Machines. *Cell* **92**, 351-366 (1998).

115. Doyle, S.M., Genest, O. & Wickner, S. Protein rescue from aggregates by powerful molecular chaperone machines. *Nat Rev Mol Cell Biol* **14**, 617-629 (2013).
116. Skjaerven, L., Cuellar, J., Martinez, A. & Valpuesta, J.M. Dynamics, flexibility, and allostery in molecular chaperonins. *FEBS Lett* **589**, 2522-32 (2015).
117. Kawe, M. & Pluckthun, A. GroEL walks the fine line: the subtle balance of substrate and co-chaperonin binding by GroEL. A combinatorial investigation by design, selection and screening. *J Mol Biol* **357**, 411-26 (2006).
118. Yan, X. et al. GroEL Ring Separation and Exchange in the Chaperonin Reaction. *Cell* **172**, 605-617 (2018).
119. Horst, R., Fenton, W.A., Englander, S.W., Wüthrich, K. & Horwich, A.L. Folding trajectories of human dihydrofolate reductase inside the GroEL-GroES chaperonin cavity and free in solution. *Proc Natl Acad Sci USA* **104**, 20788-20792 (2007).
120. Weaver, J. et al. GroEL actively stimulates folding of the endogenous substrate protein PepQ. *Nat Commun* **8**, 15934 (2017).
121. Xu, Z., Horwich, A.L. & Sigler, P.B. The crystal structure of the asymmetric GroEL-GroES-(ADP)7 chaperonin complex. *Nature* **388**, 741-50 (1997).
122. Vabulas, R.M., Raychaudhuri, S., Hayer-Hartl, M. & Hartl, F.U. Protein folding in the cytoplasm and the heat shock response. *Cold Spring Harb Perspect Biol* **2**, a004390 (2010).
123. Weiner, J.H. & Li, L. Proteome of the Escherichia coli envelope and technological challenges in membrane proteome analysis. *Biochim Biophys Acta* **1778**, 1698-713 (2008).
124. Quan, S. et al. Genetic selection designed to stabilize proteins uncovers a chaperone called Spy. *Nat Struct Mol Biol* **18**, 262-9 (2011).
125. Tapley, T.L., Franzmann, T.M., Chakraborty, S., Jakob, U. & Bardwell, J.C. Protein refolding by pH-triggered chaperone binding and release. *Proc Natl Acad Sci USA* **107**, 1071-6 (2010).
126. Srivastava, S.K., Lambadi, P.R., Ghosh, T., Pathania, R. & Navani, N.K. Genetic regulation of spy gene expression in Escherichia coli in the presence of protein unfolding agent ethanol. *Gene* **548**, 142-8 (2014).
127. Kwon, E., Kim, D.Y., Gross, C.A., Gross, J.D. & Kim, K.K. The crystal structure Escherichia coli Spy. *Protein Sci* **19**, 2252-9 (2010).
128. Guo, M.S. & Gross, C.A. Stress-Induced Remodeling of the Bacterial Proteome. *Curr Biol* **24**, 424-434 (2014).
129. Quan, S. et al. Super Spy variants implicate flexibility in chaperone action. *Elife* **3**, e01584 (2014).
130. He, L., Sharpe, T., Mazur, A. & Hiller, S. A molecular mechanism of chaperone-client recognition. *Sci Adv* **2**, e1601625 (2016).
131. Stull, F., Koldewey, P., Humes, J.R., Radford, S.E. & Bardwell, J.C.A. Substrate protein folds while it is bound to the ATP-independent chaperone Spy. *Nat Struct Mol Biol* **23**, 53-58 (2016).
132. Tapley, T.L., Franzmann, T.M., Chakraborty, S., Jakob, U. & Bardwell, J.C.A. Protein refolding by pH-triggered chaperone binding and release. *Proc Natl Acad Sci USA* **107**, 1071-1076 (2010).

133. Hong, W. et al. Periplasmic protein HdeA exhibits chaperone-like activity exclusively within stomach pH range by transforming into disordered conformation. *J Biol Chem* **280**, 27029-34 (2005).
134. Yang, F., Gustafson, K.R., Boyd, M.R. & Wlodawer, A. Crystal structure of Escherichia coli HdeA. *Nat Struct Biol* **5**, 763-4 (1998).
135. Gajiwala, K.S. & Burley, S.K. HDEA, a periplasmic protein that supports acid resistance in pathogenic enteric bacteria. *J Mol Biol* **295**, 605-12 (2000).
136. Ahlstrom, L.S., Dickson, A. & Brooks, C.L., 3rd. Binding and folding of the small bacterial chaperone HdeA. *J Phys Chem B* **117**, 13219-25 (2013).
137. Dahl, J.U. et al. HdeB Functions as an Acid-Protective Chaperone in Bacteria. *J Biol Chem* **290**, 65-75 (2014).
138. Chen, R. & Henning, U. A periplasmic protein (Skp) of Escherichia coli selectively binds a class of outer membrane proteins. *Mol Microbiol* **19**, 1287-94 (1996).
139. Schafer, U., Beck, K. & Muller, M. Skp, a molecular chaperone of gram-negative bacteria, is required for the formation of soluble periplasmic intermediates of outer membrane proteins. *J Biol Chem* **274**, 24567-74 (1999).
140. Bothmann, H. & Pluckthun, A. Selection for a periplasmic factor improving phage display and functional periplasmic expression. *Nat Biotechnol* **16**, 376-80 (1998).
141. Denoncin, K., Schwalm, J., Vertommen, D., Silhavy, T.J. & Collet, J.F. Dissecting the Escherichia coli periplasmic chaperone network using differential proteomics. *Proteomics* **12**, 1391-401 (2012).
142. Ge, X. et al. Identification of FkpA as a key quality control factor for the biogenesis of outer membrane proteins under heat shock conditions. *J Bacteriol* **196**, 672-80 (2014).
143. McMorran, L.M., Bartlett, A.I., Huysmans, G.H., Radford, S.E. & Brockwell, D.J. Dissecting the effects of periplasmic chaperones on the in vitro folding of the outer membrane protein PagP. *J Mol Biol* **425**, 3178-91 (2013).
144. Li, G. et al. Single-Molecule Detection Reveals Different Roles of Skp and SurA as Chaperones. *ACS Chem Biol* **13**, 1082-1089 (2018).
145. Lundin, V.F. et al. Molecular clamp mechanism of substrate binding by hydrophobic coiled-coil residues of the archaeal chaperone prefoldin. *Proc Natl Acad Sci USA* **101**, 4367-72 (2004).
146. Baker, N.A., Sept, D., Joseph, S., Holst, M.J. & McCammon, J.A. Electrostatics of nanosystems: Application to microtubules and the ribosome. *Proc Natl Acad Sci* **98**, 10037-10041 (2001).
147. Walton, T.A., Sandoval, C.M., Fowler, C.A., Pardi, A. & Sousa, M.C. The cavity-chaperone Skp protects its substrate from aggregation but allows independent folding of substrate domains. *Proc Natl Acad Sci USA* **106**, 1772-7 (2009).
148. Callon, M., Burmann, B.M. & Hiller, S. Structural mapping of a chaperone-substrate interaction surface. *Angew Chem* **53**, 5069-72 (2014).

149. Burmann, B.M., Wang, C. & Hiller, S. Conformation and dynamics of the periplasmic membrane-protein-chaperone complexes OmpX-Skp and tOmpA-Skp. *Nat Struct Mol Biol* **20**, 1265-72 (2013).
150. Jarchow, S., Luck, C., Gorg, A. & Skerra, A. Identification of potential substrate proteins for the periplasmic Escherichia coli chaperone Skp. *Proteomics* **8**, 4987-94 (2008).
151. Qu, J., Mayer, C., Behrens, S., Holst, O. & Kleinschmidt, J.H. The trimeric periplasmic chaperone Skp of Escherichia coli forms 1:1 complexes with outer membrane proteins via hydrophobic and electrostatic interactions. *J Mol Biol* **374**, 91-105 (2007).
152. Saul, F.A. et al. Structural and functional studies of FkpA from Escherichia coli, a cis/trans peptidyl-prolyl isomerase with chaperone activity. *J Mol Biol* **335**, 595-608 (2004).
153. Horne, S.M. & Young, K.D. Escherichia coli and other species of the Enterobacteriaceae encode a protein similar to the family of Mip-like FK506-binding proteins. *Arch Microbiol* **163**, 357-65 (1995).
154. Missiakas, D., Betton, J.M. & Raina, S. New components of protein folding in extracytoplasmic compartments of Escherichia coli SurA, FkpA and Skp/OmpH. *Mol Microbiol* **21**, 871-84 (1996).
155. Hu, K., Galius, V. & Pervushin, K. Structural plasticity of peptidyl-prolyl isomerase sFkpA is a key to its chaperone function as revealed by solution NMR. *Biochem J* **45**, 11983-91 (2006).
156. Kim, S., Grant, R.A. & Sauer, R.T. Covalent linkage of distinct substrate degrons controls assembly and disassembly of DegP proteolytic cages. *Cell* **145**, 67-78 (2011).
157. Spiess, C., Beil, A. & Ehrmann, M. A temperature-dependent switch from chaperone to protease in a widely conserved heat shock protein. *Cell* **97**, 339-47 (1999).
158. Kim, S. & Sauer, R.T. Distinct regulatory mechanisms balance DegP proteolysis to maintain cellular fitness during heat stress. *Genes Dev* **28**, 902-11 (2014).
159. Li, S. et al. Thermal-triggerd proteinquake leads to disassembly of DegP hexamer as an imperative activation step. *Sci Rep* **4**, 4834 (2014).
160. Pan, K.L., Hsiao, H.C., Weng, C.L., Wu, M.S. & Chou, C.P. Roles of DegP in prevention of protein misfolding in the periplasm upon overexpression of penicillin acylase in Escherichia coli. *J Bacteriol* **185**, 3020-30 (2003).
161. Krojer, T. et al. Structural basis for the regulated protease and chaperone function of DegP. *Nature* **453**, 885-90 (2008).
162. Tormo, A., Almiron, M. & Kolter, R. surA, an Escherichia coli gene essential for survival in stationary phase. *J Bacteriol* **172**, 4339-47 (1990).
163. Lazar, S.W., Almiron, M., Tormo, A. & Kolter, R. Role of the Escherichia coli SurA protein in stationary-phase survival. *J Bacteriol* **180**, 5704-11 (1998).
164. Lazaar, S.W. & Kolter, R. SurA assists the folding of Escherichia coli outer membrane proteins. *J Bacteriol* **178**, 1770-3 (1996).
165. Behrens, S., Maier, R. Cock, H. , Schmid, F. and Gross, C. The SurA periplasmic PPIase lacking its parvulin domains functions in vivo and has chaperone activity. *EMBO* **20**, 285-94 (2001).

166. Justice, S.S. et al. Periplasmic Peptidyl Prolyl cis-trans Isomerases Are Not Essential for Viability, but SurA Is Required for Pilus Biogenesis in Escherichia coli. *J Bacteriol* **187**, 7680-7686 (2005).
167. Tamae, C. et al. Determination of antibiotic hypersensitivity among 4,000 single-gene-knockout mutants of Escherichia coli. *J Bacteriol* **190**, 5981-8 (2008).
168. Rouviere, P.E. & Gross, C.A. SurA, a periplasmic protein with peptidyl-prolyl isomerase activity, participates in the assembly of outer membrane porins. *Genes Dev* **10**, 3170-82 (1996).
169. Rizzitello, A.E., Harper, J.R. & Silhavy, T.J. Genetic evidence for parallel pathways of chaperone activity in the periplasm of Escherichia coli. *J Bacteriol* **183**, 6794-800 (2001).
170. Vertommen, D., Ruiz, N., Leverrier, P., Silhavy, T.J. & Collet, J.F. Characterization of the role of the Escherichia coli periplasmic chaperone SurA using differential proteomics. *Proteomics* **9**, 2432-43 (2009).
171. Chai, Q. et al. Diverse sequences are functional at the C-terminus of the E. coli periplasmic chaperone SurA. *Protein Eng Des Sel* **27**, 111-6 (2014).
172. Zhong, M., Ferrell, B., Lu, W., Chai, Q. & Wei, Y. Insights into the function and structural flexibility of the periplasmic molecular chaperone SurA. *J Bacteriol* **195**, 1061-7 (2013).
173. Alcock, F.H. et al. Conserved substrate binding by chaperones in the bacterial periplasm and the mitochondrial intermembrane space. *Biochem J* **409**, 377-87 (2008).
174. Behrens-Kneip, S. The role of SurA factor in outer membrane protein transport and virulence. *Int J Med Microbiol* **300**, 421-8 (2010).
175. Bitto, E. & McKay, D.B. The periplasmic molecular chaperone protein SurA binds a peptide motif that is characteristic of integral outer membrane proteins. *J Biol Chem* **278**, 49316-22 (2003).
176. Hennecke, G., Nolte, J., Volkmer-Engert, R., Schneider-Mergener, J. & Behrens, S. The periplasmic chaperone SurA exploits two features characteristic of integral outer membrane proteins for selective substrate recognition. *J Biol Chem* **280**, 23540-8 (2005).
177. Bitto, E. & McKay, D.B. Binding of phage-display-selected peptides to the periplasmic chaperone protein SurA mimics binding of unfolded outer membrane proteins. *FEBS Lett* **568**, 94-8 (2004).
178. Xu, X., Wang, S., Hu, Y.X. & McKay, D.B. The periplasmic bacterial molecular chaperone SurA adapts its structure to bind peptides in different conformations to assert a sequence preference for aromatic residues. *J Mol Biol* **373**, 367-81 (2007).
179. Webb, H.M., Ruddock, L.W., Marchant, R.J., Jonas, K. & Klappa, P. Interaction of the periplasmic peptidylprolyl cis-trans isomerase SurA with model peptides. The N-terminal region of SurA id essential and sufficient for peptide binding. *J Biol Chem* **276**, 45622-7 (2001).
180. Wang, Y. et al. A Supercomplex Spanning the Inner and Outer Membranes Mediates the Biogenesis of beta-Barrel Outer Membrane Proteins in Bacteria. *J Biol Chem* **291**, 16720-9 (2016).

181. Thoma, J., Burmann, B.M., Hiller, S. & Muller, D.J. Impact of holdase chaperones Skp and SurA on the folding of beta-barrel outer-membrane proteins. *Nat Struct Mol Biol* **22**, 795-802 (2015).
182. Bennion, D., Charlson, E.S., Coon, E. & Misra, R. Dissection of beta-barrel outer membrane protein assembly pathways through characterizing BamA POTRA 1 mutants of Escherichia coli. *Mol Microbiol* **77**, 1153-71 (2010).
183. Vuong, P., Bennion, D., Mantei, J., Frost, D. & Misra, R. Analysis of YfgL and YaeT Interactions through Bioinformatics, Mutagenesis, and Biochemistry. *J Bacteriol* **190**, 1507-1517 (2008).
184. Watts, K.M. & Hunstad, D.A. Components of SurA Required for Outer Membrane Biogenesis in Uropathogenic Escherichia coli. *PLoS ONE* **3**, e3359 (2008).
185. Raivio, T.L. Envelope stress responses and Gram-negative bacterial pathogenesis. *Mol Microbiol* **56**, 1119-28 (2005).
186. Duguay, A.R. & Silhavy, T.J. Quality control in the bacterial periplasm. *Biochim Biophys Acta* **1694**, 121-34 (2004).
187. Bury-Mone, S. et al. Global analysis of extracytoplasmic stress signaling in Escherichia coli. *PLoS Genet* **5**, e1000651 (2009).
188. Chen, S., Thompson, K.M. & Francis, M.S. Environmental Regulation of Yersinia Pathophysiology. *Front Cell Infect Microbiol* **6**(2016).
189. Dartigalongue, C., Missiakas, D. & Raina, S. Characterization of the Escherichia coli sigma E regulon. *J Biol Chem* **276**, 20866-75 (2001).
190. Johansen, J., Rasmussen, A.A., Overgaard, M. & Valentin-Hansen, P. Conserved Small Non-coding RNAs that belong to the σE Regulon: Role in Down-regulation of Outer Membrane Proteins. *J Mol Biol* **364**, 1-8 (2006).
191. Schiene-Fischer, C. Multidomain Peptidyl Prolyl cis/trans Isomerases. *Biochim Biophys Acta* **1850**, 2005-16 (2015).
192. Gollan, P.J., Bhave, M. & Aro, E.M. The FKBP families of higher plants: Exploring the structures and functions of protein interaction specialists. *FEBS Lett* **586**, 3539-47 (2012).
193. Gothel, S.F. & Marahiel, M.A. Peptidyl-prolyl cis-trans isomerases, a superfamily of ubiquitous folding catalysts. *Cell Mol Life Sci* **55**, 423-36 (1999).
194. Wedemeyer, W.J., Welker, E. & Scheraga, H.A. Proline cis-trans isomerization and protein folding. *Biochemistry* **41**, 14637-44 (2002).
195. Fanghanel, J. & Fischer, G. Insights into the catalytic mechanism of peptidyl prolyl cis/trans isomerases. *Front Biosci* **9**, 3453-78 (2004).
196. Fujiyama-Nakamura, S. et al. Parvulin (Par14), a Peptidyl-Prolyl cis-trans Isomerase, Is a Novel rRNA Processing Factor That Evolved in the Metazoan Lineage. *Mol Cell Proteomics* **8**, 1552-1565 (2009).
197. Sievers, F. & Higgins, D.G. Clustal omega. *Curr Protoc Bioinformatics* **48**, 3.13.1-16 (2014).
198. Harding, M.W., Galat, A., Uehling, D.E. & Schreiber, S.L. A receptor for the immuno-suppressant FK506 is a cis–trans peptidyl-prolyl isomerase. *Nature* **341**, 758 (1989).
199. Rahfeld, J.U., Schierhorn, A., Mann, K. & Fischer, G. A novel peptidyl-prolyl cis/trans isomerase from Escherichia coli. *FEBS Letters* **343**, 65-69 (1994).

200. Wang, P. & Heitman, J. The cyclophilins. *Genome Biol* **6**, 226 (2005).
201. Weininger, U., Jakob, R.P., Kovermann, M., Balbach, J. & Schmid, F.X. The prolyl isomerase domain of PpiD from Escherichia coli shows a parvulin fold but is devoid of catalytic activity. *Protein Sci* **19**, 6-18 (2010).
202. Henriksson, L.M., Johansson, P., Unge, T. & Mowbray, S.L. X-ray structure of peptidyl-prolyl cis-trans isomerase A from Mycobacterium tuberculosis. *Eur J Biochem* **271**, 4107-13 (2004).
203. Stymest, K.H. & Klappa, P. The periplasmic peptidyl prolyl cis-trans isomerases PpiD and SurA have partially overlapping substrate specificities. *FEBS J* **275**, 3470-9 (2008).
204. Hoffmann, A. et al. Concerted action of the ribosome and the associated chaperone trigger factor confines nascent polypeptide folding. *Mol Cell* **48**, 63-74 (2012).
205. Roman-Hernandez, G., Peterson, J.H. & Bernstein, H.D. Reconstitution of bacterial autotransporter assembly using purified components. *Elife* **3**, e04234 (2014).
206. Morgner, N. & Robinson, C.V. Massign: an assignment strategy for maximizing information from the mass spectra of heterogeneous protein assemblies. *Anal Chem* **84**, 2939-48 (2012).
207. Schneider, C.A., Rasband, W.S. & Eliceiri, K.W. NIH Image to ImageJ: 25 years of image analysis. *Nat Methods* **9**, 671-5 (2012).
208. Xue, C., Lin, T.Y., Chang, D. & Guo, Z. Thioflavin T as an amyloid dye: fibril quantification, optimal concentration and effect on aggregation. *R Soc Open Sci* **4**, 160696 (2017).
209. Vranken, W.F. et al. The CCPN data model for NMR spectroscopy: development of a software pipeline. *Proteins* **59**, 687-96 (2005).
210. Delaglio, F. et al. NMRPipe: a multidimensional spectral processing system based on UNIX pipes. *J Biomol NMR* **6**, 277-93 (1995).
211. Piotto, M., Saudek, V. & Sklenar, V. Gradient-tailored excitation for single-quantum NMR spectroscopy of aqueous solutions. *J Biomol NMR* **2**, 661-5 (1992).
212. Costello, S.M., Plummer, A.M., Fleming, P.J. & Fleming, K.G. Dynamic periplasmic chaperone reservoir facilitates biogenesis of outer membrane proteins. *Proc Natl Acad Sci USA* **113**, 4794-800 (2016).
213. Schrodinger, L. The PyMOL Molecular Graphics System, Version 2.0.
214. Danoff, E.J. & Fleming, K.G. The soluble, periplasmic domain of OmpA folds as an independent unit and displays chaperone activity by reducing the self-association propensity of the unfolded OmpA transmembrane beta-barrel. *Biophys Chem* **159**, 194-204 (2011).
215. Danoff, E.J. & Fleming, K.G. Aqueous, Unfolded OmpA Forms Amyloid-Like Fibrils upon Self-Association. *PLoS One* **10**, e0132301 (2015).
216. Kramer, R.A., Zandwijken, D., Egmond, M.R. & Dekker, N. In vitro folding, purification and characterization of Escherichia coli outer membrane protease ompT. *Eur J Biochem* **267**, 885-93 (2000).
217. Ebie Tan, A., Burgess, N.K., DeAndrade, D.S., Marold, J.D. & Fleming, K.G. Self-association of unfolded outer membrane proteins. *Macromol Biosci* **10**, 763-7 (2010).
218. Pautsch, A. & Schulz, G.E. Structure of the outer membrane protein A transmembrane domain. *Nat Struct Biol* **5**, 1013 (1998).

219. Kennell, W.L. & Holt, S.C. Extraction, purification, and characterization of major outer membrane proteins from Wolinella recta ATCC 33238. *Infect Immun* **59**, 3740-3749 (1991).
220. Burgess, N.K., Dao, T.P., Stanley, A.M. & Fleming, K.G. Beta-barrel proteins that reside in the Escherichia coli outer membrane in vivo demonstrate varied folding behavior in vitro. *J Biol Chem* **283**, 26748-58 (2008).
221. Kabsch, W. & Sander, C. Dictionary of protein secondary structure: pattern recognition of hydrogen-bonded and geometrical features. *Biopolymers* **22**, 2577-637 (1983).
222. Lees, J.G., Miles, A.J., Wien, F. & Wallace, B.A. A reference database for circular dichroism spectroscopy covering fold and secondary structure space. *Bioinformatics* **22**, 1955-62 (2006).
223. Plummer, A. Johns Hopkins University (2017).
224. Chen, Y. & Barkley, M.D. Toward understanding tryptophan fluorescence in proteins. *Biochemistry* **37**, 9976-82 (1998).
225. Batey, S., Nickson, A.A. & Clarke, J. Studying the folding of multidomain proteins. *HFSP J* **2**, 365-377 (2008).
226. Batey, S. & Clarke, J. Apparent cooperativity in the folding of multidomain proteins depends on the relative rates of folding of the constituent domains. *Proc Natl Acad Sci* **103**, 18113-8 (2006).
227. Jerabek-Willemsen, M., Wienken, C.J., Braun, D., Baaske, P. & Duhr, S. Molecular interaction studies using microscale thermophoresis. *Assay Drug Dev Technol* **9**, 342-53 (2011).
228. Stefan, M.I. & Le Novere, N. Cooperative binding. *PLoS Comput Biol* **9**, e1003106 (2013).
229. Ko, T.P., Liao, C.C., Ku, W.Y., Chak, K.F. & Yuan, H.S. The crystal structure of the DNase domain of colicin E7 in complex with its inhibitor Im7 protein. *Structure* **7**, 91-102 (1999).
230. Bartlett, A.I. & Radford, S.E. Desolvation and development of specific hydrophobic core packing during Im7 folding. *J Mol Biol* **396**, 1329-45 (2010).
231. Capaldi, A.P., Kleanthous, C. & Radford, S.E. Im7 folding mechanism: misfolding on a path to the native state. *Nat Struct Biol* **9**, 209-16 (2002).
232. Pashley, C.L. et al. Conformational properties of the unfolded state of Im7 in nondenaturing conditions. *J Mol Biol* **416**, 300-18 (2012).
233. Capaldi, A.P., Shastry, M.C., Kleanthous, C., Roder, H. & Radford, S.E. Ultrarapid mixing experiments reveal that Im7 folds via an on-pathway intermediate. *Nat Struct Biol* **8**, 68-72 (2001).
234. Whittaker, S.B., Spence, G.R., Gunter Grossmann, J., Radford, S.E. & Moore, G.R. NMR analysis of the conformational properties of the trapped on-pathway folding intermediate of the bacterial immunity protein Im7. *J Mol Biol* **366**, 1001-15 (2007).
235. Dennis, C.A. et al. A structural comparison of the colicin immunity proteins Im7 and Im9 gives new insights into the molecular determinants of immunity-protein specificity. *Biochem J* **333** 183-91 (1998).
236. Olaru, A., Bala, C., Jaffrezic-Renault, N. & Aboul-Enein, H.Y. Surface plasmon resonance (SPR) biosensors in pharmaceutical analysis. *Crit Rev Anal Chem* **45**, 97-105 (2015).

237. Brouwer, A.C. & Kirsch, J.F. Investigation of diffusion-limited rates of chymotrypsin reactions by viscosity variation. *Biochemistry* **21**, 1302-7 (1982).
238. Xu, Y. & Matthews, S. TROSY NMR spectroscopy of large soluble proteins. *Top Curr Chem* **335**, 97-119 (2013).
239. Selkrig, J., Leyton, D.L., Webb, C.T. & Lithgow, T. Assembly of β-barrel proteins into bacterial outer membranes. *Biochim Biophys Act* **1843**, 1542-1550 (2014).
240. Libich, D.S., Tugarinov, V. & Clore, G.M. Intrinsic unfoldase/foldase activity of the chaperonin GroEL directly demonstrated using multinuclear relaxation-based NMR. *Proc Natl Acad Sci USA* **112**, 8817-23 (2015).
241. Wu, S. et al. Interaction between bacterial outer membrane proteins and periplasmic quality control factors: a kinetic partitioning mechanism. *Biochem J* **438**, 505-11 (2011).
242. Penzkofer, A., Shirdel, J., Zirak, P., Breitkreuz, H. & Wolf, E. Protein aggregation studied by forward light scattering and light transmission analysis. *Chem Phys* **342**, 55-63 (2007).
243. Lawler, D.M. Turbidity, Turbidimetry, and Nephelometry. in *Reference Module in Chemistry, Molecular Sciences and Chemical Engineering* (Elsevier, 2016).
244. Hamilton, R.G. Methods (In Vitro and In Vivo): Nephelometry and Turbidimetry. in *Encyclopedia of Medical Immunology: Allergic Diseases* (eds. Mackay, I.R., Rose, N.R., Ledford, D.K. & Lockey, R.F.) 484-486 (Springer New York, New York, NY, 2014).
245. Lee, H.C. & Bernstein, H.D. The targeting pathway of Escherichia coli presecretory and integral membrane proteins is specified by the hydrophobicity of the targeting signal. *Proc Natl Acad Sci USA* **98**, 3471-3476 (2001).
246. Moon, C.P., Zaccai, N.R., Fleming, P.J., Gessmann, D. & Fleming, K.G. Membrane protein thermodynamic stability may serve as the energy sink for sorting in the periplasm. *Proc Natl Acad Sci USA* **110**, 4285-90 (2013).
247. Beck, K., Wu, L.F., Brunner, J. & Muller, M. Discrimination between SRP- and SecA/SecB-dependent substrates involves selective recognition of nascent chains by SRP and trigger factor. *EMBO* **19**, 134-43 (2000).
248. Lian, H.Y. et al. Hsp40 interacts directly with the native state of the yeast prion protein Ure2 and inhibits formation of amyloid-like fibrils. *J Biol Chem* **282**, 11931-40 (2007).
249. Oroz, J., Kim, J.H., Chang, B.J. & Zweckstetter, M. Mechanistic basis for the recognition of a misfolded protein by the molecular chaperone Hsp90. *Nat Struct Mol Biol* **24**, 407-413 (2017).
250. Willander, H. et al. BRICHOS domains efficiently delay fibrillation of amyloid beta-peptide. *J Biol Chem* **287**, 31608-17 (2012).
251. Meisl, G. et al. Differences in nucleation behavior underlie the contrasting aggregation kinetics of the Abeta40 and Abeta42 peptides. *Proc Natl Acad Sci USA* **111**, 9384-9 (2014).
252. Arosio, P., Knowles, T.P. & Linse, S. On the lag phase in amyloid fibril formation. *Phys Chem Chem Phys* **17**, 7606-18 (2015).

253. Hou, L. et al. Solution NMR studies of the A beta(1-40) and A beta(1-42) peptides establish that the Met35 oxidation state affects the mechanism of amyloid formation. *J Am Chem Soc* **126**, 1992-2005 (2004).
254. Young, L.M. et al. Screening and classifying small-molecule inhibitors of amyloid formation using ion mobility spectrometry-mass spectrometry. *Nat Chem* **7**, 73-81 (2015).
255. Stirling, P.C., Bakhoum, S.F., Feigl, A.B. & Leroux, M.R. Convergent evolution of clamp-like binding sites in diverse chaperones. *Nat Struct Mol Biol* **13**, 865-70 (2006).
256. Crooke, E. & Wickner, W. Trigger factor: a soluble protein that folds pro-OmpA into a membrane-assembly-competent form. *Proc Natl Acad Sci USA* **84**, 5216-20 (1987).
257. Soltes, G.R., Schwalm, J., Ricci, D.P. & Silhavy, T.J. The Activity of Escherichia coli Chaperone SurA Is Regulated by Conformational Changes Involving a Parvulin Domain. *J Bacteriol* **198**, 921-929 (2016).
258. Popot, J.L. Folding membrane proteins in vitro: a table and some comments. *Arch Biochem Biophys* **564**, 314-26 (2014).
259. Hohr, A.I.C. et al. Membrane protein insertion through a mitochondrial beta-barrel gate. *Science* **359**(2018).
260. Noinaj, N., Gumbart, J.C. & Buchanan, S.K. The [beta]-barrel assembly machinery in motion. *Nat Rev Micro* **15**, 197-204 (2017).
261. Grabowicz, M., Koren, D. & Silhavy, T.J. The CpxQ sRNA Negatively Regulates Skp To Prevent Mistargeting of β-Barrel Outer Membrane Proteins into the Cytoplasmic Membrane. *MBio* **7**, e00312-16 (2016).
262. Takahashi, H., Nakanishi, T., Kami, K., Arata, Y. & Shimada, I. A novel NMR method for determining the interfaces of large protein-protein complexes. *Nat Struct Biol* **7**, 220-3 (2000).
263. Hagan, C.L., Kim, S. & Kahne, D. Reconstitution of outer membrane protein assembly from purified components. *Science* **328**, 890-2 (2010).
264. Patel, G.J. & Kleinschmidt, J.H. The lipid bilayer-inserted membrane protein BamA of Escherichia coli facilitates insertion and folding of outer membrane protein A from its complex with Skp. *Biochemistry* **52**, 3974-3986 (2013).
265. Hartmann, J.B., Zahn, M., Burmann, I.M., Bibow, S. & Hiller, S. Sequence-Specific Solution NMR Assignments of the β-Barrel Insertase BamA to Monitor Its Conformational Ensemble at the Atomic Level. *J Am Chem Soc* **140**, 11252-11260 (2018).
266. Lilly, A.A., Crane, J.M. & Randall, L.L. Export chaperone SecB uses one surface of interaction for diverse unfolded polypeptide ligands. *Pro Sci* **18**, 1860-8 (2009).
267. Roche, J., Shen, Y., Lee, J.H., Ying, J. & Bax, A. Monomeric Aβ(1–40) and Aβ(1–42) Peptides in Solution Adopt Very Similar Ramachandran Map Distributions That Closely Resemble Random Coil. *Biochemistry* **55**, 762-775 (2016).
268. Masuda, T., Saito, N., Tomita, M. & Ishihama, Y. Unbiased quantitation of Escherichia coli membrane proteome using phase transfer surfactants. *Mol Cell Proteomics* **8**, 2770-7 (2009).

269. Kramer, G. et al. Trigger factor peptidyl-prolyl cis/trans isomerase activity is not essential for the folding of cytosolic proteins in Escherichia coli. *J Biol Chem* **279**, 14165-70 (2004).
270. Hartl, F.U., Lecker, S., Schiebel, E., Hendrick, J.P. & Wickner, W. The binding cascade of SecB to SecA to SecY/E mediates preprotein targeting to the E. coli plasma membrane. *Cell* **63**, 269-79 (1990).
271. Zhou, J.M. & Xu, Z. Structural determinants of SecB recognition by SecA in bacterial protein translocation. *Nat Struct Biol* **10**, 942 (2003).
272. Obi, I.R. & Francis, M.S. Demarcating SurA activities required for outer membrane targeting of Yersinia pseudotuberculosis adhesins. *Infect Immun* **81**, 2296-308 (2013).
273. Storek, K.M. et al. Monoclonal antibody targeting the β-barrel assembly machine of Escherichia coli is bactericidal. *Proc Natl Acad Sci USA* **115**, 3692-3697 (2018).